DEPARTMENT OF MECHANICAL ENGINEERING

UNIVERSITY OF GLASGOW

AN INVESTIGATION OF RESIDUAL STRESSES IN TUBING.

GEORGE B. SIMPSON.

Ph.D. THESIS, JANUARY 1976, VOLUME I.

ACKNOWLEDGEMENTS.

The author wishes to record his gratitude to the Senate of the University of Glasgow for the award of a Gray, Law and Watt Scholarship, to Professor J.D. Robson for his interest and the use of laboratory facilities, to Mr. R. Fletcher for his supervision and assistance, and to Messrs. N. McGhie and A.B. Ramsay for the construction of experimental apparatus.

CONTENTS.

VOLUME I.

(continued overleaf)

CONTENTS.

VOLUME I. (continued)

VOLUME II.

(continued overleaf)

CONTENTS.

VOLUME II. (continued)

SUMMARY.

Residual stresses fall naturally into two categories; macrostresses and microstresses. An indication of the origins of both types is given. The presence of residual macrostresses in a body can be recognized by the occurrence of distortions on making cuts in the body. In bodies of regular geometry, the distortions which occur on gradual removal of uniform layers from one surface can often be used to assess the magnitude of the residual stresses in the removed material. Over the years, many techniques based on this principle have been developed. The Sachs method (ref.5) for the determination of triaxial axisymmetric residual stresses in solid bars, hollow cylinders and tubes, is one such technique. A brief account of the method and the assumptions on which it is based is presented. A number of important refinements are described.

The residual stresses in thin-walled cylinders and tubing have been the subject of many experimental investigations. Although some studies of quenching and machining stresses have been carried out, the residual stresses produced during tube-drawing have attracted the most attention. Recent work on this topic is briefly reviewed, and the origins of residual stress in drawn tubing are discussed.

Although it has long been realised that tubing drawn under commercial conditions almost always exhibits some

degree of eccentricity, only Knights (82) has suggested that this should be taken into account when determining residual stresses in such tubing. The same author has also suggested that significant circumferential variations of the residual stresses may occur in drawn tubing, possibly associated with plastic bending at entry or exit from the drawing die.

The present work was carried out to determine whether circumferential variations of residual stress existed in drawn tubing, to establish the effect of eccentricity on the determination of residual stress by the Sachs method, and to evaluate the bending deflection method (which is the usual alternative to the Sachs technique) in the presence of eccentricity and possibly suggest some improvements.

The results obtained from an experimental investigation of the longitudinal and circumferential variation of the deformations produced on cutting drawn tubing to length suggest the presence of additional residual stresses not previously reported. The terms 'type A' and 'type B' residual stresses are introduced to distinguish between normal residual stresses and the additional residual stresses. (ie B)

'Type B' longitudinal residual stresses exist as alternate regions of tension and compression round the circumference of drawn tubing and 'type B' circumferential residual stresses exist as opposing bending stresses in adjacent lengths. Both appear to be completely relieved

in what are normally regarded as 'long' specimens (i.e. for the tubing used, in specimens with length/diameter ratios less than 5). 'Type B' longitudinal residual stresses may possibly be associated with imperfect lubrication during drawing. The origin of 'type B' circumferential residual stresses is not clear.

The determination of circumferential and radial 'type A' residual stresses in a uniform cylinder by the Sachs technique is based on the assumption that the relief of these stresses in part of the cylinder (by layer removal) is equivalent to the application of a uniform pressure to the remainder. Since the application of a uniform pressure to an eccentric cylinder produces circumferential variations of stress on both boundaries, the Sachs technique cannot readily be applied where eccentricity is appreciable.

Experimental results suggest that the Sachs technique can be applied in practice to determine the circumferential and radial 'type A' residual stresses over about 80% of the wall thickness of drawn tubing with I.D./O.D. = 0.941 and an initial wall thickness variation less than $\pm 6\%$, provided that these residual stresses do not vary circumferentially. Where the circumferential stresses applied by layer removal are compressive, the procedure may be complicated by the occurrence of elastic pre-buckling deformations of a circumferential lobar form, and a stage may even be reached at which plastic buckling takes place.

The determination of longitudinal 'type A' residual stresses in the presence of eccentricity is complicated by the development of longitudinal shear stresses as the variation of wall thickness is increased by layer removal. The possibility of applying a simple modification of the Sachs analysis which takes account of wall thickness variation, but not shear stresses, is examined.

The limitations of the Sachs method in the presence of eccentricity are discussed.

Although the bending deflection method has certain advantages over the Sachs technique for the determination of 'type A' longitudinal residual stresses in the presence of eccentricity, its usefulness is restricted since no satisfactory method of determining the coexistent circumferential residual stresses is available. A method which incorporates a recently developed technique for the determination of local residual stress (91,100), is proposed and is shown to have considerable advantages.

NOTATION.

σ	Stress.
ε	Strain.
μ	Poisson's ratio.
$\mathcal{L}, \mathcal{b}$	Longitudinal and circumferential strain parameters.
a	Internal radius.
b	External radius.
ρ, ρ'	General radius, radial position.
R	Radius, radius of curvature.
D	Diameter.
h	Wall thickness.
ℓ	Length.
c	Centre distance.
e	Eccentricity.
f	$\pi\rho^2$
τ	Shear stress.
γ	Shear strain.
M	Bending moment.
I	Second moment of area.
P	Normal force.
W	Weight loss.
ω	Weight density.
θ	Angular position.
p	Pressure.
$F(\rho,\theta)$	Dimensionless function of ρ and θ.
x	Lengthwise position.
w	Radial deflection.
d	Depth, groove depth.

S	Stress.
G	Gap width.
s	Groove width.
t	Thickness of material beneath groove.

Subscripts.

a	'At inner surface'.
b	'At outer surface'.
$b\rho$	'At outer surface by removal of a layer at position ρ ' (internal layer removal).
$a\rho$	'At inner surface by removal of a layer at position ρ ' (external layer removal).
$\rho\rho'$	'At position ρ by removal of a layer at position ρ' '.
L, C, R	'Longitudinal, circumferential, radial'.
M	'Bending'.
P	'Normal'.
m	'Mean'.
θ	'At position θ '.
$0, 1 \ldots r, \ldots n$	General subscripts.
nr	'In n^{th} layer by removal of r^{th} layer'.
ar	'At inner surface by removal of r^{th} layer'.
an	'At inner surface by removal of n^{th} layer'.

SECTION 1.

INTRODUCTION AND REVIEW OF LITERATURE.

1.01. RESIDUAL STRESSES.

Since the earliest recorded reference to the subject in 1889 (63,68) an extensive literature has become available on the origins and effects of residual stresses in a wide variety of bodies and structures (1-4,68,78,79) and a large number of methods for the determination of residual stresses have been developed. Reviews have been produced at regular intervals over the past forty years (63-72,82), the most recent being the comprehensive review by Denton in 1966. With improved data-processing equipment becoming more readily available, particular emphasis appears to have been placed recently on speeding-up the process of residual stress determination (18-21,92,95,99,108).

Residual stresses have been defined by Orowan (2,4) as those existing in bodies upon which no external forces are acting. It is usual to distinguish between body stresses and textural stresses. The former arise in homogeneous bodies from a non-uniform expansion, contraction or shear distortion of mechanical, chemical or thermal origin. The latter from textural or structural inhomogeneities, even when the overall deformations are uniform. Stresses of the first group are usually on a much larger scale than those of the second group; for this reason the two groups are often referred to as macrostresses and microstresses. Many of the ways in which residual stresses of both groups arise in practice are discussed in references 2 and 4.

The presence of residual macrostresses in a body can be recognized by the occurrence of distortions on making cuts in the body. These distortions can often be used to assess the magnitude of the residual stresses which existed in the body prior to cutting. In general, the deformations which occur on gradual removal of uniform layers from one surface of a residually-stressed body are the most useful and the easiest to analyse, especially if the body is geometrically regular.

The determination of residual macrostresses in hollow cylinders and tubes has become a favourite topic for research projects since Sachs (in 1927), and Davidenkov (in 1932), developed the methods (5,76) which now bear their names.

Although containing an error (82,89,90), the Davidenkov method is generally recognized as the most fundamental of the so-called bending deflection methods for residual stress determination (63-95). Unfortunately, it is limited in its application to biaxial stress systems and so can only be applied to thin-walled tubing, in which the radial residual stress is practically zero. A review of the various bending deflection methods is presented in a later section.

The Sachs method, with which a major part of the present work is concerned, makes possible the determination of triaxial axisymmetric residual stresses in solid bars and thick-walled tubes, and may easily be applied to thin-walled tubing. An account of the method and the assump-

tions on which it is based is given in the following section; a number of refinements are examined, and some recent applications described.

1.02. THE SACHS METHOD.

Although it was realised by Heyn in 1914 (8) that the deformations produced by machining cold-drawn bars could be used to predict the residual stresses which existed in the uncut bars, it was not until 1927 that a satisfactory solution was obtained. The equations derived by Sachs in that year made possible the determination of triaxial residual stresses in cylinders from the dimensional changes produced by removing successive concentric layers from the surface of a centrally-bored hole.

If σ_L , σ_c and σ_R denote the axisymmetric residual stresses at position ρ in the isotropic cylinder of fig.1 then:

$$\sigma_L = E'\left[(f_b - f)\left(\frac{d\ell}{df}\right)_{b\rho} - \ell_{b\rho}\right]$$

$$\sigma_c = E'\left[(f_b - f)\left(\frac{d\ell\theta}{df}\right)_{b\rho} - \left(\frac{f_b + f}{2f}\right).\ell\theta_{b\rho}\right]$$

$$\sigma_R = E'\left[\left(\frac{f_b - f}{2f}\right).\ell\theta_{b\rho}\right] \qquad \text{----------1.01.}$$

where $E' = \frac{E}{1-\mu^2}$, $f_b = \pi b^2$, and $f = \pi\rho^2$ is the bored-out area. In the case of a hollow cylinder of internal radius a , the initial value of f is πa^2 . The parameters $\ell_{b\rho} = \varepsilon_L + \mu.\varepsilon_c$ and $\ell\theta_{b\rho} = \varepsilon_c + \mu.\varepsilon_L$ are determined from the measured strain changes ε_L and ε_c at the outer surface.

Hollow cylinders may also be investigated by removing concentric layers from the outer surface and measuring the surface strains produced at the bore. The equations for this case are:

$$\sigma_L = E'\left[(f-f_a)\left(\frac{d\mathcal{L}}{df}\right)_{ap} - \mathcal{L}_{ap}\right]$$

$$\sigma_c = E'\left[(f-f_a)\left(\frac{d\ell_0}{df}\right)_{ap} - \left(\frac{f+f_a}{2f}\right).\ell_{0ap}\right]$$

$$\sigma_R = -E'\left[\left(\frac{f-f_a}{2f}\right).\ell_{0ap}\right] \quad \text{---------1.02.}$$

where $f = \pi\rho^2$ and $f_a = \pi a^2$.

Although the derivation of the equations 1.01 and 1.02 is well known (5-7,49,83,87) an outline of the procedure has been included as appendix 3, to illustrate the 'double-subscript' notation adopted, in the present work, for stress and strain changes. The derivation of the expressions for σ_c and σ_R is based on the assumption that the relief of the circumferential and radial residual stresses in part of the cylinder (by layer removal), is equivalent to the application of a uniform (internal or external) pressure to the remainder. The derivation of the expressions for σ_L follows from consideration of the longitudinal equilibrium of the cylinder.

Over the years, two different forms of the equations for external layer removal have appeared. If $\Delta\rho$ is taken as positive for decreasing ρ , the equations 1.02 are obtained (1,6,64,67,69): If, however, $\Delta\rho$ is taken as negative for decreasing ρ , the gradients in equations 1.02 change sign (12,48,49,83,87). In the form

given by Barrett (65) a minus sign is omitted in the expression for σ_R, and in the form given by Denton (72) a similar omission occurs in the expression for σ_L.

Strictly speaking, equations 1.01 and 1.02 only apply to a cylinder of infinite length. In practical applications of the method, a specimen length of $3D_m$ is generally considered to be sufficient (section 4).

The method has been applied in its basic form many times (6,7,9-15,34,48-50,82,83,87). In large scale applications, metal removal has generally been accomplished by machining, while for smaller scale applications or thin-walled cylinders, acid-etching has been used with some success (48,50,83). The following list gives some idea of the types of problem which can be investigated; auto-frettaged cylinders (7,13,14), heat-treated cylinders (10,49), spot-welded plates (15), forgings (11,12), piston-rods (6,9), semicontinuously-cast pipes (34), extruded rod (50), ironed tubing (48) and cold-drawn tubing (82,83,87).

In all the above applications, the same basic assumptions were made; that the cylindrical body was isotropic, that the residual stresses were axisymmetric, and that the inner and outer surfaces were concentric at all times during layer removal. The assumption of isotropy is clearly questionable in the last three examples, and the assumption about concentricity, in the last two.

Two specimens are normally required for the complete

determination of residual stresses in a cylindrical body by the Sachs method; one for internal layer removal, and one for external layer removal. If only one specimen is available, it is necessary to estimate the residual stresses in the remaining wall thickness by linear extrapolation; a procedure which can often introduce errors where rapidly-changing surface stresses are involved. The following modification, proposed by Barker and Hardy (11) and developed by Weiss (16), improves the accuracy of residual stress predictions from incomplete strain measurements.

Equations 1.01 and 1.02 may be rewritten:

$$\sigma_L = E' \cdot \frac{d}{df}\left[(f_b - f) \cdot \mathcal{L}_{b\rho}\right]$$

$$\sigma_C = E' \cdot \frac{d}{d\rho}\left[\left(\frac{b^2-\rho^2}{2\rho}\right) \cdot \ell_{b\rho}\right]$$

$$\sigma_R = E' \cdot \left[\left(\frac{b^2-\rho^2}{2\rho^2}\right) \cdot \ell_{b\rho}\right] \qquad \text{1.03.}$$

$$\sigma_L = E' \cdot \frac{d}{df}\left[(f - f_a) \cdot \mathcal{L}_{a\rho}\right]$$

$$\sigma_C = E' \cdot \frac{d}{d\rho}\left[\left(\frac{\rho^2-a^2}{2\rho}\right) \cdot \ell_{a\rho}\right]$$

$$\sigma_R = -E' \left[\left(\frac{\rho^2-a^2}{2\rho^2}\right) \cdot \ell_{a\rho}\right] \qquad \text{1.04.}$$

Since the expressions in the square brackets all $\rightarrow$ zero as $\rho \rightarrow b$ (or $\rho \rightarrow a$), extrapolation may be replaced by linear interpolation between the last

measured value and zero at the outer (inner) surface. The equivalence of equations 1.03 and 1.01, and of equations 1.04 and 1.02, may easily be verified by substituting $f = \pi\rho^2$, $f_b = \pi b^2$ and $f_a = \pi a^2$, and completing the differentiation. In the case of equations 1.04, $\frac{d}{d\rho}(\rho)$ and $\frac{d}{df}(f)$ must be taken as minus one during this process, in accordance with the sign convention for external layer removal.

The determination of the gradients $\frac{d\mathcal{L}}{df}$ and $\frac{d\ell o}{df}$ in equations 1.01 and 1.02 is usually carried out graphically, from plots of $\mathcal{L}$ and ℓo against f. In an effort to minimise the errors in this process, Buhler (49) adopted a step-wise approach.

If the interval from $f = 0$ to $f = f_b$ is divided into P equal parts the equations for internal layer removal may be written:

$$\sigma_L = E'\left[\frac{P-n}{2}\left(\mathcal{L}_{n+1} - \mathcal{L}_{n-1}\right)_b - \left(\mathcal{L}_n\right)_b\right]$$

$$\sigma_c = E'\left[\frac{P-n}{2}\left(\ell o_{n+1} - \ell o_{n-1}\right)_b - \left(\frac{P+n}{2n}\right)\left(\ell o_n\right)_b\right]$$

$$\sigma_R = E'\left[\frac{P-n}{2n}\cdot\left(\ell o_n\right)_b\right] \qquad \text{----------1.05.}$$

In the case of external layer removal, the interval from $f=0$ to $f=f_a$ is divided into N equal parts, and the subdivision is continued until f_b is exceeded. In accordance with the sign convention: $\Delta\rho$ positive

for decreasing ρ , equations 1.02 become:

$$\sigma_L = E'\left[\frac{n-N}{2}(\mathcal{L}_{n-1}-\mathcal{L}_{n+1})_a - (\mathcal{L}_n)_a\right]$$

$$\sigma_c = E'\left[\frac{n-N}{2}(\ell\ell_{n-1}-\ell\ell_{n+1})_a - \left(\frac{n+N}{2n}\right)(\ell\ell_n)_a\right]$$

$$\sigma_R = -E'\left[\frac{n-N}{2n}\cdot(\ell\ell_n)_a\right] \qquad \text{---------1.06.}$$

In Denton's review (72), there is an error in the definition of N .

The following equilibrium conditions apply to the infinite residually-stressed cylinder:

$$\int \sigma_L \cdot df = 0 \qquad \text{----------1.07.}$$

$$\int \sigma_c \cdot d\rho = 0 \qquad \text{----------1.08.}$$

$$\sigma_R = 0 \quad (\rho = a, b) \text{----------1.09.}$$

$$\sigma_c - \sigma_R = \rho \cdot \frac{d\sigma_R}{d\rho} \text{----------1.10.}$$

The first condition implies that the sum of the longitudinal stresses over the cross-sectional area of the cylinder must be zero, or that in a plot of σ_L against f , the area under the curve on the tension side must equal the area under the curve on the compression side. The second condition implies that the sum of the circumferential stresses across any

diametrical section must be zero (plot σ_c against ρ). The third condition expresses the force equilibrium of the free inner and outer surfaces, and the fourth describes the interdependence of the radial and circumferential stress distributions.

It may easily be shown (49) that the Sachs equations fulfil all the above conditions.

The general form of the radial residual stress distribution is a smooth curve from zero at one surface, through a maximum (or a minimum), to zero at the other surface. The fact that $\sigma_c = \sigma_R$ at the turning point (from equation 1.10) has been suggested by Shur (17) as a further means of checking the calculated stress values.

The validity of the curves for ℓ_{bp} and ℓ_{ap} obtained from two identical specimens may be checked using the equation:

$$\ell_{bp} = -\left(\frac{f-f_a}{f_b-f}\right).\ell_{ap}$$

which follows directly from the expressions for σ_R in equations 1.01 and 1.02.

Large errors in σ_c may result if graphical methods are used for the analysis of experimental data obtained from discs or thick-walled cylinders. By using a polynomial approximation for σ_R (based on a few measured points, and the zero surface values) and the equilibrium

condition 1.10, Yakunin (18,19) obtained σ_c without plotting the deformation curve. The polynomial approximation was obtained by the method of least squares, and the calculations were simplified by rewriting the Sachs equations in terms of the dimensionless parameter ρ/b .

Fourier series may be used for the mathematical description of residual stress and released strain diagrams. Kobrin and Birulya (20) have recently shown that a given residual stress diagram may be expressed:

$$\sigma_i = m\left[A_0 + \sum_{k=1}^{n/2} A_k \cos k\alpha_i + \sum_{k=1}^{n/2} B_k \sin k\alpha_i + C_i\right] \qquad \text{---------1.11.}$$

where m is the scale on which the diagram is plotted. With $f_i = \pi \rho_i^2$ as the independent variable, and σ_0 and σ_n as the initial and final stress values, α_i and C_i may be written in the form:

$$\alpha_i = \frac{2\pi\left[(f_i)^{1/2} - (f_0)^{1/2}\right]}{(f_n)^{1/2} - (f_0)^{1/2}}$$

$$C_i = \frac{\sigma_n - \sigma_0}{(f_n)^{1/2} - (f_0)^{1/2}}\left[(f_i)^{1/2} - (f_0)^{1/2}\right]$$

To test the procedure, Kobrin and Birulya approximated four different experimentally-obtained circumferential residual stress diagrams, which essentially covered all the basic types normally encountered, by 48-term series.

The number of terms in each approximation was reduced until the r.m.s. error relative to the 48-term series exceeded $9.8 N/mm^2$ ($1kg\ mass/mm^2$). The most difficult curve to approximate was found to be the circumferential residual stress produced in a case-hardened disc, annealed at $150^{\circ}C$ (fig.2), for which at least twenty-four terms were required.

By substituting the expression 1.11 into the appropriate equation from 1.03 (or 1.04), and integrating, the mathematical equivalent of the original deformation measurements was obtained. In the case of the 24-term approximation to fig.2 , the maximum discrepancy between the measured and calculated values was less than 10%, and in the other three cases this was less than 3%.

Standard programmes were produced for the computation of the Fourier coefficients, the residual stress functions, and the strain functions, and the method was applied to a number of practical problems. For example, the mathematical equivalent of the residual stresses in ingots was used to predetermine final stress levels in finished parts, and the strains which would be produced during manufacture. The authors found that a certain amount of control over the final stress level could be exercised by judicious machining.

Kobrin, Proshko and Sorkin (21) have used an analog computer for speeding-up residual stress calculations. Their structure diagram for equations 1.01 is

reproduced as fig.3 . The experimental plots for $\mathcal{L}_{b\rho}$ and $\mathcal{l}\theta_{b\rho}$ were converted to a suitable form for processing, by piecewise-linear approximation. The method was applied to the calculation of the residual stresses in a a roller-hardened steel cylinder 156mm in diameter and 134mm long.

In addition to the above refinements, a number of new applications for the Sachs technique have recently been developed.

Peiter (22,23) has derived equations which make possible the determination of torsional residual stress in cylinders. In the case of the hollow cylinder of fig.4 , the residual shear stress τ_{LC} may be determined from measurements of ϕ , the relative angle of twist of the end-faces during layer removal, by using either of the following equations:

$$\tau_{LC} = \pm G\left[\rho.\theta_I + \frac{\rho^2}{4}\left(1-\frac{b^4}{\rho^4}\right).\frac{d\theta_I}{d\rho}\right] \quad \text{---- 1.12.}$$

$$\tau_{LC} = \pm G\left[\rho.\theta_E + \frac{\rho^2}{4}\left(1-\frac{a^4}{\rho^4}\right).\frac{d\theta_E}{d\rho}\right] \quad \text{---- 1.13.}$$

θ_I and θ_E denote the angle of twist per unit length (ϕ/l) in the case of internal and external layer removal, respectively. If it is assumed that the torque released by layer removal produces the condition of pure shear in the cylinder, then:

$$\gamma_b = b.\theta_I$$
$$\gamma_a = a.\theta_E$$

where γ_b denotes the shear strain on the outer surface during internal layer removal, and γ_a the shear strain on the inner surface during external layer removal. Equations 1.12 and 1.13 may therefore be rewritten:

$$\tau_{Lc} = \pm \frac{G}{b}\left[\rho.\gamma_b + \frac{\rho^2}{4}\left(1 - \frac{b^4}{\rho^4}\right).\frac{d\gamma_b}{d\rho}\right] \quad \text{---- 1.14.}$$

$$\tau_{Lc} = \pm \frac{G}{a}\left[\rho.\gamma_a + \frac{\rho^2}{4}\left(1 - \frac{a^4}{\rho^4}\right).\frac{d\gamma_a}{d\rho}\right] \quad \text{---- 1.15.}$$

The surface shear strains γ_a and γ_b may be determined by mounting three strain gauges in the longitudinal, circumferential and 45° directions, and using the strain transformation relation:

$$\varepsilon_{45^\circ} = \frac{\varepsilon_L + \varepsilon_c}{2} + \frac{\gamma}{2}$$

The method is unaffected by the presence of the direct stresses σ_L, σ_c and σ_R, and may also be applied to solid cylinders by putting $a = 0$ in equation 1.13.

The torsional residual stresses produced in springs during manufacture have been investigated by Murakami and Fujitani (24). Removal of uniform layers from the outer surface of the springs by acid-etching produced changes in length X, which were magnified 150 times by the lever and mirror system shown in fig.5, and continuously monitored. The following formula was derived to relate the shear stress at radius ρ to the measured extension:

$$\tau = \frac{G\rho}{8\pi n R^2}\left[\rho \cdot \frac{dX}{d\rho} - 4X\right] \qquad \text{---------- 1.16.}$$

R is the mean radius of the spring coil and n the effective number of turns.

The authors chose to neglect the possible presence of triaxial residual stresses σ_L , σ_C and σ_R in the spring-wire. This could affect the accuracy of the procedure, since the release of the stress σ_L could also contribute to the extension X .

It has already been noted that equations 1.01 and 1.02 are limited to elastically isotropic materials, Doi and Kataoka (25) and Olson and Bert (26), working independently, have recently modified the Sachs analysis so that triaxial residual stresses in polar-anisotropic (orthotropic) cylinders may be determined. In the case of internal layer removal, the modified equations (25) are:

$$\sigma_L = \frac{E_L}{1-\mu_{CL}\cdot\mu_{LC}}\left[\left(\frac{b^2-\rho^2}{2\rho}\right)\left(\frac{d\mathcal{L}^*}{d\rho}\right)_{b\rho} - \mathcal{L}^*_{b\rho}\right]$$

$$\sigma_C = \frac{E_C}{2K\left(1-\mu_{CL}\cdot\mu_{LC}\right)}\left\{\rho\left[\left(\frac{b}{\rho}\right)^{K+1} - \left(\frac{\rho}{b}\right)^{K-1}\right]\left(\frac{d\mathcal{L}^*}{d\rho}\right)_{b\rho} - K\left[\left(\frac{b}{\rho}\right)^{K+1} + \left(\frac{\rho}{b}\right)^{K-1}\right]\cdot\mathcal{L}^*_{b\rho}\right\}$$

$$\sigma_R = \frac{E_C}{2K\left(1-\mu_{CL}\cdot\mu_{LC}\right)}\left[\left(\frac{b}{\rho}\right)^{K+1} - \left(\frac{\rho}{b}\right)^{K-1}\right]\cdot\mathcal{L}^*_{b\rho} \qquad \text{---------- 1.17.}$$

where $k = \left(\frac{E_C}{E_R}\right)^{1/2}$, $\overset{*}{\ell}_{bp} = \varepsilon_L + \mu_{CL} \cdot \varepsilon_C$ and $\overset{*}{\ell\theta}_{bp} = \varepsilon_C + \mu_{LC} \cdot \varepsilon_L$.

Using the sign convention: $\Delta\rho$ positive for decreasing ρ, the equations for external layer removal (25) become:

$$\sigma_L = \frac{E_L}{1-\mu_{CL}\cdot\mu_{LC}}\left[\left(\frac{\rho^2-a^2}{2\rho}\right)\left(\frac{d\overset{*}{\ell}}{d\rho}\right)_{ap} - \overset{*}{\ell}_{ap}\right]$$

$$\sigma_C = \frac{E_C}{2k(1-\mu_{CL}\cdot\mu_{LC})}\left\{\rho\left[\left(\frac{\rho}{a}\right)^{k-1} - \left(\frac{a}{\rho}\right)^{k+1}\right]\left(\frac{d\overset{*}{\ell\theta}}{d\rho}\right)_{ap} - k\left[\left(\frac{a}{\rho}\right)^{k+1} + \left(\frac{\rho}{a}\right)^{k-1}\right]\cdot\overset{*}{\ell\theta}_{ap}\right\}$$

$$\sigma_R = \frac{-E_C}{2k(1-\mu_{CL}\cdot\mu_{LC})}\left[\left(\frac{\rho}{a}\right)^{k-1} - \left(\frac{a}{\rho}\right)^{k+1}\right]\cdot\overset{*}{\ell\theta}_{ap} \qquad \text{---------- 1.18}$$

The original Sachs formulae may be obtained as a special case, by substituting $E_L = E_C = E_R = E$ and $\mu_{CL} = \mu_{LC} = \mu$ in either of the above sets of equations.

If the presence of annual-rings and cardinal-points are ignored, and macroscopic average values of the elastic compliances in the longitudinal, circumferential and radial directions are taken, a tree-trunk may be considered as a polar-anisotropic body (25), and equations 1.17 and 1.18 may be used to determine growth-stresses.

Large errors can result (26) if the basic Sachs equations are applied to cylindrically-orthotropic

materials, although, in the case of thin-walled tubing (a/b greater than 0.9), errors are generally small.

One application of the basic Sachs technique not already mentioned, is in the investigation of residual stress in cylinders which have been built up by welding. It is necessary to assume that the built-up cylinder is isotropic, or that the deposited metal has the same elastic properties as the material of the original cylinder. Ksendzyk (27) describes a comparative study of the circumferential residual stresses produced in rolling-mill rolls built up by the electroslag and the submerged-arc deposition processes. In each case the grades of the deposited and original steels were identical. Results indicated that the arc-deposited metal contained tensile residual stresses, while the electroslag-deposited metal contained compressive stresses.

A disadvantage of the Sachs method is that the specimen must be destroyed to obtain the necessary experimental data. Dekhtyar, Temrin and Petrov (28) have overcome this problem in the case of built-up cylinders by monitoring the surface strains during metal deposition. With the assumption that the built-up cylinder is isotropic, the technique is equivalent to the Sachs method in reverse, and a careful choice of strain-variables and sign convention produces equations which are identical in form to equations 1.01 and 1.02.

In the case of external deposition up to radius k

on a cylinder with initial radii a and b (fig.6), the values of the strain parameters $\mathcal{L}_{ap}$ and $\mathscr{l}_{ap}$ are determined from strain measurements at the bore. If the strain-variables $(\mathcal{L}_{ap} - \mathcal{L}_{ak})$ and $(\mathscr{l}_{ap} - \mathscr{l}_{ak})$, where $\mathcal{L}_{ak}$ and $\mathscr{l}_{ak}$ represent the values of $\mathcal{L}_{ap}$ and $\mathscr{l}_{ap}$ on addition of the final layer, are chosen, and the sign convention; $\Delta\rho$ negative for increasing ρ, is adopted, the residual stresses in the deposited metal may be determined from the equations:

$$\sigma_L = E'\left[(f-f_a)\frac{d}{df}(\mathcal{L}_{ap}-\mathcal{L}_{ak}) - (\mathcal{L}_{ap}-\mathcal{L}_{ak})\right]$$

$$\sigma_C = E'\left[(f-f_a)\frac{d}{df}(\mathscr{l}_{ap}-\mathscr{l}_{ak}) - \left(\frac{f+f_a}{2f}\right)(\mathscr{l}_{ap}-\mathscr{l}_{ak})\right]$$

$$\sigma_R = -E'\left[\left(\frac{f-f_a}{2f}\right)(\mathscr{l}_{ap}-\mathscr{l}_{ak})\right] \qquad \text{-------1.19.}$$

which are identical in form to the original Sachs equations for external layer removal.

In the case of internal deposition down to radius k (fig.7), $(\mathcal{L}_{bp} - \mathcal{L}_{bk})$ and $(\mathscr{l}_{bp} - \mathscr{l}_{bk})$ are determined at the outer surface. With the sign convention $\Delta\rho$ negative for decreasing ρ, the residual stresses may be determined from the equations:

$$\sigma_L = E'\left[(f_b-f)\frac{d}{df}(\mathcal{L}_{bp}-\mathcal{L}_{bk}) - (\mathcal{L}_{bp}-\mathcal{L}_{bk})\right]$$

$$\sigma_C = E'\left[(f_b-f)\frac{d}{df}(\mathscr{l}_{bp}-\mathscr{l}_{bk}) - \left(\frac{f_b+f}{2f}\right)(\mathscr{l}_{bp}-\mathscr{l}_{bk})\right]$$

$$\sigma_R = E'\left[\left(\frac{f_b-f}{2f}\right)(\mathscr{l}_{bp}-\mathscr{l}_{bk})\right] \qquad \text{-------1.20.}$$

which have the same form as the Sachs equations for internal layer removal.

The residual stresses in deposited coatings are generally always of the same sign (33), so that as deposition proceeds, balancing reactive stresses build up in the original cylinder. In the longitudinal direction, either uniform tensile or uniform compressive stress is produced, while in the circumferential and radial directions, uniform pressure stresses are established.

In an earlier paper (29) Dekhtyar, Andreichuk and Beznosov, considered the possibility of determining longitudinal residual stress in the case where the coating and the original cylinder had different elastic moduli. The method developed was, however, limited in application to long cylinders and rods of small cross-sectional area, since the effect of circumferential and radial residual stresses on the calculation, was not considered.

The complete solution to the problem of determining triaxial residual stresses in bimetallic cylinders was finally obtained by Dekhtyar (30), using a layer-removal approach.

The method is based on the assumptions that the residual stresses are axisymmetric, that the interface between the dissimilar metals is clearly defined, and that no axial slippage or radial separation of the two

parts can occur. In view of the complexity of the final equations, the following general parameters are defined for the cylinder of fig.8 :

$$\begin{aligned} A &= (1-\mu_1)k^2 + (1+\mu_1)a^2 \\ B &= (1-\mu_2)k^2 + (1+\mu_2)b^2 \\ C &= E_2(b^2-k^2) \\ D &= E_1(k^2-a^2) \end{aligned} \qquad \text{---------- 1.21.}$$

In the case of internal layer removal (fig.9) a . is replaced by the general radius ρ , so that the parameters A and D become $A(\rho)$ and $D(\rho)$. With $\Delta\rho$ positive for increasing ρ the residual stresses up to the interface (i.e. for $a \leq \rho < k$), may be determined from the equations:

$$\sigma_L = \frac{1}{2\rho}\left[\frac{C}{1-\mu_2^2} + \frac{D(\rho)}{1-\mu_1^2}\right]\left(\frac{d\ell}{d\rho}\right)_{b\rho} - \frac{E_1}{1-\mu_1^2}\cdot\ell_{b\rho}$$

$$\sigma_C = \frac{1}{1-\mu_2^2}\left\{\left[\frac{A(\rho).C + B.D(\rho)}{4k^2.\rho}\right]\left(\frac{d\ell_\theta}{d\rho}\right)_{b\rho} - \left[\frac{A(\rho).C + B.D(\rho)}{4k^2.\rho^2} - \frac{(1+\mu_1).C - E_1.B}{2k^2}\right].\ell_{\theta\, b\rho}\right\}$$

$$\sigma_R = \frac{1}{1-\mu_2^2}\cdot\frac{A(\rho).C + B.D(\rho)}{4k^2.\rho^2}\cdot\ell_{\theta\, b\rho} \qquad \text{---------- 1.22.}$$

Beyond the interface (i.e. for $k < \rho < b$), σ_L , σ_C and σ_R may be determined from equations 1.01 ,

with E and μ replaced by E_2 and μ_2. Abrupt changes in gradient of the experimental plots of $\varepsilon_{b\rho}$ and $\theta_{b\rho}$ may be expected as a result of the discontinuity at $\rho = k$.

In the case of external layer removal (fig.10) b is replaced by ρ in equations 1.21, so that B and C become $B(\rho)$ and $C(\rho)$. With $\Delta\rho$ positive for decreasing ρ the residual stresses down to the interface (i.e. for $k < \rho \leq b$) may be determined from:

$$\sigma_L = \frac{1}{2\rho}\left[\frac{C(\rho)}{1-\mu_2^2} + \frac{D}{1-\mu_1^2}\right]\left(\frac{d\varepsilon}{d\rho}\right)_{a\rho} - \frac{E_2}{1-\mu_2^2}\cdot\varepsilon_{a\rho}$$

$$\sigma_C = \frac{1}{1-\mu_1^2}\left\{\left[\frac{A.C(\rho)+B(\rho).D}{4k^2\rho}\right]\left(\frac{d\theta}{d\rho}\right)_{a\rho} - \left[\frac{(1+\mu_2)D + E_2.A}{2k^2} - \frac{A.C(\rho)+B(\rho).D}{4k^2\rho^2}\right].\theta_{a\rho}\right\}$$

$$\sigma_R = -\frac{1}{1-\mu_1^2}\cdot\frac{A.C(\rho)+B(\rho).D}{4k^2\rho^2}\cdot\theta_{a\rho} \qquad \text{--------- 1.23.}$$

Beyond the interface (i.e. for $a < \rho < k$), equations 1.02 with E and μ replaced by E_1 and μ_1 should be used.

The method is of considerable practical importance, and may be applied, for example, to bushings, to lined bearings and to cylinders built up by various processes such as filling, metallization, electrolysis and welding.

Recently the method has been generalised to n layers by Deev (31), to make possible the determination of triaxial residual stresses in multi-layer components. The final equations, which are identical in form to equations 1.22 and 1.23, are omitted here, for the sake of brevity.

Typical examples of multi-layer bodies are; high-frequency induction hardened shafts and axles, built-up cylinders with corrosion-resistant or wear-resistant coatings, and tree-trunks, when the presence of annual-rings is considered.

Deev describes an experimental investigation of the residual stresses in 53mm diameter built-up cylinders manufactured from steel by automatic welding. Examination of the specimens indicated that three distinct layers existed; the welded layer, the heat-affected zone, and the base material.

In all the investigations discussed so far, the distribution of the stresses σ_L , σ_C and σ_R has been assumed to be axisymmetric. Lambert (32) has extended the Sachs technique so that antisymmetric longitudinal residual stresses in round bars (produced by plastic bending) can be determined. The method is based on the assumption that the relief of the longitudinal stresses $\sigma_L(y)$ (fig.11), which are antisymmetric ($|\sigma_L(y)| = |\sigma_L(-y)|$), by boring-out, produces simple bending of the remaining bar.

If the antisymmetrical longitudinal strain at distance k from the nuetral axis ($y = 0$) is $\overset{*}{\varepsilon}_L$ then:

$$\frac{EI}{k} \cdot \overset{*}{\varepsilon}_L = 4\int_0^{\rho} \sigma_L(y) \cdot y(\rho^2 - y^2)^{1/2} \cdot dy \qquad \text{-----1.24.}$$

where $I = \frac{\pi}{4}(b^4 - \rho^4)$ is the second moment of area of the bored-out cross-section.

Equation 1.24 is a Volterra integral equation of the first kind, and is best solved (32) by a finite difference approach.

The method is limited to long solid bars or long thick-walled cylinders to which the simple bending assumption might be expected to apply. It may, however, be used in the presence of axisymmetric triaxial stresses since the antisymmetrical longitudinal strain $\overset{*}{\varepsilon}_L$ may be easily distinguished.

1.03. RESIDUAL STRESSES IN THIN-WALLED TUBING.

The residual stresses in thin-walled cylinders or tubing have been the subject of many investigations. Although some studies of quenching and machining stresses have been carried out (35,64), most interest has been centred on drawn tubing and the effect of the various drawing variables on the final residual stress distribution (36-40,82,87).

It is generally recognized that the longitudinal and circumferential residual stresses in hollow-drawn or sunk tubing vary in an approximately linear manner from high compressive stresses at the bore, to high tensile stresses near the outer surface, with a rapid stress reversal frequently evident in the outermost layers where the material has been almost in contact with the drawing-die. Loxley (87) obtained results which suggested that these surface stresses in mild steel tubes were affected by friction and could be reduced by the use of an efficient drawing lubricant.

In the case of plug-drawn tubing, overall stress levels tend to be lower (36,37,82) and more variation in the form of the stress distribution has been observed. If the process is carried out with little reduction in wall thickness the stress distributions which result, tend to be similar to those in sunk tubing (37,82).

The mechanism by which residual stresses are produced during tube-drawing is well known, and is best explained (37), by considering that the tubing is composed of a large number of concentric, perfectly smooth, elemental layers of equal thickness. The maintenance of dimensional compatibility during reduction, results in the occurrence of plastic deformation of varying severity in adjacent layers, and the final residual stress pattern is established by elastic relaxation on emergence from the die.

In the particular case of sunk tubing (fig.12), the drawing (longitudinal) stress for the layer 1. is small while the compressive circumferential stress is near the yield value (37). As a result, the longitudinal strain is small, and the constant volume requirement during drawing is met primarily by wall thickening. Since:

$$\frac{D_o - 2h_1}{D_o' - 2h_1'} > \frac{D_o}{D_o'}$$

the percentage reduction for layer 2. is greater than that for layer 1. A higher drawing stress is therefore required, and consequently a greater elongation results. Layer 2. must therefore be forcibly shortened to fulfil the condition of dimensional compatibility at the interface. As a result, a residual longitudinal tension is induced in the first layer. Repetition of this reasoning with layers 3,4,etc., leads to a longitudinal residual stress distribution which varies from tensile at the outer surface to compressive at the inner surface. The circumferential and radial residual stresses develop in a similar manner. The forcible longitudinal shortening of layer 2. with respect to layer 1. causes it to expand circumferentially and radially, so that a residual circumferential tension is established in the first layer, and a residual circumferential compression is established in the second. Repetition of this reasoning with layers 3,4,etc., again results in tensile residual stress at the outer surface and compressive residual stress at the bore. The tendency of each layer to expand radially is accounted for partially by wall

thickening, and partially by the development of a radial residual stress distribution which is entirely compressive except for the zero surface values.

In the case of plug or mandrel drawn tubing, the presence of the plug or mandrel prevents wall thickening, and friction at the various interfaces has a significant effect on the relative elongation of adjacent layers. Since the frictional resistance at the plug or mandrel is generally higher than at the more easily lubricated die, the outer layers tend to be deformed more than the inner, and a reversed residual stress pattern can result (37,36).

Knights (82) found that one of the most important variables in determining the magnitude of residual stresses in steel tubes was the ratio of sink to draft (or the proportion of the reduction of area achieved by diametral reduction to that obtained by reduction in thickness). This was subsequently confirmed in the case of the circumferential stresses in 70/30 brass tubing by Meadows (36) who showed that the maximum observed tensile residual stress in both sunk and plug-drawn tubing was related to the strain disparity (= % reduction in bore - % reduction in outside diameter).

In contrast to Loxley's findings, Meadows found that lubrication, by lowering the emergent surface temperature of the tubing, tended to produce higher overall stress levels than were produced by dry-drawing.

Misra and Polakowski (37) have recently described the results of a comprehensive study of the various tube-drawing processes, with a view to the in-process manipulation of stress levels. Plug-drawing, mandrel-drawing and sinking were the main subjects studied, but the effects of reeling and rock-rolling were also investigated to a limited extent. The materials used were 304 and 321 stainless steel, Incoloy 800 and cold-drawn copper. Overall stress levels were found to be significantly lower in plug-drawn tubing than in sunk tubing, with intermediate stress levels produced by rock-rolling. Drastic reductions in the stress levels in mandrel-drawn tubing were effected by tandem drawing using a second, low-reduction (2%) or skin-pass die, with a 1^{o} taper. In the case of plug-drawn tubing, tandem drawing was found to reduce the average stress levels and reverse the sign of normally tensile surface stresses, but in the case of sunk tubing, tandem drawing had little beneficial effect, and high stresses were always observed.

The recent papers by Buhler et.al. (38-40) report the effects of plug-drawing, sinking and expanding on the residual stresses in tubing produced from a variety of steels including 9SMn28, 9SMnPb28 and 9CrMo9 10, and discuss the possibility of calculating the stress levels with the aid of dimensionless parameters.

Despite the large amount of information available about the effects of altering the conditions of manufacture on the final residual stress distribution in

drawn tubing, there are certain aspects of the actual process of residual stress determination in such tubing, which have received little attention.

In all the above investigations, either the Sachs or the Davidenkov technique was used for the analysis of experimental data. In almost every case the following assumptions were accepted without question; that the tube material was isotropic, that the inner and outer surfaces were concentric, and that the residual stresses were distributed axisymmetrically.

The possibility that directional variation of the elastic properties might occur in tubing drawn with large reductions does not appear to have been considered in the literature, and only Knights (82) has questioned the assumptions about concentricity and axial symmetry.

Since the modified Sachs equations 1.17 and 1.18 may be used at any stage to correct strain data obtained from tubing previously thought to be isotropic, for the effects of anisotropy, an investigation of this point was not thought to be worthwhile. Information on experimental methods of determining the elastic constants in orthotropic cylinders can be found in ref.26.

Although it has long been recognized that tubing drawn under commercial conditions almost always exhibits some degree of eccentricity (the normal commercial tolerance for wall thickness variation in drawn tubing is $\pm 10\%$),

only Knights (82) has considered the possible effect of such eccentricity on the determination of residual stresses.

The most interesting features of Knights's work on eccentricity are discussed in a later section. It is sufficient for the purposes of the present section to reproduce his conclusion - that the effect of eccentricity on the bending deflection method of residual stress determination could be neglected in tubing with an initial wall thickness variation of less than $\pm 5\%$, provided the common practice of etching one specimen from the outside and one specimen from the inside was adopted.

Knights also considered the possibility that significant circumferential variation of the residual stresses might occur in drawn tubing, and suggested that the occurrence of plastic bending at entry and exit from the drawing-die might result in an overall longitudinal residual stress distribution similar to the familiar pattern shown in fig.13 . He was, however, unable to obtain experimental evidence which confirmed the existence of such a stress distribution.

In view of Knights's results using bending deflection methods, it was felt that an investigation of the effect of eccentricity on the determination of residual stress in drawn tubing by the Sachs method, and a detailed examination of the circumferential variation of the deformations produced on cutting specimens to length

and on layer removal, might yield some interesting results.

1.04. OBJECTIVES OF THE PRESENT WORK.

(a) The development of experimental techniques for cutting thin-walled tubing to length and for layer removal.

(b) The development of a technique for the detection and measurement of small longitudinal and circumferential variations in the effects of cutting-out and layer removal.

(c) A theoretical investigation of the effect of eccentricity on the determination of residual stress by the Sachs method.

(d) An experimental investigation of the effect of eccentricity on the determination of residual stress in drawn tubing by the Sachs method.

(e) An experimental investigation of the longitudinal and circumferential variation of the deformations produced on cutting drawn tubing to length.

(f) A critical evaluation of the bending deflection method in the presence of eccentricity.

(g) An examination of possible alternatives to the conventional Sachs and Davidenkov techniques, in the presence of eccentricity.

The tubing used in the experimental work was manufactured by Yorkshire Imperial Metals from de-oxidised non-arsenical copper, by the following production schedule:

3" round billets, pierced to 3.5" bore,
drawn 'hard' two passes,
annealed at about 650°C,
drawn 'hard' two passes to 2"I.D., 2.125"O.D.

The metric equivalents of the above final sizes give: a = 25.40mm, b = 26.99mm, R_m = 26.20mm and a/b = 0.941.

SECTION 2.

APPARATUS AND EXPERIMENTAL TECHNIQUES.

2.01. INTRODUCTION.

It is the purpose of this section to provide a general description of the various experimental techniques and items of apparatus used in conducting the investigation outlined in section 1.04. More detailed information on particular aspects of individual experiments will be found in sections 4 and 5.

It is convenient to divide the section into three parts; the first part dealing with the process of cutting specimens, the second with the process of layer removal, and the third with the process of strain measurement.

2.02. SPECIMEN CUTTING.

In order to carry out the investigation of specimen length described in section 4 it was necessary to devise a suitable technique for cutting the thin-walled copper tubing ($\frac{a}{b}$ = 0.941) to length. Although this operation could easily have been performed on a lathe it was felt that the degree of clamping necessary to hold the specimen might introduce unwanted stresses (72). In order to avoid clamping difficulties, the possibility of using acid-etching was considered. This method had been used successfully by Loxley (80,81) but proved to be extremely laborious, especially since an even finish on the end-face was required on all specimens. The possibility of using an ordinary (?) a standard hacksaw was also

considered, but rejected, since it seemed desirable at that point to avoid performing any operations on the tubing which were asymmetrical.

The apparatus shown in fig.14 was devised to rotate the tubing against a high-speed screw-slotting cutter. In this way, the cut took the form of a narrow (0.25mm) groove which could be gradually deepened by turning the hand-wheel H. The speeds of the tube and the contra-rotating cutter were 20 r.p.m. and 1500 r.p.m. respectively, and a plentiful supply of 'Rapid-Tap' fluid was used as coolant. The final drive to the rotating tubing was accomplished by means of the specially adapted gear-wheel shown in fig.15 , and power was transmitted to the cutter by means of a flexible shaft. Since the torque required to rotate the tubing against the cutter was relatively small, only light clamping by means of the socket screws was necessary. The tubing was supported in four bearings (fig.16) which could be moved longitudinally and locked in any desired position. Each was equipped with spring-loaded rollers and a removable top half, which was also spring-loaded. Lateral movement of the tubing during cutting was prevented by using two of the adapted gear-wheels back-to-back against the bearings, with large nylon disc-washers interposed to reduce friction. The apparatus was powered by a 0.17 h.p. electric motor with reduction gearing to the tubing and a direct drive to the cutter. With this arrangement each cut on tubing with a/b = 0.941 and R_m = 26.20mm took about four minutes to complete. Any attempt to

reduce this time tended to cause excessive vibration because of the coupling between tube and cutter.

2.03. LAYER REMOVAL.

An excellent summary of the various techniques available for layer removal can be found in Denton's review (72).

Acid-etching was chosen for the present work since it was known (80,81,88) to be an almost stress-free method of layer removal, and also since its use would avoid all difficulty over clamping the thin-walled copper specimens. A further advantage, discovered in the course of the experimental work, was that layer removal could be continued down to wall thicknesses of 0.01mm .

The main difficulties with acid-etching are in the achievement of a uniform rate of dissolution all over the exposed surface, and in the prevention of unwanted corrosion.

Preliminary experiments with copper specimens suspended vertically in beakers of acid indicated that the reaction rate increased with depth within the acid, and therefore that the best method of achieving uniformity of layer removal was to rotate the specimen about a horizontal axis while etching was in progress.

The most suitable rate of dissolution was achieved with 50% nitric acid at a temperature between 30-35°C. It was therefore necessary to find a stopping-off compound which would adhere to copper and resist this solution. The proprietary stopping-off waxes favoured by previous investigators (80-82,88) were felt to be unsuitable on account of their low melting-point (37°C). The compound finally selected was the I.C.I. silicone rubber 'Silicoset 100'. This proved to be completely unaffected by prolonged exposure to the etchant, and bonded strongly to the copper specimens when used in conjunction with the appropriate I.C.I. primer.

A three-quarter sectional elevation of the acid bath developed for layer removal is shown in fig.17 . Apart from the stopcock and the heating tubes which were glass, the entire apparatus was constructed from perspex. Power was transmitted from a slow-speed motor/gearbox outside the bath (fig.18) to the spindle, on which a specimen would normally be mounted, by means of the perspex gear-wheels. The spindle (fig.19) was mounted on two split bearings 305mm apart, and could be removed and replaced easily. Although similar in certain respects to an apparatus used by Botros (48) for etching steel cylinders, this arrangement had in fact been constructed before Botros's paper was obtained.

The motor/gearbox output speed was 1 r.p.m. with the direction of rotation automatically reversed every half-revolution, by the mechanism shown in figs.18,20,21 .

With a 1:2 step-up gear ratio the spindle revolved at 2 r.p.m. and was reversed every revolution, this being necessary to avoid winding the strain gauge leads into the acid bath. The reversing mechanism, which consisted of two microswitches back-to-back and wired as shown in fig.21 , was operated by the rotating arm on the motor shaft coming into contact with the vertical trigger-pin. The movable arms were held in contact with adjusting screws by the spring-loaded microswitch buttons B, and when properly adjusted, a small lateral movement of the trigger-pin was sufficient to reverse the direction of rotation of the motor.

In view of the known toxicity of mixtures of oxides of nitrogen (brief exposure to 200 p.p.m. can be fatal), an outlet was provided from the acid bath to a fume cupboard extractor through flexible plastic piping. This proved to be an extremely effective method of containing the toxic fumes; the partial vacuum maintained in the apparatus when the cover plate was in position on the observation hole, was so large that the bath lid could not be removed.

Acid was supplied and extracted through the glass stopcock by means of the arrangement shown in fig.22 ; by using either the compressed-air supply, or the suction provided by a tap-mounted air ejector, it was possible to fill or drain the acid bath rapidly. The capacity of the carboy when two-thirds full was 20 litres and that of the acid bath when filled to the 150mm level, about 18 litres.

The acid was stored permanently in the carboy when not in use.

The acid was heated by passing hot water through twenty-two, 5mm bore glass heating tubes, which were arranged along the bottom of the acid bath, as shown in fig.23 . These were sealed on the outside of the bath with 'Araldite' and on the inside by a solution of perspex in chloroform (which proved to be ideal for all sealing purposes within the bath). A continuous circulation of hot water at 45°C was maintained by the apparatus shown in fig.24 , which consisted of two 1kW thermostatically-controlled bath heaters arranged in parallel, and a by-pass valve. The capacity of the system was approximately 28 litres, with small additions being necessary from time to time to replace evaporative losses. With this arrangement, 18 litres of acid could be heated from 12-31°C in twenty-five minutes.

The general arrangement of the whole apparatus is shown in fig.25 . An auxiliary fume extractor pipe was suspended near the acid bath since it was occasionally necessary to remove the bath lid while etching was in progress. A levelling platform for the acid bath was also provided.

For reasons which will be discussed in section 2.04, it was necessary to remove the specimens from the acid bath to measure the strains produced by layer removal. To facilitate this process, each specimen was mounted in a

sealed unit which was easily removable from the spindle.

In the case of internal layer removal, the first stage in the construction of the sealed unit was to mount a perspex disc or end-ring at each end of the specimen. After priming the surfaces indicated in fig.26a , the the specimen and end-ring were placed in their correct relative positions on a polythene sheet which had been lightly smeared with 'Durofix' to provide a temporary seal. Using a small syringe, the 9.5mm-wide annular space so formed, was filled with overthinned 'Silicoset 100' solution (obtained by mixing 6ml of 'Silicoset 100' with an equal volume of the I.C.I. thinning fluid F111/500 and adding one drop of curing agent 'A'). After curing was complete (overnight at room temperature) the polythene sheet was easily peeled off, leaving an acid resistant joint between the specimen and the end-ring which was extremely flexible (fig.36). When both end-rings had been attached in this way the sealed unit was completed by mounting the specimen inside a large perspex cylinder as shown in figs.27,28,29 . The manner in which the strain gauges were installed and protected, will be discussed in section 2.04. The completed unit was mounted on the spindle by means of two perspex supports as shown in figs.30,31 .

For the case of external layer removal, end-discs were fitted inside the specimen, as shown in fig.32 . Basically the procedure was the same as for the end-rings, except that the annular space between the end-disc and

the outer ring was filled with overthinned 'Silicoset 100' before the specimen was lowered into position. Both the outer ring and the polythene sheet were easily removed after curing, leaving the end-disc mounted as shown in fig.32c . To avoid an air-lock when fitting the second end-disc, the disc with the holes for the gauge leads was always fitted first. The completed, sealed-unit for external layer removal is shown in fig.33 . The four locating holes enabled the unit to be fitted easily onto a modified spindle, as shown in figs.34,35 .

Although, under normal circumstances, contact with the acid only occurred when inserting or removing the sealed units from the drained bath, rubber gloves were worn at all times when working with the etching apparatus. As a further precaution, several litres of dilute potassium hydroxide solution were kept nearby in case of spillage.

An investigation of the uniformity of internal layer removal from two copper specimens with a/b = 0.941, R_m = 26.20mm and ℓ = 182mm was carried out by measuring the change in wall thickness Δh at the fifty-six evenly spaced points indicated in fig.37 , after a period of acid attack. The initial wall thickness at the points 9-48 was obtained by linear interpolation between the end values on the same generator, and the change Δh was measured after cutting the specimen into seven lengths of 26mm . The wall thickness reduction was 24% in the case of the first specimen and 81% in the case of the second specimen, and there was no sign of prefer-

ential etching in either case. The Δh values were randomly distributed as shown in fig.38 . The wider scatter obtained in the case of the first specimen was almost certainly due to local inhibition of the reaction by surface dirt. In subsequent experiments the surface to be exposed to the acid was always thoroughly cleaned and degreased.

In the case of internal layer removal, the bore radius ρ , was determined using the formula:

$$\rho^2 = a^2 + \frac{W}{\pi\omega(l-l_1)} - \frac{l_1}{(l-l_1)}(b^2-a^2) \quad \text{------2.01.}$$

which follows directly from fig.39 . W represents the weight loss of the sealed unit, ω the weight density of copper and l_1 the reduction in specimen length (since the end-faces as well as the bore of the specimen were exposed to the acid).

For the case of external layer removal, the radius ρ of the outer surface after a period of acid attack was determined in a similar manner from the expression:

$$\rho^2 = b^2 - \frac{W}{\pi\omega(l-l_1)} + \frac{l_1}{(l-l_1)}(b^2-a^2) \quad \text{------2.02.}$$

which follows from fig.40 .

Both W and l_1 were measured when the sealed units were removed from the acid bath for strain measurement; W after every etch, by using a pan balance, and

l_1 less frequently, by means of a steel rule. A plot of l_1 against W obtained from a specimen with a/b = 0.941, R_m = 26.20mm and l = 208.8mm is shown in fig.41 . Intermediate values of l_1 were taken from this curve.

The accuracy of equation 2.01 was checked by using the values of W and l_1 for the two specimens concerned in the investigation of the uniformity of layer removal. In the case of the first specimen (24% wall thickness reduction) the difference between the calculated value of Δh and the mean of the measured values was 1%, and in the case of the second specimen (81% wall thickness reduction) the difference was less than 0.5% .

The feasibility of using a chemical volumetric analysis for the estimation of W was also studied. The technique examined was the iodine-thiosulphate titration method described in ref.41 . Although it was possible to estimate the copper content of a sample of to within $\pm$0.5%, it proved difficult to obtain a representative sample from the acid bath and to estimate the total volume of etchant, so that the overall accuracy was $\pm$3% .

2.04. STRAIN MEASUREMENT.

Since the proposed investigation was likely to involve the detection and measurement of small longitudinal and circumferential variations in the effects of cutting-

out and layer removal, the strain gauge method of strain measurement was chosen. Micro-Measurements series EA-09 epoxy-backed 120 ohm gauges, which were temperature-compensated for copper, were used in conjunction with a Philips P9205 portable strain recorder (repeatability $\pm 5 \times 10^{-6}$), and a Farnell 7.5 volt D.C. stabilized power supply. Gauge lengths of 6.35mm and 2.29mm (0.250" and 0.090") were chosen, the larger gauges being used mainly in preliminary experiments. A balanced half-bridge circuit using a common dummy was employed for all strain measurements.

Preliminary experiments were conducted to examine the feasibility of continuously monitoring the surface strain while layer removal was in progress. These experiments were carried out in conjunction with the examination of the volumetric method for estimating W and it was hoped that a rapid method of determining residual stress could be developed by combining the two techniques. Unfortunately the heat of reaction liberated as the copper dissolved made it impossible to equalize the temperature of the test and dummy specimens, although both were submerged in the same solution, and no useful results were obtained.

Since stability of the gauge zeros was of prime importance, a discontinuous technique was adopted, and, as mentioned in section 2.03, the specimens were mounted in easily removable, sealed units which were washed and dried before the strains produced by layer removal were

measured. As an additional precaution against zero drift due to changes in ambient conditions, a constant temperature chamber was constructed in which the dummy specimen remained permanently, and to which the test specimens were returned after each etch.

A disadvantage of the discontinuous strain measuring circuit is that some means must be found of disconnecting and reconnecting the active gauges without introducing resistance variations. The figures recently quoted by Peekel (42) illustrate the magnitude of the problem; for a balanced circuit using 120 ohm gauges with gauge factor 2, a change in resistance of 0.00024 ohm is equivalent to 1 microstrain. Denton (72) quotes an example where silver-plated brass plugs gave a repeatability better than $\pm$1 microstrain, while Knights (82) elected to solder and resolder the connections every time. Lynch (69) describes a method for immersing the leads in small pots of mercury, but gives no figures for repeatability. The technique used in the present work was to solder a spade connector on the end of each gauge lead, as shown in fig.42 , and to make the connection to the bridge circuit by means of screw-down terminals. Since only three such terminals were provided on the strain recorder, the small terminal box shown in fig.44 was constructed to enable the test specimen to be removed or replaced without disturbing the connections to the dummy. By degreasing each spade terminal before every measurement, a repeatability better than $\pm$2 microstrain was obtained. The arrangement shown in fig.45 was used to minimise the possibility of

corrosion of the spade terminals by stray fumes or accidental spillage while etching was in progress.

The adhesive used for all strain gauge installations was a liquid hardener/liquid resin of the 'Araldite' range, formulated to be dimensionally stable over long periods. This required 2-4 hours to set, and an overnight cure during which, externally-mounted gauges were held in position by a rubber pad and 'Sellotape', and internally-mounted gauges by a small clamp specially designed for the purpose. All gauge leads were P.V.C.-covered 7/0.1mm, and a thin layer of overthinned 'Silicoset 100' was used to protect the gauges and their soldered connections against humidity or accidental corrosion.

In the investigations described in section 4 , all the gauges were mounted, wired-up and protected before the specimens were cut from the parent tubing. During cutting, which was performed with the apparatus described in section 2.02 , the gauge leads and spade connectors were wrapped round the outside of the tubing and covered with polythene sheeting and P.V.C. tape. Once the specimens (1A-1,1A-2,2A-1 and 3A-1 in figs.63,64,65) had been freed, it was necessary to cut the gauge leads in order to construct the sealed units for internal layer removal. The manner in which the leads were rejoined and the join protected is illustrated in fig.43 . The sections of the gauge leads exposed to the etchant were additionally protected by 1mm bore P.V.C. sleeving, and the sealing at the end-ring was 'Araldite'.

In the case of external layer removal (specimen 2B-1 in fig.61c) it was necessary to cut the specimen to length before the strain gauges could be mounted.

Three sectional views of the constant temperature chamber are shown in figs.46,47,48 . The innermost tank was constructed from 2.5mm brass, and the walls, roof and floor of the controlled air space from 1mm brass. The capacity of the water jacket was 56 litres, with the temperature controlled by a sensitive 1kW heater/stirrer unit. A small propellor assisted air circulation within the controlled space.

The most effective control was achieved with the apparatus set about 15°C above room temperature; fig.49 shows the frequency distribution of 302 measurements of chamber temperature taken over a period of two weeks at a nominal setting of 33°C.

The general arrangement of the strain measuring circuit is shown schematically in fig.50 . Although errors can occur with this type of circuit if the active and dummy gauge leads differ in length (42) these were effectively eliminated by using the constant temperature chamber.

Recently (43) some doubts have arisen about the stability of Micro-Measurements series EA epoxy-backed strain gauges. It should therefore be pointed out that all gauge installations used in the present investigation

were zero-checked over a length of time at least equal to the expected test duration, and the maximum observed drift was less than 10 microstrain.

SECTION 3.

THE EFFECT OF ECCENTRICITY ON THE DETERMINATION OF RESIDUAL STRESS BY THE SACHS METHOD.

3.01. THE ECCENTRIC CYLINDER.

The cross-section of an eccentric cylinder or tube may be represented, as shown in fig.51 , by the area between two non-concentric circles radius a and b (a less than b), where the centre distance c does not exceed the difference of the radii.

The eccentricity of the cross-section, denoted by e , is defined by the equation:

$$e = \frac{c}{b-a} \qquad \text{---------} \quad 3.01.$$

from which it follows that e varies from zero to one as c changes from zero to $b-a$.

Expressed as a percentage, e represents the maximum deviation of the wall thickness from the mean value $b-a$. The normal commercial tolerance for wall thickness variation in drawn tubing (section 1.03) may therefore be expressed: $e < 0.10$.

The removal of uniform layers from either (or both) surfaces of an eccentric tube does not change the centre distance, but increases the eccentricity. If the internal radius increases from a to ρ then:

$$e(\rho) = \frac{c}{b-\rho} \qquad \text{----------} \quad 3.02.$$

or in the case of layer removal from the outer surface:

$$e(\rho) = \frac{c}{\rho - a} \qquad \text{---------- 3.03.}$$

In a uniform tube, the wall thickness h, defined as the distance between two parallel tangents, is easily measured by a standard tube micrometer. In the eccentric tube, where the axes of the two cylinders which form the inner and outer surfaces do not coincide, the precise definition and measurement of the wall thickness h_θ is not so straightforward (82). If the angular position of the point P in fig.52 is defined by the angle θ from maximum wall thickness, then h_θ must be defined as the distance PQ. Since the tangents at P and Q are not parallel, it is clearly difficult, if not impossible, to ensure that the hemispherical anvil of the tube micrometer makes contact with the inner surface exactly at the position Q. If, however, c is small compared to a and b, the error produced by this tendency of the inner anvil to 'wander', will be small, and may be neglected.

It may easily be shown from fig.52 that:

$$h_\theta = b - \left[(a^2 - c^2\sin^2\theta)^{1/2} - c\cos\theta\right]$$

and if c^2 is very much less than a^2:

$$\begin{aligned} h_\theta &= b - a + c.\cos\theta \\ &= (b-a)(1 + e.\cos\theta) \\ &= h_m(1 + e.\cos\theta) \end{aligned} \qquad \text{-------- 3.04.}$$

and if the internal radius is increased from a to ρ then:

$$h_\theta = (b-\rho)[1 + e(\rho).\cos\theta]$$
$$= h_m[1 + e(\rho).\cos\theta] \qquad \text{-------3.05.}$$

3.02. THE ECCENTRIC CYLINDER UNDER UNIFORM INTERNAL AND EXTERNAL PRESSURE.

The theoretical investigation described in this section was carried out to assess the effect of the increase in eccentricity which occurs on layer removal, on the determination of σ_c and σ_R by the Sachs method.

Whereas the analysis of the radial deformations produced in a uniform cylinder by internal or external pressure represents a relatively simple problem in polar co-ordinates, the solution in the case of the pressurised eccentric cylinder requires the use of the bipolar co-ordinate system (44,46,47), which is a system of curvilinear co-ordinates derived from the bilinear transformation or mapping:

$$\zeta = \log \frac{z+i.k}{z-i.k} \qquad \text{-------3.06.}$$

where $z = x + i.y$, and k is a positive real length.

If:

$$\frac{1}{\zeta} = \alpha + i.\beta$$

$$z + i.k = z_1 = r_1.\exp(i\phi_1)$$

$$z - i.k = z_2 = r_2.\exp(i\phi_2)$$

then:

$$\alpha + i\beta = \log \frac{z_1}{z_2} = \log \frac{r_1}{r_2}.\exp[i(\phi_1 - \phi_2)]$$

and using the property of the logarithmic function that:

$$\log w = \log|w| + i.\arg.w$$

it follows that:

$$\alpha + i\beta = \log \frac{r_1}{r_2} + i(\phi_1 - \phi_2) \qquad \text{--------3.07.}$$

so that:

$$\alpha = \log \frac{r_1}{r_2}$$

$$\beta = \phi_1 - \phi_2 \qquad \text{----------3.08.}$$

The general scheme of the co-ordinates in the complex z -plane is shown in fig.53 , which has been adapted from an illustration in ref.44 . The distances r_1 and r_2 provide a means of fixing the point P relative to the two origins O and O' (47). It may be shown by expressing α and β in terms of the Cartesian co-ordinates x and y that the curves in the z - plane corresponding to α = constant are a set of co-axial non-concentric circles having O and O' for limiting points (fig.54), and that the curves corresponding to

β = constant are circles passing through O and O', cutting the first set of circles orthogonally.

By limiting α to positive values in the range $\alpha_a \leqslant \alpha \leqslant \alpha_b$ it is possible to define the cross-section of an eccentric cylinder.

Both Jeffrey (44), using classical elasticity theory, and Stevenson (46), using complex potential theory, have obtained solutions in bipolar co-ordinates for the surface stresses and displacements in the pressurised eccentric cylinder.

It may be shown (44) for the cylinder of fig.55 that the circumferential surface stresses at the points Q and P are given respectively by the expressions:

$$\sigma_c(\beta)_a = -p_a + 4(p_a - p_b)(\cosh\alpha_a - \cos\beta_a)H\left[\sinh(\alpha_a - \alpha_b)\cos\beta_a + \sinh\alpha_a \cdot \cosh(\alpha_a - \alpha_b)\right] \quad \text{-------- 3.09.}$$

$$\sigma_c(\beta)_b = -p_b - 4(p_a - p_b)(\cosh\alpha_b - \cos\beta_b)H\left[\sinh(\alpha_a - \alpha_b)\cos\beta_b - \sinh\alpha_b \cdot \cosh(\alpha_a - \alpha_b)\right] \quad \text{--------- 3.10.}$$

where: $$H = \frac{\operatorname{cosech}(\alpha_a - \alpha_b)}{2(\sinh^2\alpha_a + \sinh^2\alpha_b)}$$

By putting p_b or p_a equal to zero in turn,

the effect of internal or external pressure, acting alone, may be examined. With $p_b = 0$, equations 3.09 and 3.10 reduce to:

$$\sigma_c(\beta)_a = -p_a + 4p_a(\cosh\alpha_a - \cos\beta_a)H[\sinh(\alpha_a-\alpha_b)\cos\beta_a + \sinh\alpha_a.\cosh(\alpha_a-\alpha_b)] \quad \text{-----3.11.}$$

$$\sigma_c(\beta)_b = -4p_a(\cosh\alpha_b - \cos\beta_b)H[\sinh(\alpha_a-\alpha_b)\cos\beta_b - \sinh\alpha_b.\cosh(\alpha_a-\alpha_b)] \quad \text{------3.12.}$$

If a and b denote the radii of the curves α_a and α_b, and c denotes the distance between their centres, then it may be shown (44) that:

$$\sigma_c(\beta)_a = -p_a + \frac{2p_a b^2[(b^2-c^2)^2 - a^2(a+2c.\cos\beta_a)^2]}{(b^2+a^2)[b^2-(a+c)^2][b^2-(a-c)^2]} \quad \text{--------3.13.}$$

$$\sigma_c(\beta)_b = \frac{2p_a a^2[b^2(b-2c.\cos\beta_b)^2 - (a^2-c^2)^2]}{(b^2+a^2)[b^2-(a+c)^2][b^2-(a-c)^2]} \quad \text{---------3.14.}$$

from which the distribution of the circumferential stresses on the inner and outer surfaces may be calculated, for the case of uniform internal pressure.

Coker and Filon (45) verified equations 3.13 and 3.14 experimentally by comparing measured and calculated values of $\sigma_c(\beta)_a$ and $\sigma_c(\beta)_b$ at the points D,E,F and G in fig.55, for four cases in which a, b and c

were varied over a considerable range. In all cases excellent agreement was found.

With $p_a = 0$ in equations 3.09 and 3.10 it may similarly be shown (44) that the surface circumferential stresses in the externally pressurised cylinder are:

$$\sigma_c(\beta)_a = - \frac{2p_b b^2\left[(b^2-c^2)^2 - a^2(a+2c.\cos\beta_a)^2\right]}{(b^2+a^2)\left[b^2-(a+c)^2\right]\left[b^2-(a-c)^2\right]} \quad \text{----------3.15.}$$

$$\sigma_c(\beta)_b = -p_b - \frac{2p_b a^2\left[b^2(b-2c.\cos\beta_b)^2 - (a^2-c^2)^2\right]}{(b^2+a^2)\left[b^2-(a+c)^2\right]\left[b^2-(a-c)^2\right]} \quad \text{----------3.16.}$$

In the case of the residually-stressed eccentric cylinder, equations 3.13-3.16 may be used to assess the uniformity of the stress or pressure applied by layer removal, and hence, to assess the uniformity of the stress components σ_c'' and σ_R'' (appendix 3).

If $\varepsilon\theta(\beta)_{b\rho}$ and $\varepsilon\theta(\beta)_{a\rho}$ denote the surface strain parameters for internal and external layer removal respectively, then by replacing a , (internal layer removal) or b , (external layer removal) by the general radius ρ , equations 3.14 and 3.15 may be written:

$$\sigma_c(\beta)_{b\rho} = E'.\varepsilon\theta(\beta)_{b\rho} = \frac{2p_a\rho^2\left\{b^2\left[b-2c.\cos\beta_b(\rho)\right]^2 - (\rho^2-c^2)^2\right\}}{(b^2+\rho^2)\left[b^2-(\rho+c)^2\right]\left[b^2-(\rho-c)^2\right]}$$

$$a \leq \rho < b-c \quad \text{----------3.17.}$$

$$\sigma_c(\beta)_{qp} = E'.\varepsilon_b(\beta)_{qp} = \frac{-2p_b\rho^2\left\{(\rho^2-c^2)^2 - a^2\left[a+2c.\cos\beta_a(\rho)\right]^2\right\}}{(\rho^2+a^2)\left[\rho^2-(a+c)^2\right]\left[\rho^2-(a-c)^2\right]}$$

$$a+c < \rho \leq b \qquad \text{--------3.18.}$$

So that the uniformity of the stress or pressure applied at one boundary, at each stage ρ of the layer removal process, may be investigated by comparing the measured and calculated values of $\varepsilon_b(\beta)$ at the other boundary.

From the point of view of practical strain measurement, the definition of angular position by means of β_a and β_b (fig.55) is not convenient. If θ_a and θ_b are defined as indicated, it may be shown (appendix 4) that:

$$\cos\beta_b(\rho,\theta) = \frac{2bc + \cos\theta_b\left[b^2-(\rho^2-c^2)\right]}{2bc\cos\theta_b + \left[b^2-(\rho^2-c^2)\right]} \qquad \text{-----3.19.}$$

$$\cos\beta_a(\rho,\theta) = \frac{2ac + \cos\theta_a\left[\rho^2-(a^2+c^2)\right]}{2ac\cos\theta_a + \left[\rho^2-(a^2+c^2)\right]} \qquad \text{----- 3.20.}$$

and if the dimensionless functions $F_a(\rho,\theta)$ and $F_b(\rho,\theta)$ are defined by the expressions:

$$F_a(\rho,\theta) = \frac{-2\rho^2\left\{(\rho^2-c^2)^2 - a^2\left[a+2c.\cos\beta_a(\rho,\theta)\right]^2\right\}}{(\rho^2+a^2)\left[\rho^2-(a+c)^2\right]\left[\rho^2-(a-c)^2\right]}$$

$$a+c < \rho \leq b \qquad \text{---------3.21.}$$

$$F_b(\rho,\theta) = \frac{2\rho^2\left\{b^2\left[b - 2c.\cos\beta_b(\rho,\theta)\right]^2 - (\rho^2-c^2)^2\right\}}{(b^2+\rho^2)\left[b^2-(\rho+c)^2\right]\left[b^2-(\rho-c)^2\right]}$$

$$a \leq \rho < b-c \qquad \text{---------- 3.22.}$$

then equations 3.17 and 3.18 may be written:

$$\frac{\sigma_c(\theta)_{b\rho}}{p_a} = \frac{E'.\varepsilon_\theta(\theta)_{b\rho}}{p_a} = F_b(\rho,\theta) \qquad \text{---------- 3.23.}$$

$$\frac{\sigma_c(\theta)_{a\rho}}{p_b} = \frac{E'.\varepsilon_\theta(\theta)_{a\rho}}{p_b} = F_a(\rho,\theta) \qquad \text{---------- 3.24.}$$

Given the initial dimensions a , b and c and a number of angular positions θ_b or θ_a at which the surface stress value is required, the calculation of the functions $F_b(\rho,\theta)$ or $F_a(\rho,\theta)$ is carried out in two stages, as follows:

(a) The determination of $\cos\beta_b(\rho,\theta)$ or $\cos\beta_a(\rho,\theta)$ at each position θ_b or θ_a for a range of ρ values, using equation 3.19 or 3.20 .

(b) The substitution of the values ρ , $\cos\beta_b(\rho,\theta)$ or ρ , $\cos\beta_a(\rho,\theta)$ in equation 3.22 or 3.21 .

It is convenient for the purposes of this calculation to rewrite equations 3.19-3.22 in terms of the dimensionless radii ρ/b or ρ/a . In the case of the expression for $F_b(\rho,\theta)$ this leads to:

$$F_b(\rho/b,\theta) = \frac{2\frac{\rho^2}{b^2}\left\{\left[1-2.\frac{c}{b}.\cos\beta_b(\rho/b,\theta)\right]^2-\left(\frac{\rho^2}{b^2}-\frac{c^2}{b^2}\right)^2\right\}}{\left(1+\frac{\rho^2}{b^2}\right)\left[1-\left(\frac{\rho}{b}+\frac{c}{b}\right)^2\right]\left[1-\left(\rho/b-c/b\right)^2\right]}$$

$$\frac{a}{b} \leq \frac{\rho}{b} < 1-\frac{c}{b} \qquad \text{----------3.25.}$$

An experimental investigation of the surface stress distribution produced by removal of uniform internal layers from a residually-stressed specimen with a/b = 0.941, c/b = 3.553×10^{-3} and e = 0.06 was carried out, and will be described in section 5 .

The calculation of $F_b(\rho/b,\theta)$, at each stage of the layer removal process, was a necessary preliminary to an examination of the data obtained. Since c was very much less than a or b , it was assumed during this calculation that $\theta_b = \theta_a = \theta$. Table 1 shows the values of $F_b(\rho/b,\theta)$ for a number of θ values at each of the following stages of layer removal:

ρ/b = 0.940(0.005)0.970(0.002)0.990(0.001)0.995

The mean value of $F_b(\rho/b,\theta)$ at each stage ρ/b is shown in the row marked F_m .

The angular positions θ were chosen, with the exception of θ = 90°, 180° and 270°, to correspond to the positions of circumferential strain gauges on the test specimen (table 3).

Fig.56 shows $F_b(\rho/b, \theta)$ plotted against θ for a range of ρ/b values. It is clear that the variation of the circumferential stress on the outer surface increases rapidly as ρ/b approaches the limiting value $1 - c/b$ (= 0.9965), and that the maximum value of stress always occurs at minimum wall thickness. For ρ/b = 0.940 and 0.995 the circumferential stress on the outer surface at minimum wall thickness is respectively 16 times and 688 times the applied internal pressure.

The values of $F_b(\rho/b, \theta)$ for θ = 90° and 270° are numerically equal to the ratio of the circumferential stress on the outer surface to the applied internal pressure obtained using Lame's equation for a uniform cylinder with a wall thickness equal to the mean wall thickness $b - \rho$ of the eccentric cylinder.

Table 2 was obtained by recalculating part of table 1 in the form $F_b(\rho/b, \theta) / F_m$. The additional columns for ρ/b = 0.973, 0.980 and 0.985 were obtained by linear interpolation. The significance of this table will be discussed in section 5 in relation to the measured strain distribution on the outer surface of the test specimen.

By extending the calculation of $F_b(\rho/b, \theta)$ to include ρ/b values less than 0.941, the circumferential surface stress variation produced by uniform internal pressure in thicker cylinders with the same centre distance may be investigated. It is clear from fig.56 that in cylinders with c/b less than 0.9, the inner and outer

surfaces may be regarded as concentric without significant error.

3.03. THE SACHS METHOD IN THE PRESENCE OF ECCENTRICITY.

(a) Circumferential and radial residual stresses.

Since even the application of a uniform radial stress or pressure to an eccentric cylinder will produce θ - varying circumferential stresses on both boundaries, it is clear that stress components of the type σ' (appendix 3) will vary with θ in the presence of eccentricity. It follows from the equation:

$$\sigma'' = \sigma + \sigma'$$

that the stresses relieved in all layers (with the possible exception of the first) will vary with θ , and that the effect will be cumulative as layer removal proceeds, and eccentricity increases.

Under these circumstances the determination of σ_c and σ_R represents a difficult task. The extent to which the Sachs analysis can be applied in practice is investigated in section 5 .

(b) Longitudinal residual stress.

The determination of σ_L in the presence of eccen-

tricity is complicated by the fact that longitudinal shearing actions must be considered. Since the response of a given section of the tube wall to the longitudinal forces applied by layer removal will obviously depend on the local wall thickness, it is clear that longitudinal shear stresses will develop as the variation in h_θ increases, and that the effect will be amplified by the presence of circumferential variations of σ_L .

The possibility of applying a simple modification of the Sachs analysis which takes account of wall thickness variation, but not shear stresses, is examined in section 5 .

SECTION 4.

AN INVESTIGATION OF THE EFFECT OF SPECIMEN LENGTH.

4.01. INTRODUCTION.

It is assumed in the derivation of the Sachs equations that the cylinder length is infinite. Since in any practical application of the technique a specimen of finite length must be used, it is clear that the effect of specimen length on the residual stress determination is of fundamental importance.

Since complete relief of the longitudinal residual stress σ_L must take place at the free surfaces created by cutting-out, it follows that a region of stress disturbance must exist in the vicinity of the end-faces of any cylinder of finite length. The extent of this region of stress disturbance is dependent on the character of the longitudinal residual stress distribution and, in the case of hollow cylinders, on the ratio of R_m/h .

In order to obtain an accurate estimate of the residual stress distribution in a long (infinite) cylinder from measurements made on a relatively short specimen, it is necessary that the specimen length should be sufficient to avoid overlap of the regions of stress disturbance and to provide a central region, several times the gauge length, in which no stress disturbance takes place.

Over the years, a number of investigations of the effect of specimen length have been carried out. Sachs and Espey (64) suggested that a specimen length of between two and three times the diameter was suitable.

Buhler (49) showed by some careful experiments on quenched steel cylinders that a length/diameter ratio of two would suffice in the case of solid or thick-walled ($R_m/h = 1$) cylinders, and that even shorter specimens might be used if $R_m/h = 1.5$. Botros (48) used a length/diameter ratio of two for aluminium and mild steel tubes with R_m/h in the range 5-10 , and more recently Osakada, Shiraishi and Oyane (50) used the same figure for specimens of hydrostatically-extruded copper rod.

A theoretical analysis by Kawagoe (51) indicated that a minimum length/diameter ratio between 2 and 2.25 should be used, and this figure was subsequently (52) verified experimentally for solid steel cylinders.

A recent investigation by Hanke and Tiemann (53) of the longitudinal distribution of the surface strains produced in case-hardened steel cylinders by 'end-facing' confirmed a minimum length/diameter ratio of two for solid or thick-walled ($R_m/h = 1$) cylinders. With strain gauge pairs mounted as shown in fig.57 the cylinders were progressively shortened by removal of material from end 'A' . In all cases, the measured longitudinal and circumferential strains were found to vary identically with the distance x , and the relationship:

$$\frac{\sigma_L(x)}{\sigma_{L\infty}} = 1 - \exp.(-0.235x) \qquad \text{----------4.01.}$$

where $\sigma_{L\infty}$ represented the undisturbed stress level, was found to describe the longitudinal residual stress variation in the vicinity of the end-faces. It is clear from fig.58 that the stress disturbance produced by the 'end-facing' operation rapidly decreased, and was negligible for x greater than 30mm (i.e. $x > D$ in the case of the solid cylinder, or $x > D_m$ in the case of the hollow cylinder).

4.02. THE DETERMINATION OF A SUITABLE LENGTH FOR THIN-WALLED SPECIMENS.

Since most of the available data on the effect of specimen length had been obtained from solid or thick-walled cylinders which had been quenched to obtain an axially symmetrical residual stress distribution, an investigation of the effect in the case of thin-walled drawn tubing (R_m/h = 16.5), in which circumferential and longitudinal variations of stress might be present, was carried out.

(a) Theoretical considerations.

If it is assumed, as a first approximation, that the residual stresses present in a thin-walled tube ($R_m/h > 11$) are axisymmetric and do not vary with length; the surface strains and deformations produced by a cut at right-angles to the axis of the tube may be predicted by the theory of beams on an elastic found-

ation (54,96).

It follows from the longitudinal equilibrium condition 1.07 that no direct longitudinal force, only a bending moment will be produced on making a cut at right-angles to the tube axis. If this bending moment (produced by the complete relief of the approximately linear longitudinal residual stress distribution) is denoted by M_L per unit length of circumference, and the inward radial displacement of the tube wall is denoted by w (fig.59), then it may be shown (55) that:

$$w(x) = \frac{-6M_L}{E'.h^3\beta^2}\phi(\beta x) \qquad \text{---------4.02.}$$

where: $\phi(\beta x) = (\cos\beta x - \sin\beta x)\exp.(-\beta x)$

and: $\beta^4 = \frac{3(1-\mu^2)}{R_m^2 h^2}$

It follows from axial symmetry that:

$$\varepsilon_c(x) = -\frac{w(x)}{R_m} = \frac{6M_L}{E'.R_m h^3\beta^2}\phi(\beta x) \qquad \text{-------4.03.}$$

$\phi(\beta x)$ is a rapidly damped oscillatory curve of wavelength $\frac{2\pi}{\beta}$ (fig.60).

With R_m/h = 16.5 and R_m = 26.20mm, it may be shown that β = 0.199mm^{-1}, and it is clear from fig.60 that for x greater than $\frac{2\pi}{\beta}$ (or $1.2R_m$ or 31.6mm) the disturbance produced by the cut will be negligible.

(b) Experimental investigation.

Preliminary theoretical consideration based on the assumption of complete axial symmetry and of an approximately linear longitudinal residual stress distribution, indicated that the region of disturbance produced by a cut at right-angles to the axis of a residually-stressed tube with R_m/h = 16.5 extended $0.6\,D_m$ on either side of the cut. Since this result was in agreement with the figures mentioned in section 4.01 for solid and thick-walled cylinders, it appeared that a length/diameter ratio greater than two was universally applicable.

The following experimental work was carried out on thin-walled drawn tubing to determine whether circumferential variations in the effect of cutting-out occurred.

Two 4.57m lengths of 'hard' copper tubing with a/b = 0.941 or R_m/h_m = 16.5, and R_m = 26.20mm were marked-off as shown in fig.61a . By designating one end of each length as 'end-1' and numbering each subdivision as shown, a record was kept of the position each individual specimen occupied in the parent tubing.

Three $12\,D_m$ lengths (629mm) were carefully cut from tube 'A' using a hacksaw and a plentiful supply of coolant. The clamp shown in fig.66 was adjusted until rotational movement of the tubing was just prevented. Tests indicated that this method of clamping introduced

no additional stresses.

Measurement of the circumferential variation of the wall thickness at both ends of each $12D_m$ length showed that the centre distance c (and therefore the eccentricity) changed slowly over the combined length of $36D_m$, with c = 0.098mm, 0.097mm and 0.096mm for tubes 1A, 2A and 3A respectively. No significant (?) rotation of the axis of symmetry of the cross-section was observed. Fig.62 compares the circumferential variation in wall thickness at each end of tube 3A. The angle θ was measured from maximum wall thickness in a clockwise direction, looking on end-1.

Strain gauges were applied to the outer surfaces of the three tubes at the positions shown in figs.63,64,65. The gauge positions on tube 2A were chosen so that the longitudinal distribution of the strains produced by cutting specimen 2A-1 could be examined, while those on tubes 1A and 3A enabled the investigation of the circumferential variation of the strains at the mid-sections of specimens 1A-2 and 3A-1. The angular position of each gauge on specimens 1A-2 and 3A-1 is shown in fig.67 and table 3 respectively, as before, the angle θ was measured from maximum wall thickness in a clockwise direction, looking on end-1. All the gauges on tube 2A, and the single gauge pair on specimen 1A-1 were mounted on the generator of maximum wall thickness.

The gauges were protected by applying a coating of

'Silicoset primer' followed by a thin layer of 'Silicoset 100' which had been overthinned with the silicone fluid F111/500 as described in section 2.03 .

All strain measurements were made with the tubing in the constant temperature chamber.

After noting the gauge zeros for a period of fifty-eight hours, during which time the maximum observed drift was 3×10^{-6}, the first cut was performed on tube 2A using the apparatus described in section 2.02 . The distance x from each gauge to the new end-face was measured and is shown in fig.63b . After returning the tube to the constant temperature chamber, the longitudinal and circumferential strain changes were measured and repeated until constant (thermal equilibrium was reached in less than two hours due to the relatively small thermal capacity of the thin-walled copper tubing). The results obtained are shown in fig.68 . It is clear that the extent of the region of disturbance was far greater than the theoretical predictions of section (a) .

The gauges were rezeroed and the whole procedure repeated for the second cut. The distance x for each gauge is shown in fig.63c and the measured strains and surface stresses in fig.69 . Although the extent of the region of disturbance was almost identical to that produced by the first cut, the magnitude of the disturbance was almost doubled.

The overall effect of the two cuts was to apply $19.4 N/mm^2$ longitudinal compression and $3.7 N/mm^2$ circumferential compression at maximum wall thickness on the mid-section of specimen 2A-1 .

Using the same experimental technique, tubes 1A and 3A were subdivided as indicated in figs.64,65 . The surface strains and stresses produced by each cut on tube 1A are shown in table 4 while those produced at mid-section on specimen 3A-1 are shown in figs.70-74 .

(c) Discussion of results.

The results obtained from tube 2A showed that the stress distribution produced by 'end-facing', greatly exceeded the theoretical predictions of section (a) . The extent of the region of disturbance (approximately 250mm or $5D_m$) appeared to be a function of the tube dimensions, rather than the stress level at the cut section.

The magnitude of the longitudinal surface compressive stress produced by each cut decayed approximately linearly with x as shown in fig.75a . $\sigma_L(x)$ represents the surface stress produced at x from the end-face and $\sigma_L(0)$, the surface stress produced at $x = 0$.

Since the external effect of the relief of stress of one sense in a fibre by 'end-facing' is equivalent to the

application of an equal stress of the opposite sense, it follows from figs.68,69 that the residual stress which existed in the outer layers at the first and second cut sections was $+12.5N/mm^2$ and $+25.0N/mm^2$ respectively, and also that the residual stress at the second cut section before the first cut was made was: $+25.0 + 0.6x12.5 = +32.5N/mm^2$ (fig.75b). Due to the proximity of end-2 , considerable stress relief must have occurred at both sections prior to the strain gauges being mounted, and it follows that neither of the values shown in fig.75b represents the undisturbed level of stress which was present in the uncut tubing. This point will be discussed more fully in section 4.05 .

Estimates of longitudinal curvature from diameter measurements indicated that longitudinal bending was negligible in tube 2A and therefore that the measured strains were the result of direct stress relief at maximum wall thickness. It followed from equilibrium considerations that direct stresses of the opposite sense should be present at other points round the circumference, and this was subsequently confirmed by the results obtained from tube 3A .

Even if allowance is made for the different position of each specimen relative to the ends of each $12D_m$ length, it is clear that considerable variation of the effects of 'end-facing' occurred from specimen to specimen. Table 5 shows the surface stresses produced at maximum wall thickness on the mid-section of each

specimen.

The highest stress levels occurred in tube 2A and the lowest in tube 1A . Of particular interest were the unexpectedly large circumferential surface stress levels produced in specimen 3A-1 (figs.72,73), which indicated that considerable circumferential stress relief had occurred during both cutting processes. The sinusoidal nature of the distribution of these stresses and the fact that the cutting process had involved rotation of the tube suggested that periodic plastic deformation might have occurred during cutting. On further examination, this possibility was ruled out, since the stress distributions produced by each cut varied identically with θ despite the fact that the tube orientation with respect to the clamps and the cutter, differed each time.

The only other possible cause of the type of deformation indicated in figs.72,73 was mismatch between specimen 3A-1 and the discarded sections on either side (fig.76). Measurement of the inside diameter at the mid-section confirmed that the cross-section of specimen 3A-1 was distorted as shown in fig.77 , with the maximum and minimum inside diameters occurring at $\theta = 30^\circ$ and $(180 + 30)^\circ$ respectively. The mean inside diameter was found to be 50.821mm .

Theoretical confirmation that the circumferential surface stress distribution $E' \frac{E' \varepsilon_{(\theta)_b}}{1-\nu_b}$ shown in fig.74

was entirely due to the deformation of the bore of specimen 3A-1 from a perfect circle to the shape indicated in fig.77 , was obtained as follows:

The deflection of an elemental ring in the central region of a long, thin-walled ($R_m/h > 11$) cylinder, is governed (56) by the equation:

$$\frac{d^2w}{d\theta^2} + w = -\frac{12\,M_c(\theta).R_m^2}{E'.h^3} \qquad \text{--------- 4.04.}$$

where $w(\theta)$, the radial displacement of the tube wall, is taken as positive inward, and the factor E' occurs since lateral (longitudinal) curvature of the elemental ring is prevented. The minus sign on the right-hand side follows from the fact that the bending moment $M_c(\theta)$ is taken as positive when it produces a decrease in curvature of the tube wall (fig.78).

It follows directly that:

$$M_c(\theta) = -\frac{E'h^3}{12R_m^2}\left(\frac{d^2w}{d\theta^2} + w\right) \qquad \text{--------4.05.}$$

and therefore that the circumferential bending stress on the outer surface is given by:

$$\sigma_M(\theta)_b = -\frac{6M_c(\theta)}{h^2} = \frac{E'h}{2R_m^2}\left(\frac{d^2w}{d\theta^2} + w\right) \qquad \text{---------- 4.06.}$$

Depending on the nature of the applied loading, circumferential direct stresses may also be present, and must be taken into account. For the loading system shown in fig.79 where the cylinder is compressed along a diameter by the forces P per unit length, the circumferential compressive stress increases from zero at the points E and F to the value $0.5\,P/h$ at G and H, and it may be shown (56) that the circumferential bending moment $M_c(\theta)$ varies sinusoidally between the value $\frac{PR_m}{2}\left(\frac{2}{\pi}\right)$ at E and F, and $-\frac{PR_m}{2}\left(1-\frac{2}{\pi}\right)$ at G and H . If these results are applied to specimen 3A-1, for which $R_m/h = 16.5$, it follows from equation 4.06 that $\sigma_{M(\theta)_b}$ has the value $-31.6\,P/h$ at E and F and the value $+18\,P/h$ at G and H, so that the direct stress may be neglected in comparison to the bending stress without significant error.

It follows that the radial displacement of the tube wall $w(\theta)$ may be related to the measured surface strains by the expression:

$$\ell_{\theta(\theta)_b} = \frac{h}{2R_m}\left(\frac{d^2w}{d\theta^2} + w\right) \qquad \text{----------4.07.}$$

Fig.80 was constructed from the measurements of the inside diameter of specimen 3A-1 by assuming that the inward radial displacement of the tube wall $w(\theta)$ was equal to half the difference between the actual inside diameter and the mean inside diameter. Although this method of construction was based on the assumption that the uncut tubing had a perfectly circular cross-

section, and meant that $w(\theta)$, and therefore the calculated value of $\rho(\theta)_b$, was the average of the values at two points diametrically opposite each other, agreement between the measured values of $\rho(\theta)_b$ and those calculated from equation 4.07 was excellent (fig.81). The values for $\frac{d^2w}{d\theta^2}$ were obtained graphically, and the slight variation in wall thickness ($\pm 6\%$) caused by specimen eccentricity, was neglected.

If ΔD_{EF} and ΔD_{GH} represent the changes in the diameters EF and GH under the action of the force P per unit length, then it may be shown (56) that:

$$|\Delta D_{EF}| = \frac{3P}{E'}\left(\frac{R_m}{h}\right)^3\left(\pi - \frac{8}{\pi}\right)$$

$$|\Delta D_{GH}| = \frac{6P}{E'}\left(\frac{R_m}{h}\right)^3\left(\frac{4}{\pi} - 1\right)$$

so that P may be determined if either ΔD_{EF} or ΔD_{GH} are known.

In the case of specimen 3A-1, ΔD_{EF} = -0.018mm and ΔD_{GH} = +0.017mm (fig.77), from which P = 0.28N/mm or 0.29N/mm over the central region of the specimen length.

(d) Conclusions.

The longitudinal surface stress produced on cutting-out specimen 3A-1 appears to confirm the existence in drawn tubing of a type of longitudinal residual

stress distribution similar to that suggested by Knights (section 1.03), with regions of direct stress of the opposite sense existing in equilibrium round the circumference.

The circumferential surface stress distribution obtained from the same specimen, which was shown to be equivalent to the application of two radial inward forces of 0.29N per millimetre specimen length along the diameter at $\theta = 30°$, suggests the presence of circumferential mismatch between adjacent lengths of drawn tubing. plug chatter?

4.03. INVESTIGATION OF THE RESIDUAL STRESSES AT MAXIMUM WALL THICKNESS IN SPECIMENS 2A-1, 1A-1, 1A-2 AND 3A-1.

Although theoretical considerations indicated that the region of disturbance for the tubing used should extend only $0.6D_m$ from each specimen end, it appeared from the results discussed in the previous section that almost total stress relief had occurred in the specimens chosen for further examination.

A comparative investigation of the residual stresses remaining at maximum wall thickness in specimens 2A-1, 1A-1, 1A-2 and 3A-1 was carried out by removing uniform internal layers from each specimen.

Using the apparatus described in sections 2.03 and

2.04 the wall thickness of each specimen was reduced in small steps by acid-etching, and the longitudinal and circumferential strain changes on the outer surface were recorded. The number of measurements taken was twenty, twenty-one, twenty-eight and thirty, in specimens 2A-1, 1A-1, 1A-2 and 3A-1 respectively.

The surface stress parameters $\mathcal{L}_{bp}$ and $\mathcal{b}_{bp}$ were plotted against the bore radius ρ, and are shown in figs.82-85. Although additional strain gauges were mounted on specimens 1A-2 and 3A-1, as part of the investigation of the circumferential variation of the residual stress in the tubing (section 5), only the results obtained from the gauges at maximum wall thickness will be considered in this section.

The residual stresses present at maximum wall thickness in specimen 2B-1, for which $\ell = 3D_m$, $\%_b$ = 0.941 and c = 0.103mm (fig.61c), were investigated by removing uniform layers from the outer surface. This was mainly to determine whether this method of layer removal was practicable, but also to compare the strains detected on the inner surface with those obtained by etching in the opposite direction. The values obtained for $\mathcal{L}_{ap}$ and $\mathcal{b}_{ap}$ are shown plotted against decreasing ρ in fig.86. The excellent agreement between these curves and those obtained from specimens 1A-1, 1A-2 and 3A-1, may be taken as an indication that no plastic deformation occurred during layer removal, a basic requirement in any experimental investigation of residual stress by

the Sachs method.

Despite the fact that considerable residual stress relief had already occurred on cutting-out, it was clear that high stress levels still existed in all the specimens. Both the level and the distribution of stress showed little variation from specimen to specimen, except in the case of specimen 2A-1 ($\ell = 2D_m$), in which reduced stress levels were observed.

4.04. EXPLANATION OF THE SURFACE STRESSES PRODUCED BY 'END-FACING'.

Over the years, the experimental procedure described in section 4.03 has become the standard technique for assessing the minimum length/diameter ratio of specimens for residual stress analysis. It is based on the assumption that reduced residual stress levels will be observed in specimens with a length/diameter ratio less than a certain 'critical' value.

Apart from the recent investigation by Hanke and Tiemann (53), and the present work, no observations of the strains produced during cutting-out have been made.

The fact that the results discussed in section 4.03 confirm the findings of previous investigators (48-52,64), while those discussed in section 4.02 appear to refute them, suggests that two distinct types of residual stress

existed in the uncut drawn tubing; 'type A' or normal residual stresses on which cutting-out had only a local effect similar to that described in section 4.02a , and 'type B' residual stresses, hitherto unreported and almost completely relieved by cutting to produce in specimens with a length/diameter ratio less than 5 .

On this basis the surface stresses shown in figs.68, 69,72,73 would be the result of 'type B' stress relief on cutting-out, while those in figs.82-85 would be the result of 'type A' stress relief on layer removal.

A detailed examination of the 'type B' residual stresses in specimen 3A-1 is presented in the following section. The 'type A' stresses in the same specimen will be discussed in section 5 , with reference to the results obtained from the additional gauges which were mounted round the circumference.

4.05. 'TYPE B' RESIDUAL STRESSES.

(a) Longitudinal stresses.

The results shown in figs.68,69 suggest that the extent of the region of disturbance of 'type B' longitudinal stresses by a cut at right-angles to the tube axis ($5D_m$ in the tubing tested), depended upon the tube dimensions rather than the stress level at the cut section, and that the magnitude of the stress

relieved decayed linearly with α as shown in fig.75a . If these two principles are assumed to apply to all the tubing tested, it is clear that the surface stresses detected at the gauged section after the first cut on tube 3A, represent approximately 60% of the surface stresses released at the cut section. It follows that the longitudinal 'type B' residual stresses which existed at the cut section, may be represented by curve 2 in fig.72a , which was obtained from the curve for the surface stress at the gauged section, by multiplying by -1.67 . The fact that this curve is almost identical to that obtained for the total residual stresses released at mid-section (the dotted curve in fig.74a), confirms that almost complete relief of the 'type B' longitudinal stresses occurred on cutting-out specimen 3A-1 .

Unfortunately, the undisturbed stress level which was present in the uncut tubing at the first cut section cannot be determined exactly since no measurements of the surface strains produced by the hacksaw cut between tube 2A and tube 3A were taken. An indication can however be obtained from fig.87a , by putting σ = 0, 10, 20, 30 .....N/mm^2 , in turn, as shown in fig.87b . The series of stress levels obtained with σ = 20N/mm^2 appears to be the most likely, suggesting that the undisturbed stress level at the first cut section on tube 3A was about 40% higher than the measured value (curve 3 in fig.72a).

Irrespective of the exact value of the undisturbed 'type B' stress at the various sections, it is evident that considerable longitudinal variation occurred in the tubing tested, possibly associated with plastic bending during drawing, as suggested by Knights (section 1.03), or perhaps with a variable frictional effect such as imperfect lubrication.

selective annealing

(b) Circumferential stresses.

The circumferential 'type B' residual stress relieved at any position θ in specimen 3A-1 , may be determined as follows:

Recalling from equation 4.06 that the circumferential bending stress on the outer surface of a cylinder with the deformation pattern $w(\theta)$ is given by:

$$\sigma_M(\theta)_b = \frac{E'h}{2R_m^2}\left(\frac{d^2w}{d\theta^2} + w\right)$$

and noting that small variations in wall thickness may be accounted for by replacing h by h_θ , (provided $R_m/h_\theta > 11$), it follows that:

$$\sigma_M(\theta)_b = \frac{E'h_\theta}{2R_m^2}\left(\frac{d^2w}{d\theta^2} + w\right)$$

and since the relief of residual stress of one sense in a circumferential fibre is equivalent to the application of an equal stress of the opposite sense, $\sigma_{CM}(\theta)_b$, the circumferential residual bending stress

which existed in the outermost layer prior to cutting-out, may be determined from:

$$\sigma_{CM}(\theta)_b = -\sigma_M(\theta)_b = -\frac{E' h_\theta}{2R_m^2}\left(\frac{d^2w}{d\theta^2} + w\right)$$

Since R_m/h_θ was large for the tubing used, it may be assumed that the bending stress relieved at any section varied linearly through the wall thickness (96), so that $\sigma_{CM}(\theta)$, the residual bending stress relieved at depth d from the outer surface (fig.88), may be obtained from:

$$\sigma_{CM}(\theta) = \left(\frac{h_\theta - 2d}{h_\theta}\right).\sigma_{CM}(\theta)_b \quad \text{----------4.08.}$$

$$= -\frac{E'}{2R_m}(h_\theta - 2d)\left(\frac{d^2w}{d\theta^2} + w\right) \quad \text{---------4.09.}$$

This equation makes possible the determination of the residual bending stress at any position θ, d from measurements of $w(\theta)$.

Since 'type B' circumferential residual stresses arise because of circumferential mismatch between adjacent lengths of tubing, a certain amount of direct circumferential stress relief must always occur on cutting-out, if these stresses are present. However, in the case of specimen 3A-1 , the direct stress component has already been shown to be negligible in comparison to the bending component, so that equation 4.08 may be written:

$$\sigma_c(\theta) = -E'.\left(\frac{h_\theta - 2d}{h_\theta}\right).\varepsilon(\theta)_b \qquad \text{--------4.10.}$$

and the 'type B' circumferential residual stress $\sigma_c(\theta)$ may easily be determined from fig.74b .

It is clear that 'type B' circumferential residual stresses vary with θ and with ℓ , and also vary linearly through the wall thickness. They appear to be relatively small in comparison to 'type B' longitudinal stresses, and may even be negligible in the majority of cases.

(c) It is evident that the complete investigation of the 'type B' residual stresses over a length of tubing would require a considerable number of strain gauges. The arrangement shown in fig.89 would probably prove to be the most economical, since it would also provide several gauged specimens of suitable length for the complete investigation of 'type A' residual stresses (sections 5 and 6).

Provided the first cut is made at a distance of at least $5D_m$ from the end of the tubing, subsequent cuts may be made with a closer spacing. The interference of the regions of disturbance of the longitudinal stress pattern may be accounted for as indicated in section (a).

Due to the relatively wide spacing of the cut sections the method is probably not the most sensitive

which could be devised for the investigation of circumferential 'type B' stresses, but since these appear to be relatively small in comparison to those in the longitudinal direction, it would probably be suitable in most cases.

The dimensions $5D_m$ and $3D_m$ apply specifically to the tubing discussed in the present work, and would require preliminary investigation in any future work.

SECTION 5.

THE CIRCUMFERENTIAL VARIATION OF 'TYPE A' RESIDUAL STRESSES IN SPECIMEN 3A-1.

5.01. INTRODUCTION.

The object of the work described in this section was to investigate experimentally the circumferential variation of the 'type A' or normal residual stresses in specimen 3A-1 (for which $a/b = 0.941$ and $C = 0.096$mm) and to determine the extent to which the initial eccentricity of the specimen (and its increase on layer removal) affected the surface strain changes. The possibility of using the Sachs method in the presence of eccentricity was also examined.

5.02. EXPERIMENTAL TECHNIQUE.

Although the general experimental technique has already been outlined in section 4.03 in connection with the strains released at maximum wall thickness in specimens 2A-1, 1A-1 and 1A-2, certain aspects of the procedure in the case of specimen 3A-1 require more detailed consideration.

Twenty-six strain gauges, thirteen longitudinal, and thirteen circumferential, were mounted at mid-section in the angular positions shown in table 3 . Two (soldered) common terminals were used in wiring-up the gauges, one for the longitudinal gauges and one for the circumferential gauges. Care was taken to ensure that the length of each lead exactly matched the length via the common terminal, in order to avoid as far as possible, resistive imbalance

in the circuit.

Altogether, twenty-eight wires plus sleeving were led out of the end-ring in the manner indicated in fig.29 , and spade terminals were attached as described in section 2.04; little difficulty was experienced in handling these leads except that the process of washing and drying the specimen proved somewhat tedious. During weighing, the leads were wrapped round the circumference of the perspex cylinder, and prior to each strain measurement, all the spade terminals were degreased using carbon tetrachloride.

The wall thickness of the specimen was reduced in thirty stages of between 0.02mm and 0.07mm by etching with 50% nitric acid. The total weight of copper removed was 4.466N in 329 minutes actual etching time. The thickness of the first and last few layers removed was reduced in order to obtain extra measuring points (table 6). This was carried out, in the case of the first few layers, by reducing the length of each etch, and in the case of the last few layers, by dropping the acid level, so that the rotating specimen was only just breaking the surface of the acid; a procedure which minimised the possibility of plastic deformation occurring in the thin shell due to hydrostatic pressure (in the case of external etching) or to the weight of acid it contained (in the case of internal etching). The acid temperature was maintained between 30°C and 35°C throughout.

The change in specimen length due to etching of the end-faces was measured periodically and the length reduction ℓ_1 was plotted against the weight loss W as shown in fig.41 . The manner in which this curve was used in the determination of ρ has already been discussed in section 2.03 .

One complete cycle i.e. etching, washing, drying, weighing and the measurement of strain occupied about three hours, on average. Previous experience with the constant temperature chamber suggested that gauge zero drift would be less than 10 microstrain during the five consecutive days needed to complete the whole series of readings.

The longitudinal and circumferential strains $\varepsilon_L(\theta)$ and $\varepsilon_c(\theta)$ released on layer removal are shown in table 7 . These were plotted against θ (not shown), and from the curves, the circumferential distribution of the parameters $\ell(\theta)_{bp}$ and $\ell\varrho(\theta)_{bp}$ was obtained. The curves for $\ell(\theta)_{bp}$ and $\ell\varrho(\theta)_{bp}$ against θ for all thirty stages of layer removal are shown in figs.90-119 . The circled points represent the surface stresses produced at $\theta = 0^\circ$, 90°, 180° and 270° on specimen 1A-2, these were obtained by linear interpolation between two measured values when the stages of the etching process did not coincide.

Figs.120,121 were constructed to show more clearly the sequence of events which occurred during layer removal.

Periodically, the sealed unit was rotated 180° about its axis in the constant temperature chamber. This was carried out in order to determine if any additional stresses were imposed by the specimen bending longitudinally under its own weight. The changes in the surface stress parameters detected at maximum, minimum and mean wall thickness are shown in table 8 , and are clearly negligible at all stages in comparison to the changes produced by layer removal.

The restraint imposed by the 'Silicoset' mountings after the thirtieth etch (when R_m/h_m = 250 and R_m/h_{MIN} = 2000 approx.) was investigated by carefully cutting them away with a scalpel and allowing the specimen to rest in the cylinder on the perspex end-rings. The changes in surface stress which resulted, are shown in fig.122 . The circumferential stresses are clearly a result of the specimen 'sagging' under its own weight, and indicate that the major effect of the mountings was to preserve the circular cross-section at each end of the specimen. Apart from the high circumferential compressive stress at minimum wall thickness, which could be the result of local yielding, the effect of freeing the specimen is everywhere small in comparison to the effect produced by removal of the thirtieth layer.

5.03. 'TYPE A' LONGITUDINAL RESIDUAL STRESSES.

It is clear from figs.90a-119a that the circum-

ferential variation of the longitudinal surface stresses produced by layer removal increased progressively as ρ/b and $e(\rho)$ increased. Up to the tenth etch no significant circumferential variation of $\mathcal{L}(\theta)_{bp}$ was observed. Beyond this point a definite pattern began to emerge, with stress peaks occurring at regular intervals round the circumference. By the sixteenth etch, peaks were evident at $\theta = 0^\circ, \pm 45^\circ, \pm 90^\circ, \pm 130^\circ$ and 180° and the overall stress distribution was clearly symmetrical about the axis of symmetry of the eccentric cross-section. On further layer removal, the magnitude of the stress variations increased, but no new stress peaks appeared. A considerable degree of symmetry about the position $\theta = 0^\circ$ was maintained throughout the remaining etching processes. Three stages in the development of the longitudinal surface stress pattern are shown in fig.120 .

The circled points in figs.90a-119a represent the results obtained at $\theta = 0^\circ, 90^\circ, 180^\circ$ and 270° on specimen 1A-2 . Up to the twenty-fifth etch, agreement at all points is excellent. Beyond this point, the surface stresses detected at minimum wall thickness begin to diverge, probably due to the occurrence of plastic deformation in either or both specimens.

At first sight the uniform distribution of $\mathcal{L}(\theta)_{bp}$ obtained during the first ten etches suggests that no significant variation of the longitudinal residual stress occurred in this region of the specimen. However, this data may also be interpreted as suggesting that the

specimen was initially insensitive to small circumferential variations in the loading applied by layer removal.

Apart from an overall symmetry with respect to the position $\theta = 0^\circ$, the magnitude of the changes in surface stress on layer removal appeared to be unrelated to the variation in wall thickness as predicted by equation 3.05 . Up to the nineteenth etch, the process of layer removal produced only compressive surface stress changes at all points round the circumference. Beyond this point tensile surface stress changes began to occur at the positions $\theta = \pm 45^\circ$ and $\pm 130^\circ$, while compressive surface stress changes continued to occur at all other points. By the twenty-fifth etch, tensile surface stress changes were occurring at all points except $\theta = \pm 90^\circ$, and after the twenty-sixth etch, all surface stress changes were tensile.

Even without the additional complexity introduced by the variation of ρ and h_θ, and the constantly-changing loading system, the problem of the thin-walled cylinder under the action of a θ-varying longitudinal load, represents a fairly advanced application of shell theory (57), it being necessary to take account of longitudinal shearing actions in addition to normal stresses. It is therefore extremely unlikely that an exact determination of the 'type A' longitudinal residual stresses which were present in specimen 3A-1 could be carried out using the data of figs.90a-119a . The

possibility of applying an approximate method, which accounts for the wall thickness variation, but not the shearing actions, is examined in the remainder of this section.

The Sachs analysis (appendix 3) may be modified and applied to the results obtained from specimen 3A-1 if the presence of longitudinal shearing actions is ignored. This obvious approximation, which is equivalent to assuming that the thin strip at position θ in fig.123 behaves independently of all other thin strips when the residual stress $\sigma_L(\theta)$ is relieved, may be justified on the grounds that it enables some account to be taken of the effect of wall thickness variation on the results, without introducing complex mathematics.

The longitudinal residual stress $\sigma_L(\theta)$ at the position ρ may be determined from the equation:

$$\sigma_L''(\theta) = \sigma_L(\theta) + \sigma_L'(\theta) \qquad \text{--------5.01.}$$

where $\sigma_L''(\theta)$ is the stress present in the small arc $\rho.\Delta\theta$ of the layer of thickness $\Delta\rho$ at radius ρ on its removal, and $\sigma_L'(\theta)$ is the stress induced at the position ρ,θ by removal of internal layers up to radius ρ .

If longitudinal shearing actions are ignored, it may be assumed that the stress $\sigma_L''(\theta)$ present in the small arc $\rho.\Delta\theta$ is redistributed uniformly over the area ABCD on removal of the layer at radius ρ . It

follows that:

$$\sigma_L''(\theta) \cdot \rho \cdot \Delta\theta \cdot \Delta\rho = \Delta\sigma_L(\theta)_{b\rho} \cdot h_\theta \cdot \rho \cdot \Delta\theta$$

where $\Delta\sigma_L(\theta)_{b\rho}$ is the change in surface stress at position θ.

So that:

$$\sigma_L''(\theta) = h_\theta \cdot \frac{\Delta\sigma_L(\theta)_{b\rho}}{\Delta\rho}$$

and since: $$\Delta\sigma_L(\theta)_{b\rho} = E' \cdot \Delta\mathcal{L}(\theta)_{b\rho}$$

it follows that: $$\sigma_L''(\theta) = E' \cdot h_\theta \cdot \frac{\Delta\mathcal{L}(\theta)_{b\rho}}{\Delta\rho} \quad \text{-----5.02.}$$

It follows from the definition of $\sigma_L'(\theta)$ that:

$$\sigma_L'(\theta) = \sum_{\rho'=a\to\rho} \Delta\sigma_L(\theta)_{\rho\rho'}$$

where $\Delta\sigma_L(\theta)_{\rho\rho'}$ is the stress induced at the position ρ, θ by removal of the layer, thickness $\Delta\rho$, at the radius $\rho' < \rho$. Since the stress relieved in the small arc $\rho' \cdot \Delta\theta$ may be assumed to be uniformly distributed over the area A'B'CD it follows that:

$$\Delta\sigma_L(\theta)_{\rho\rho'} = E' \cdot \Delta\mathcal{L}(\theta)_{b\rho'}$$

so that: $$\sigma_L'(\theta) = E' \sum_{\rho'=a\to\rho} \Delta\mathcal{L}(\theta)_{b\rho'}$$

or: $$\sigma_L'(\theta) = E' \cdot \mathcal{L}(\theta)_{b\rho} \quad \text{--------5.03}$$

and using equation 5.01 it follows that:

$$\sigma_L(\theta) = \lim_{\Delta\rho \to 0} E' \left[h_\theta \cdot \frac{\Delta \mathcal{L}(\theta)_{b\rho}}{\Delta \rho} - \mathcal{L}(\theta)_{b\rho} \right] \qquad \text{--------5.04.}$$

Figs.124-127 show $\mathcal{L}(\theta)_{b\rho}$ plotted against ρ at the positions θ = 0°, +45°, -45°, +90°, -85°, +130°, -140° and 180°, with the curve for θ = 0° repeated for easier comparison. These curves show clearly the way in which the various stress peaks developed, with the close correspondence during the first few etches giving way to wide variations as layer removal proceeded. The relative magnitude of the wall thickness at the positions θ = 0°, 45°, 90°, 130° and 180° at various stages of layer removal is shown in fig.128 which was constructed using equation 3.05 . Apart from a general tendency towards larger changes in gradient as $\theta \to 180°$ and $\rho/b \to 1$, there appears to be little connection between the curves in figs.124-127 and the variation of h_θ . Fig.128 does however indicate the need to take account of wall thickness variations, especially as ρ/b approaches the limiting value $1 - c/b$ or 0.9965 .

The determination of the gradient $\frac{\Delta \mathcal{L}(\theta)_{b\rho}}{\Delta \rho}$ was carried out by a step-wise technique which used the marked points in figs.124-127 rather than the trend curves. This produced the scatter in the final curves for $\sigma_L(\theta)$ which are shown in figs.129-132 . Again the curve for θ = 0° is repeated to facilitate comparison.

The most striking feature of the various curves for

$\sigma_L(\theta)$ is their similarity. During the early stages of layer removal, this is almost certainly the result of neglecting longitudinal shearing stiffness, and in consequence, assessment of the true magnitude of the circumferential variation of $\sigma_L(\theta)$ near the inner surface is difficult. However, the close correspondence of the curves in the later stages of layer removal, when the resistance to longitudinal shear-type deformations appears, from the measured strain changes, to have been reduced, suggests that the circumferential variations of $\sigma_L(\theta)$ in this region were relatively small. This, in turn, suggests that the wide variation in magnitude of the surface strain in the later stages of the experiment was the cumulative result of relatively small variations in stress in the layers removed previously, rather than the result of large scale local stress variation.

The overall impression conveyed by the results is of relatively small but definite stress variations occurring at the same angular positions in consecutive layers. The greatest changes in stress occur at the positions $\theta = 0^\circ$ and $\theta = 180^\circ$, and in identical pairs at $\pm 45^\circ$, $\pm 90^\circ$ and $\pm 130^\circ$, so that the axis of symmetry of the eccentric cross-section is also an axis of symmetry for the stress variations. The basic radial distribution of $\sigma_L(\theta)$, which may be taken as the average of all the curves shown in figs.129-132, indicates that compressive stresses existed in the inner half of the wall thickness, with tensile stresses in the outer half.

To obtain the undisturbed distribution of longitudinal residual stress, the 'type B' stresses released on cutting specimen 3A-1 to length, must be superimposed. It is clear from fig.72a that tensile stresses of magnitude $15N/mm^2$, $7N/mm^2$ and $12N/mm^2$ must therefore be added at the positions $\theta = 0^\circ$, $+45^\circ$ and 180°, and that compressive stresses of magnitude $13N/mm^2$ and $8N/mm^2$ must be added at the positions $\theta = +90^\circ$ and $+130^\circ$ respectively.

5.04. 'TYPE A' CIRCUMFERENTIAL AND RADIAL RESIDUAL STRESSES.

The circumferential surface stresses produced on layer removal are shown in figs.90b-119b . Circumferential variations of stress could just be discerned from the sixth etch onward, and six distinct stress peaks were visible by the twelfth etch. The mean circumferential surface compression at this point was approximately $7.5N/mm^2$. By the twenty-second etch, additional stress peaks had developed at $\theta = 60^\circ$, 90°, 120° and 140° and the mean circumferential surface compression had increased to $15N/mm^2$. No further stress peaks formed beyond this point, although those already present increased rapidly in magnitude. The mean surface compression gradually declined and tended to zero as P/b approached the limiting value 0.9965 . No obvious axis of symmetry was found to exist, and the results showed little agreement with those obtained from

specimen 1A-2 , which are indicated, as before, by the circled points.

Following the method of Sachs, the relief of the circumferential and radial residual stresses $\sigma_c(\theta)$ and $\sigma_R(\theta)$ in an eccentric cylinder may be represented by the equations:

$$\sigma_c''(\theta) = \sigma_c(\theta) + \sigma_c'(\theta) \quad \text{----------} \quad 5.05$$

$$\sigma_R''(\theta) = \sigma_R(\theta) + \sigma_R'(\theta) \quad \text{----------} \quad 5.06$$

where the components σ'' represent the stresses existing in a particular layer as it is removed, and the components σ' represent the stresses induced in the layer by removal of previous layers.

In section 3 it was shown that the circumferential stress $\sigma_c(\theta)_{bp}$ produced on the outer surface of an eccentric cylinder by the application of a uniform internal pressure p_a could be determined from the equation 3.23 :

$$\frac{\sigma_c(\theta)_{bp}}{p_a} = \frac{E' \ell_\theta(\theta)_{bp}}{p_a} = F_b(\rho/b, \theta)$$

Since the effect of layer removal from a residually-stressed cylinder is equivalent to the application of a uniform pressure to the newly created surface if, and only if, the stress components σ'' are uniform, the above equation provides a means of examining the uniformity of $\sigma_c''(\theta)$ and $\sigma_R''(\theta)$ in the eccentric cylinder at

each stage of layer removal.

If, at a given stage of layer removal, the stress components $\sigma_c''(\theta)$ and $\sigma_R''(\theta)$ are independent of θ, it follows from equation 3.23 that the general form of the distribution of $\varepsilon(\theta)_{bp}$ should be similar to that shown for $F_b(\rho/b,\theta)$ in fig.56 . To facilitate the comparison of theoretical and experimental data, equation 3.23 may be rewritten in the form:

$$\varepsilon(\theta)_{bp} = \frac{F_b(\rho/b,\theta)}{F_m} \cdot \varepsilon_m \quad \text{---------} \quad 5.07.$$

so that by using the mean value ε_m of a set of experimental points, their actual distribution with respect to θ may be compared to the distribution which would be produced by a uniform stress applied at the bore.

Fig.133 shows a plot of ε_m against ρ for specimen 3A-1 , the circled points indicate the values of ε_m after the tenth, eighteenth, twenty-first, twenty-third, twenty-sixth and twenty-ninth etches respectively. The circumferential variation of $F_b(\rho/b,\theta)/F_m$ at each of these stages of layer removal is shown in table 2 . Figs.134-136 were constructed to compare the curves of $F_b(\rho/b,\theta).\varepsilon_m/F_m \; v \; \theta$ with the experimentally observed values of $\varepsilon(\theta)_{bp}$.

It appears that, up to the twenty-sixth etch, the measured surface stress $E'\varepsilon(\theta)_{bp}$ may be considered as consisting of two components; one resulting from the

application of a uniform (negative) pressure at the bore, and the other resulting from local circumferential bending deformations which increased in magnitude as layer removal proceeded. The manner in which the various circumferential stress peaks developed (fig.121) suggests that they could have been the result of elastic pre-buckling deformations similar to those reported by Montague (58) in thin shells subjected to external pressure. In this way the unexpectedly large variations in the measured circumferential surface stress may be attributed to the uniform negative pressure applied to the bore by layer removal, rather than to the rather unlikely occurrence, in such thin-walled, nearly-concentric tubing, of large periodic circumferential variations in the stress components σ_c'' and σ_R'' . Before this hypothesis can be examined, a brief review of the relevant literature on buckling is necessary.

When a thin-walled cylinder is subjected to an increasing externally-applied pressure, many factors combine to determine the critical pressure at which yielding will occur, and the eventual failure mode. Among the more important factors enumerated by Cox (59) are; the presence of irregularities or imperfections in the circular cross-section, the presence of longitudinal applied stresses, and the presence of circumferential variations in wall thickness or in the applied loading. Recently (60) the presence of residual stresses has also been recognized as having a significant effect.

Two distinct types of behaviour have been noted (58); collapse by elastic instability, and rigid-plastic collapse. The first is characterised by the appearance of circumferential lobes after yielding, and the second by an hour-glass or waisted configuration, also following yielding. Whichever is the most appropriate to a particular specimen, depends on a combination of geometric and material properties. These may be assessed most conveniently by determining the thinness ratio T from the expression:

$$T^4 = \frac{2(l/R)^2}{(h/R)^3}\left(\frac{\sigma_y}{E}\right)^2 \qquad \text{---------} \quad 5.08.$$

where l in this case is the unsupported length between sections held round. In relatively thick cylinders (for which T is less than 1), failure is generally by plastic collapse, and a reasonably good prediction of the critical pressure $p_{CRIT.}$ may be obtained from the formula: $\sigma_y = p_{CRIT.} R/h$, based on simple circumferential yielding. For thin cylinders (T greater than 2.5) the elastically unstable mode of failure predominates. Between these two extremes there is a transition region where initial imperfections can be decisive in causing collapse.

In the case of the thin cylinder, the number of circumferential lobes in the elastically unstable (or critical) collapse mode can be predicted quite reliably provided the unsupported length l , the ratio R/h , the end conditions and the type of loading are known. The

following formula for the elastic critical pressure is quoted by Timoshenko and Gere (56) and in a less general form by Cox (59) :

$$p_{CRIT.} = \frac{E'}{c_3 + c_4 \frac{\phi_L}{\phi_C}} \left[c_1 \cdot \frac{h}{R} + \frac{c_2}{12} \cdot \left(\frac{h}{R}\right)^3 \right] \qquad \text{--------5.09.}$$

with:

$$c_1 = (1-\mu^2)\lambda^4$$

$$c_2 = (\lambda^2+n^2)^4 - 2\left[\mu\lambda^6 + 3\lambda^4 n^2 + (4-\mu)\lambda^2 n^4 + n^6\right] + 2(2-\mu)\lambda^2 n^2 + n^4$$

$$c_3 = n^2(\lambda^2+n^2)^2 - (3\lambda^2 n^2 + n^4)$$

$$c_4 = \lambda^2(\lambda^2+n^2)^2 + \lambda^2 n^2$$

$$\lambda = \frac{m\pi R}{l}$$

where m is the number of axial half waves and $2n$ is the number of circumferential half waves in the buckled form, and where l is the length between the simply-supported ends of the cylinder. The factor ϕ_L/ϕ_C represents the ratio of the principal stresses produced by the applied loading.

By means of a formula similar to equation 5.09 , Windenburg and Trilling (61) produced a chart for all-around pressure ($\phi_L/\phi_C = 0.5$) from which the figures shown in table 9 are taken. Arkmenakas and Herrmann (62) have recently published extended charts for lateral pressure only, which give identical figures in the same range of R/h . In general, the thinner the specimen, the greater the number of lobes in the elastic critical mode shape.

Montague (58) describes the results of external radial and hydrostatic pressure tests on twelve mild steel, thin-walled cylindrical shells with R/h values in the range 21-94 . Despite the fact that the cylinders were nominally uniform, the radial measured deformations at mid-section were not axisymmetrical. In every case there was a discernible elastic deformation pattern which took the form of lobes spaced round the circumference and which was similar in both form and manner of development to the curves shown in figs.90b-119b . Irrespective of the eventual failure mode, the number of lobes which developed during this elastic pre-buckling phase, was always found to equal the number of lobes in the predicted elastic critical mode shape for the specimen. Figs.90b-119b clearly suggest that the elastic critical mode for specimen 3A-1 should contain 5 lobes.

The correct failure analysis for specimen 3A-1 was selected by calculating the thinness ratio T at each stage of layer removal. The ratio of h/R was based on mean wall thickness, and although the 'Silicoset' mountings offered little restraint in the early stages of layer removal, l was taken as being equal to the specimen length of 208.8mm as a first approximation. It was clear from the T values obtained (fig.137) that failure predictions in the later stages of layer removal should be based on elastic instability theory, i.e. that equation 5.09 should be used to determine the elastic critical pressure.

Preliminary calculations indicated that the critical pressure was of most interest for $\rho/b > 0.980$ or $R_m/h_m > 50$. Because of the relative increase in stiffness of the 'Silicoset' mountings, the accuracy of the assumption: $\ell = 208.8$mm , improved as $\rho/b \rightarrow 0.9965$. The factor ϕ_L/ϕ_c was taken as the ratio of the mean longitudinal and circumferential stresses i.e. σ_m/σ_m , and m was taken as 1 .

Two sets of calculations were performed; one with R/h based on mean wall thickness, and the other with R/h based on minimum wall thickness. In the first case $p_{CRIT.}$ was determined for $n = 3$, 4 and 5 , and in the second case for $n = 3$, 4, 5 and 6 . The figures obtained are shown in table 10 , and clearly, the thinner the specimen, the lower the elastic critical pressure for a given number of circumferential lobes.

In order to compare the loading applied by layer removal with the values of $p_{CRIT.}$ shown in table 10 , an equivalent external pressure $p_{EQU.}$ was calculated using the formula:

$$p_{EQU.} = E' \sigma_m \left[\frac{1-(\rho/b)^2}{1+(\rho/b)^2} \right]$$

which follows directly from Lame's equations (96) for a uniform cylinder of wall thickness $b-\rho$. Since the mean surface compression σ_m actually resulted from a negative pressure at the bore, this approach is not strictly correct. However, the error is small for $\rho/b > 0.94$, and insignificant for $\rho/b > 0.98$. Fig.138 shows

a plot of $p_{EQV.}$ against ρ/b and figs.139,140 compare $p_{EQV.}$ and $p_{CRIT.}$ for $\rho/b > 0.98$. These curves indicate that at least 50% of the circumference of specimen 3A-1 was in a condition for plastic buckling in three or four lobes by the twenty-seventh etch, or ρ/b = 0.992 . Bearing in mind the large variations in wall thickness and the many other factors which could have affected the values of n and $p_{CRIT.}$, the agreement between this result and the observed number of lobes is extremely satisfactory, and it seems reasonable to conclude that the circumferential stress peaks of figs.90b-119b were produced by elastic pre-buckling deformations, rather than by variations in the stress components $\sigma_c''(\theta)$ and $\sigma_r''(\theta)$.

It appears from figs.134-136 that $\sigma_c''(\theta)$ and $\sigma_r''(\theta)$ may be considered as independent of θ up to the twenty-sixth etch or ρ/b = 0.990 , which is the point at which the curve for $F_b(\rho/b,\theta).\omega_m/F_m$ begins to diverge from the 'buckling base-line' . It follows from equations 5.05 and 5.06 that the stress components $\sigma_c'(\theta)$ and $\sigma_r'(\theta)$, and the original stresses $\sigma_c(\theta)$ and $\sigma_r(\theta)$ may all be considered as independent of θ up to this point. On the basis of this result the Sachs equations may be used to determine the circumferential and radial 'type A' residual stresses from the surface stress changes which occurred at $\theta = \frac{\pi}{2}$.

Since the stress component $\sigma_c''(\theta)$ may be regarded as independent of θ up to the point ρ/b = 0.990 , it

follows from equation 3.23 and appendix 3 that:

$$E' \cdot \Delta b(\theta)_{b\rho} = F_b(\rho/b, \theta) \cdot \frac{\Delta\rho}{\rho} \cdot \sigma_c''(\theta)$$

or:

$$\sigma_c''(\theta) = E' \cdot \left[\frac{\rho}{F_b(\rho/b, \theta)} \cdot \frac{\Delta b(\theta)_{b\rho}}{\Delta\rho} \right]$$

where the expression in brackets is independent of θ. It may easily be shown from table 1 that $F_b(\rho/b, \frac{\pi}{2})$ is numerically equal to $\frac{2\rho^2}{b^2-\rho^2}$ so that:

$$\sigma_c''(\theta) = E' \cdot \frac{b^2-\rho^2}{2\rho} \cdot \frac{\Delta b(\frac{\pi}{2})_{b\rho}}{\Delta\rho} \quad \text{.....5.10..}$$

It follows from the definition of stress components of the type σ' that:

$$\sigma_c'(\theta) = \sum_{\rho' = a \to \rho} \Delta\sigma_c(\theta)_{\rho\rho'}$$

and by using Lame's equation for a uniform cylinder, it may easily be shown that:

$$\Delta\sigma_{c\,\rho\rho'} = \frac{b^2+\rho^2}{2\rho^2} \cdot \Delta\sigma_{c\,b\rho'}$$

It is reasonable to expect that the error involved in using this expression at $\theta = \pi/2$ in a thin-walled nearly-concentric specimen would be small, so that:

$$\Delta\sigma_c(\tfrac{\pi}{2})_{\rho\rho'} = \frac{b^2+\rho^2}{2\rho^2} \cdot \Delta\sigma_c(\tfrac{\pi}{2})_{b\rho'}$$

and since $\Delta\sigma_c(\theta)_{\rho\rho'}$ may be regarded as independent of θ until $\rho/b = 0.990$ it follows that:

$$\Delta\sigma_c(\theta)_{\rho\rho'} = \frac{b^2+\rho^2}{2\rho^2} \cdot \Delta\sigma_c\left(\frac{\pi}{2}\right)_{b\rho'}$$

or that:

$$\Delta\sigma_c(\theta)_{\rho\rho'} = E' \cdot \frac{b^2+\rho^2}{2\rho^2} \cdot \Delta\ell\varrho\left(\frac{\pi}{2}\right)_{b\rho'}$$

so that:

$$\sigma_c'(\theta) = E' \cdot \frac{b^2+\rho^2}{2\rho^2} \sum_{\rho'=a\to\rho} \Delta\ell\varrho\left(\frac{\pi}{2}\right)_{b\rho'}$$

or:

$$\sigma_c'(\theta) = E' \cdot \frac{b^2+\rho^2}{2\rho^2} \cdot \ell\varrho\left(\frac{\pi}{2}\right)_{b\rho} \quad \text{.....5.11.}$$

Using equation 5.05 it follows that:

$$\sigma_c(\theta) = E' \left[\left(\frac{b^2-\rho^2}{2\rho}\right) \cdot \frac{\Delta\ell\varrho\left(\frac{\pi}{2}\right)_{b\rho}}{\Delta\rho} - \left(\frac{b^2+\rho^2}{2\rho^2}\right) \cdot \ell\varrho\left(\frac{\pi}{2}\right)_{b\rho}\right]$$

$\Delta\rho \to 0$ .....5.12.

and by similar reasoning it may be shown that:

$$\sigma_R(\theta) = E' \left[\frac{b^2-\rho^2}{2\rho^2} \cdot \ell\varrho\left(\frac{\pi}{2}\right)_{b\rho}\right] \quad \text{.....5.13.}$$

The curve for the surface stress parameter $\ell\varrho\left(\frac{\pi}{2}\right)_{b\rho}$ was obtained by multiplying $\ell\varrho_m$ by the factor $F_b(\rho/b, \frac{\pi}{2}) / F_m$. A plot of $F_b(\rho/b, \frac{\pi}{2})/F_m$ v ρ/b is shown in fig.141, and the corrected curve for $\ell\varrho_m$ is shown dotted in fig.133. The residual stress distributions are shown in figs.142,143. $\sigma_R(\theta)$ is clearly negligibly small in comparison to $\sigma_c(\theta)$.

To obtain the undisturbed circumferential residual stresses which existed in the uncut tubing, the 'type B'

residual stresses must be determined, using equation 4.10, and superimposed.

5.05. CONCLUSIONS.

Measurement of the surface strains produced on removal of uniform internal layers from specimen 3A-1 revealed large circumferential variations in the surface stress parameters ℓ_{bp} and ℓ_{bp} . The variations in longitudinal surface stress were found to be the cumulative result of relatively small variations in the residual stress at the same angular position in successive layers, while the variations in circumferential surface stress appeared to be due largely to elastic pre-buckling deformations. The longitudinal surface stress distribution was found to be symmetrical about the axis of symmetry of the eccentric cross-section, which suggests some connection between misalignment during drawing and the variations of $\sigma_L(\theta)$. In the case of the circumferential surface stresses, the form of the 'buckling base-line' was shown to be directly attributable to the effect of specimen eccentricity.

On the whole, the effect of eccentricity, and its increase on layer removal, on the determination of the residual stresses was small for ρ/b less than 0.980 (figs. 56, 128).

The approximate methods used to determine the

'type A' residual stresses σ_L , σ_C and σ_R suggested that all three were substantially independent of θ in the tubing tested.

Despite the large amount of information obtained about the overall deformation changes on layer removal, it is clear that the Sachs method is of limited usefulness for the determination of local circumferential variations of the 'type A' residual stresses in tubing. Its main disadvantages are lack of selectivity, and sensitivity; i.e. material is removed from the whole circumference rather than from one specific angular position, and the whole cylinder is deformed rather than just one specific part.

The method discussed in the next section does not suffer from these disadvantages, and may also be applied to tubing with a higher degree of eccentricity.

SECTION 6.

AN ALTERNATIVE APPROACH TO THE DETERMINATION OF 'TYPE A' RESIDUAL STRESSES IN ECCENTRIC TUBING.

6.01. INTRODUCTION.

The bending deflection method has certain advantages over the Sachs method in the determination of longitudinal residual stress in eccentric tubing, but its usefulness is restricted since no satisfactory method of determining the coexistent circumferential residual stress is available.

In the present section, the problems involved in the determination of circumferential residual stress in the presence of eccentricity are examined, and a method incorporating a recently developed technique for the determination of local residual stress (91,100) is shown to overcome them.

6.02. BENDING DEFLECTION METHODS FOR THE DETERMINATION OF RESIDUAL STRESS.

The bending deflection method for the determination of residual stress (63-95) is the usual alternative to the Sachs technique in the case of thin-walled tubing, where σ_R may be neglected in comparison to σ_L and σ_C. The method is based (fig.144a) on the measurement of ΔD_o, the change in diameter on slitting a specimen longitudinally (for circumferential stresses), and of $\Delta\left(\frac{1}{R}\right)_o$, the change in curvature of a thin longitudinal strip cut from the specimen (for longitudinal stresses). From these and subsequent measurements

(fig.144b) of diameter $\Delta D_1 \ldots\ldots \Delta D_n$, and curvature $\Delta\left(\frac{1}{R}\right)_1 \ldots\ldots\ldots \Delta\left(\frac{1}{R}\right)_n$ after layer removal from one surface of the slit specimen and strip, it is possible to estimate the residual stresses originally present in the tubing.

In common with the Sachs technique, the method depends on the following assumptions; that the tubing is isotropic and of uniform wall thickness, and that the residual stresses are distributed axisymmetrically.

Since the slit specimen and the thin longitudinal strip are much more flexible than an untouched specimen, the method offers a greater response for the removal of a given layer than the Sachs technique.

Davidenkov's method (76) was the first bending deflection method which made possible the complete determination of residual stresses in tubing. Earlier workers (73-75) had only considered the deformations ΔD_o and $\Delta\left(\frac{1}{R}\right)_o$, and not the effects of layer removal.

Denoting the circumferential and longitudinal residual stresses at position ρ by S_c and $\hat{S}_L$, Davidenkov's equations were:

$$S_c = S_{c1} + S_{c2} + S_{c3} \quad \ldots\ldots\ldots 6.01.$$

$$\hat{S}_L = \hat{S}_{L1} + \hat{S}_{L2} + \hat{S}_{L3} \quad \ldots\ldots\ldots 6.02.$$

where S_{c1} and $\hat{S}_{L1}$ were the stresses relieved by slitting or cutting-out (the so-called residual bending stresses), S_{c3} and $\hat{S}_{L3}$ were the stresses relieved at

position ρ by removal of material up to ρ and S_{C2} and $\hat{S}_{L2}$ were the stresses relieved when the layer, thickness $\Delta\rho$, at ρ was removed. It is sufficient for the purposes of the present section to refer to the above general equations. Specific formulae will be quoted where necessary in later sections.

Sachs and Espey (77) modified Davidenkov's expressions to effect an improvement in computation time, although this has since been disputed by Knights (82).

$$S_c = S_{cA} + S_{cB} + S_{cC} + S_{cD} \quad \text{---------6.03}$$

$$\hat{S}_L = \hat{S}_{LA} + \hat{S}_{LB} + \hat{S}_{LC} + \hat{S}_{LD} \quad \text{---------6.04}$$

The stress components S_A and S_B corresponded to Davidenkov's components S_1 and S_2 , while the stress components S_C and S_D represented the direct and bending components of S_3 . This rather artificial subdivision has attracted some criticism (90).

In the method of cutting-out the thin strips for longitudinal residual stress determination (fig.145) the longitudinal strain ε_L is constrained to be zero during the first two cuts. Since the circumferential residual stress in the thin strip is completely relieved by these cuts, a reduction in the longitudinal residual stress of $\mu.\sigma_c$ must occur. The methods of both Davidenkov and Sachs and Espey failed to account for this effect, so that each of the stress components $\hat{S}$ in equations 6.02 and 6.04 must be increased in value by μ x the corres-

ponding circumferential stress component. This error was first noticed by Knights (82) and subsequently by others (89,90). The corrected equations are:

$$S_L = S_{L1} + S_{L2} + S_{L3} \quad \text{---------- 6.05.}$$

where:

$$S_{L1} = \hat{S}_{L1} + \mu . S_{C1}$$
$$S_{L2} = \hat{S}_{L2} + \mu . S_{C2}$$
$$S_{L3} = \hat{S}_{L3} + \mu . S_{C3}$$

and:

$$S_L = S_{LA} + S_{LB} + S_{LC} + S_{LD} \quad \text{-------6.06.}$$

where:

$$S_{LA} = \hat{S}_{LA} + \mu . S_{CA}$$
$$S_{LB} = \hat{S}_{LB} + \mu . S_{CB}$$
$$\text{.....etc.....}$$

The Davidenkov theory as represented by equations 6.01 and 6.05 , has been generally accepted as the most fundamental of the bending deflection methods, although Denton and Alexander (90) have recently indicated three additional (minor) sources of error.

It is interesting to note the similarity in the reasoning behind the definition of the stress components in equations 6.01 and 6.05 , and the definition of the stress components in appendix 3 . A distinction should however be made between the component σ' , which has been defined in the present work as the stress induced at radius ρ , and the components S_1 and S_3 , which were defined by Davidenkov as the stresses relieved at radius ρ .

Over the years, several workers (75,77,82,87) have observed what has become known as the 'length effect' in the determination of circumferential residual stress from the changes in diameter on slitting and subsequent layer removal. Starting with a short specimen and progressively increasing the length, the diameter changes were found to increase approximately linearly with the ratio of length/diameter. Above a certain 'critical' value of this ratio the diameter changes were found to remain constant. Although it has long (87) been realised that longitudinal residual stresses were in some way involved, only recently has a satisfactory explanation for the effect emerged.

Denton (90) explained the apparently reduced values of circumferential stress in short specimens by suggesting that, during parting-off, the circumferential strain ε_c or the longitudinal curvature in the vicinity of the end-face (fig.146) was in some way constrained to be zero. Since:

$$\varepsilon_c = \frac{1}{E}(\sigma_c - \mu.\sigma_L)$$

the complete relief of the longitudinal residual stress σ_L would therefore result in a reduction of the circumferential stress in the short specimen by an amount $\mu.\sigma_L$. In other words, if the residual stresses originally present in the long tube were σ_L and σ_c, there would be residual stresses of $\sigma_c - \mu.\sigma_L$ in the circumferential direction, and zero in the longitudinal direction, in the short specimen.

Although the above explanation might perhaps apply

to thick-walled tubing, it has already been shown in section 4.02 that considerable longitudinal curvature or circumferential strain is produced on relief of σ_L in thin-walled tubing. A more satisfactory explanation of the 'length effect' in terms of the occurrence rather than the prevention of longitudinal (anticlastic) curvature in short specimens has recently been provided by Pomeroy (107).

Using the theory of beams on an elastic foundation it may be shown that the mean value of the longitudinal or anticlastic curvature adopted by a thin tube due to the relief of the longitudinal residual stress σ_L at both end-faces is:

$$K_m = \frac{2M_L}{B\ell . EI}\left(\frac{\cosh B\ell - \cos B\ell}{\sinh B\ell + \sin B\ell}\right)$$

$$= \frac{M_L}{EI} . f(B\ell)$$

where M_L is the moment of the longitudinal residual stress, ℓ is the tube length, $B^4 = 3(1-\mu^2)/R_m^2 h^2$ and $f(B\ell)$ is the average moment function.

This curvature effectively stiffens a slit tube against circumferential bending deformations, and the bending moment M_c applied by the relief of the circumferential residual stress is effectively reduced to:

$$M_c - \mu . M_L . f(B\ell) \quad \text{---------- 6.07.}$$

Fig.147 shows a plot of the average moment function $f(B\ell)$ against $B\ell$, and it is clear that for $B\ell$ less than 1 the applied moment becomes:

$$M_C - \mu . M_L$$

so that the circumferential stress in the short specimen is apparently reduced to:

$$\sigma_c - \mu . \sigma_L$$

For $B\ell$ greater than 20 the slope of the curve for $f(B\ell)$ becomes small and might well be called zero. Since the absolute value of $f(B\ell)$ is also small in this region, experimental estimates of the circumferential residual stress might well appear to be constant and equal to σ_c.

In order to minimise the effect of anticlastic curvature on the measurement of circumferential residual stress, a specimen with $B\ell$ greater than 30 would appear to be essential. For thin-walled tubing (R_m/h greater than 11), ℓ should therefore be at least $3.5D_m$, and for tubing with R_m/h = 16.5 (as used in sections 4 and 5), ℓ should be at least $3D_m$.

6.03. THE BENDING DEFLECTION METHOD IN THE PRESENCE OF ECCENTRICITY.

In the case of eccentric tubing, all the stress components in equations 6.01 and 6.05 may vary in the

circumferential as well as in the radial direction, so that:

$$S_c(\theta) = S_{c1}(\theta) + S_{c2}(\theta) + S_{c3}(\theta) \quad \text{-----6.08.}$$

$$S_L(\theta) = S_{L1}(\theta) + S_{L2}(\theta) + S_{L3}(\theta) \quad \text{------6.09.}$$

Only Knights (82) has considered the effect of specimen eccentricity on the determination of residual stress by the bending deflection method. A discussion of the more important features of his work occupies the remainder of this section.

It is assumed throughout that R_m/h_θ is greater than 11 , so that simple bending theory may be used for the analysis of circumferential bending deformations (96,97).

(a) Circumferential bending stress $S_{c1}(\theta)$.

Since the circumferential bending moment M_c released on slitting an eccentric tube must, from static equilibrium, be independent of the angular position of the slot, the surface values of the circumferential bending stress at any position θ may be determined directly from the expression:

$$\sigma_c = \pm \frac{6M_c}{l.h_\theta^2} \quad \text{----------6.10.}$$

which follows from simple bending theory. Since $S_{c1}(\theta)$ may be assumed to be linearly distributed through the wall thickness (96) the determination of the circum-

ferential bending stress at any depth is an easy matter, once the value of M_c has been determined from the measured changes in diameter or gap-width on slitting, (in practice the change in gap-width is taken as the relative displacement of two reference marks on either side of the slitting position).

Knights found by an investigation of the effect of different positions for slitting and for deflection measurement that the difference between the surface value of $S_{c1}(\frac{\pi}{2})$ and the surface value of S_{c1}, the bending stress calculated by assuming that the eccentric tube had a uniform wall thickness h_m, was a minimum when the slot was made at mean wall thickness and the deflection was measured on the diameter perpendicular to the plane of slitting, as shown in fig.148. In fact, for this particular case, Knights showed that:

$$\frac{\text{SURFACE VALUE OF } S_{c1}(\pi/2)}{\text{SURFACE VALUE OF } S_{c1}} = (1-e^2)^2$$

By using the expression 6.10, this equation may be rewritten:

$$\frac{M_c}{M_{cm}} = (1-e^2)^2 \qquad \text{---------- 6.11.}$$

where M_{cm} is the value of the bending moment calculated by assuming that the tube wall thickness is uniform and equals h_m.

It may easily be shown using equation 6.11 that for e less than 0.07 the effect of eccentricity on the

calculation of M_c (and therefore on the calculation of $S_{c1}(\theta)$) is negligible.

For any other slitting position or measurement position, the effect of eccentricity is more pronounced, and must be taken into account or serious errors will result.

(b) The stress component $S_{c2}(\theta)$.

By assuming that $S_{c2}(\theta)$ was independent of θ in tubing with e less than 0.05 , Knights found, for the case of internal layer removal, that:

$$\frac{S_{c2}(\theta)}{S_{c2}} = 1 - \frac{e^2 h_m^2}{[h_m - (\rho - a)]^2} \quad \text{------ 6.12.}$$

where the component S_{c2} was calculated without regard to eccentricity.

It may easily be shown using this expression that, for e less than 0.05 , the effect of eccentricity on the determination of the (assumed constant) value of $S_{c2}(\theta)$ is negligible, provided $\rho - a$ does not exceed $0.5 h_m$, i.e. provided the common practice of etching duplicate specimens in opposite directions is adopted.

(c) The stress component $S_{c3}(\theta)$.

By a similar argument to that used in (b) , Knights concluded that the stress component $S_{c3}(\theta)$ could be

assumed to be independent of θ and equal to S_{c3}, the value calculated by assuming the specimen had the uniform wall thickness h_m, provided e was less than 0.05 and $\rho - a$ did not exceed $0.5 h_m$, (for the case of internal layer removal).

(d) Circumferential residual stress $S_c(\theta)$ in specimens with e less than 0.05.

Provided the processes of slitting and deflection measurement are carried out as indicated in fig.148, and the total thickness of the material removed does not exceed 50% of the wall thickness, the stress components $S_{c1}(\theta)$, $S_{c2}(\theta) = S_{c2}$ and $S_{c3}(\theta) = S_{c3}$ may be calculated without regard to the effects of eccentricity, and equation 6.08 may be rewritten:

$$S_c(\theta) = S_{c1}(\theta) + S_{c2} + S_{c3}$$

Formulae for the various stress components in terms of the changes in diameter on slitting and subsequent layer removal may be found in ref.82.

(e) Longitudinal residual stress $S_L(\theta)$.

The corrected Davidenkov strip method for the determination of longitudinal residual stress has the considerable advantage that a small region of the circumference is isolated and examined, thus avoiding the longitudinal shear effects which may arise on layer removal from eccentric tubing (section 5.03).

If a thin longitudinal strip is cut out at position θ in the manner indicated in figs.145,149 , the longitudinal residual stress $\hat{S}_L(\theta)$ may be determined from equation 6.02 :

$$\hat{S}_L(\theta) = \hat{S}_{L1}(\theta) + \hat{S}_{L2}(\theta) + \hat{S}_{L3}(\theta)$$

It is necessary to assume that the residual stresses are independent of θ within the limits of the thin strip, and that the cross-section of the strip is rectangular. Since the dimension s can be made very small and R_m/h_θ is large, these are reasonable assumptions.

The original Davidenkov formulae for $\hat{S}_{L1}$, $\hat{S}_{L2}$ and $\hat{S}_{L3}$ in terms of the change in longitudinal curvature of the strip (82) may easily be modified for the effects of eccentricity by replacing the uniform wall thickness h by the local wall thickness h_θ . So that the determination of $\hat{S}_L(\theta)$ is relatively straightforward, even in specimens with e greater than 0.05 .

Unfortunately, the longitudinal stress originally present at position θ must be calculated from the equation:

$$S_L(\theta) = \hat{S}_L(\theta) + \mu . S_c(\theta) \quad \text{.....6.13.}$$

which follows from equation 6.05 .

The appearance of the circumferential stress $S_c(\theta)$ in this equation restricts the method to tubing with e less than 0.05 .

(f) Conclusions.

The method outlined in (a)-(e) may be used for the determination of residual stresses in eccentric tubing, provided the tubing is nearly-concentric (e less than 0.05), the stress component $S_{c1}(\theta)$ is measured as indicated in fig.148 , the stress components $S_{c2}(\theta)$ and $S_{c3}(\theta)$ can be assumed to be independent of θ , and the layer removal process does not take place beyond a depth of $0.5h_m$.

In the determination of circumferential residual stress, the method suffers from the same disadvantages as the Sachs technique, since $S_{c2}(\theta)$ and $S_{c3}(\theta)$ must both be assumed to be independent of θ for $\rho - a$ less than $0.5h_m$. Although this is well supported by the experimental results obtained from specimen 3A-1 , for which e = 0.06 , it is unlikely to be the case in tubing with a higher degree of initial eccentricity.

In the determination of longitudinal residual stress the method is potentially applicable to tubing with e greater than 0.05 , although the problem of determining $S_c(\theta)$ in such tubing must first be overcome.

A method for the determination of local values of circumferential residual stress in tubing with a high degree of initial eccentricity is developed in the remainder of this section. The method is based on a technique proposed by Denton (72,91,100) for the deter-

mination of local residual stress.

6.04. THE IMPORTANCE OF SEREBRENNIKOV'S METHOD.

It has already been noted that the major advantage of the corrected Davidenkov strip method lies in the fact that a small region of the circumference of the specimen may be isolated and examined. The method of Serebrennikov (101) for the determination of longitudinal residual stress in small diameter shafts, offers a similar advantage.

With the object of ultimately controlling production stresses Serebrennikov showed that the local value of the longitudinal surface stress in small diameter shafts could be determined by etching a shallow longitudinal groove or channel at the position where the stress value was required (fig.150a). In shafts where the length/diameter ratio exceeded 15 the stress which existed in the removed material was determined from the lateral deflection of the shaft at the mid-point of the groove, and in shafts with a smaller length/diameter ratio, from the relative angular deflection of the ends of the shaft (figs.150b,c).

Although Serebrennikov's technique is not applicable to the determination of residual stress in thin-walled tubing, his method of stress relief by groove-cutting is of particular interest. Since only the section of the residually-stressed body beneath the groove is deformed (figs.150b,c) the shape of the rest of the body has no

effect on the residual stress calculation.

The determination of the circumferential stress components $S_{c2}(\theta)$ and $S_{c3}(\theta)$ in tubing with a high e value may therefore be carried out by slitting the tubing (to release the residual bending stress $S_{c1}(\theta)$) then cutting and gradually deepening a narrow longitudinal groove at the position θ (fig.151) while monitoring the change in curvature of the section BC . The variation in the wall thickness over the sections AB and CD need not be considered.

6.05. A METHOD FOR THE DETERMINATION OF 'TYPE A' CIRCUMFERENTIAL RESIDUAL STRESS IN TUBING WITH e GREATER THAN 0.1.

(a) Preliminary assumptions.

(i) The material of the tubing is isotropic and only elastic strains are produced by slitting and layer removal.

(ii) The specimens are sufficiently long to avoid the 'length effect' described in section 6.02 .

(iii) The 'type B' residual stresses in the specimens have been completely relieved by cutting-out, and predetermined by the method outlined in section 4.05 .

(iv) The tubing is sufficiently thin for radial stress

to be neglected and the ratio of R_m/h_θ large enough (greater than 11 for all θ) to make the use of curved bar theory unnecessary in the calculation of circumferential bending deflections. So that, for small strains (less than 2%), plane sections will remain plane and the strain in any fibre will be proportional to the distance from the neutral axis (96,97,104).

(v) The techniques employed for cutting, slitting and layer removal are stress free or introduce only stresses which are consistently predictable.

(b) Definition of the stress components.

The circumferential residual stress $\sigma_c(\theta)_n$ in the n^{th} layer (counting from the outer surface) of a specimen of tubing with e greater than 0.1 may be determined in two parts:

$$\sigma_c(\theta)_n = \sigma_{c1}(\theta)_n + \sigma_{c2}(\theta)_n \quad \text{---------- 6.14.}$$

where $\sigma_{c1}(\theta)_n$ is the residual bending stress relieved in the n^{th} layer by a longitudinal slot ($\equiv S_{c1}(\theta)$), and $\sigma_{c2}(\theta)_n$ is the stress remaining in the n^{th} layer after slitting ($\equiv S_{c2}(\theta) + S_{c3}(\theta)$).

(c) Determination of the circumferential bending stress $\sigma_{c1}(\theta)_n$.

The stress component $\sigma_{c1}(\theta)_n$ is calculated from the deformations ΔD_o or ΔG_o which occur when the

specimen is slit along a generator (fig.152).

(i) The first stage in the calculation is the determination of $\sigma_{c1}(\theta)_n$ in terms of M_c the bending moment released on slitting.

Since the ratio R_m/h_θ is large, $\sigma_{c1}(\theta)_n$ may be assumed to vary linearly through the wall thickness (fig.153). If the depth from the outer surface to the mid-point of the n^{th} layer is denoted by d_n then:

$$\sigma_{c1}(\theta)_n = \left(\frac{h_\theta - 2d_n}{h_\theta}\right) \sigma_{c1}(\theta)_b \quad \text{------- 6.15.}$$

where $\sigma_{c1}(\theta)_b$ denotes the bending stress relieved at the outer surface.

Taking moments which tend to decrease curvature as positive (fig.152) it may be shown from simple bending theory that:

$$\sigma_{c1}(\theta)_b = \frac{6M_c}{l.h_\theta^2} \quad \text{---------- 6.16.}$$

i.e. the relief of tensile residual stress in the outer fibres by slitting, produces a decrease in curvature.

It follows from equation 6.15 that:

$$\sigma_{c1}(\theta)_n = \frac{6M_c}{l}\left(\frac{h_\theta - 2d_n}{h_\theta^3}\right) \quad \text{---------- 6.17.}$$

(ii) The second stage in the calculation is the determination of M_c in terms of the deformations ΔD_o or ΔG_o

which occur on slitting.

Since M_c is independent of θ (section 6.03a) and can be determined by slitting along any generator, the slitting position can be chosen to satisfy particular requirements; Knights, for example, found for nearly-concentric tubing that the effect of eccentricity on the calculation of M_c could be neglected when the slit was made at mean wall thickness.

Since the effect of eccentricity cannot be neglected in the present discussion, a different criterion can be used to select the most suitable slitting position. From the point of view of mathematical simplicity, the three most suitable slitting positions are at maximum, minimum and mean wall thickness, as shown in fig.154 , (it is assumed that the centre distance c is so small that mean wall thickness occurs at $\theta = \pi/2$). Since the bending moment produced in each case is the same, the most useful criterion for selecting the best position of the three, is the relative magnitude of the deformations which occur on slitting.

Taking the change in diameter perpendicular to the plane of each slot as the basis for comparison and denoting it by ΔD_{00} , $\Delta D_{0\pi}$ and $\Delta D_{0\pi/2}$ respectively, it may be shown (appendix 4) using Castigliano's theorem that:

$$\Delta D_{oo} = \frac{24 M_c . R_m^2}{E' . l . h_m^3 (1-e^2)^2}\left\{1 + \frac{e^2}{2} + \frac{3e}{(1-e^2)^{1/2}}\left[\frac{\pi}{2} - \tan^{-1}\frac{(1-e^2)^{1/2}}{1+e}\right]\right\}$$

------6.18.

$$\Delta D_{o\pi} = \frac{24 M_c . R_m^2}{E' . l . h_m^3 (1-e^2)^2}\left\{1 + \frac{e^2}{2} - \frac{3e}{(1-e^2)^{1/2}}\left[\tan^{-1}\frac{(1-e^2)^{1/2}}{1+e}\right]\right\}$$

------6.19.

$$\Delta D_{o\pi/2} = \frac{24 M_c . R_m^2}{E' . l . h_m^3 (1-e^2)^2}$$

----------6.20.

The factor $E' = \frac{E}{1-\mu^2}$ appears in the above expressions due to the suppression of anticlastic (longitudinal) curvature at the centre of the long (approx. $3{\cdot}5 D_m$) specimens.

By substitution of numerical values it may easily be shown that:

$$\Delta D_{o\pi} < \Delta D_{o\pi/2} < \Delta D_{oo}$$

for $0 < e < 1$

i.e. the greatest change in diameter is produced by slitting along the generator at maximum wall thickness.

It may similarly be shown for the change in gap-width ΔG_o that:

$$\Delta G_{o\pi} < \Delta G_{o\pi/2} < \Delta G_{oo}$$

for $0 < e < 1$

Since ΔG_o will always be greater than ΔD_o (intuitively obvious) the maximum deflection for a given applied moment will occur at the slot, on slitting at maximum wall thickness.

It may be shown (appendix 4) that:

$$\Delta G_{oo} = \frac{24.M_c R_m^2}{E'.l.h_m^3(1-e^2)^2}\left[\frac{(1+e)(2+e)}{(1-e^2)^{1/2}}.\frac{\pi}{2}\right] \qquad \text{--------6.21.}$$

Knights (82) quotes the following simplified formulae for ΔD_{oo} and ΔG_{oo} , without proof:

$$\Delta D_{oo} = \frac{24.M_c R_m^2}{E'.l.h_m^3}\left(1+\frac{3\pi e}{4}+e^2\right)$$

$$\Delta G_{oo} = \frac{24.M_c R_m^2}{E'.l.h_m^3}\pi\left(1+\frac{3}{2}e+3e^2\right)$$

The accuracy of these expressions deteriorates rapidly for e greater than 0.05 , and where e is greater than 0.10 , it is necessary to use equation 6.18 or equation 6.21 to determine M_c .

Using equations 6.17 , 6.18 and 6.21 , the circumferential bending stress at any angle θ and depth d_n is given by:

$$\sigma_{c1}(\theta)_n = \frac{E'(h_\theta-2d_n)h_m^3.\Delta D_{oo}}{4R_m^2.h_\theta^3}\left\{\frac{(1-e^2)^2}{1+\frac{e^2}{2}+\frac{3e}{(1-e^2)^{1/2}}\left[\frac{\pi}{2}-\tan^{-1}\frac{(1-e^2)^{1/2}}{1+e}\right]}\right\}$$

$$= \frac{E'(h_\theta-2d_n)h_m^3.\Delta G_{oo}}{4R_m^2.h_\theta^3}\left[\frac{2(1-e^2)^{5/2}}{\pi(1+e)(2+e)}\right] \qquad \text{--------6.22.}$$

The exact solution to this problem has been obtained by Mori (103) using bipolar co-ordinates. For R_m/h_θ large and h_θ small, the expressions 6.22 are satisfactory.

(iii) The error produced by neglecting the effect of eccentricity in the calculation of M_c when the slot is made at maximum wall thickness.

If M_m is the value of M_c calculated by neglecting the effect of eccentricity, then from equations 6.18,6.21:

$$\frac{M_c}{M_m} = \frac{(1-e^2)^2}{1+\frac{e^2}{2}+\frac{3e}{(1-e^2)^{1/2}}\left[\frac{\pi}{2}-\tan^{-1}\frac{(1-e^2)^{1/2}}{1+e}\right]}$$

when the change in diameter ΔD_{oo} is measured, and:

$$\frac{M_c}{M_m} = \frac{2(1-e^2)^{5/2}}{(1+e)(2+e)}$$

when the change in gap-width ΔG_{oo} is measured.

Table 11 indicates that substantial errors are produced in both cases if the effect of eccentricity is neglected.

(d) Determination of the stress component $\sigma_{c2}(\theta)_n$.

The inadequacy of conventional methods for the determination of the stress component $\sigma_{c2}(\theta)_n$ $(\equiv S_{c2}(\theta)+S_{c3}(\theta))$ when the initial eccentricity e exceeds 0.05 has already been discussed in section 6.03 . The technique described in this section has the twofold advantage that circumferential variations of this stress component may be investigated without regard to the initial eccentricity of the specimen or the increase in eccentricity which occurs on layer removal.

The specimen under examination is slit longitudinally and the circumferential bending stresses determined as described in section (c) . The fact that the specimen may have considerable eccentricity may be disregarded in the remainder of the investigation.

The stress within a small arc of the circumference of the specimen is determined from the deformations produced by cutting, and gradually deepening, a rectangular groove along the entire length of a generator (fig.151). Since only that part of each layer lying within the limits of the arc s is removed when the groove is deepened, an estimate of the local circumferential stress in each layer is obtained. It must be assumed that the stress component $\sigma_{c2}(\theta)_n$ is independent of length, and is independent of θ over the arc BC . The arc-length s should therefore be small (about $4h_\theta$). It is also assumed that the effect of lateral (longitudinal) curvature produced by the complete relief of longitudinal residual stress at the end-faces, is negligible in the long (approx. $3{\cdot}5D_m$) specimens.

Provided it can be assumed that the region of deformation on layer removal is confined to the section BC , the sections AB and CD can be considered as rigid lever arms which magnify the relative angular rotation of the sides of the groove. Under these circumstances, the deformation of the section BC may be determined from the changes in gap-width on layer removal.

Since R_m/h_θ is large the section of the tube wall beneath the groove after the removal of n layers, may be considered as a simple rectangular beam of length s, depth t_n and breadth ℓ (fig.155) and simple bending theory of the type: $\frac{1}{R} = \frac{M}{E'I}$ may be used to determine the stresses released on layer removal (100).

The stress remaining at the position θ in the n^{th} layer after slitting is calculated in two parts:

$$\sigma''(\theta)_n = \sigma_{c2}(\theta)_n + \sigma'(\theta)_n \qquad \text{-------6.23}$$

where $\sigma''(\theta)_n$ denotes the stress at position θ in the n^{th} layer when it is removed, and $\sigma'(\theta)_n$ is the stress induced at position θ in the n^{th} layer by the removal of the $n-1$ previous layers.

(i) Determination of $\sigma''(\theta)_n$.

Fig.156 shows a groove cut at the angle θ from maximum wall thickness. $\delta\psi(\theta)_n$ is the small angle turned through by the sides of the groove on removal of the n^{th} layer, thickness Δt_n, containing the stress $\sigma''(\theta)_n$.

Provided it can be assumed that only the material under the groove is deformed by layer removal, the edges of the slot at A and D remain at a constant distance from the point P and are deflected by $\delta_A(\theta)_n$ and $\delta_D(\theta)_n$ in the directions shown.

Increase in gap-width is taken as positive in accordance with the sign convention adopted in section (c).

It is clear from fig.156 that:

$$\delta_A(\theta)_n \propto z_A \quad \text{and} \quad \delta_D(\theta)_n \propto z_D \quad \text{for all} \quad \theta \ .$$

By fitting rigid extensions (91,100) on both edges as shown in fig.157 it is possible to arrange that:

$$z_A = z_D = z \quad \text{for all} \quad \theta \ ,$$

and for this case:

$$\delta_A(\theta)_n = \delta_D(\theta)_n = \delta(\theta)_n$$

If the overall increase in gap-width on removal of the n^{th} layer is $\Delta G(\theta)_n$ then:

$$\Delta G(\theta)_n = 2\,\delta(\theta)_n \cdot \cos\phi \qquad \text{------ 6.24.}$$

where: $\phi = 180^\circ - (\theta + \alpha)$

If the change in curvature of the material beneath the groove on removal of the n^{th} layer is denoted by $\Delta\left(\frac{1}{R}\right)_n$ then using simple bending theory:

$$\Delta\left(\frac{1}{R}\right)_n = -\frac{M_c(\theta)_n}{E' \cdot I_c(\theta)_n} \qquad \text{------- 6.25.}$$

where $M_c(\theta)_n$ is the circumferential bending moment applied to the section BC due to the removal of the layer of thickness Δt_n containing the stress $\sigma''(\theta)_n$ (fig.158), and $I_c(\theta)_n$ is the moment of inertia of the cross-section at B (or C) after removal of the n^{th} layer. E' is used due to the suppression of lateral (anticlastic) curvature of the material beneath the groove

in the long specimen, and the minus sign results from the fact that positive moments cause a decrease in curvature.

Since only direct strain is produced by the release of the longitudinal stress $\sigma_L(\theta)_n$ in the removed layer, it has no effect on the circumferential curvature between B and C or on the change in gap-width, and can therefore be neglected in this instance.

If all deflections are small, it follows from fig.159 that:

$$\Delta\left(\frac{1}{R}\right)_n = -\frac{2}{s}.\delta\psi(\theta)_n$$

where the minus sign results from the fact that an increase in ψ causes a decrease in curvature.

Since: $$\delta(\theta)_n = z.\delta\psi(\theta)_n$$

it follows that:

$$\Delta\left(\frac{1}{R}\right)_n = -\frac{2\,\delta(\theta)_n}{z.s}$$

and using equation 6.24 gives:

$$\Delta\left(\frac{1}{R}\right)_n = -\frac{\Delta G(\theta)_n}{z.s.\cos\phi} \qquad \text{--------6.26.}$$

The bending moment applied to the section BC on removal of the n^{th} layer is given by:

$$M_c(\theta)_n = -\frac{1}{2}\sigma''(\theta)_n . \Delta t_n . \ell . (t_n + \Delta t_n)$$

where ℓ is the specimen length. The minus sign results from the fact that removal of a layer containing tensile residual stress produces an increase in curvature of the material beneath the groove, or a decrease in gap-width.

Using equations 6.25 and 6.26 gives:

$$\sigma''(\theta)_n = -\frac{2E' . I_c(\theta)_n . \Delta G(\theta)_n}{\Delta t_n . (t_n + \Delta t_n) \ell . z . S . \cos\phi} \quad ----6.27.$$

for all n .

This equation may be used for the determination of the stress component $\sigma''(\theta)_n$ at any angle θ provided the angle ϕ and the length z can be determined accurately, and provided the initial groove-width S is held constant during the layer removal process.

It should be pointed out that a direct force $P_c(\theta)_n = \sigma''(\theta)_n . \ell . \Delta t_n$ is also applied to the section BC on removal of the n^{th} layer. The effect on the gap-width of the resultant change in length is however small in comparison to the magnified effect of the curvature change, and may be neglected.

(ii) Determination of $\sigma'(\theta)_n$.

$\sigma'(\theta)_n$ is the stress induced at position θ in the n^{th} layer by removal of the $n-1$ previous layers.

From equation 6.27 the stress released by removal of the first layer of thickness Δt_1 (fig.160) is given by:

$$\sigma''(\theta)_1 = \frac{-2E'.I_c(\theta)_1.\Delta G(\theta)_1}{\Delta t_1(t_1+\Delta t_1)\ell.z.S.\cos\phi}$$

$\sigma'(\theta)_{n1}$, the stress induced in the n^{th} layer by removal of the first layer, is calculated in two parts:

$$\sigma'(\theta)_{n1} = \sigma'_p(\theta)_{n1} + \sigma'_M(\theta)_{n1} \quad \text{.....6.28.}$$

where $\sigma'_p(\theta)_{n1}$ is the direct stress induced in the n^{th} layer and $\sigma'_M(\theta)_{n1}$ is the bending stress induced in the n^{th} layer.

The removal of the layer of thickness Δt_1 containing the stress $\sigma''(\theta)_1$ is equivalent to the application of a force $P_c(\theta)_1$ and a moment $M_c(\theta)_1$ to the material beneath the groove, where:

$$P_c(\theta)_1 = \sigma''(\theta)_1.\Delta t_1.\ell$$

$$M_c(\theta)_1 = -\tfrac{1}{2}.\sigma''(\theta)_1.\Delta t_1.\ell(t_1+\Delta t_1)$$

the minus sign occurs because moments which cause a decrease in curvature are taken as positive.

The direct stress induced in the n^{th} layer is given by: $\frac{P_c(\theta)_1}{\ell t_1}$, so that:

$$\sigma'_p(\theta)_{n1} = \sigma''(\theta)_1.\frac{\Delta t_1}{t_1}$$

The bending stress induced in the n^{th} layer is given by: $\frac{-M_c(\theta)_1.z_1}{I_c(\theta)_1}$, where $z_1 = h_\theta - d_n - \frac{t_1}{2}$

is the distance from the mid-point of the n^{th} layer to the nuetral axis (fig.160), so that:

$$\sigma'_M(\theta)_{n1} = \frac{\sigma''(\theta)_1 . \Delta t_1 . \ell (t_1 + \Delta t_1)(h\theta - d_n - \frac{t_1}{2})}{2 I_c(\theta)_1}$$

where $h\theta$ is the local wall thickness and d_n is the depth from the outer surface to the mid-point of the n^{th} layer.

From equation 6.27 the stress released by removal of the second layer of thickness Δt_2 is given by:

$$\sigma''(\theta)_2 = \frac{-2E' . I_c(\theta)_2 . \Delta G(\theta)_2}{\Delta t_2 (t_2 + \Delta t_2) \ell . z . s . \cos\phi}$$

and $\sigma'(\theta)_{n2}$, the stress induced in the n^{th} layer by removal of the second layer, is given by:

$$\sigma'(\theta)_{n2} = \sigma'_p(\theta)_{n2} + \sigma'_M(\theta)_{n2} \quad \text{..... 6.29.}$$

where $\sigma'_p(\theta)_{n2}$ and $\sigma'_M(\theta)_{n2}$ are respectively the direct and the bending stresses induced in the n^{th} layer.

The nuetral axis of bending of the material under the groove will shift due to the removal of the layer of thickness Δt_2 , and in this case:

$$\eta_2 = h\theta - d_n - \frac{t_2}{2}$$

It may easily be shown that:

$$\sigma'_p(\theta)_{n2} = \sigma''(\theta)_2 . \frac{\Delta t_2}{t_2}$$

$$\sigma'_M(\theta)_{n2} = \frac{\sigma''(\theta)_2 . \Delta t_2 . \ell . (t_2+\Delta t_2)(h\theta - d_n - \frac{t_2}{2})}{2 I_c(\theta)_2}$$

If the stresses induced in the n^{th} layer by removal of the 3rd, 4th, 5th, ... $(n-1)^{th}$ layers are denoted by: $\sigma'(\theta)_{n3}$, $\sigma'(\theta)_{n4}$, $\sigma'(\theta)_{n5}$, ... $\sigma'(\theta)_{n\,n-1}$, it is clear that:

$$\sigma'(\theta)_n = \sigma'(\theta)_{n1} + \sigma'(\theta)_{n2} + \ldots\ldots\ldots + \sigma'(\theta)_{n\,n-1}$$

i.e. :

$$\sigma'(\theta)_n = \sum_{r=1\to n-1} \sigma'(\theta)_{nr} \qquad n>1 \qquad \text{----------6.30}$$

or:

$$\sigma'(\theta)_n = \sum_{r=1\to n-1} \left[\sigma'_p(\theta)_{nr} + \sigma'_M(\theta)_{nr} \right] \qquad n>1 \qquad \text{.....6.31}$$

where:

$$\sigma'_p(\theta)_{nr} = \sigma''(\theta)_r . \frac{\Delta t_r}{t_r}$$

$$\sigma'_M(\theta)_{nr} = \frac{\sigma''(\theta)_r . \Delta t_r . \ell (t_r+\Delta t_r)(h\theta - d_n - \frac{t_r}{2})}{2 I_c(\theta)_r}$$

$$\sigma''(\theta)_r = \frac{-2 E' . I_c(\theta)_r . \Delta G(\theta)_r}{\Delta t_r (t_r+\Delta t_r) \ell . z . s \cos\phi}$$

$$d_n = -\frac{1}{2}\Delta t_n + \sum_{r=1\to n} \Delta t_r$$

$$I_c(\theta)_r = \frac{1}{12} \ell . t_r^3$$

and from fig.161 :

$$t_r = h\theta - \sum_{q=1\to r} \Delta t_q$$

so that $\sigma'(\theta)_n$ may be calculated from the measured changes in gap-width $\Delta G(\theta)_1$, $\Delta G(\theta)_2$, ... $\Delta G(\theta)_{n-1}$.

(iii) Simplification introduced by removing layers of equal thickness.

If it can, in some way, be arranged that:

$$\Delta t_1 = \Delta t_2 = \ldots\ldots \Delta t_n = \Delta t$$

equations 6.27 and 6.31 may be simplified considerably, since in this case:

$$t_r = h_\theta - r.\Delta t$$

$$I_c(\theta)_r = \frac{1}{12} l (h_\theta - r.\Delta t)^3$$

$$d_n = (n-\tfrac{1}{2}).\Delta t$$

and:

$$\sigma''(\theta)_r = \frac{-E'.(h_\theta - r.\Delta t)^3.\Delta G(\theta)_r}{6\Delta t\,[h_\theta + (1-r)\Delta t]\,z.S.\cos\phi}$$

so that equation 6.27 becomes:

$$\sigma''(\theta)_n = \frac{-E'.(h_\theta - n.\Delta t)^3.\Delta G(\theta)_n}{6\Delta t\,[h_\theta + (1-n)\Delta t]\,z.S.\cos\phi} \qquad \text{---------- 6.32.}$$

for all n ,

and since:

$$\sigma'_p(\theta)_{nr} = \sigma''(\theta)_r \cdot \frac{\Delta t}{h_\theta - r.\Delta t}$$

$$\sigma'_M(\theta)_{nr} = \frac{\sigma''(\theta)_r.3\Delta t\,[h_\theta + (1-r)\Delta t]\,[h_\theta + (1+r-2n)\Delta t]}{(h_\theta - r.\Delta t)^3}$$

$$\sigma'(\theta)_n = \sum_{r=1\to n-1} \sigma''(\theta)_r \left\{ \frac{\Delta t}{h\theta - r.\Delta t} + \frac{3\Delta t[h\theta+(1-r)\Delta t][h\theta+(1+r-2n)\Delta t]}{(h\theta - r.\Delta t)^3} \right\}$$

$$v(\theta)_n = \sum_{r=1\to n-1} v(\theta)_r \left\{ \frac{\Delta t}{h\theta - r.\Delta t} + \frac{3\Delta t[h\theta+(1-r)\Delta t][h\theta+(1+r-2n)\Delta t]}{(h\theta - r.\Delta t)^3} \right\}$$

$n > 1$ ----------6.33

(iv) Summary of technique.

It has been shown that the stress component $\sigma_{c2}(\theta)_n$ may be calculated from the measured changes in gap-width $\Delta G(\theta)_1$, $\Delta G(\theta)_2$, ... $\Delta G(\theta)_n$ which occur on removal of layers of thickness Δt_1 , Δt_2 , ... Δt_n from a groove at position θ , by using equations 6.23 , 6.27 and 6.31 .

If it can be arranged that the removed layers are of equal thickness, the simplified expressions 6.32 and 6.33 may be used.

The step-by-step method of calculation which has been used is similar to that suggested by Denton (90,100) and subsequently by Pomeroy (98,99) and Hospers and Vogelesang (105). It avoids the errors which may occur if trend curves are used, and may conveniently be carried out on a digital computer.

(e) Application to short specimens.

If the method described in sections (a)-(d) is applied to the determination of the circumferential residual stress in a short specimen in which lateral (longitudinal) curvature can occur freely, E' in equations 6.23 , 6.27 , 6.31 , 6.32 and 6.33 must be replaced by E .

For the particular case of $\theta = \pi$, it follows from fig.157 that $\phi = \alpha$, and equation 6.27 becomes:

$$\sigma''(\pi)_n = \frac{-2E.I_c(\pi)_n.\Delta G(\pi)_n}{\Delta t_n (t_n+\Delta t_n) \ell.z.S\cos\alpha} \quad \text{-----} 6.34.$$

Except for the minus sign which appears to be due to a difference in the sign convention for the changes in gap-width, this equation is equivalent to that quoted (without proof) by Denton (100) for the determination of local residual stress in narrow curved bars of uniform thickness (figs.162,163). Denton also quotes expressions which are equivalent to $\sigma'_\rho(\pi)_{nr}$ and $\sigma'_M(\pi)_{nr}$, but a less general notation is used, and a factor of two is omitted in the denominator of the expression for $\sigma'_M(\pi)_{nr}$.

It should be borne in mind, if the use of short (ℓ less than $3D_m$) specimens is planned, that the presence of longitudinal residual stress in the parent tubing will cause an apparent reduction in the value of the circumferential residual stress, due to the 'length effect'.

(f) The measurement of the changes in gap-width.

The determination of circumferential residual stress by the method described in sections (a)-(d) is complicated by the fact that the changes in gap-width produced by cutting a groove are much smaller than those produced in conventional bending deflection methods, in which layer removal takes place over an entire surface. The measurement technique for $\Delta G(\theta)_1 \ldots\ldots \Delta G(\theta)_n$ must therefore be more sensitive than those usually employed (63-72).

Denton (91,100) employed an inferometric technique to determine the changes in gap-width, in the particular case of $\theta = \pi$ (figs.162,163). The relative deflection of two optical flats was measured by means of a Twyman inferometer. By using $\theta = \pi$ maximum magnification of the bending deformations of the material under the groove was obtained. Readings were found to be repeatable to 2.0×10^{-4}mm , with normal mountings, and to 0.4×10^{-4}mm with anti-vibration mountings.

The application of this technique to the determination of the circumferential distribution of $\sigma_c(\theta)_n$ in tubing, would require grooves at a number of angular positions, so that the magnification achieved would generally be less than the maximum. For $-45^\circ < \theta < 45^\circ$ the change in gap-width might not be accurately measurable.

It has been assumed up to this stage that the sections AB and CD in fig.156 retain their original

curvature throughout the process of layer removal, and therefore that the changes in gap-width $\Delta G(\theta)_1 \ldots\ldots \ldots \Delta G(\theta)_n$ are entirely due to the deformation of section BC . Since complete relief of the circumferential stress component $\sigma_{c2}(\theta)_n$ must occur at the sides of the groove, a region of stress disturbance must exist in the vicinity of the groove. The existence of associated curvature near B and C must also be considered.

Gura (106) has reported that the deformation zone produced by cutting a groove in rectangular slugs cut from welded joints is considerably larger than the groove-width. For groove-widths of 10mm, 5mm, 3mm and 2mm respectively, the deformation zone extended 10mm, 9mm, 8mm and 7mm on either side of the groove. It is clear that the occurrence of a similar 'edge effect' at the groove in fig.156 would introduce errors in the determination of $\delta\psi(\theta)_n$ from $\Delta G(\theta)_n$.

This difficulty may however be avoided, and the presence of such additional curvature ignored, if strain gauges are used to determine the deformations between B and C.

6.06. THE ADVANTAGES OF USING STRAIN GAUGES.

If strain gauges are used to measure the deformations produced by slitting and by groove-cutting, the calculation of $\sigma_c(\theta)_n$ is considerably simplified.

The measurement of surface strain would almost certainly be simpler from a practical point of view than the measurement of changes in gap-width by the inferometric technique; possible difficulties associated with the measurement of z and $\cos\phi$, and with the mounting and alignment of optical flats, would be avoided.

(a) Determination of the circumferential bending stress $\sigma_{c1}(\theta)_n$.

By mounting a strain gauge on one surface of the specimen, prior to slitting, $\sigma_{c1}(\theta)_n$ may be easily determined. There are no restrictions on the slitting position, and the released strains may be measured on either surface of the specimen.

Fig.164 shows a strain gauge mounted on the inner surface of the specimen, at position θ_1 from maximum wall thickness. If the surface bending strain detected by the gauge on slitting is denoted by $\varepsilon_{cM}(\theta_1)_a$ then:

$$E' \cdot \varepsilon_{cM}(\theta_1)_a = -\sigma_{c1}(\theta_1)_a \quad \text{---------} \quad 6.35.$$

where $\sigma_{c1}(\theta_1)_a$ is the value of the residual bending stress at the inner surface of the specimen. The minus sign results from the fact that the release of compressive residual stress at the inner surface (by slitting) produces tensile strain on the gauge.

Since the ratio of R_m/h_θ is large, it may be assumed that:

$$\sigma_{c1}(\theta_1)_a = -\sigma_{c1}(\theta_1)_b$$

where $\sigma_{c1}(\theta_1)_b$ is the residual bending stress at the outer surface. It follows from equation 6.15 that:

$$\sigma_{c1}(\theta_1)_n = -\left(\frac{h\theta_1 - 2d_n}{h\theta_1}\right).\sigma_{c1}(\theta_1)_a$$

and from equation 6.35 that:

$$\sigma_{c1}(\theta_1)_n = E'.\left(\frac{h\theta_1 - 2d_n}{h\theta_1}\right).\varepsilon_{cM}(\theta_1)_a \qquad \text{-------6.36.}$$

The stress component at any other angular position θ may be obtained from the measured surface strain at position θ_1, by using equation 6.17 :

$$\sigma_{c1}(\theta)_n = \frac{6M_c}{\ell}\left(\frac{h\theta - 2d_n}{h\theta^3}\right)$$

Since M_c is independent of θ it follows that:

$$\sigma_{c1}(\theta_1)_n = \frac{6M_c}{\ell}\left(\frac{h\theta_1 - 2d_n}{h\theta_1^3}\right)$$

so that:

$$\frac{\sigma_{c1}(\theta)_n}{\sigma_{c1}(\theta_1)_n} = \left(\frac{h\theta - 2d_n}{h\theta_1 - 2d_n}\right).\frac{h\theta_1^3}{h\theta^3} \qquad \text{---------6.37.}$$

and using equation 6.36 :

$$\sigma_{c1}(\theta)_n = E'(h\theta - 2d_n).\frac{h\theta_1^2}{h\theta^3}.\varepsilon_{cM}(\theta_1)_a \qquad \text{-------6.38.}$$

This equation is equivalent to equation 6.22 .

(b) Determination of the stress component $\sigma_{c2}(\theta)_n$.

In section 6.05 it was shown that $\sigma_{c2}(\theta)_n$ could be determined from the changes in gap-width $\Delta G(\theta)_1$, ... $\Delta G(\theta)_n$.

By mounting a strain gauge pair on the inner surface of the specimen between B and C, as shown in fig.165, it is possible to determine $\sigma_{c2}(\theta)_n$ from the surface strain changes which occur on layer removal.

The gauge length should be less than the groove-width s, and the stress component $\sigma_{c1}(\theta)_n$ should be pre-determined.

As before, $\sigma_{c2}(\theta)_n$ is determined in two parts according to equation 6.23 :

$$\sigma''(\theta)_n = \sigma_{c2}(\theta)_n + \sigma'(\theta)_n$$

The removal of the n^{th} layer, of thickness Δt_n, containing the stress $\sigma''(\theta)_n$ (fig.158) is equivalent to applying a force $P_c(\theta)_n$ and a moment $M_c(\theta)_n$ to the material beneath the groove, where:

$$P_c(\theta)_n = \sigma''(\theta)_n . l . \Delta t_n$$

$$M_c(\theta)_n = -\frac{1}{2} . \sigma''(\theta)_n . \Delta t_n . l (t_n + \Delta t_n)$$

The stress change on the inner surface is the algebraic sum of the direct and bending stress changes (99), and is given by:

$$\sigma''(\theta)_n \left[\frac{\Delta t_n}{t_n} - \frac{\Delta t_n . t_n . \ell (t_n + \Delta t_n)}{4 I_c(\theta)_n} \right]$$

If the circumferential strain change on the inner surface on removal of the n^{th} layer is denoted by $\Delta\varepsilon_c(\theta)_{an}$ then:

$$\Delta\varepsilon_c(\theta)_{an} + \mu . \Delta\varepsilon_L(\theta)_{an} = \frac{\sigma''(\theta)_n}{E'} \left[\frac{\Delta t_n}{t_n} - \frac{\Delta t_n . t_n . \ell (t_n + \Delta t_n)}{4 I_c(\theta)_n} \right]$$

where $\Delta\varepsilon_L(\theta)_{an}$ is the longitudinal strain produced by the relief of the stress $\sigma_L(\theta)_n$ in the n^{th} layer. Although this has no effect on the circumferential curvature between B and C , and no effect on the change in gap-width, it must be considered when determining the circumferential surface stress change.

If $\Delta\varepsilon_c(\theta)_{an} + \mu . \Delta\varepsilon_L(\theta)_{an}$ is denoted by $\Delta\phi(\theta)_{an}$, and $I_c(\theta)_n$ is replaced by $\frac{1}{12}\ell . t_n^3$, the above equation may be rewritten:

$$\sigma''(\theta)_n = \frac{- E' . t_n^2 . \Delta\phi(\theta)_{an}}{\Delta t_n (2t_n + 3\Delta t_n)} \qquad \text{--------- 6.39.}$$

for all n .

This equation is equivalent to equation 6.27 , but has the advantage that the effect of the force $P_c(\theta)_n$ is automatically taken into account.

The stress component $\sigma'(\theta)_n$ may be obtained directly from equation 6.31 by using the substitution:

$$\sigma''(\theta)_r = \frac{-E'.t_r^2.\Delta b(\theta)_{ar}}{\Delta t_r(2t_r+3\Delta t_r)} \qquad \text{---------6.40.}$$

So that by using the equations 6.23 , 6.39 , 6.31 and 6.40 , the stress component $\sigma_{c2}(\theta)_n$ may be determined from the changes $\Delta b(\theta)_{a1}$, ... $\Delta b(\theta)_{an}$.

(c) If it can be arranged that layers of equal thickness are removed, the equation 6.39 becomes:

$$\sigma''(\theta)_n = \frac{-E'(h_\theta - n.\Delta t)^2.\Delta b(\theta)_{an}}{\Delta t\left[2h_\theta + (3-2n)\Delta t\right]}$$

and $\sigma''(\theta)_r$ in equation 6.33 is replaced by:

$$\sigma''(\theta)_r = \frac{-E'(h_\theta - r.\Delta t)^2.\Delta b(\theta)_{ar}}{\Delta t\left[2h_\theta + (3-2r)\Delta t\right]}$$

(d) Conclusions.

The determination of $\sigma_c(\theta)_n$ from the measurement of local surface strain changes is considerably simpler from both the theoretical and practical point of view than the method based on the measurement of changes in gap-width discussed in section 6.05 .

Provided $\sigma_c(\theta)_n$ and $\sigma_L(\theta)_n$ do not change abruptly with θ , the local changes $\Delta b(\theta)_{a1}$, ... $\Delta b(\theta)_{an}$ are unaffected by small changes in the groove-width S

during the layer removal process (equation 6.39 is independent of s).

In contrast to the changes in gap-width produced by cutting a groove, the surface strain changes between B and C would probably be of the same order of magnitude as those which would be produced by conventional layer removal techniques. The strain measurement technique described in section 2.04 could therefore be used without modification.

Since the investigation of the circumferential distribution of $\sigma_c(\theta)_n$ must be carried out by cutting grooves at a number of angular positions, it is clear that the extent of the region of circumferential stress disturbance produced by each groove will be an important factor in determining the minimum groove separation. Since R_m/h_θ is greater than 11 it seems reasonable to assume that this region of stress disturbance will extend only a few wall thicknesses on either side of each groove. On this basis, five or six equally-spaced grooves could easily be accommodated on one specimen, and four specimens would provide sufficient measuring points.

6.07. EXPERIMENTAL CHECK ON THE VALIDITY OF EQUATION 6.34.

Denton (91,100) checked the validity of the expression 6.34 by comparing the changes in gap-width

calculated from known applied stresses, with measured values. The known stresses were applied to the sides of the groove by a 'stress-tool' in the form of internal calipers, as shown in fig.166 .

For groove-depths up to $0{\cdot}4\,h_0$ the measured changes in gap-width $\delta G(\pi)_1$, ... $\delta G(\pi)_n$ were found to be consistently about 20% higher than the values $\Delta G(\pi)_1$, ... $\Delta G(\pi)_n$ obtained from equation 6.34 . Denton therefore suggested that a correction factor $K = 1.2$ should be inserted in the denominator of the expression for $\sigma''(\pi)_n$.

The accuracy of this method for determining the correction factor K is clearly dependent on the exact reproduction, by the lever system, of the loading imposed by layer removal, and also on the accurate estimation of the applied bending moment. In order to avoid uncertainty about the length of the moment-arm of the force P , it is clearly necessary that the faces F should remain in contact at all times with the bottom of the groove. There is no indication in Denton's description as to how this was achieved.

6.08. EXAMINATION OF THE TECHNIQUES AVAILABLE FOR CUTTING GROOVES.

Denton (72,100) has discussed the limitations of conventional metal removal techniques when applied to the problem of cutting a rectangular groove for the determin-

ation of local residual stress.

The main requirements of a suitable technique are that it should be dimensionally controllable and that it should either be stress-free or introduce stresses which are consistent and measurable. The operation of machining introduces local residual stresses which in most cases can be determined and taken into account. However, with thin-walled tubing of the softer metals, the relative increase in flexibility caused by slitting, tends to make clamping difficult, and variable residual stresses may result unless great care is taken.

Difficulties with clamping are usually avoided by using acid-etching or electropolishing (77,80,81,85-88, 98,99) which have both been shown to be practically stress-free techniques for metal removal. Unfortunately, both techniques lack the dimensional controllability necessary for cutting a groove of specified dimensions, the main problem being blunting at the corners and undercutting of the sides, as shown in fig.167 .

It is obvious from equation 6.27 that the changes in gap-width produced by groove-cutting are dependent on the groove-width, and therefore that the initial groove-width S must remain constant throughout the process of layer removal. Clearly, both acid-etching and electro-polishing are of limited usefulness in this respect, and in fact, Denton (100) has shown, for nitric acid and copper, that scatter becomes significant when the groove-

depth exceeds $0{\cdot}04s$. Serebrennikov (101), on the other hand, has indicated that etching may be carried out until the groove-depth exceeds $0{\cdot}57s$, but no details of the etchant, or its control, are given.

Spark erosion has been used successfully by Denton (100) for cutting grooves. It provides excellent dimensional controllability and the specimen under attack need not be clamped. It, unfortunately, introduces a tensile residual stress which falls rapidly to zero in the first 0.1mm. An adjustment must therefore be made to the measured residual stress in order to achieve an accurate value. The method of adjustment is discussed fully in ref.100.

It has already been noted in section 6.06 that the local changes $\Delta b(\theta)_{a1}$, ... $\Delta b(\theta)_{an}$ are, in theory, unaffected by small changes in the initial groove-width s during the layer removal process. The possibility of using acid-etching or electropolishing as a stress-free alternative to spark erosion, must therefore be considered in this case.

Assuming that both acid-etching and electropolishing take place at an equal rate in both the circumferential and radial directions, it is clear from fig.167 that the groove-width s_n after removal of n layers is given by:

$$s_n = s + 2(h\theta - t_n)$$

Taking the initial groove-width s as $4h_\theta$, and the practical limit on the groove-depth as $0{\cdot}8h_\theta$, it follows from this equation that $s_n = 1{\cdot}4s$; so that increases of up to 40% in the initial groove-width could be expected under normal circumstances. The extent to which the curvature of the section BC would be affected in practice by an increase in s of this order of magnitude, must be investigated experimentally before the usefulness of either acid-etching or electropolishing as an alternative to spark erosion can be reliably assessed.

The possibility of minimising circumferential etching by using some form of chemical saw, might also be worth investigating.

6.09. THE DETERMINATION OF 'TYPE A' LONGITUDINAL RESIDUAL STRESS IN TUBING WITH e GREATER THAN 0.1.

Having determined $\sigma_c(\theta)_n$ by either of the methods in sections 6.05 and 6.06, $\sigma_L(\theta)_n$ may be determined by the method discussed in section 6.03e.

Using the notation of equation 6.13, it follows that:

$$\sigma_L(\theta)_n = \hat{\sigma}_{L1}(\theta)_n + \hat{\sigma}_{L2}(\theta)_n + \hat{\sigma}_{L3}(\theta)_n + \mu \cdot \sigma_c(\theta)_n \qquad \text{-------- 6.41.}$$

where the stress components $\hat{\sigma}_{L1}(\theta)_n$, $\hat{\sigma}_{L2}(\theta)_n$ and $\hat{\sigma}_{L3}(\theta)_n$ are determined from the longitudinal surface

strain changes which result from the cutting and subsequent dissection of a thin strip at position θ (fig.149), and $\mu.\sigma_c(\theta)_n$ represents the effect of the circumferential stress relief on cutting-out the thin specimen.

In order that the relief of the circumferential residual stress in the strip should be complete, the dimension S should not exceed $2h_\theta$ (99).

It is necessary to assume that the 'type A' residual stresses do not vary with length and are independent of θ within the limits of the arc S , and that the 'type B' residual stresses have been completely relieved and pre-determined.

(a) Determination of $\hat{\sigma}_{L1}(\theta)_n$.

The longitudinal residual bending stress $\hat{\sigma}_{L1}(\theta)_n$ in the n^{th} layer (measuring from the outer surface) may be determined from the surface strain changes which occur on cutting-out the thin strip specimen at the position θ .

Since R_m/h_θ is large and S is small it may be assumed without significant error that the cross-section of the strip is rectangular and, since $M_L(\theta)$ (fig.168) is constant over the strip length, that the radius of curvature adopted by the strip is constant.

Taking moments positive as shown, the longitudinal

bending stress released in the n^{th} layer by cutting-out is given by:

$$\hat{\sigma}_{L1}(\theta)_n = \frac{M_L(\theta)\left(\frac{h\theta}{2} - d_n\right)}{I_L(\theta)}$$

where: $I_L(\theta) = \frac{1}{12} s . h\theta^3$

Since $\hat{\sigma}_{L1}(\theta)_a$, the longitudinal bending stress released at the inner surface, is given by:

$$\hat{\sigma}_{L1}(\theta)_a = -\frac{M_L(\theta) . \frac{h\theta}{2}}{I_L(\theta)}$$

it follows that:

$$\hat{\sigma}_{L1}(\theta)_n = -\left(\frac{h\theta - 2d_n}{h\theta}\right) . \hat{\sigma}_{L1}(\theta)_a \qquad \text{------ 6.42.}$$

If the surface bending strain detected by a gauge on the inner surface is denoted by $\varepsilon_{LM}(\theta)_a$, then:

$$E . \varepsilon_{LM}(\theta)_a = -\hat{\sigma}_{L1}(\theta)_a$$

The minus sign results from the fact that the release of compressive residual stress at the inner surface (by cutting-out) produces tensile strain on the gauge.

It follows from equation 6.42 that:

$$\hat{\sigma}_{L1}(\theta)_n = E\left(\frac{h\theta - 2d_n}{h\theta}\right) . \varepsilon_{LM}(\theta)_a \qquad \text{------- 6.43.}$$

(b) Determination of $\hat{\sigma}_{L2}(\theta)_n$.

The longitudinal stress component $\hat{\sigma}_{L2}(\theta)_n$ in the n^{th} layer, as it is removed, is determined from the resultant surface strain change $\Delta\varepsilon_L(\theta)_{an}$ on the inner surface.

The removal of the n^{th} layer, thickness Δt_n, containing the stress $\hat{\sigma}_{L2}(\theta)_n$ is equivalent to applying a force $P_L(\theta)_n$ and a moment $M_L(\theta)_n$ at the nuetral axis (fig.169), where:

$$P_L(\theta)_n = \hat{\sigma}_{L2}(\theta)_n . \Delta t_n . s$$

$$M_L(\theta)_n = -\frac{1}{2}\hat{\sigma}_{L2}(\theta)_n . \Delta t_n . s(t_n + \Delta t_n)$$

Again, the minus sign results from the fact that removal of a layer containing tensile residual stress produces negative curvature.

The stress change on the inner surface is the algebraic sum of the direct and bending stress changes (99), and is given by:

$$\hat{\sigma}_{L2}(\theta)_n \left[\frac{\Delta t_n}{t_n} - \frac{\Delta t_n . t_n . s . (t_n + \Delta t_n)}{4 I_L(\theta)_n} \right]$$

it follows that:

$$\Delta\varepsilon_L(\theta)_{an} = \frac{\hat{\sigma}_{L2}(\theta)_n}{E} \left[\frac{\Delta t_n}{t_n} - \frac{\Delta t_n . t_n . s . (t_n + \Delta t_n)}{4 I_L(\theta)_n} \right]$$

and putting $I_L(\theta)_n = \frac{1}{12} s . t_n^3$ leads to:

$$\hat{\sigma}_{L2}(\theta)_n = \frac{-E.t_n^2.\Delta\varepsilon_L(\theta)_{an}}{\Delta t_n(2t_n+3\Delta t_n)}$$

for all n . ---------- 6.44.

(c) Determination of $\hat{\sigma}_{L3}(\theta)_n$.

The longitudinal stress $\hat{\sigma}_{L3}(\theta)_n$ released in the n^{th} layer by removal of the $n-1$ previous layers, is determined from the surface strain changes $\Delta\varepsilon_L(\theta)_{a1}$, ... $\Delta\varepsilon_L(\theta)_{a\,n-1}$ which occur at the inner surface.

The calculation is almost identical to that for the stress component $\sigma'(\theta)_n$ in section 6.05d , so that only the final equation need be stated:

$$\hat{\sigma}_{L3}(\theta)_n = \sum_{r=1\to n-1}\left[\hat{\sigma}_p(\theta)_{nr} + \hat{\sigma}_M(\theta)_{nr}\right]$$

$n>1$ ---------- 6.45.

where:

$$\hat{\sigma}_p(\theta)_{nr} = -\hat{\sigma}_{L2}(\theta)_r.\frac{\Delta t_r}{t_r}$$

$$\hat{\sigma}_M(\theta)_{nr} = -\frac{\hat{\sigma}_{L2}(\theta)_r.\Delta t_r.s(t_r+\Delta t_r)(h\theta-d_n-\frac{t_r}{2})}{2I_L(\theta)_r}$$

$$I_L(\theta)_r = \frac{1}{12}s.t_r^3$$

$$\hat{\sigma}_{L2}(\theta)_r = \frac{-E.t_r^2.\Delta\varepsilon_L(\theta)_{ar}}{\Delta t_r(2t_r+3\Delta t_r)}$$

The minus sign in the expressions for $\hat{\sigma}_p(\theta)_{nr}$ and $\hat{\sigma}_M(\theta)_{nr}$ result from the fact that $\hat{\sigma}_{L3}(\theta)_n$ is defined as the stress released, rather than induced, in the n^{th} layer.

(d) Considerable simplification is again produced if layers of equal thickness Δt are removed.

6.10. DISCUSSION.

Although an experimental investigation is essential before a final assessment can be made, the technique described in sections 6.05-6.09 is, in theory, more suitable for the investigation of local values of stress in tubing with e greater than 0.1 than any revealed to date by an extensive literature survey.

The main advantage of the technique lies in the fact that specimen eccentricity need only be considered in the calculation of the circumferential bending stress $\sigma_{c1}(\theta)_n$ from the change in diameter or gap-width on slitting (equation 6.22). The calculation of $\sigma_{c1}(\theta)_n$ from the change in surface strain, and of $\sigma_{c2}(\theta)_n$ from the change in either surface strain or gap-width, may be carried out without regard to specimen eccentricity.

The condition R_m/h_θ greater than 11 for all θ , was chosen to make the use of curved bar theory unnecessary in the calculation of circumferential bending deformations. It also sets an upper limit on the value of the initial eccentricity of specimens to which the technique of sections 6.05-6.09 can be applied. It may be shown (appendix 6) that the upper limit for e is specified by the inequality:

$$e \leq \frac{1}{22}\left(\frac{1+a/b}{1-a/b}\right) - 1$$

In the case of the tubing used in sections 4 and 5 , for which a/b = 0.941 , the technique may be applied to specimens with e less than 0.5 , or an initial wall thickness variation up to $\pm$50%.

As mentioned earlier, the exact solution to the problem of the bending of an eccentric tube under the action of the edge moment M_c has been obtained by Mori (103) using bipolar co-ordinates. For a specimen with a/b = 0.941 and e = 0.5 , the error produced by using the approximate theories of sections 6.05c and 6.06a , is less than 3%.

A preliminary experimental investigation should give priority to the following topics:

(a) The determination of the minimum groove separation, and hence the number of grooves which could be accommodated on one specimen.

(b) A critical evaluation of the technique discussed in section 6.07 for determining the correction factor K .

(c) An investigation of the suitability of acid-etching or electropolishing as a groove-cutting technique, when surface strain is measured.

It should be noted, in conclusion, that the principles behind the analyses of sections 6.05 and 6.06 apply equally well if the groove is cut from the inner surface. If α_n were also measured from the inner surface, the derivation of the final equations for $\sigma_c(\theta)_n$ and $\sigma_L(\theta)_n$ would be almost identical to that already carried out, the only differences being due to changes in sign.

REFERENCES.

1. Sachs G. & Van Horn K.R.
Practical Metallurgy p.162, Am.Soc.Metals 1940.

2. Orowan E.
p.47 Symposium on Internal Stresses in Metals & Alloys, The Institute of Metals 1948.

3. MacGregor C.W.
p.103 Residual Stresses in Metals & Metal Construction (W.R. Osgood), Reinhold 1954.

4. Orowan E.
Internal Stresses & Fatigue in Metals (G.M. Rassweiller & W.L. Grube), Elsevier 1959.

5. Sachs G.
Zeit.Für.Metallk. 1927,19,352.

6. Hanslip R.E.
Proc.Soc.Exp.Stress Anal. 1952,10(1),97.

7. Davidson T.E., Kendall D.P. & Reiner A.N.
Proc.Soc.Exp.Stress Anal. 1963,20(2),253.

8. Heyn E.
J.Inst.Metals 1914,12,3.

9. Sachs G.
Trans.Am.Soc.Metals 1939,27,821.

10. Wishart H.B. & Potter R.K.
Trans.Am.Soc.Metals 1949,41,692.

11. Barker A. & Hardy E.H.
Proc.Inst.Mech.Engrs. 1957,171,581.

12. Mack D.R.
Proc.Soc.Exp.Stress Anal. 1962,19(1),155.

13. Acquaviva S.J.
J.Mater. 1969,4(2),286.

14. Dawson V.C.D. & Jackson J.W.
J.Basic Eng., Trans.Am.Soc.Mech.Engrs. 1969,91,63.

15. Zhdanov I.M., Korzh V.N. & Vasilenko Yu.A.
Zavod.Lab. 1970,36(2),213.

16. Weiss V.
Proc.Soc.Exp.Stress Anal. 1958,15(2),53.

17. Shur D.M.
Zavod.Lab. 1963,29(5),608.

18. Yakunin L.S.
Zavod.Lab. 1966,32(10),1246.

19. Yakunin L.S.
Zavod.Lab. 1970,36(7),858.

20. Kobrin M.M. & Birulya A.L.
Zavod.Lab. 1969,35(10),1218.

21. Kobrin M.M., Proshko V.M. & Sorkin L.S.
Zavod.Lab. 1966,32(3),377.

22. Peiter A.
Materialprüfung 1964,6(1),11.

23. Peiter A.
Materialprüfung 1966,8(3),97.

24. Murakami Y. & Fujitani K.
p.45 Proc.7th Japan.Congr.Test.Mater. 1964.

25. Doi O. & Kataoka K.
Bul.Japan.Soc.Mech.Engrs. 1968,11(43),1.

26. Olson W.A. & Bert C.W.
Proc.Soc.Exp.Stress Anal. 1966,23(2),451.

27. Ksendzyk G.V.
Automatic Welding 1968,21(10),35.

28. Dekhtyar L.I., Temrin B.V. & Petrov Yu.N.
Zavod.Lab. 1966,32(10),1270.

29. Dekhtyar L.I., Andreichuk V.K. & Beznosov A.E.
Zavod.Lab. 1966,32(8),997.

30. Dekhtyar L.I.
Zavod.Lab. 1968,34(4),471.

31. Deev V.A.
Russian Eng.J. 1974,54(6),18.

32. Lambert J.W.
Proc.Soc.Exp.Stress Anal. 1954,12(1),91.

33. Pokhmurskii V.I. & Karpenko G.V.
Soviet Mater.Sci. 1968,4(4),277.

34. Ozimin Yu.S. & Kazachkov B.M.
Russian Castings Prod. 1968,9,409.

35. Senatorova O.G. & Samoilov A.I.
Metal Sci.Heat Treatment 1969,p.322.

36. Meadows B.J.
J.Inst.Metals 1965,93,353.

37. Misra S.K. & Polakowski N.H.
J.Basic Eng., Trans.Am.Soc.Mech.Engrs. 1969,91,810.

38. Buhler H. & Kreher P.J.
Archiv.Eisen. 1968,39(5),1.

39. Buhler H. & Matting A.
Bänder.Bleche.Rohre 1969,10(12),724.

40. Buhler H., Lueg K. & Mahrenholtz O.
Archiv.Eisen. 1969,40(12),1.

41. Kolthoff I.M. & Belcher R.
Volumetric Analysis (vol.3), Wiley 1957.

42. Peekel C.

Strain 1972,8(3),112.

43. Dittbenner G.R.

Exp.Mechanics 1973,13(11),493.

44. Jeffrey G.B.

Phil.Trans.Roy.Soc. 1920,221(A),265.

45. Coker E.G. & Filon L.N.G.

Photoelasticity p.301, Cambridge Univ.Press 1931.

46. Stevenson A.C.

Proc.Roy.Soc. 1940,184(A),129.

47. Godfrey D.E.R.

Theoretical Elasticity & Plasticity for Engineers p.159, Thames & Hudson 1959.

48. Botros B.M.

Intern.J.Mech.Sci. 1960,2,195.

49. Buhler H.

p.305 Residual Stresses in Metals & Metal Construction (W.R. Osgood), Reinhold 1954.

50. Osakada K., Shiraishi N. & Oyane M.

J.Inst.Metals 1971,99,341.

51. Kawagoe H.

Bul.Japan.Soc.Mech.Engrs. 1967,10(40),588.

52. Kawagoe H.

ibid.p.595.

53. Hanke E. & Tiemann E.

Harterei-Techn.Mitt. 1970,25(2),81.

54. Kent C.H.

J.Appl.Mech., Trans.Am.Soc.Mech.Engrs. 1931,3,167.

55. Timoshenko S.P.
Theory of Plates & Shells p.393, Maple Press 1940.

56. Timoshenko S.P. & Gere J.M.
Theory of Elastic Stability p.280,281,496, McGraw-Hill 1961.

57. Turner C.E.
Introduction to Plate & Shell Theory p.186, Longmanns 1965.

58. Montague P.
J.Mech.Eng.Sci. 1969,11(1),40.

59. Cox N.L.
The Buckling of Plates & Shells, Pergamon 1963.

60. Aylward R.W., Galletly G.D. & Moffit D.G.
J.Mech.Eng.Sci. 1975,17(1),11.

61. Windenburg D.F. & Trilling C.
Trans.Am.Soc.Mech.Engrs. 1934,56,819.

62. Arkmenakas A.E. & Herrmann G.
Proc.Am.Soc.Civ.Engrs., J.Eng.Mechanics Div. 1963,89,131.

63. Barrett C.S.
Metals & Alloys 1934;5,p.131,154,170,196,224.

64. Sachs G. & Espey G.
The Iron Age 1941,Sept.18th p.63, Sept.25th p.36.

65. Barrett C.S.
Proc.Soc.Exp.Stress Anal. 1944,2(1),147.

66. Ford H.
p.3 Symposium on Internal Stresses in Metals & Alloys, The Institute of Metals 1948.

67. Baldwin W.M.

Proc.Am.Soc.Test.Mater. 1949,49,539.

68. Horger O.J.

p.459 Handbook of Experimental Stress Analysis (M. Hetenyi), Wiley-Chapman Hall 1950.

69. Lynch J.J.

p.42 Residual Stress Measurements, Am.Soc.Metals 1951.

70. Rosenthal D.

p.271 Residual Stresses in Metals & Metal Construction (W.R. Osgood), Reinhold 1954.

71. Heindelhofer K.

Evaluation of Residual Stresses, McGraw-Hill 1951.

72. Denton A.A.

Metallurgical Reviews 1966,11,review 101.

73. Hatfield W.H. & Thirkell G.L.

J.Inst.Metals 1919,22,67.

74. Anderson R.J. & Fahlman E.G.

J.Inst.Metals 1924,32,367.

75. Crampton D.K.

Trans.Am.Inst.Min.Met.Engrs. 1930,89,233.

76. Davidenkov N.

Zeit.Für.Metallk. 1932,24,25.

77. Sachs G. & Espey G.

Trans.Am.Inst.Min.Met.Engrs. 1942,147,348.

78. Greaves R.W., Kirstowsky E.C. & Lipson C.

Proc.Soc.Exp.Stress Anal. 1944,2(2),44.

79. Richards D.G.

Proc.Soc.Exp.Stress Anal. 1945,3(1),40.

80. Loxley E.M.

Brit.Iron & Steel Res.Assoc.Report MW/E/43/50.

81. Loxley E.M.

Brit.Iron & Steel Res.Assoc.Report MW/E/48/51.

82. Knights W.J.

Ph.D. thesis, Univ. of London 1952.

83. Loxley E.M. & Whiteley F.

Brit.Iron & Steel Res.Assoc.Report MW/E/53/53.

84. Waisman J.L. & Phillips A.

Proc.Soc.Exp.Stress Anal. 1953,11(2),29.

85. Demorest D.J. & Leeser D.O.

Proc.Soc.Exp.Stress Anal. 1953,11(1),45.

86. Leeser D.O. & Daane R.A.

Proc.Soc.Exp.Stress Anal. 1954,12(1),203.

87. Loxley E.M.

Ph.D. thesis, Univ. of Sheffield 1955.

88. Hundy B.B.

J.Iron & Steel Inst. 1955,179,23.

89. Birger I.A.

Zavod.Lab. 1962,28(9),1112.

90. Denton A.A. & Alexander J.M.

J.Mech.Eng.Sci. 1963,5(1),75.

91. Denton A.A. & Alexander J.M.

ibid.p.89.

92. Kasimov L.N. & Mukhin V.S.

Zavod.Lab. 1967,33(1),113.

93. Yarkovets A.I. & Kiselev N.M.

Zavod.Lab. 1970,36(11),1384.

94. Sykes J.M. & Rothwell G.P.
J.Electrochemical Soc. 1971,118(1),91.

95. Margules A.U.
Zavod.Lab. 1971,37(4),471.

96. Timoshenko S.P.
Strength of Materials (part 2) p.1,65,79,236,
Van Nostrand 1951.

97. Rembowski J.L.
Proc.Soc.Exp.Stress Anal. 1959,16(1),195.

98. Pomeroy R.J. & Johnson K.L.
J.Strain Anal. 1969,4(3),208.

99. Pomeroy R.J.
Wear 1970,16(6),393.

100. Denton A.A.
Strain 1967,3(3),19.

101. Serebrennikov G.Z.
Zavod.Lab. 1962,28(9),1108.

102. Grobner W. & Hofreiter N.
Integraltafel, Springer-Verlag 1949.

103. Mori K.
Bul.Japan.Soc.Mech.Engrs. 1964,7(27),499.

104. Denton A.A.
J.Strain Anal. 1966,1(3),196.

105. Hospers F. & Vogelesang L.B.
Exp.Mechanics 1975,15(3),107.

106. Gura P.M.
Zavod.Lab. 1971,37(10),1249.

107. Pomeroy R.J.
Intern.J.Mech.Sci. 1968,10,29.

108. Weymueller C.R.

Metal Progress 1971,99(5),66.

N.B. : The Russian periodical Zavodskaya Laboratoriya appears in English translation as Industrial Laboratory. The original volume and part numbers are retained.

DEPARTMENT OF MECHANICAL ENGINEERING

UNIVERSITY OF GLASGOW

AN INVESTIGATION OF RESIDUAL STRESSES IN TUBING.

GEORGE B. SIMPSON.

Ph.D. THESIS, JANUARY 1976, VOLUME II.

CONTENTS.

VOLUME II.

APPENDIX 1.

DIAGRAMS.

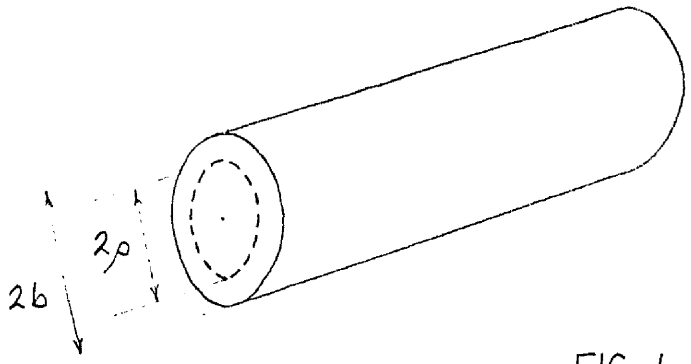

FIG. 1.

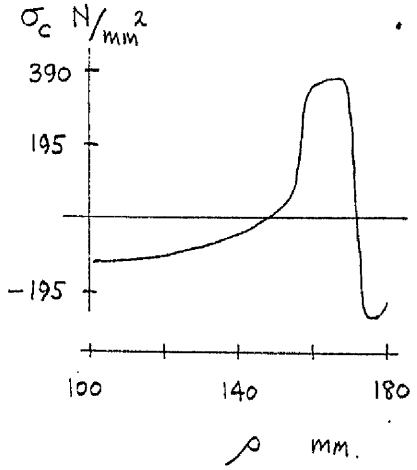

FIG. 2.

FIG. 3.

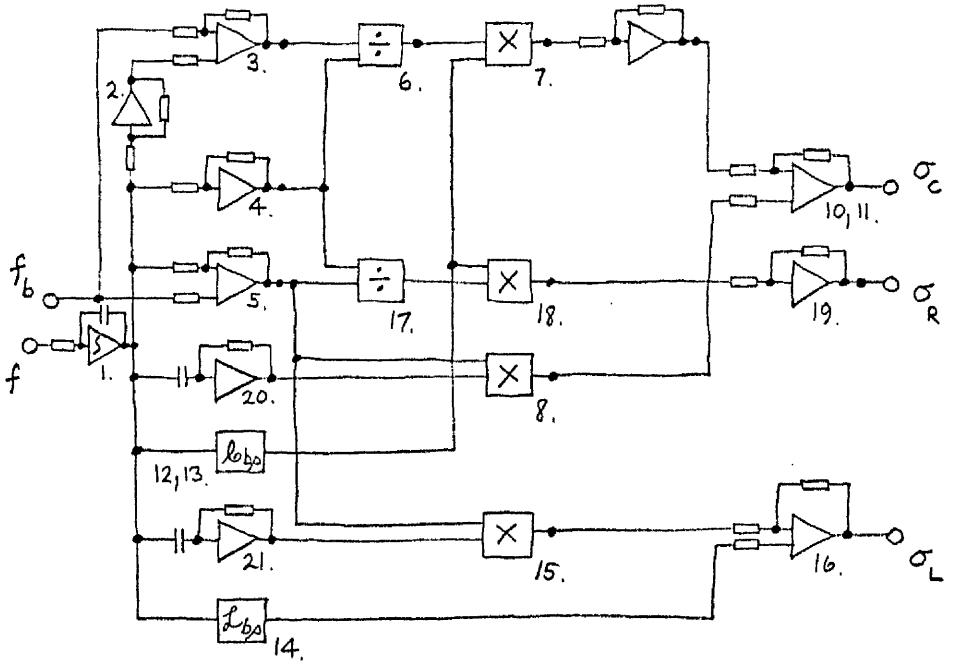

KEY : 1. INTEGRATOR ; 2-5, 9-11, 16 & 19. SUMMATORS OR INVERTERS ; 6 & 17. DIVIDERS ; 7, 8, 15 & 18. MULTIPLIERS ; 12 & 14. FUNCTIONAL CONVERTERS ; 20 & 21. DIFFERENTIATORS.

FIG. 4.

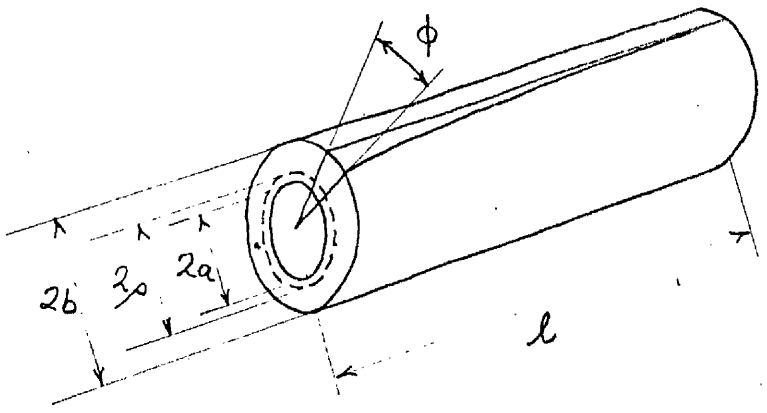

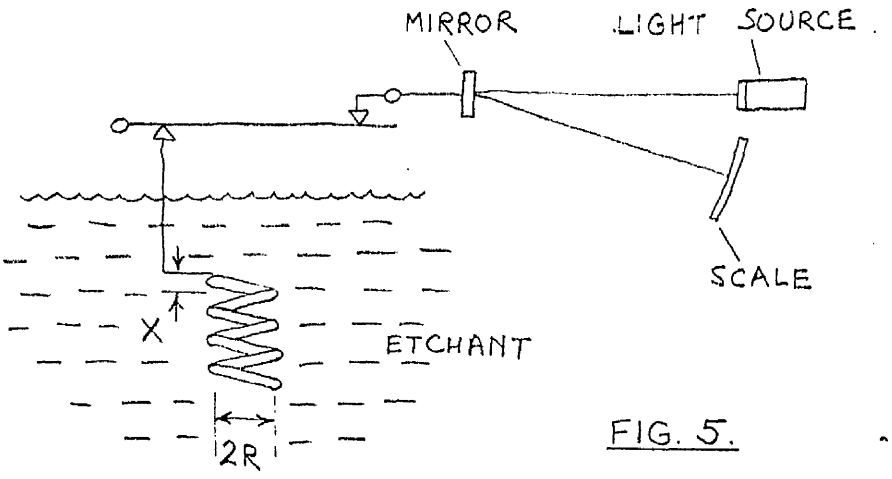

FIG. 5.

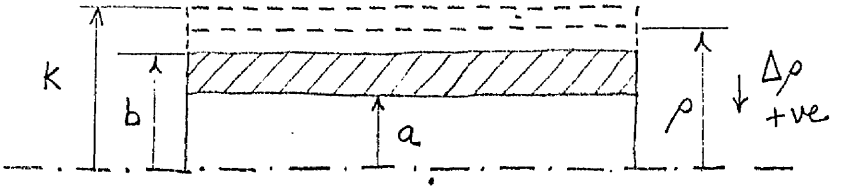

FIG. 6.

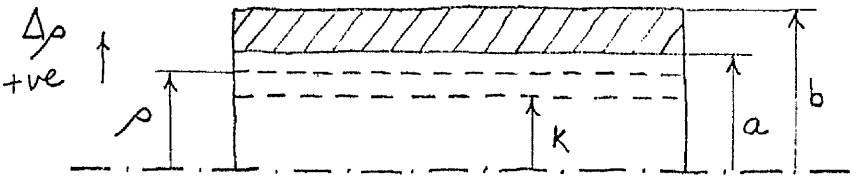

FIG. 7.

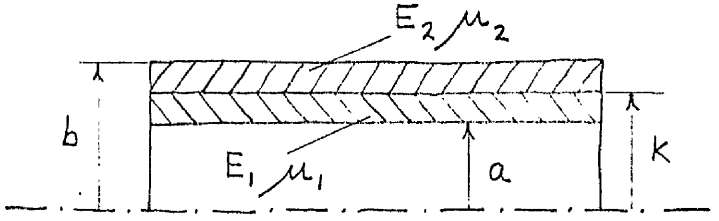

FIG. 8.

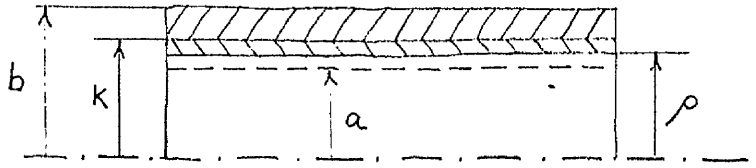

FIG. 9.

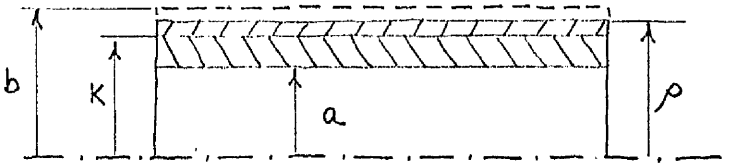

FIG. 10.

FIG. 11.

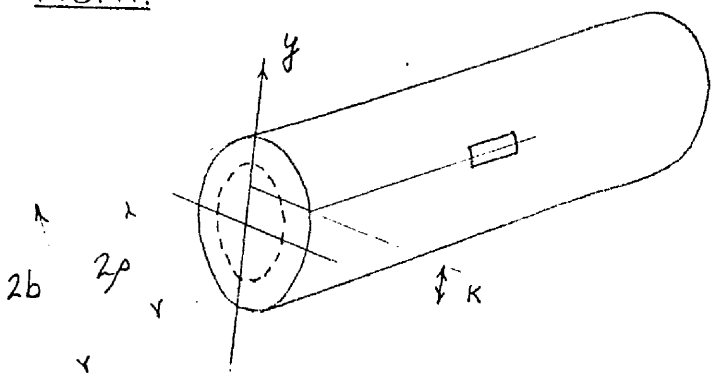

FIG. 12.

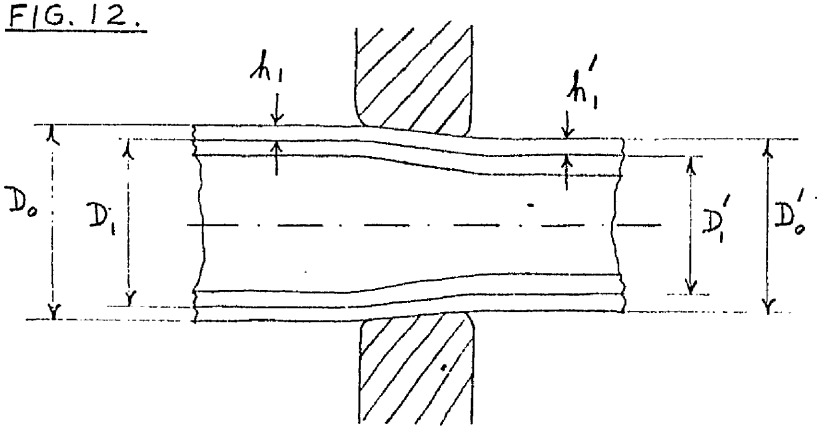

FIG. 13.

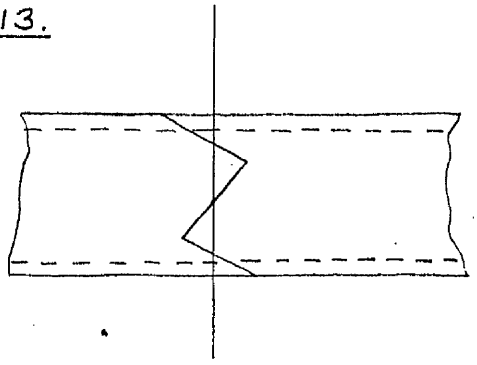

LONGITUDINAL RESIDUAL STRESS PRODUCED BY PLASTIC BENDING WITH ELASTIC SPRINGBACK.

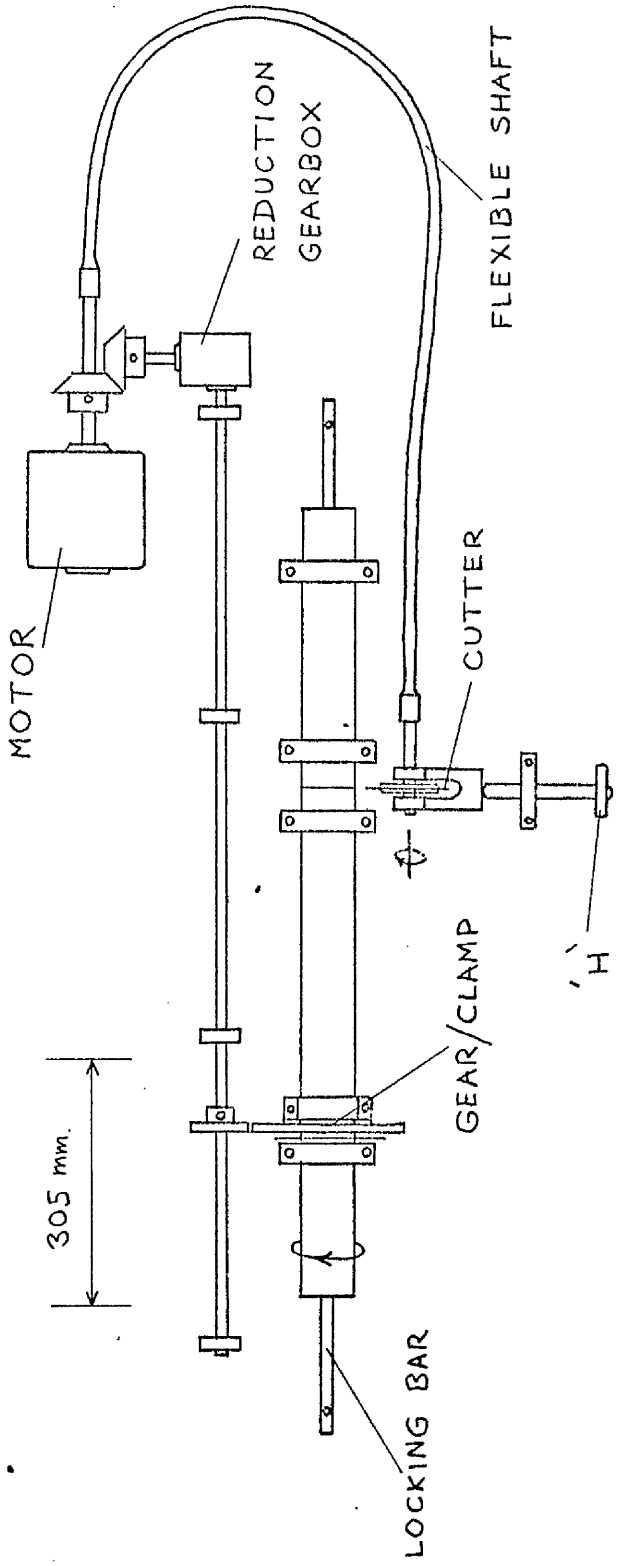

FIG. 14. PLAN VIEW OF TUBE-CUTTING APPARATUS

FIG. 15. GEAR/ CLAMP

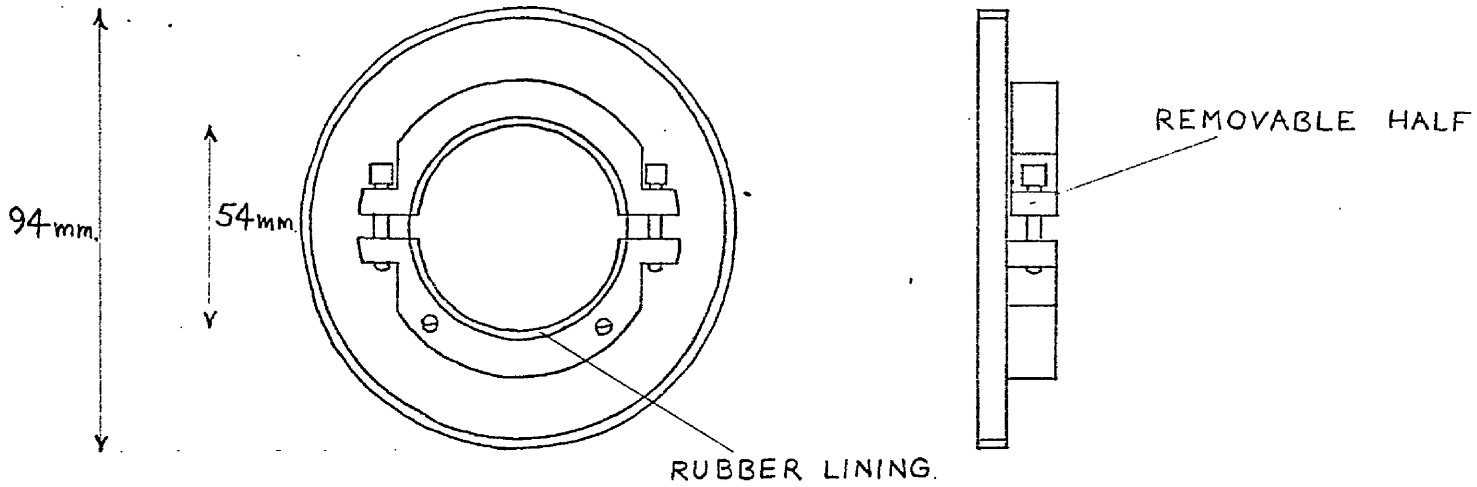

FIG. 16. BEARING

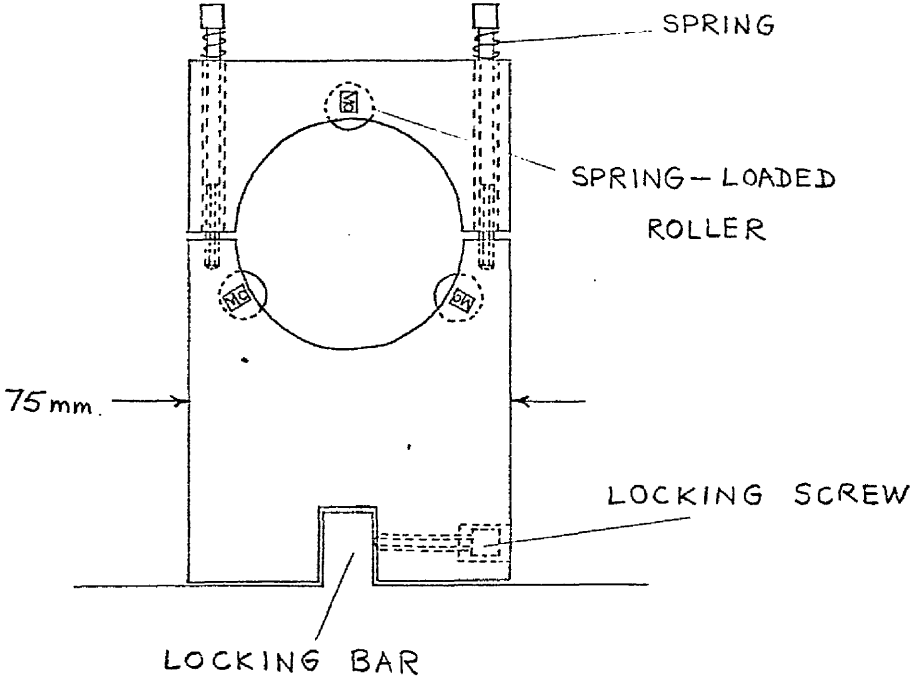

FIG. 17. SECTIONAL ELEVATION OF ACID BATH
(MOTOR AND REVERSING MECHANISM OMITTED)

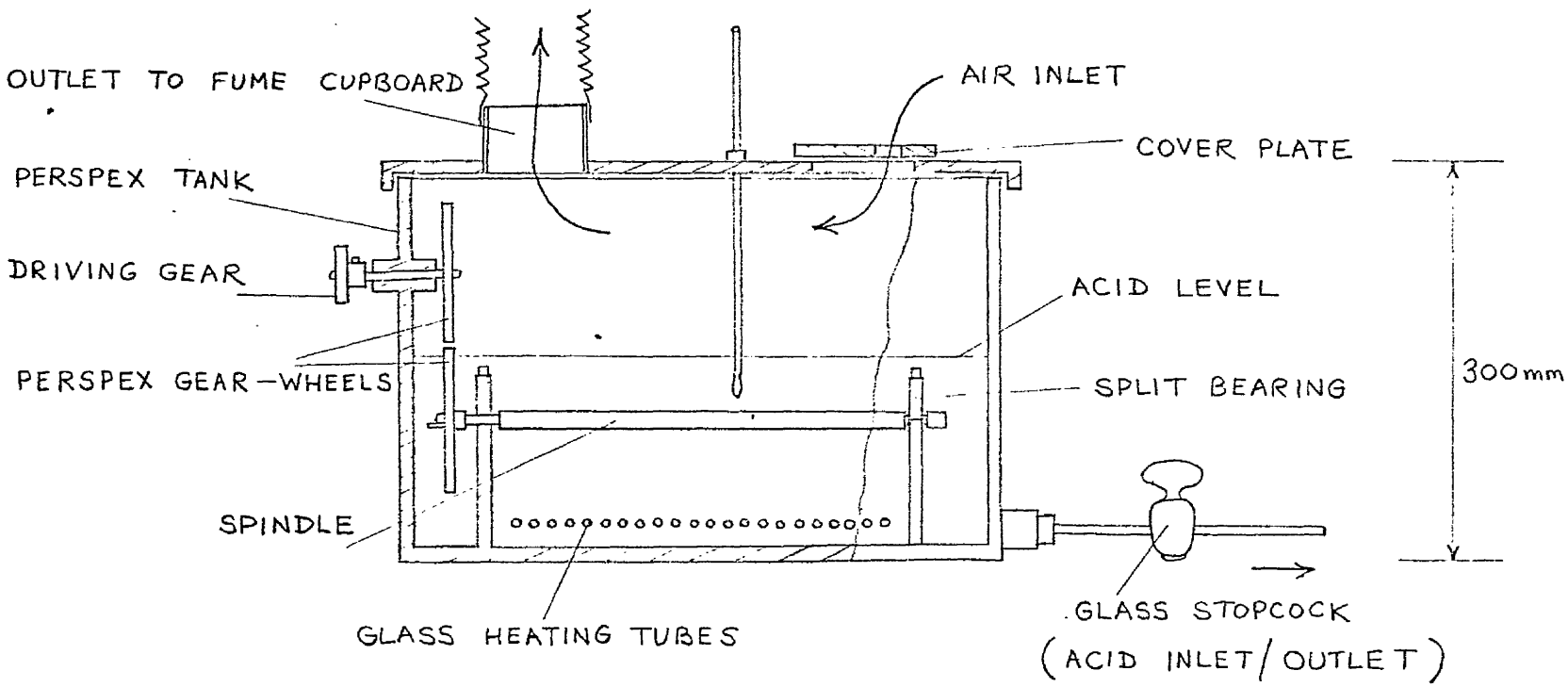

FIG. 18. MOTOR AND REVERSING MECHANISM

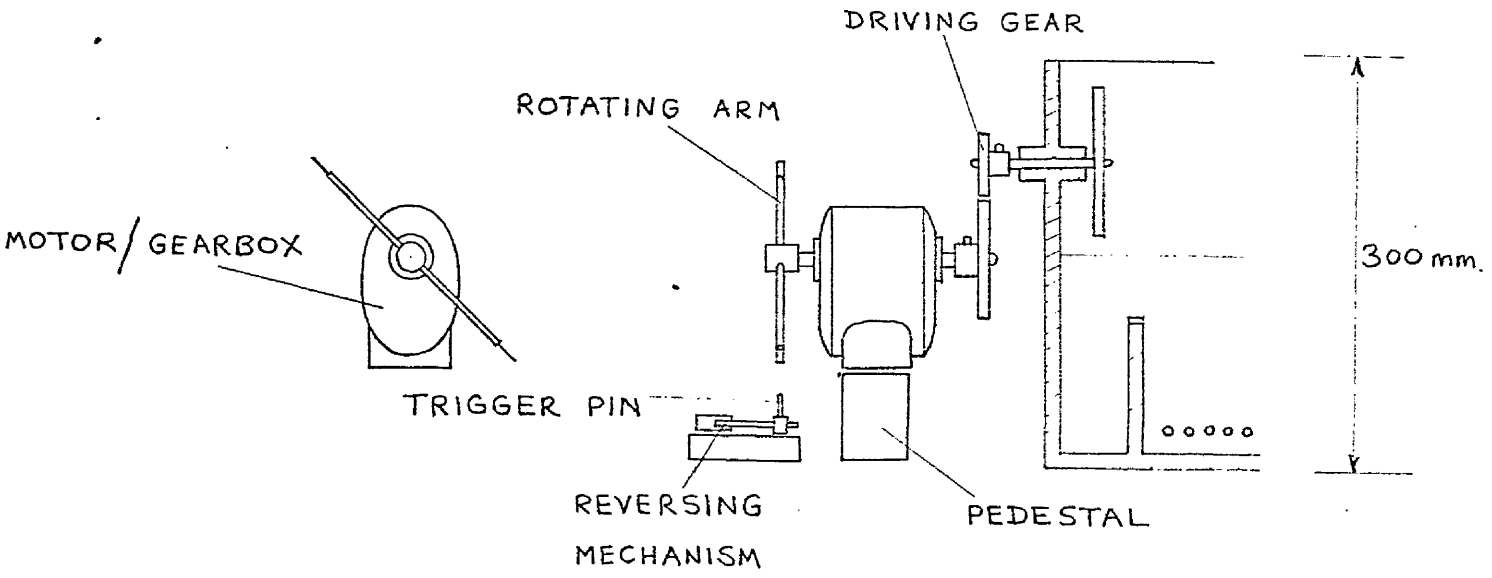

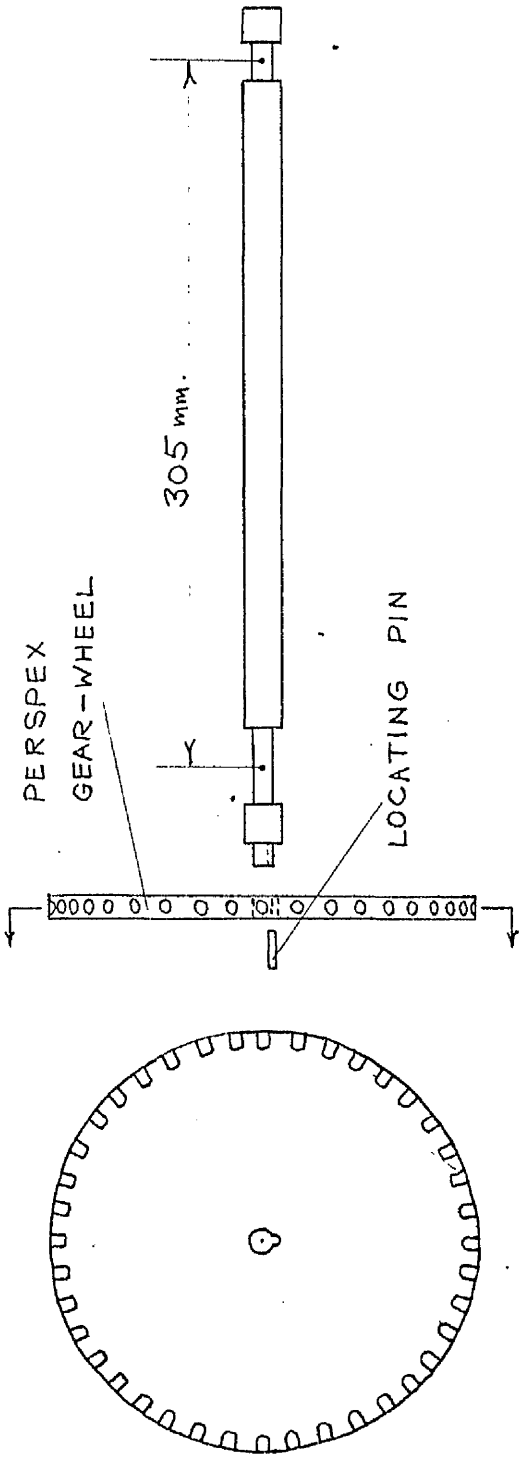

SPINDLE

F/G. 19.

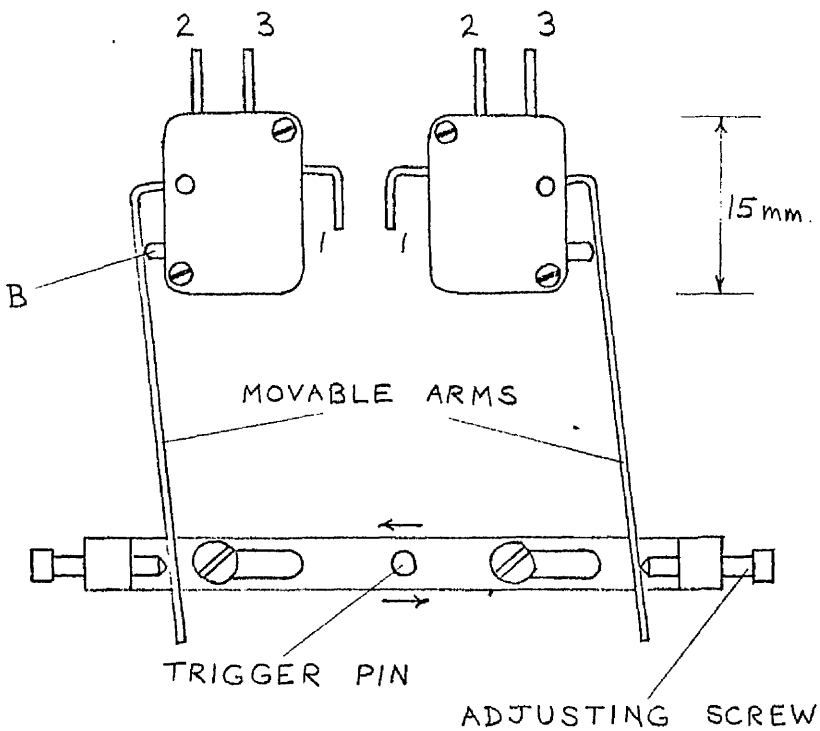

FIG. 20. PLAN OF REVERSING MECHANISM

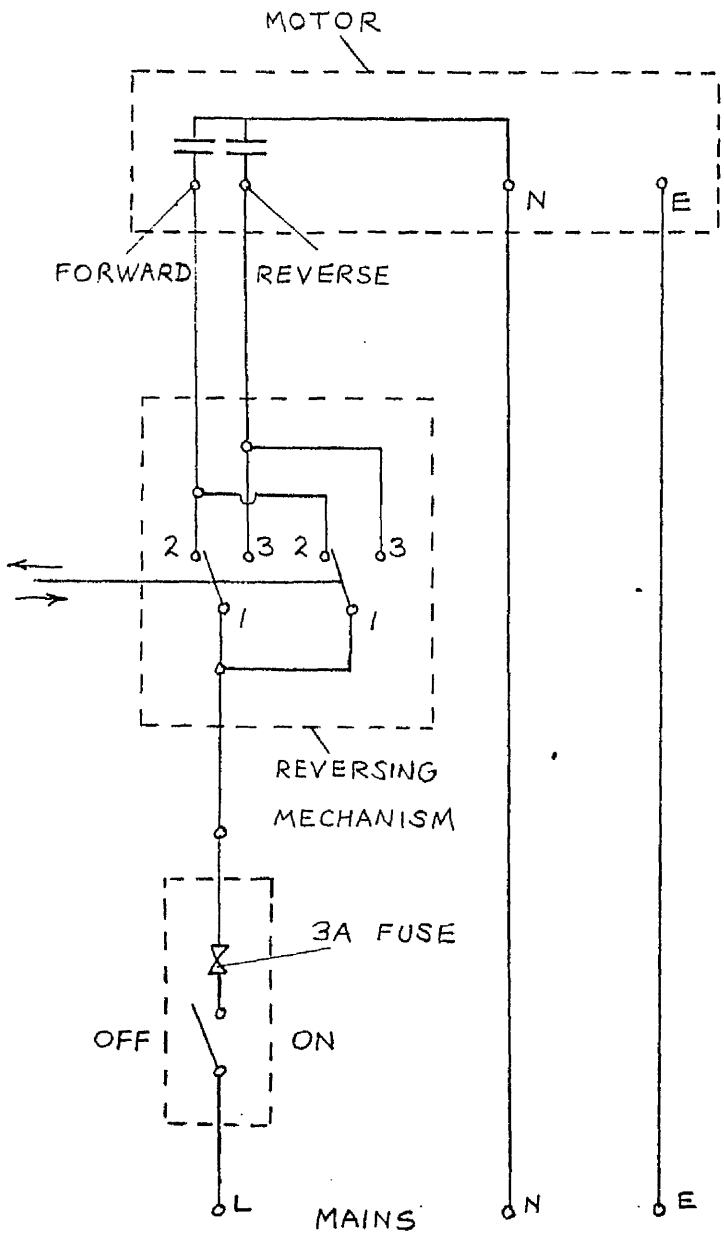

FIG. 21. CIRCUIT DIAGRAM FOR REVERSING MECHANISM

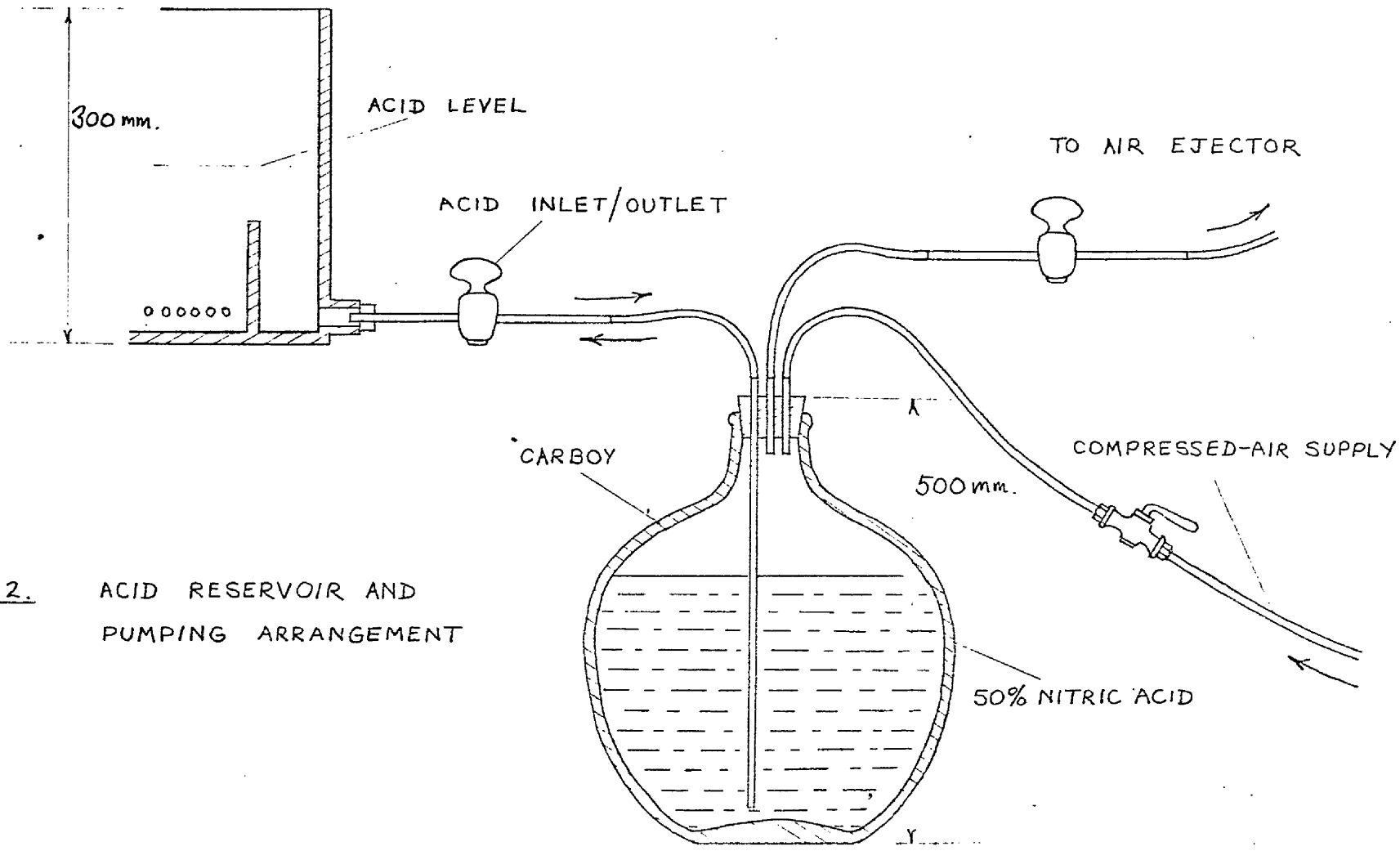

FIG. 22. ACID RESERVOIR AND PUMPING ARRANGEMENT

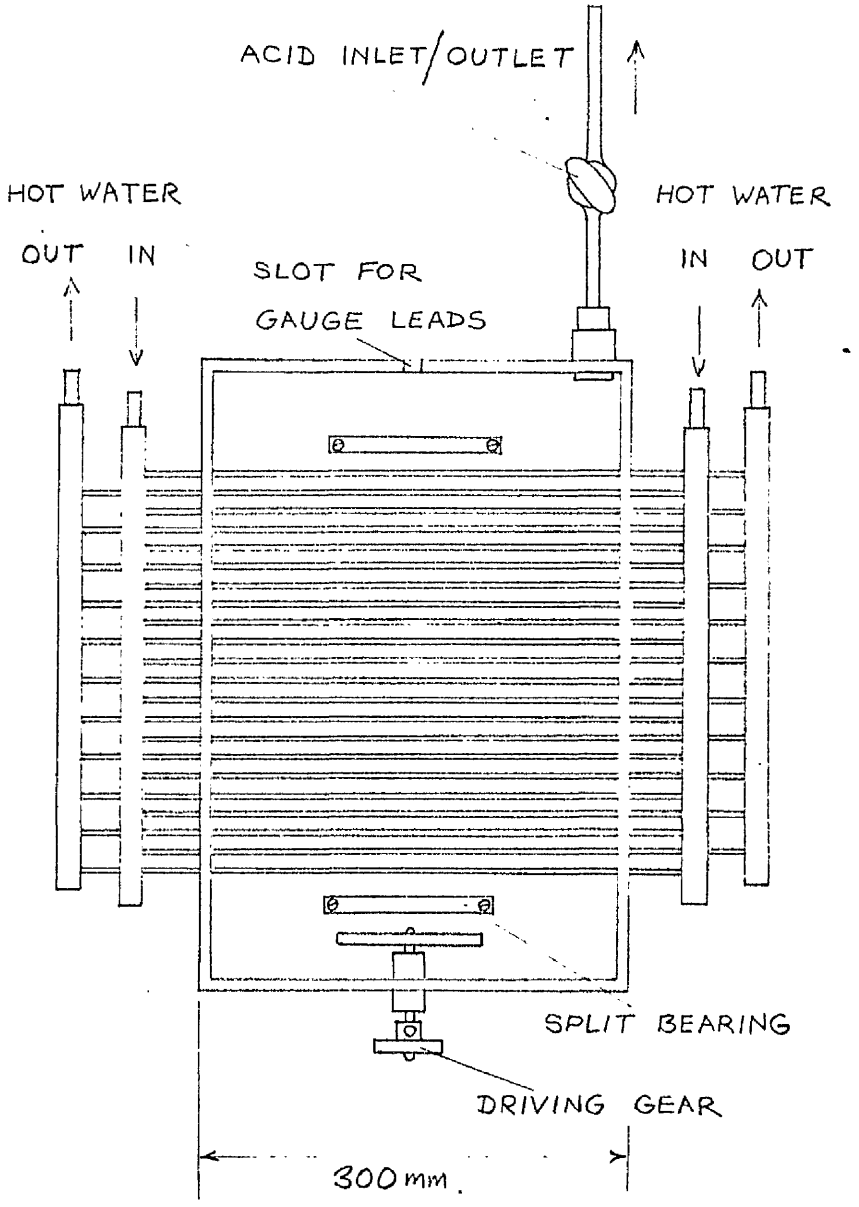

FIG. 23. PLAN VIEW OF ACID BATH.
(MOTOR, REVERSING MECHANISM AND SPINDLE OMITTED, LID REMOVED TO SHOW HEATING TUBES).

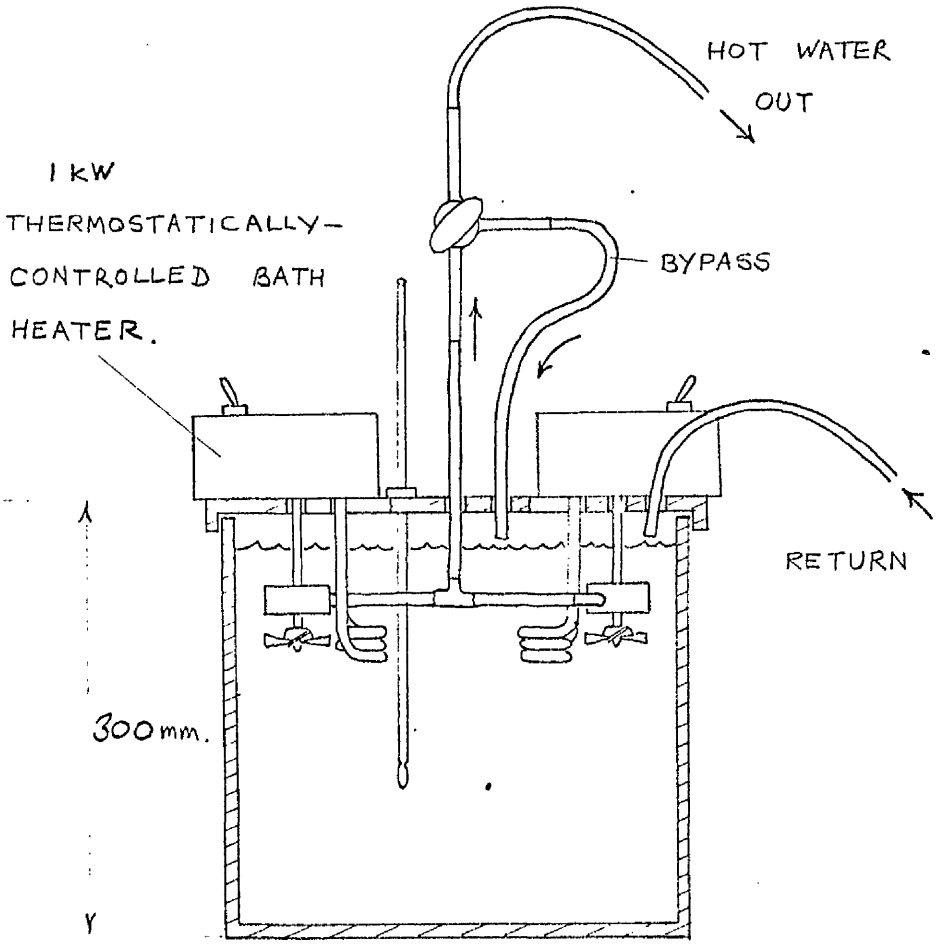

FIG. 24. HEATING-WATER SUPPLY.

FIG. 25. COMPLETE ETCHING APPARATUS.

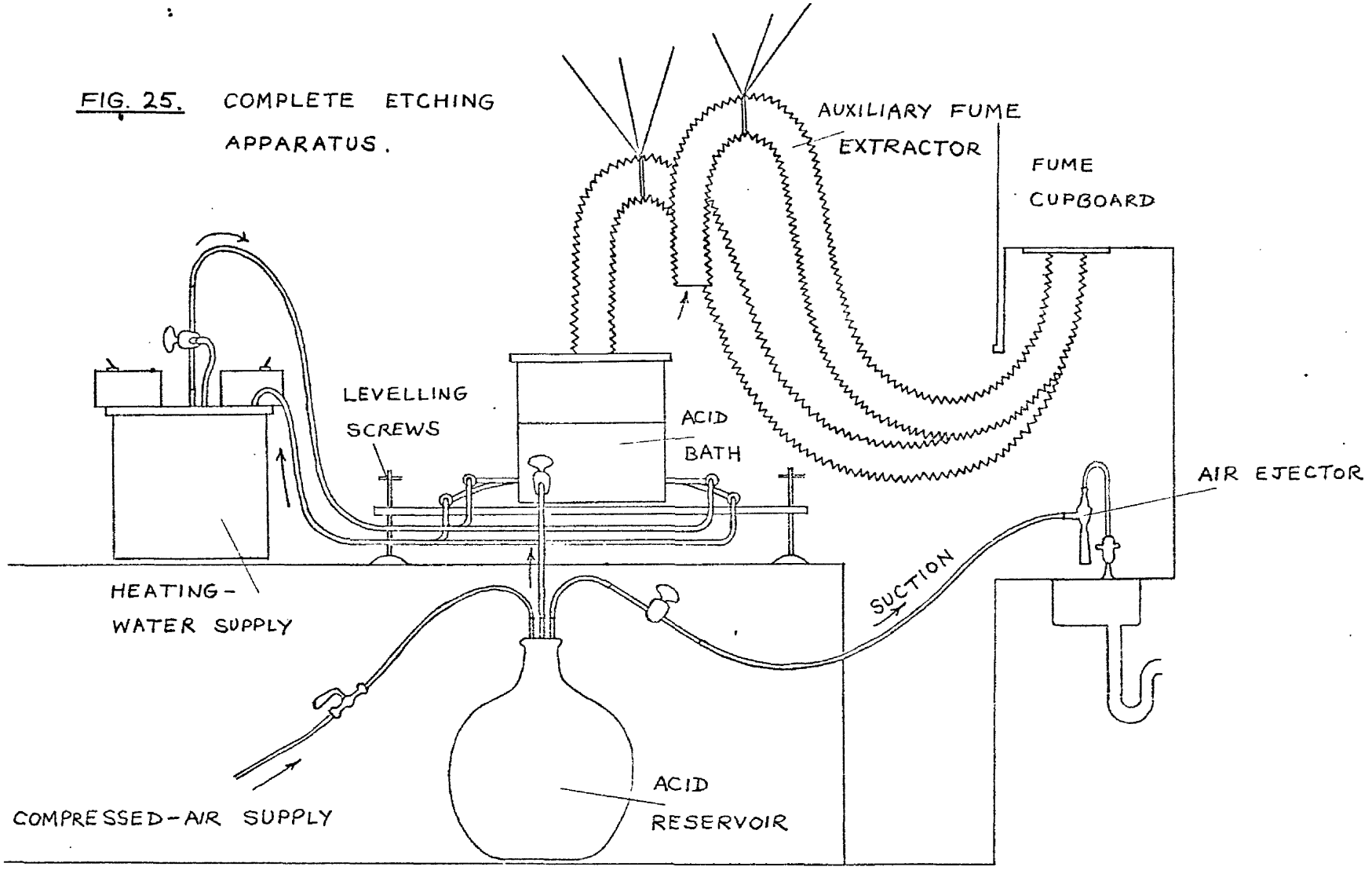

FIG. 26. ATTACHMENT OF END-RING.

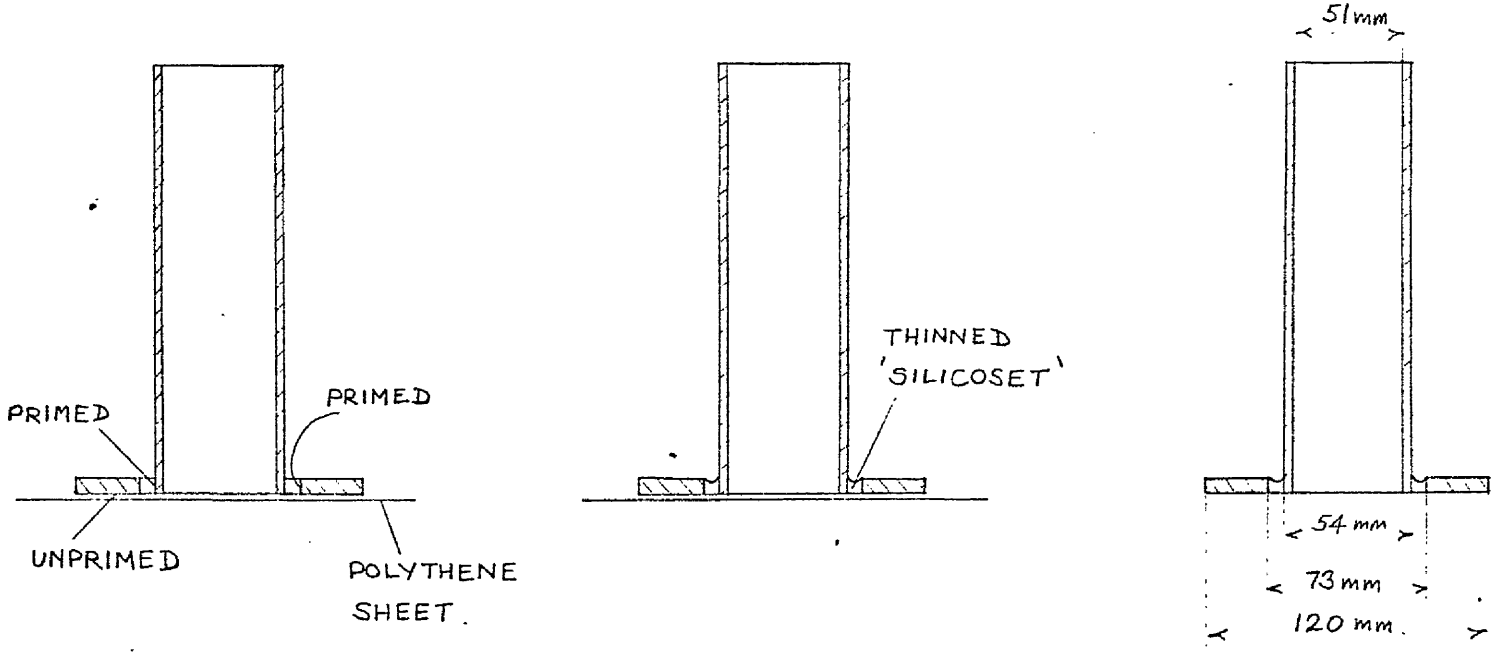

FIG. 27. SPECIMEN WITH END-RINGS.

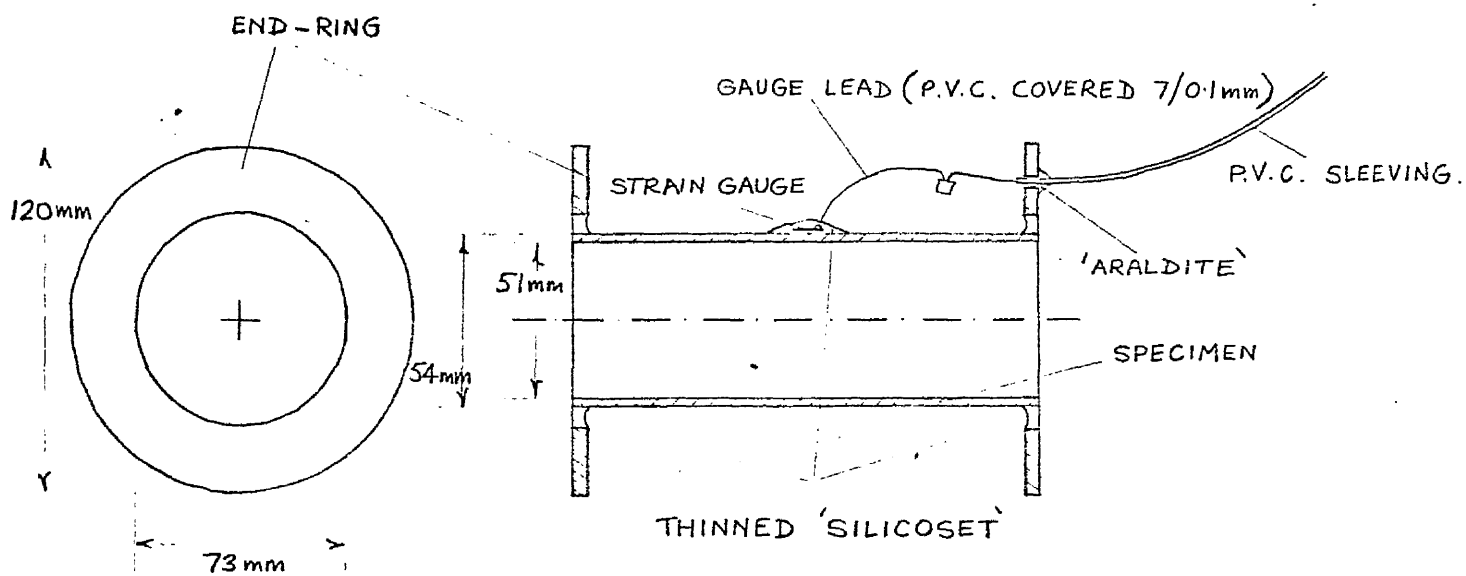

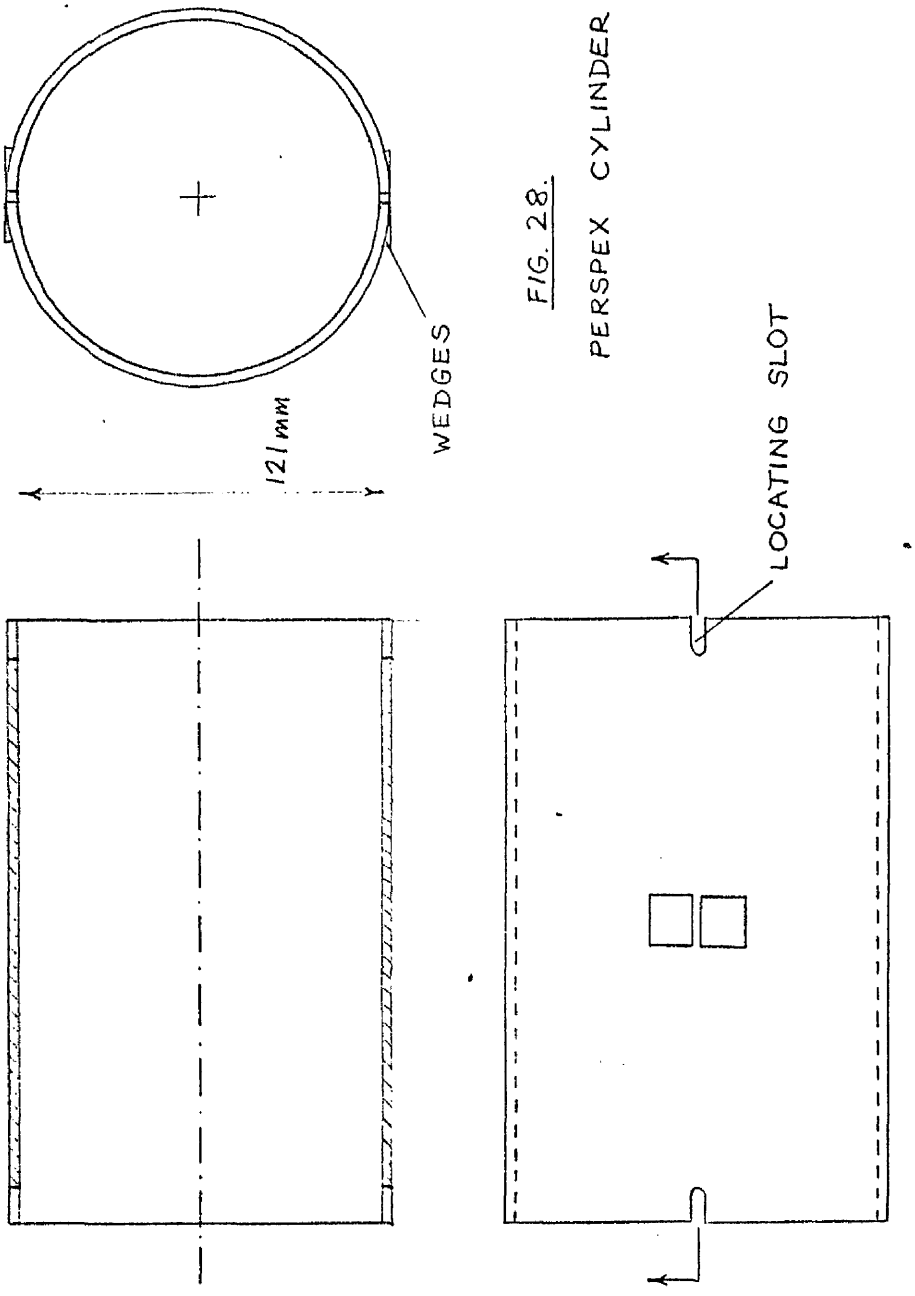

FIG. 28.

PERSPEX CYLINDER.

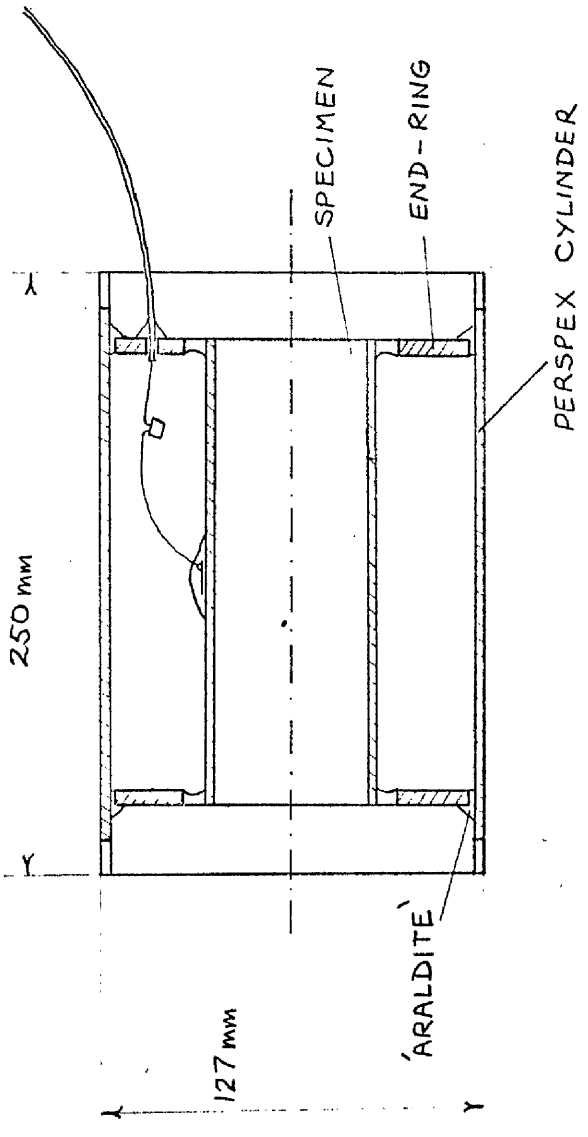

FIG. 29. SPECIMEN MOUNTED IN CYLINDER.

FIG. 30. SPINDLE + CYLINDER SUPPORTS

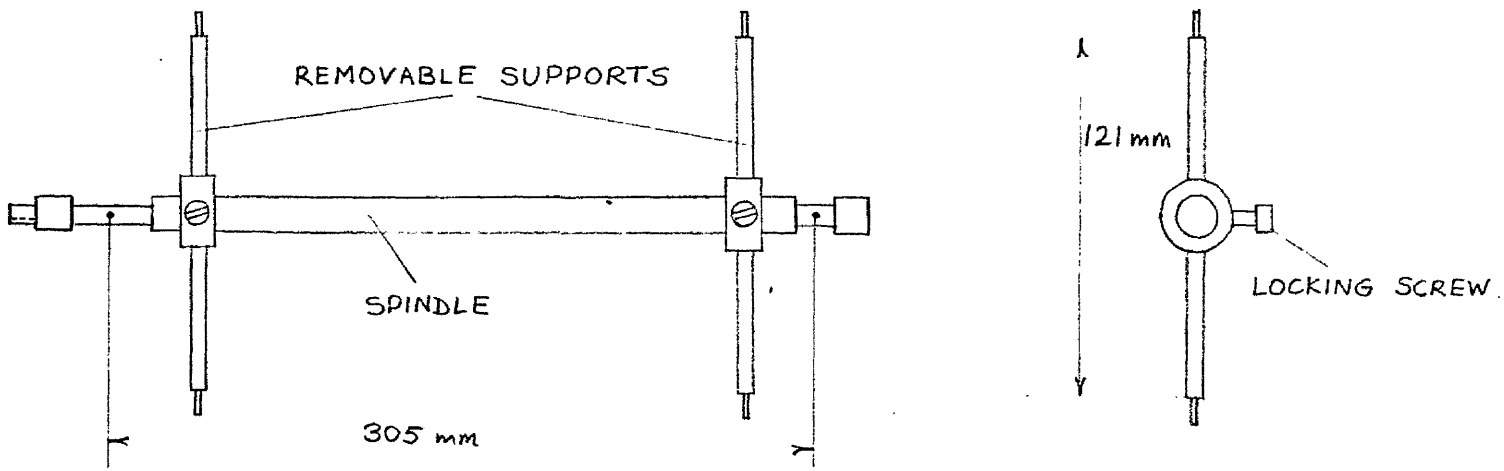

FIG. 31. COMPLETE ASSEMBLY, INTERNAL LAYER REMOVAL.

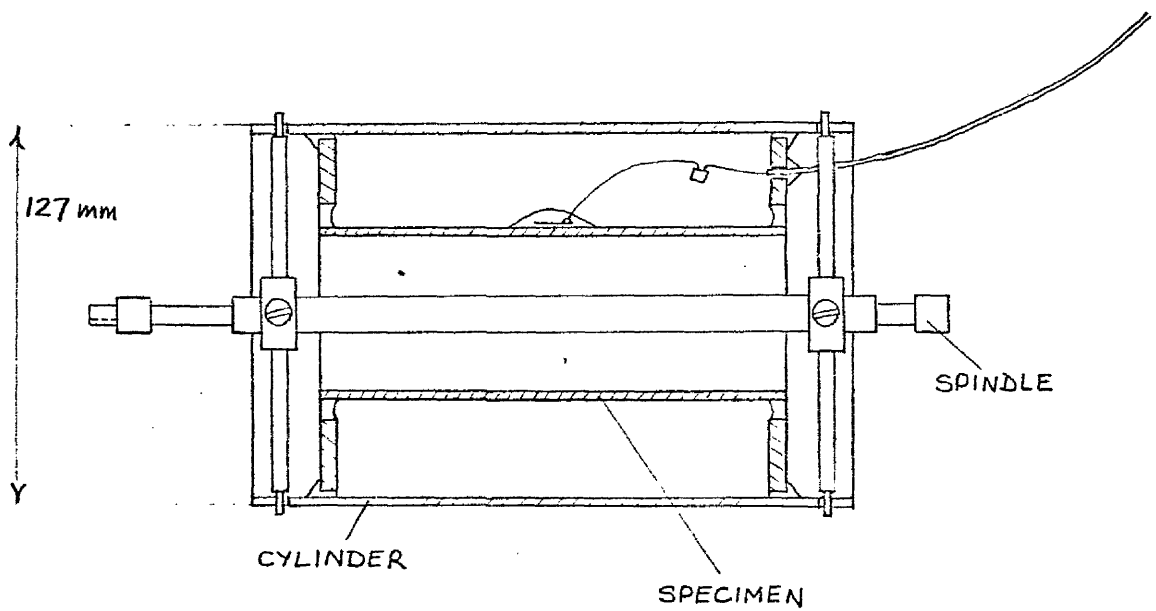

FIG. 32. ATTACHMENT OF END-DISC.

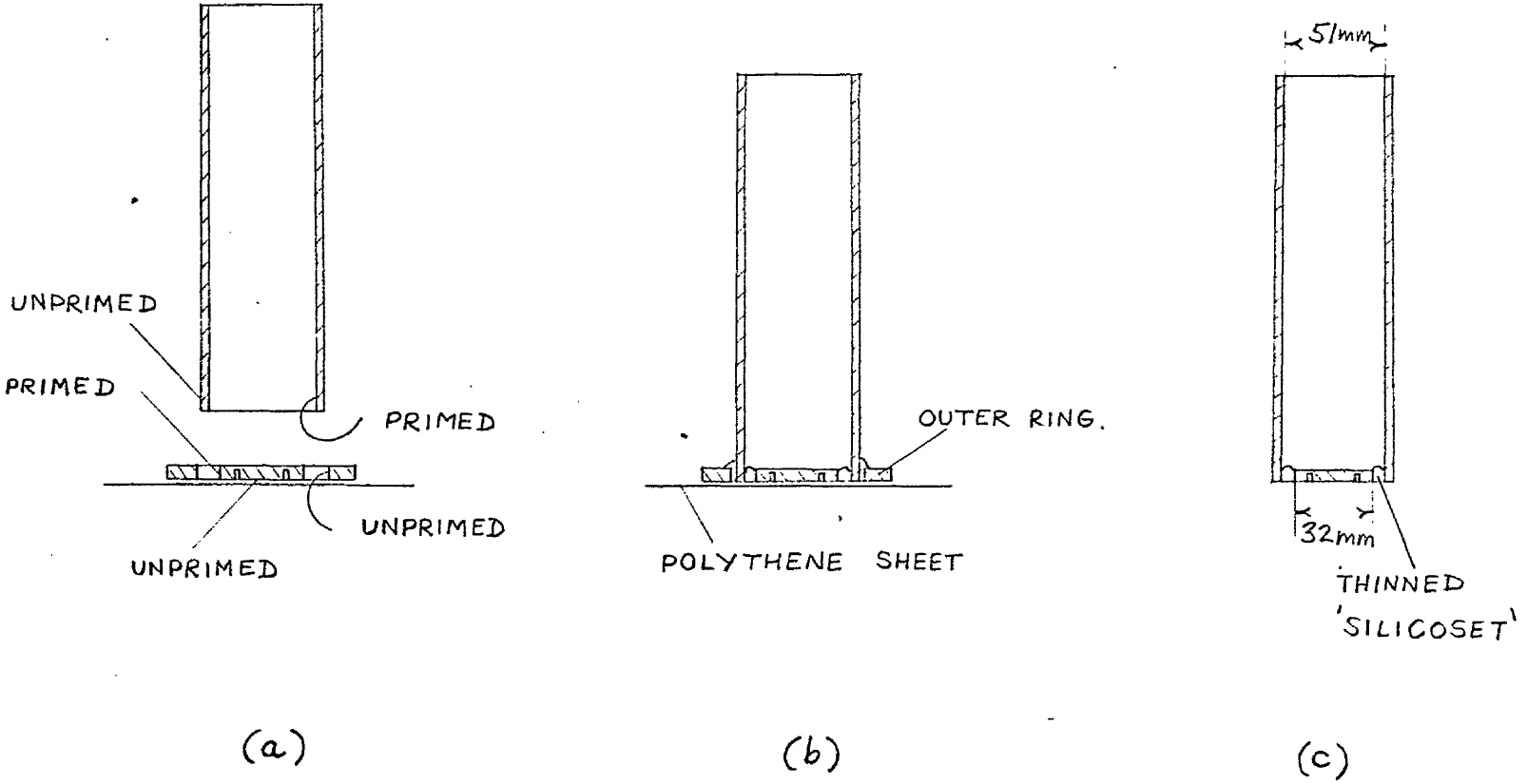

FIG. 33. SPECIMEN WITH END-DISCS.

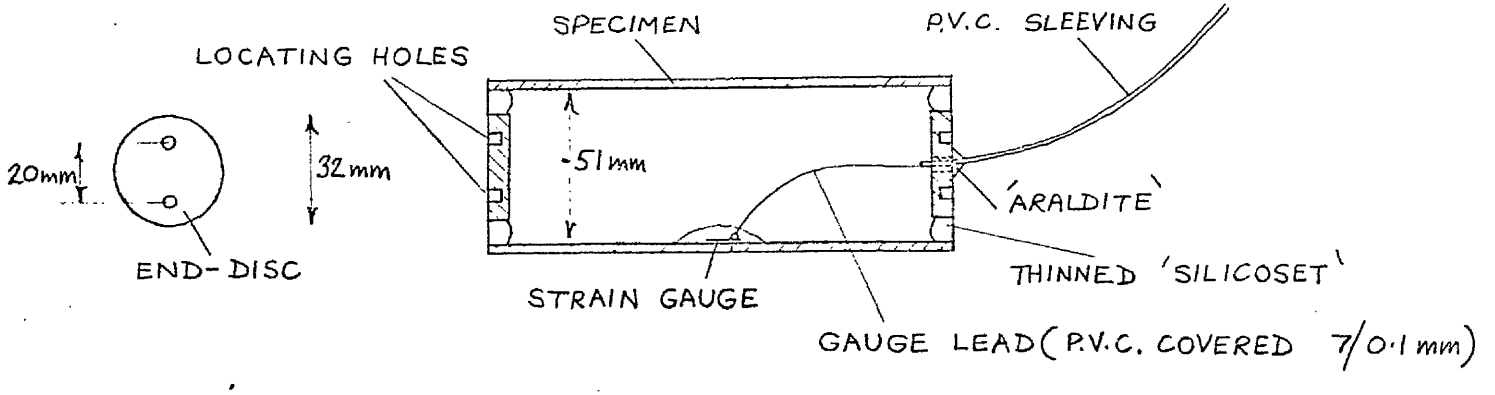

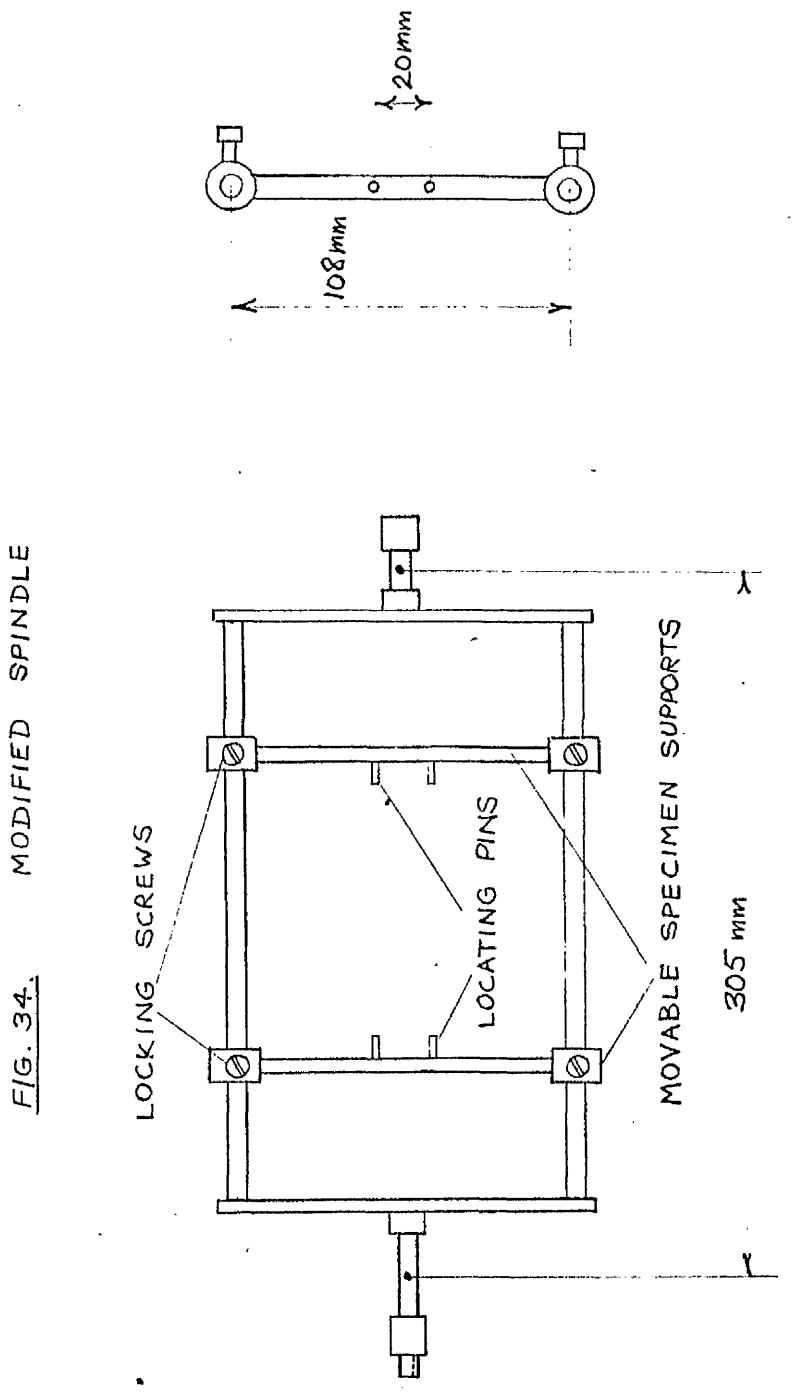

FIG. 34. MODIFIED SPINDLE

FIG. 35. COMPLETE ASSEMBLY, EXTERNAL LAYER REMOVAL.

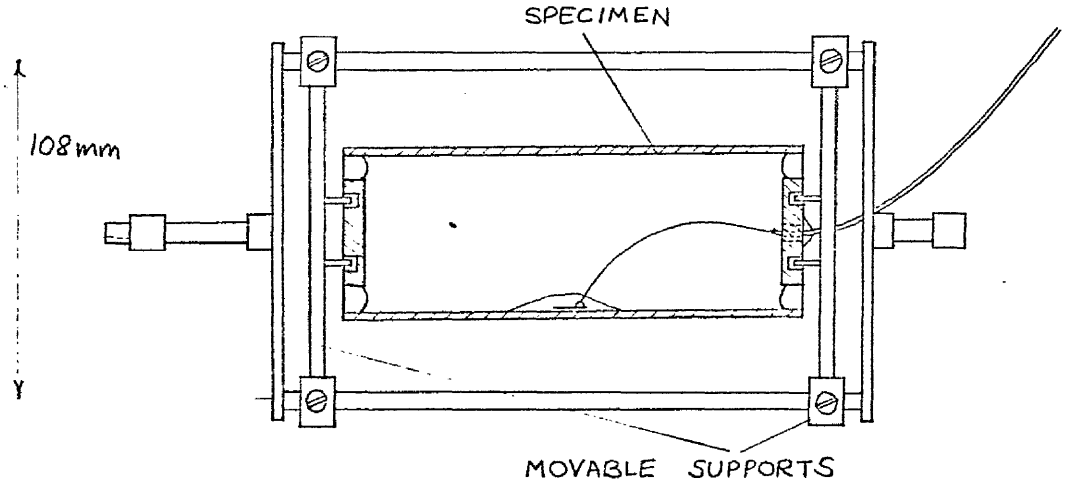

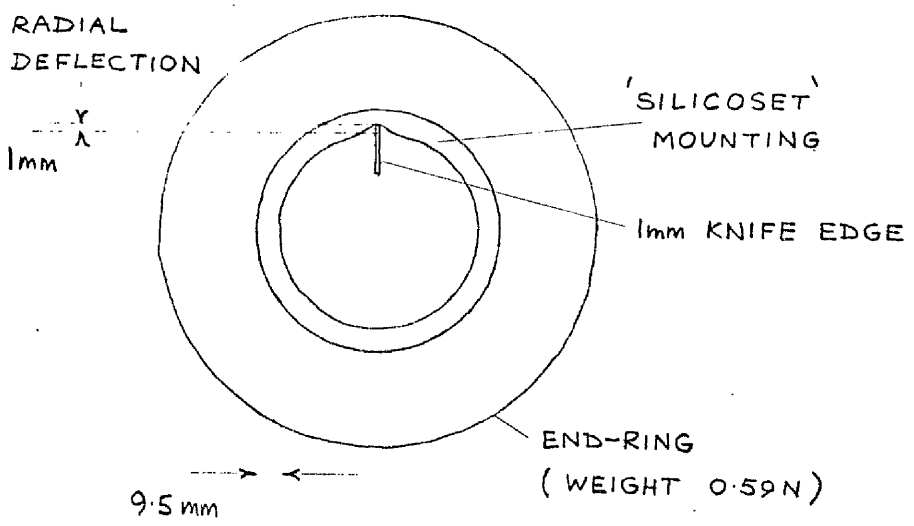

FIG. 36. FLEXIBILITY OF 'SILICOSET' MOUNTING (SPECIMEN REMOVED FOR THIS TEST).

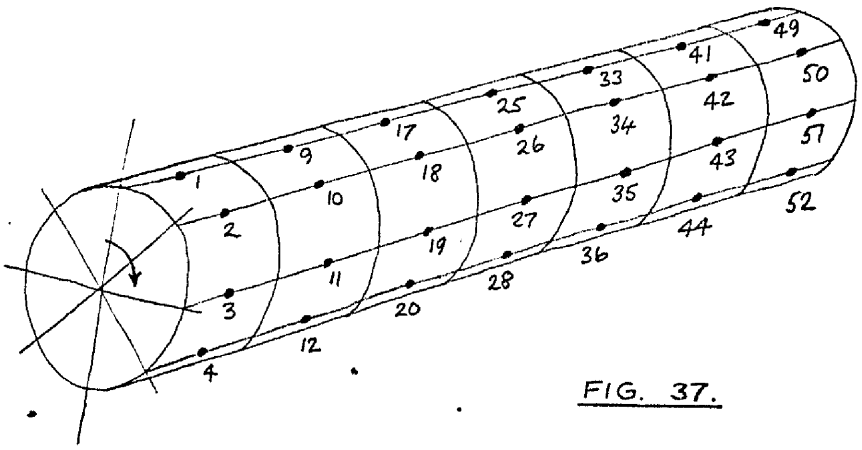

FIG. 37.

FIRST SPECIMEN 24% REDUCTION IN h

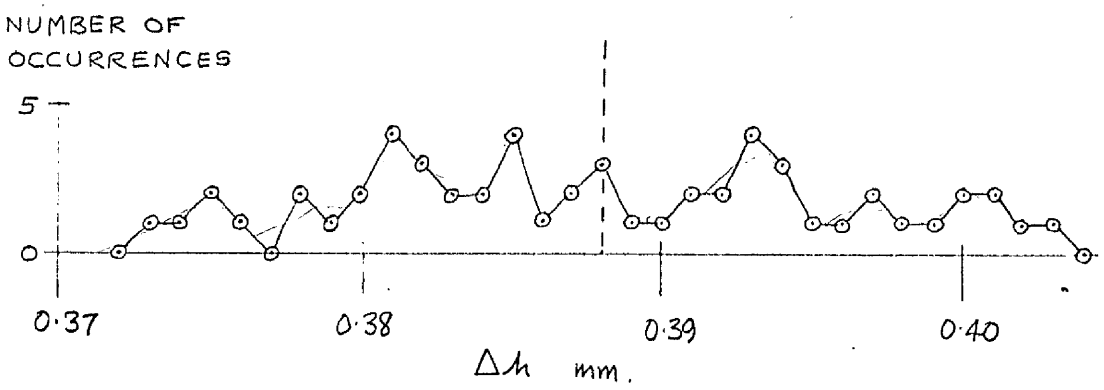

SECOND SPECIMEN 81% REDUCTION IN h

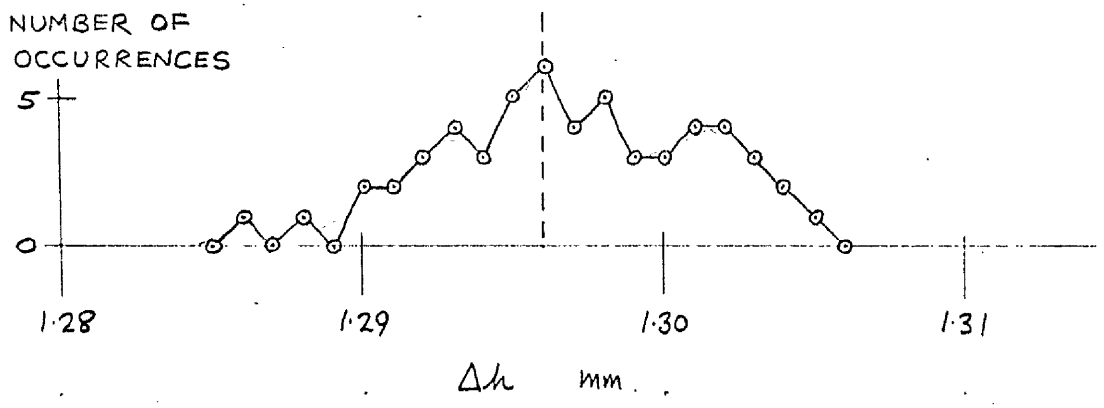

FIG. 38. UNIFORMITY OF LAYER REMOVAL

FIG. 39.

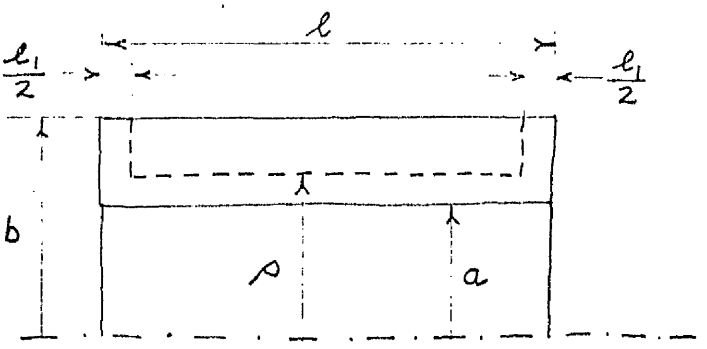

FIG. 40.

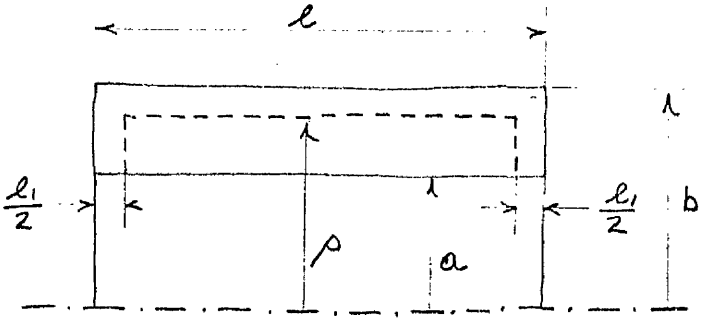

FIG. 41. SPECIMEN 3A-1, ℓ_1 v W

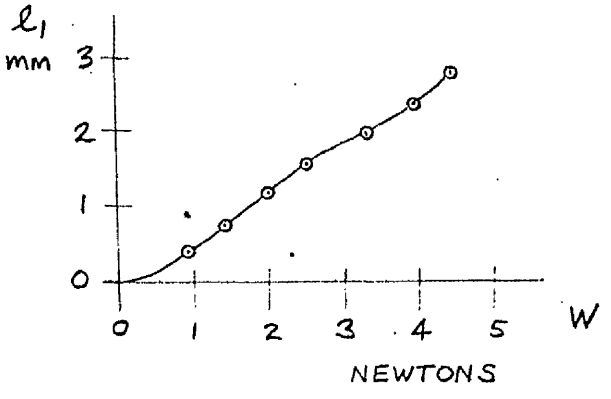

FIG. 42.

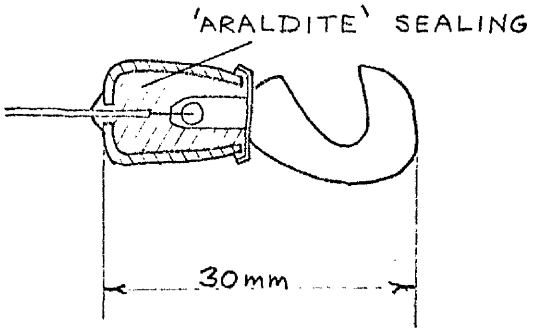
'ARALDITE' SEALING
30mm

FIG. 43.

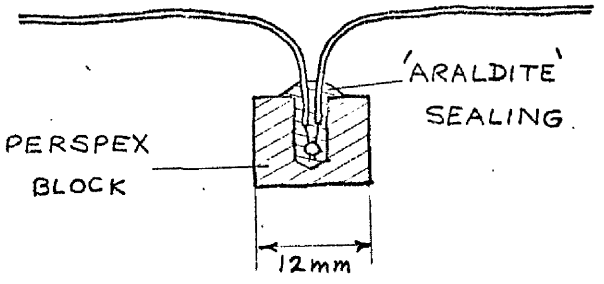
'ARALDITE'
SEALING
PERSPEX
BLOCK
12mm

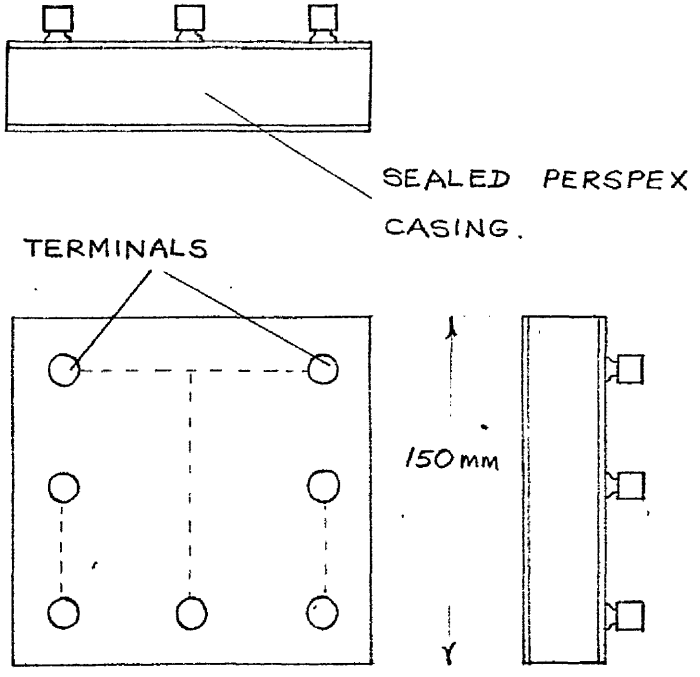

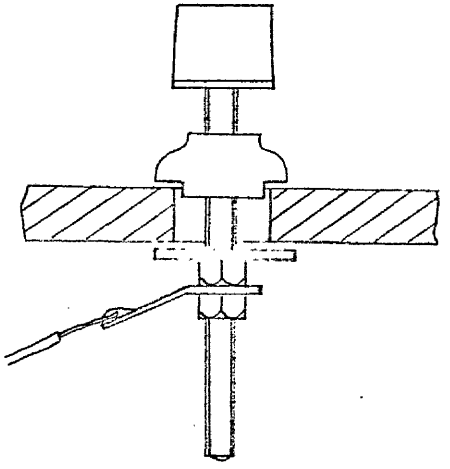

FIG. 44.

TERMINAL BOX

FIG. 45. PROTECTION OF SPADE TERMINALS

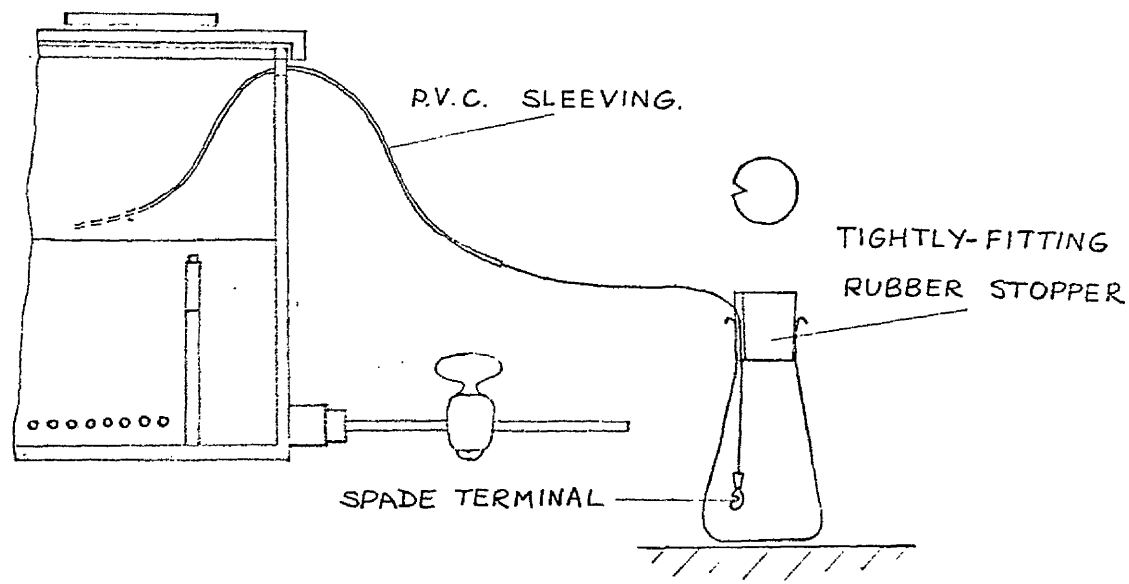

FIG. 46. SECTIONAL ELEVATION, CONSTANT TEMPERATURE CHAMBER

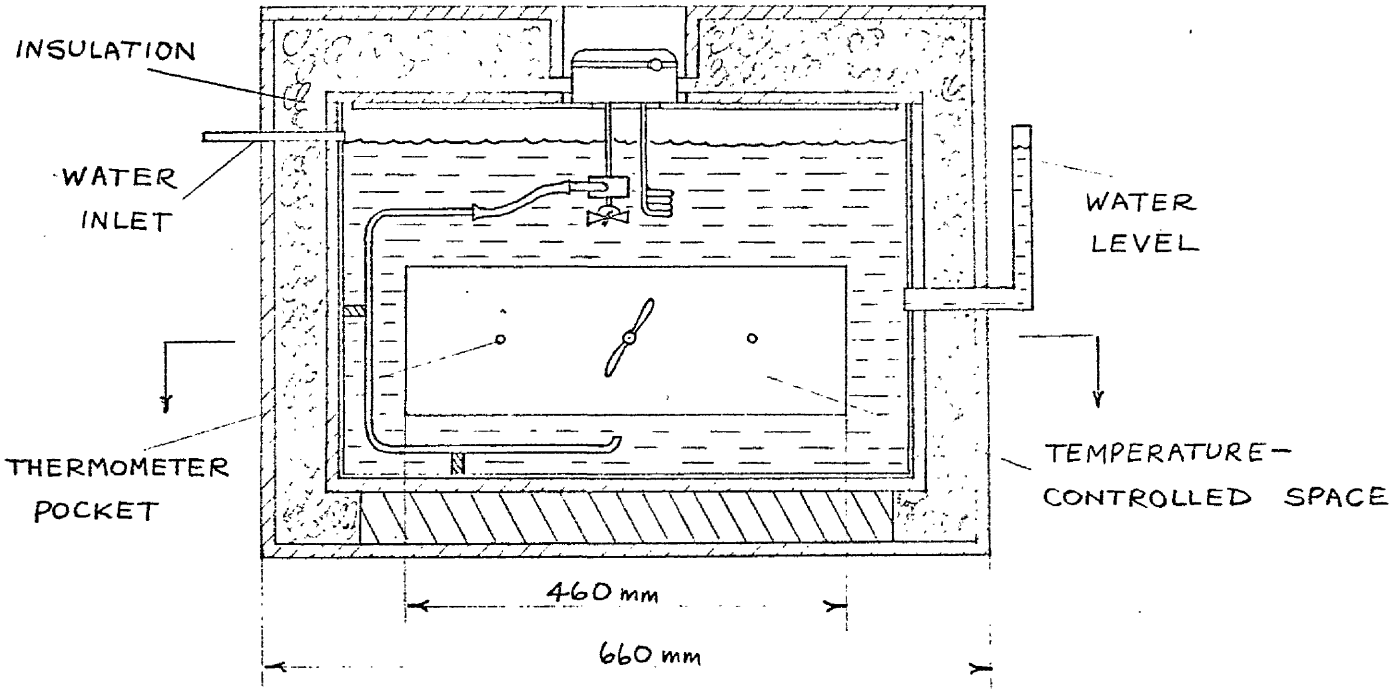

FIG. 47. SECTIONAL END ELEVATION, CONSTANT TEMPERATURE CHAMBER

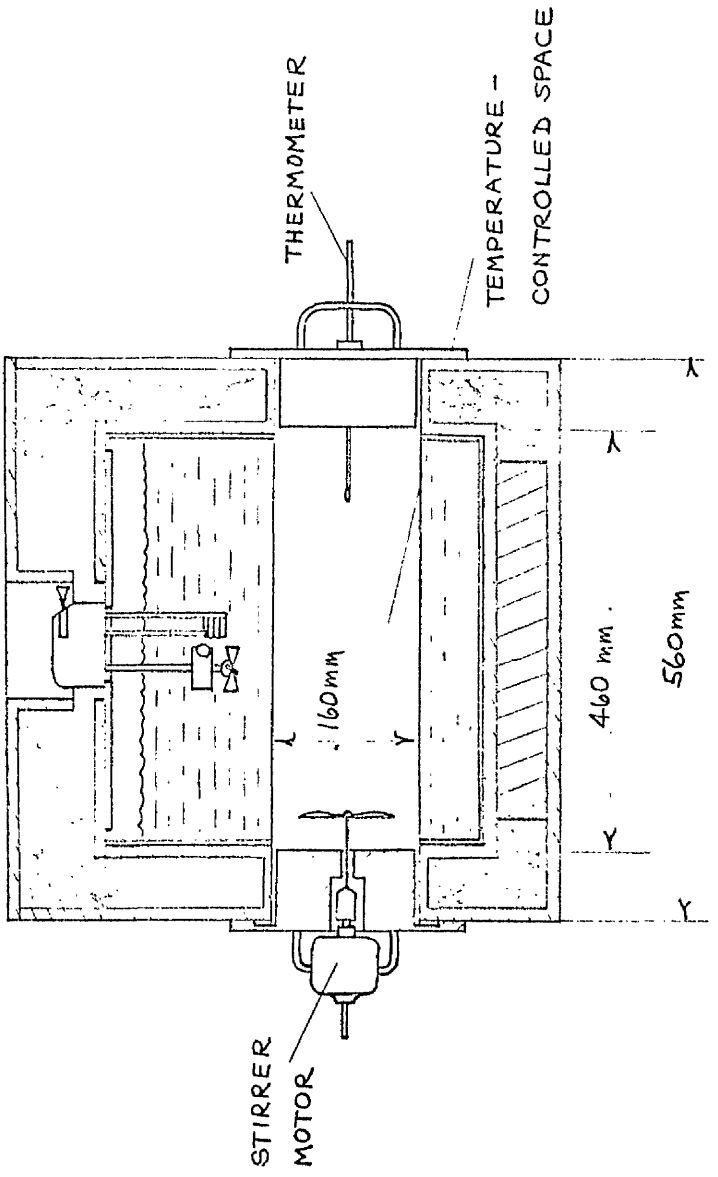

FIG. 48. SECTIONAL PLAN, CONSTANT TEMPERATURE CHAMBER

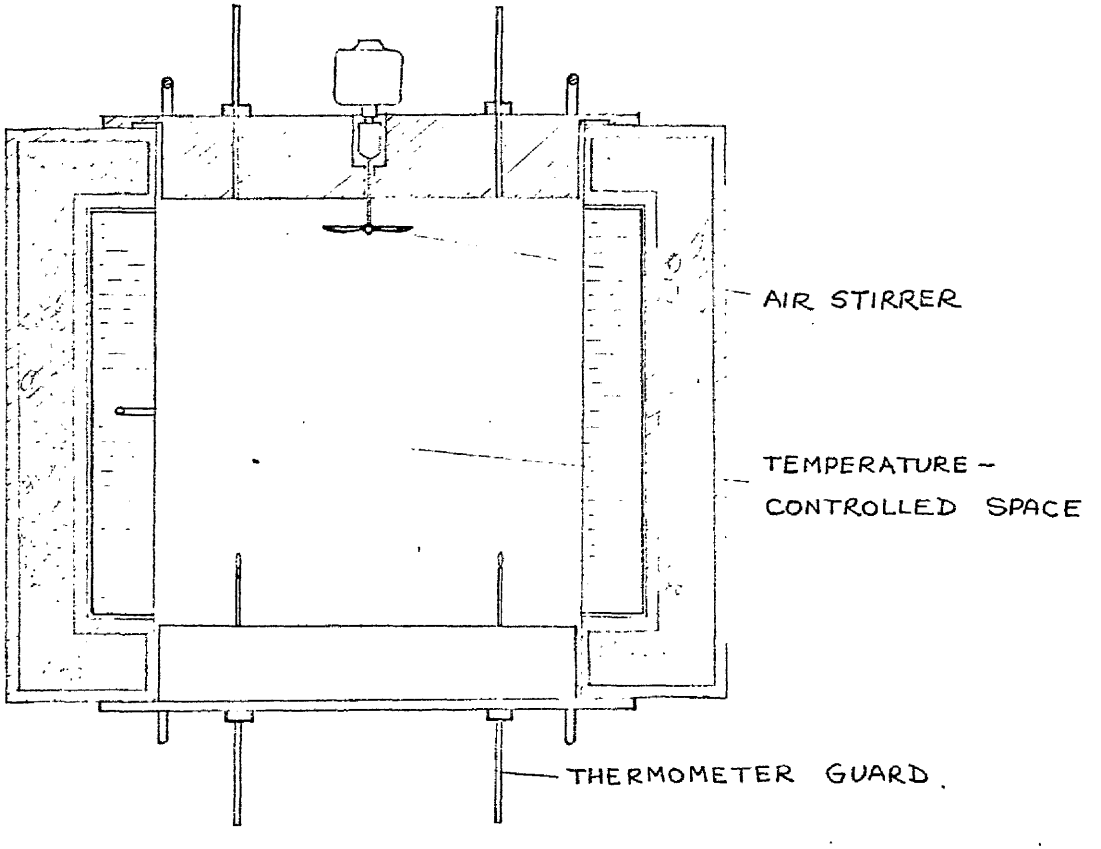

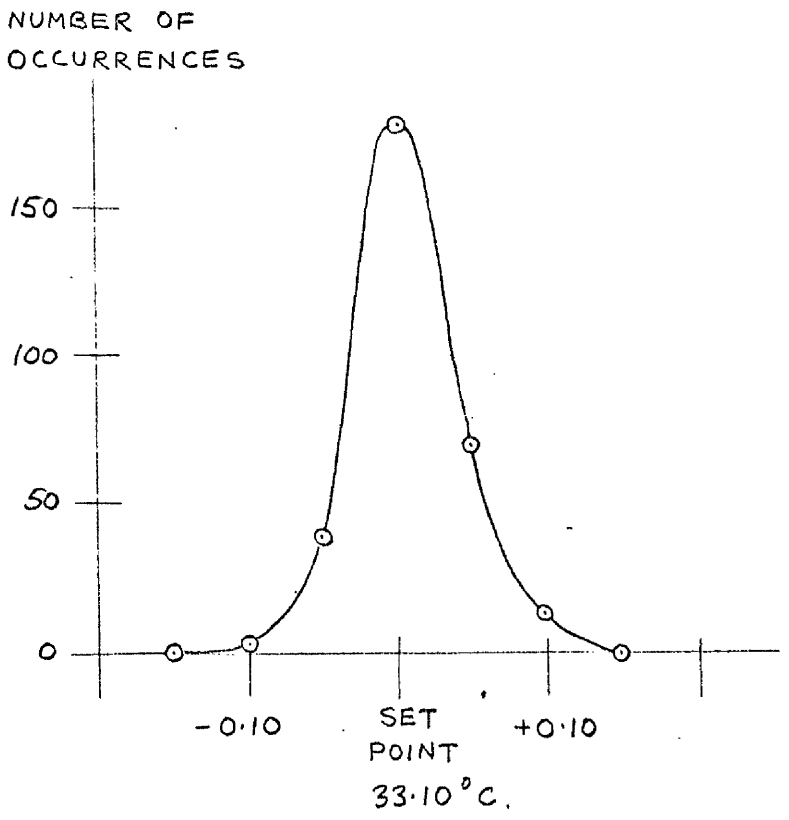

FIG. 49. STABILITY OF CONSTANT TEMPERATURE CHAMBER

FIG. 50. STRAIN-MEASURING CIRCUIT

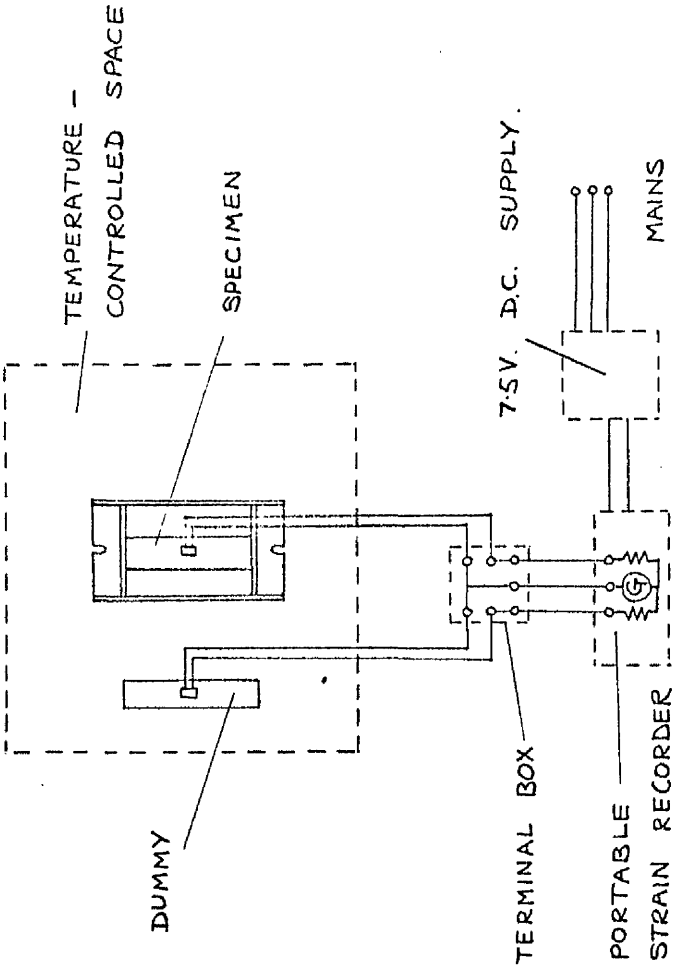

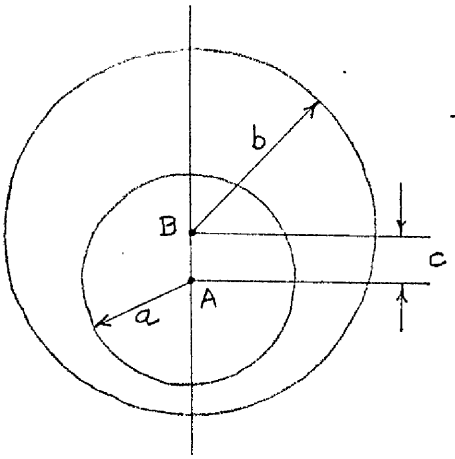

FIG. 51.

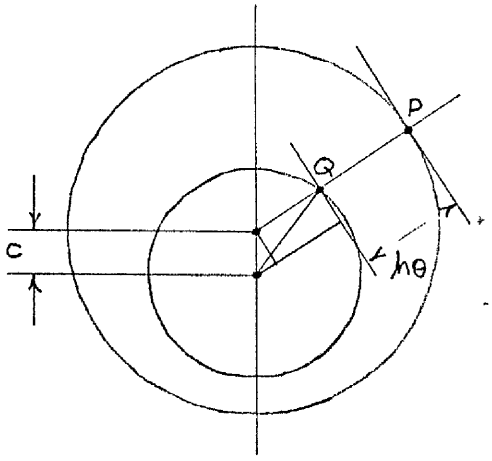

FIG. 52.

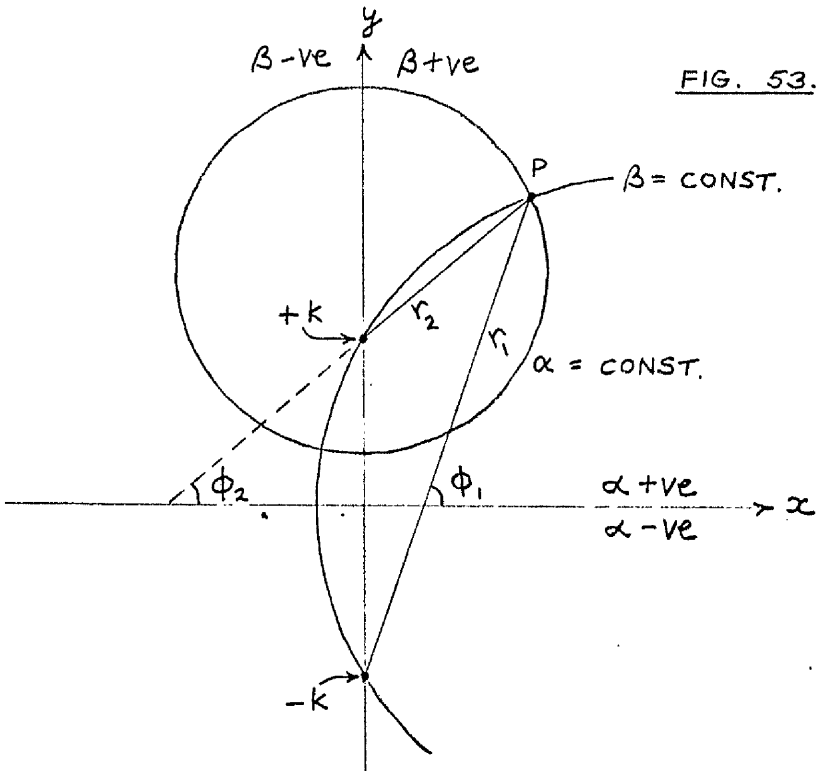

FIG. 53.

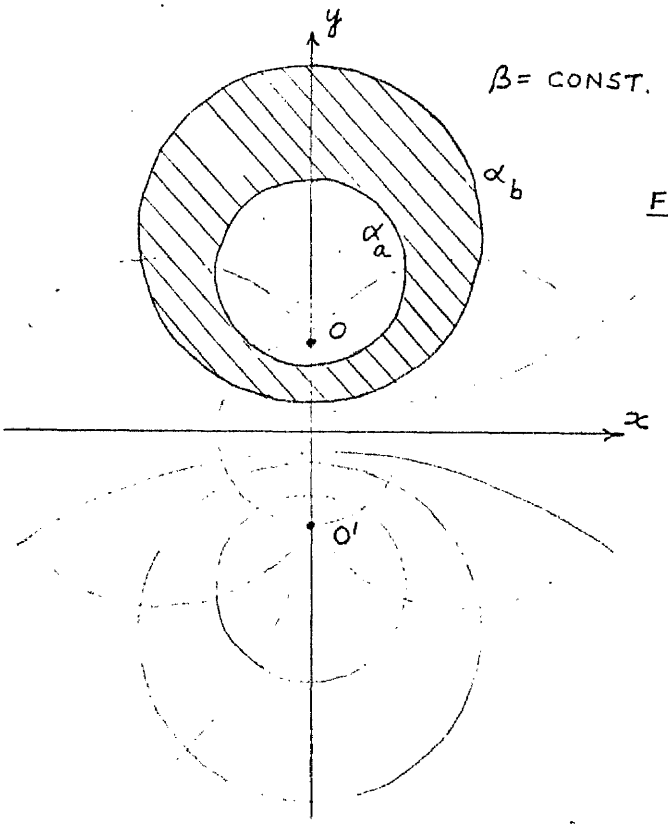
y
β = CONST.
α_b
α_a
O
x
O'

FIG. 54.

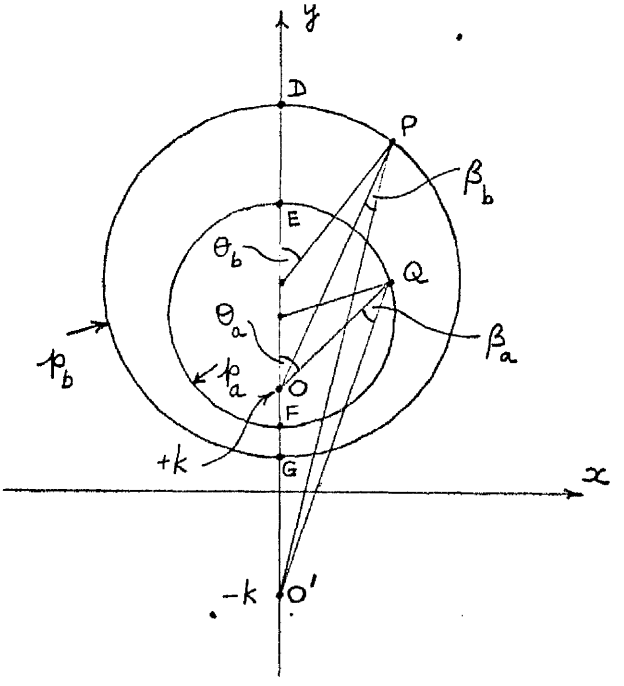
y
D
P
β_b
E
θ_b
Q
θ_a
β_a
p_b
p_a
O
F
+k
G
x
-k
O'

FIG. 55.

FIG. 56. $F_b(\rho/b, \theta)$ v θ

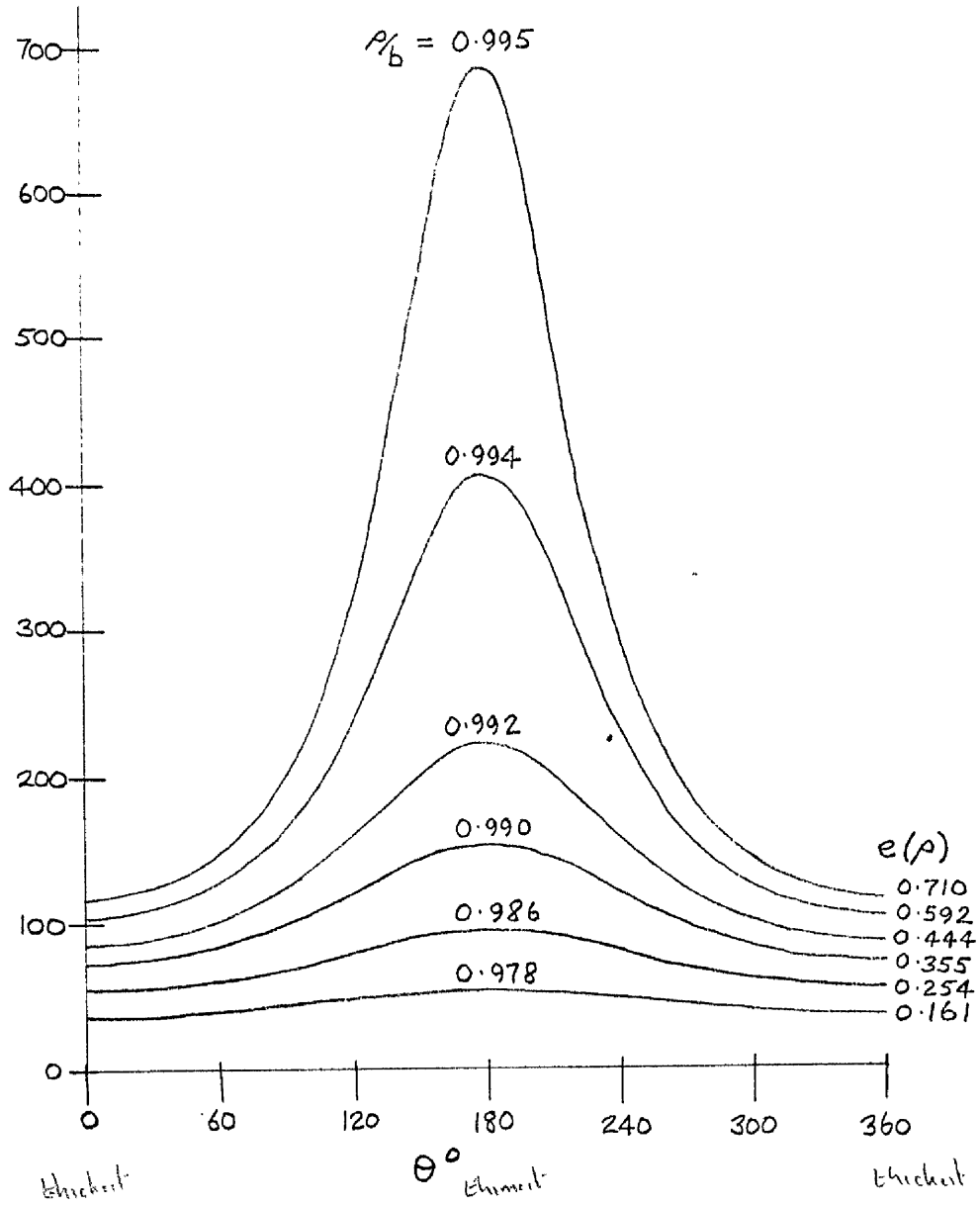

FIG. 57.

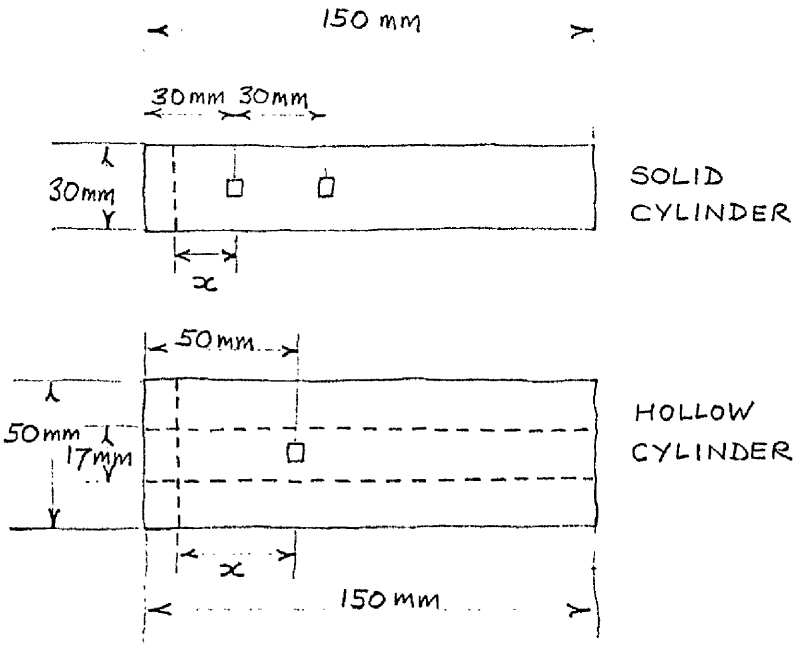
150 mm
30mm 30mm
30mm
SOLID CYLINDER
x
50mm
50mm
17mm
HOLLOW CYLINDER
x
150 mm

FIG. 58.

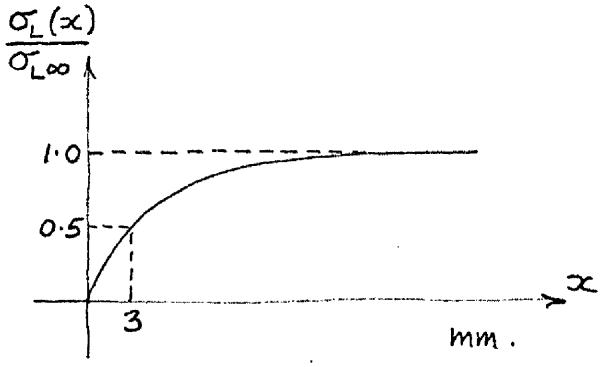
$\frac{\sigma_L(x)}{\sigma_{L\infty}}$
1·0
0·5
3
x
mm.

FIG. 59.

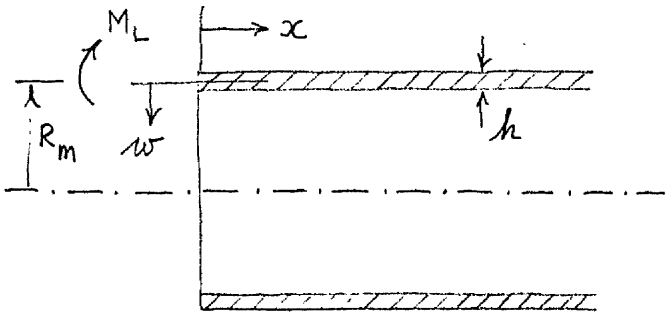

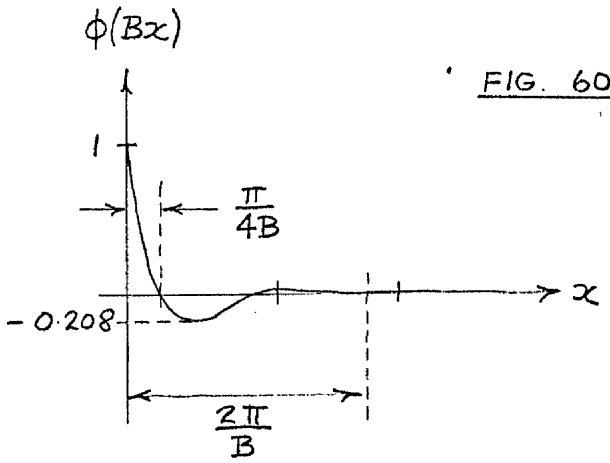

FIG. 60.

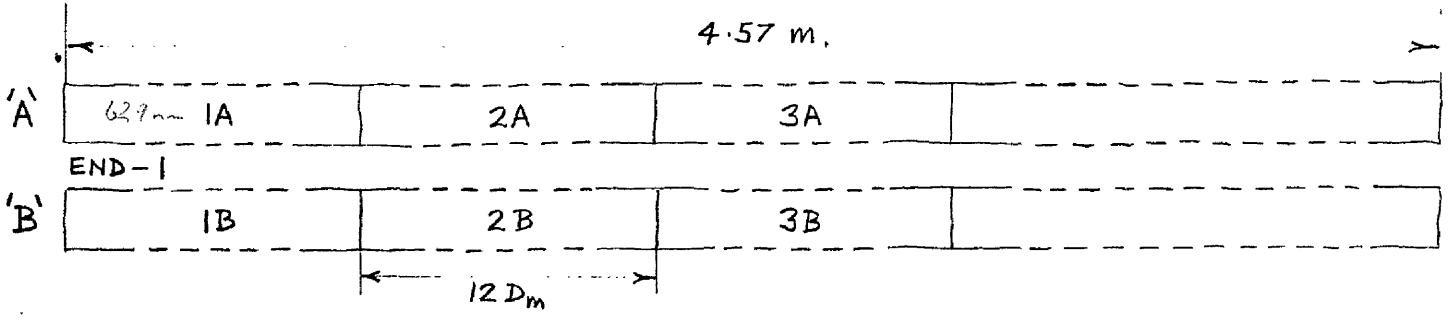

(a)

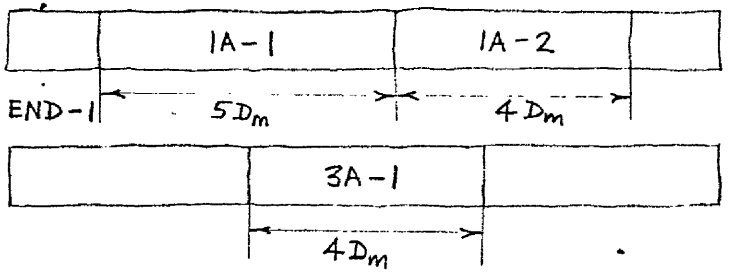

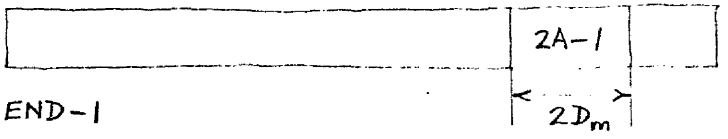

(b)

FIG. 61.

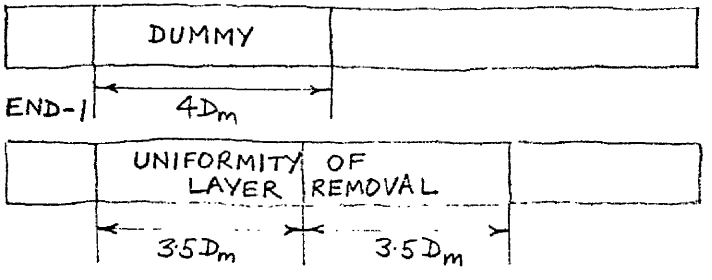

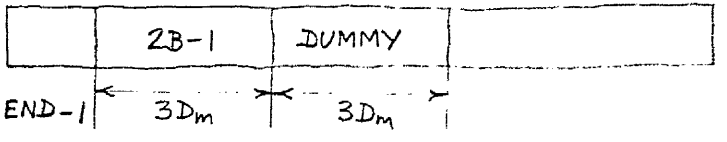

(c)

$D_m = 52{\cdot}4$ mm

FIG. 62. CIRCUMFERENTIAL VARIATION IN WALL THICKNESS, TUBE 3A.

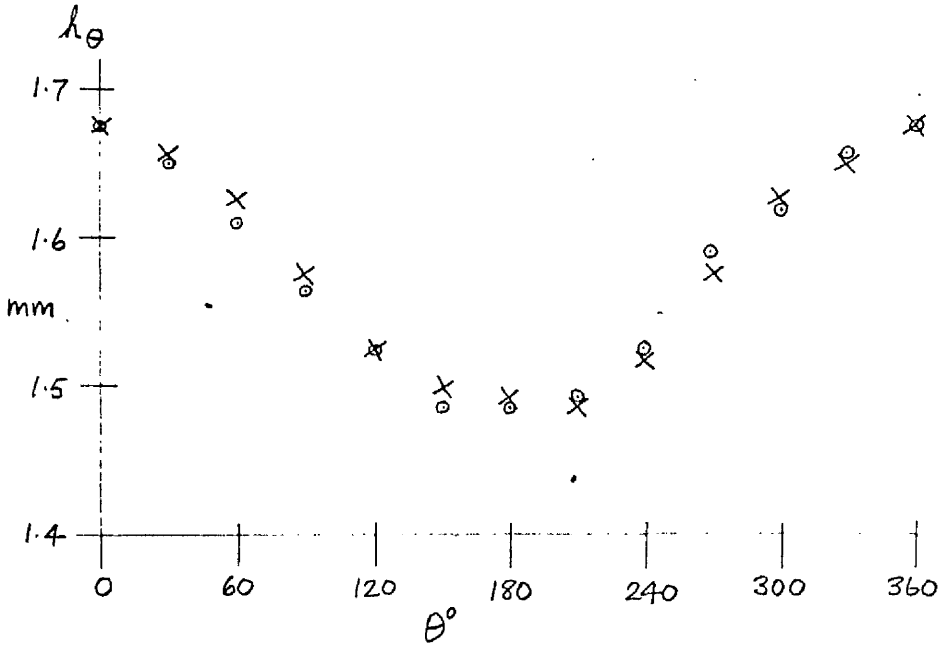

FIG. 63.

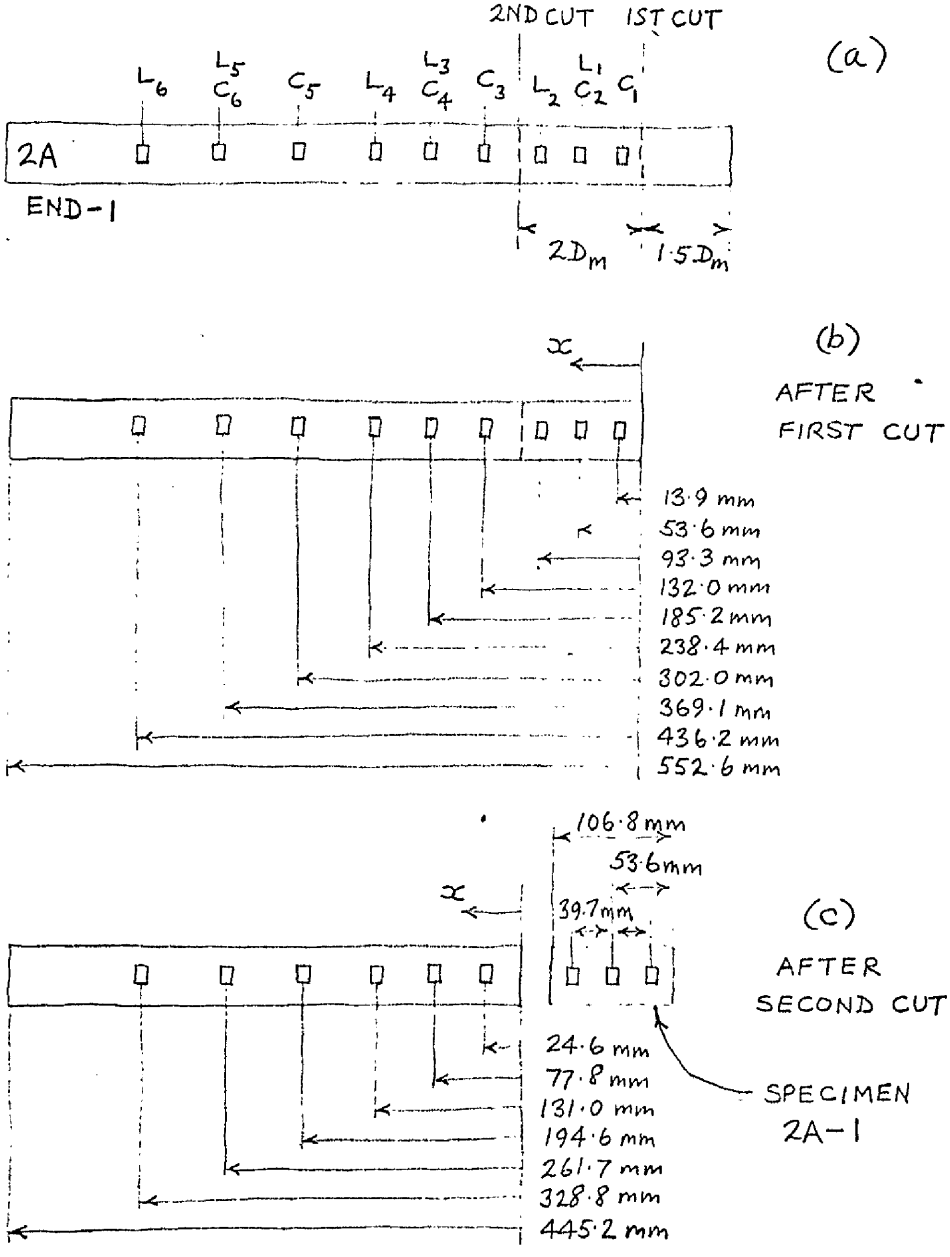
2ND CUT
1ST CUT
(a)
L_6 L_5 C_6 C_5 L_4 L_3 C_4 C_3 L_2 L_1 C_2 C_1
2A
END-1
$2D_m$
$1.5D_m$
(b)
AFTER FIRST CUT
x
13·9 mm
53·6 mm
93·3 mm
132·0 mm
185·2 mm
238·4 mm
302·0 mm
369·1 mm
436·2 mm
552·6 mm
106·8 mm
53·6mm
39·7mm
x
(c)
AFTER SECOND CUT
24·6 mm
77·8 mm
131·0 mm
194·6 mm
261·7 mm
328·8 mm
445·2 mm
SPECIMEN 2A-1

FIG. 64.

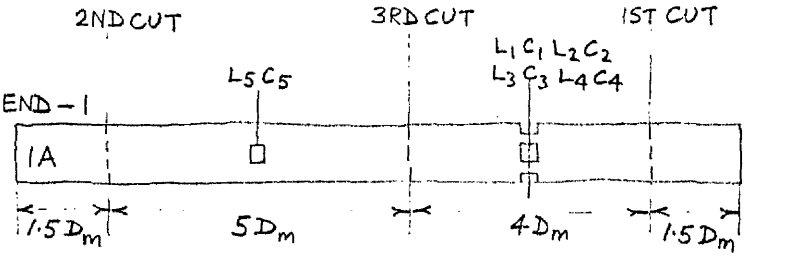

(a)

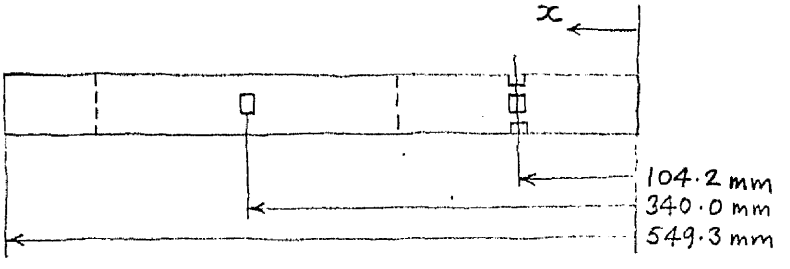

(b) AFTER FIRST CUT

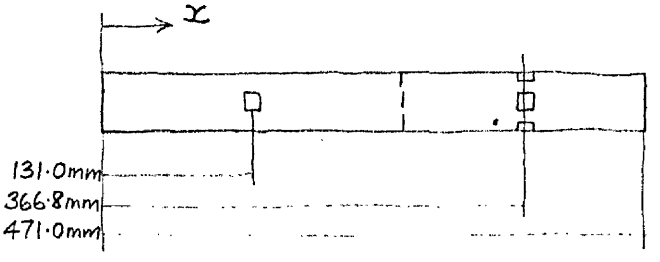

(c) AFTER SECOND CUT

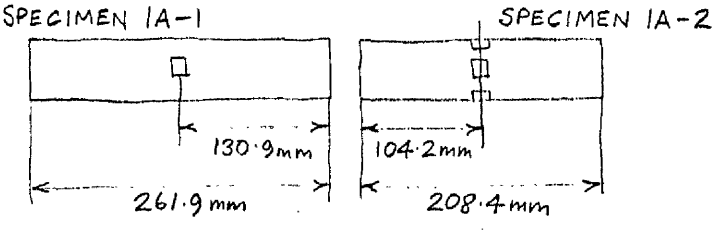

(d) AFTER THIRD CUT

FIG. 65.

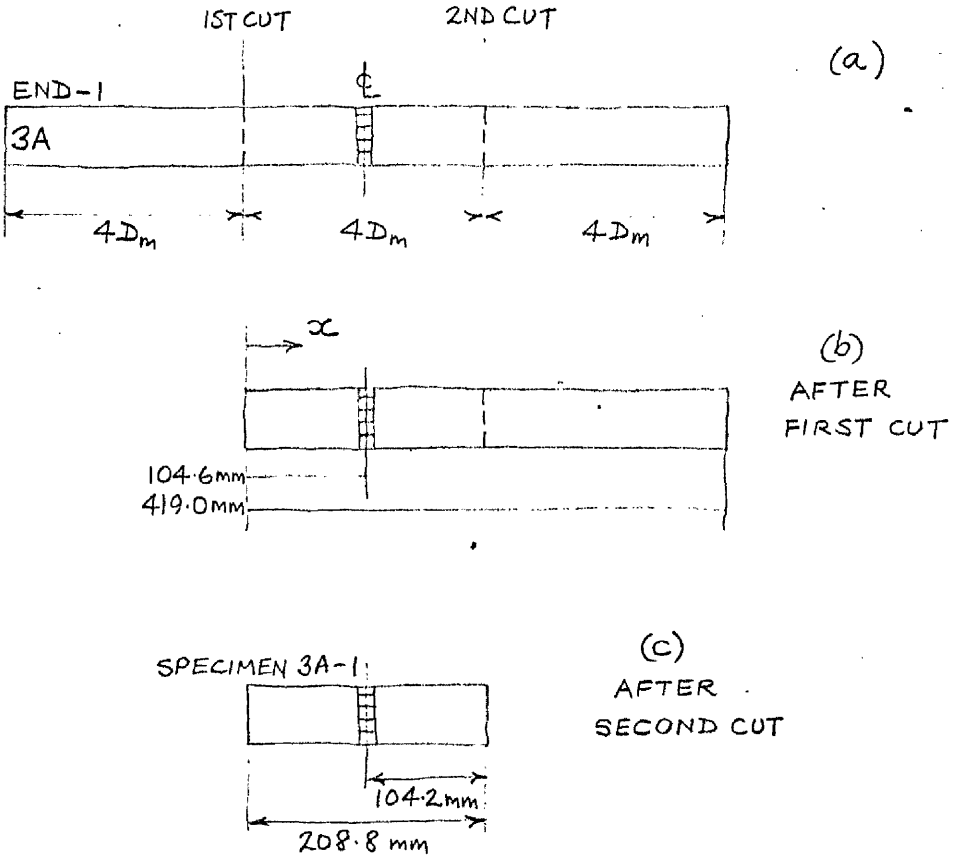
1ST CUT
2ND CUT
(a)
END-1
℄
3A
4Dm
4Dm
4Dm
x
(b)
AFTER
FIRST CUT
104·6mm
419·0mm
SPECIMEN 3A-1
(c)
AFTER
SECOND CUT
104·2mm
208·8 mm

FIG. 66.

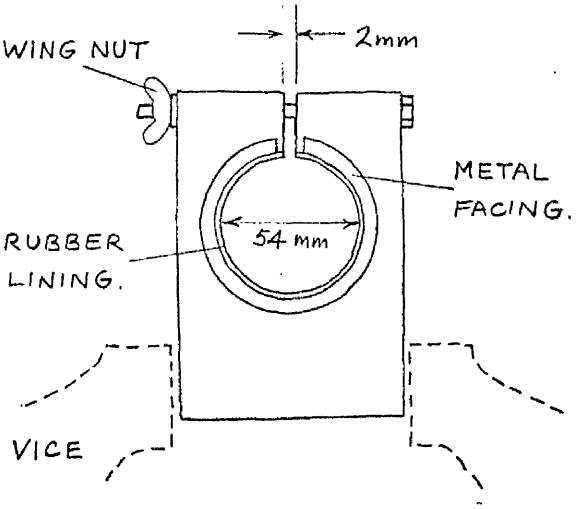

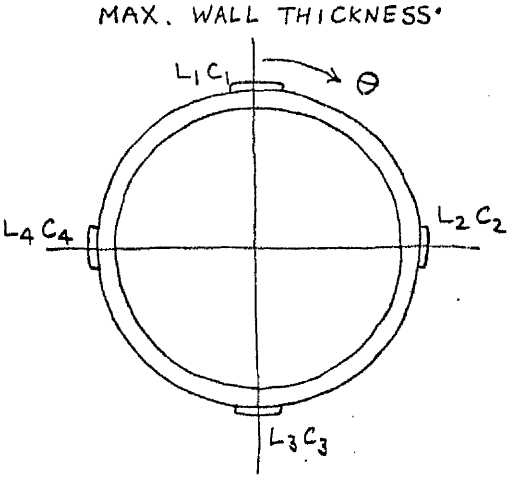

FIG. 67. GAUGE POSITIONS, SPECIMEN 1A-2 (LOOKING ON END-1).

FIG. 68. FIRST CUT, TUBE 2A

ε_L, ε_c, $\mathcal{L}_b$, ℓ_b V x

AT MAXIMUM WALL THICKNESS

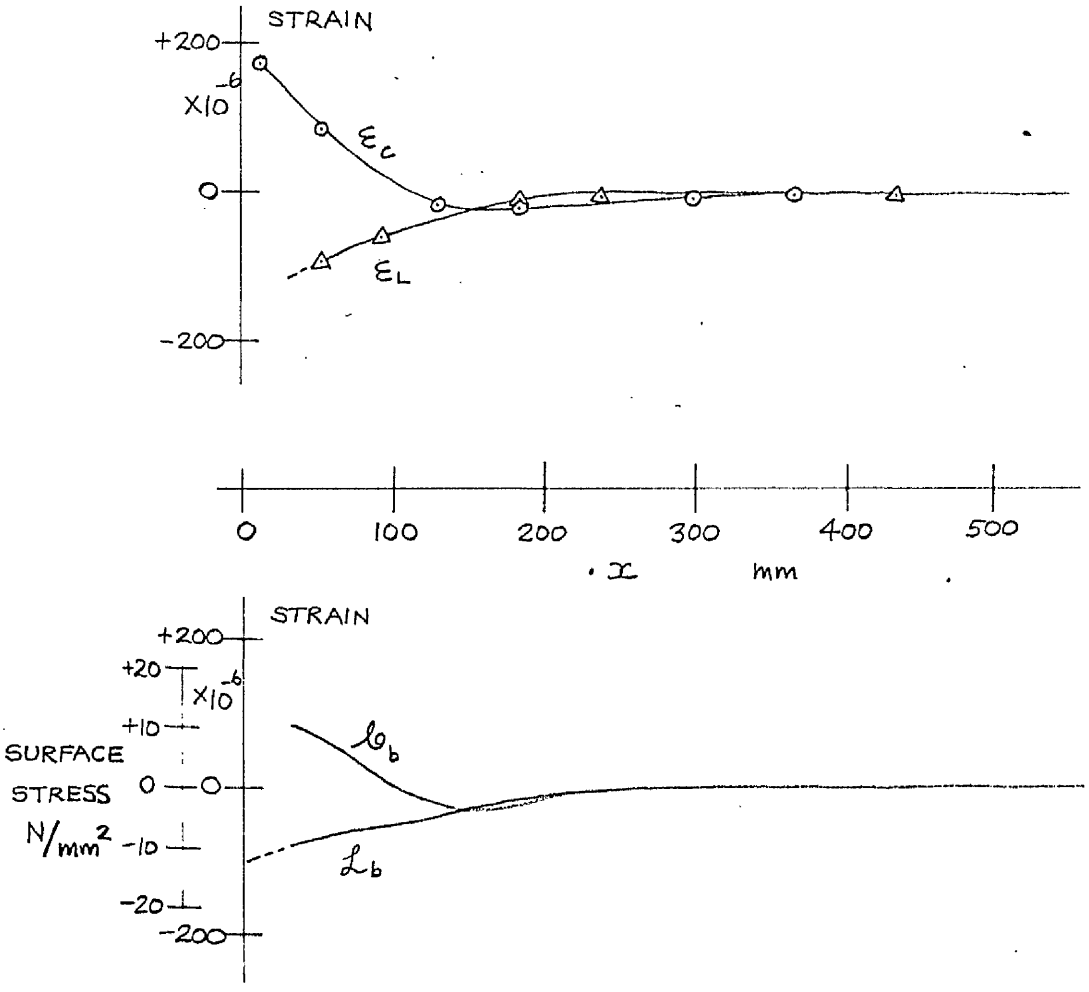

FIG. 69. SECOND CUT, TUBE 2A
ε_L, ε_c, $\mathscr{L}_b$, $\mathscr{b}_b$ V x
AT MAXIMUM WALL THICKNESS

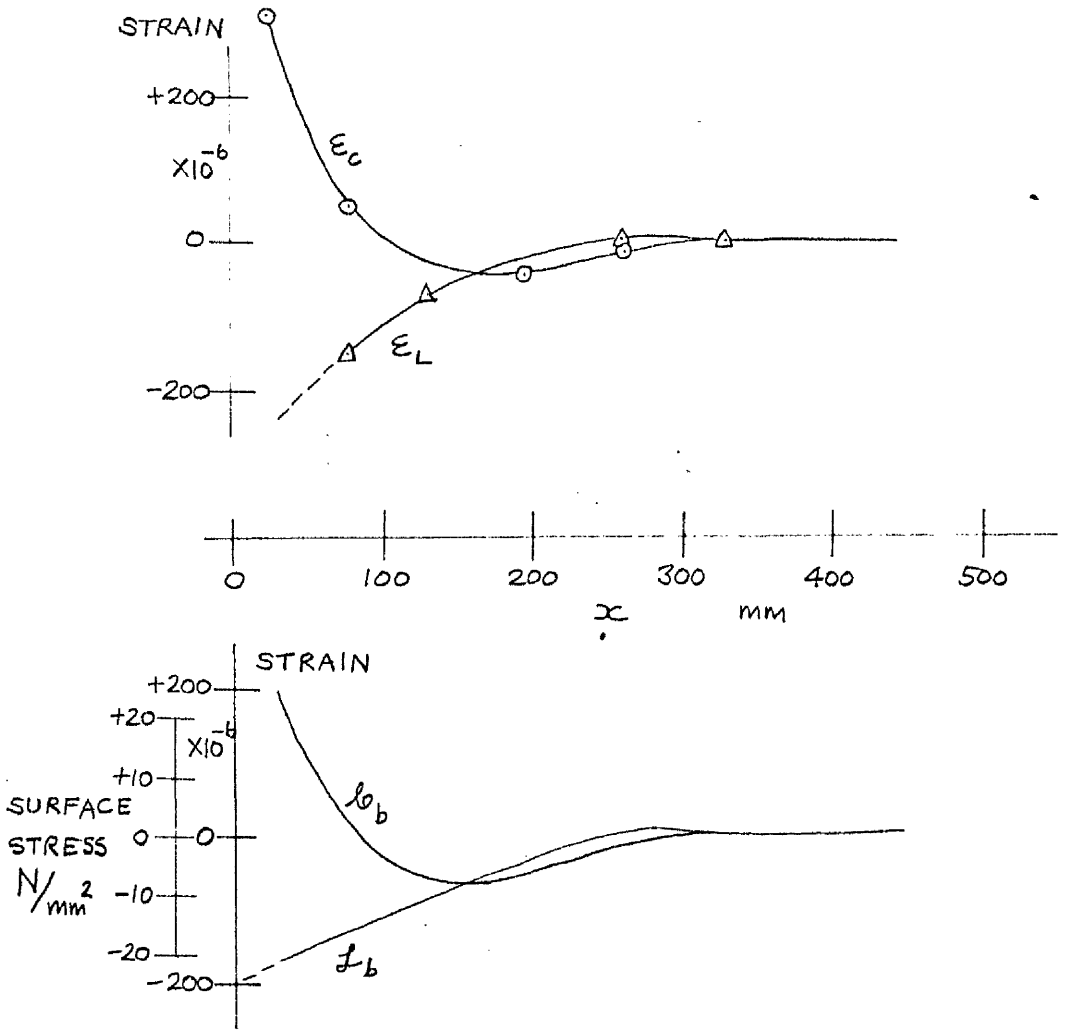

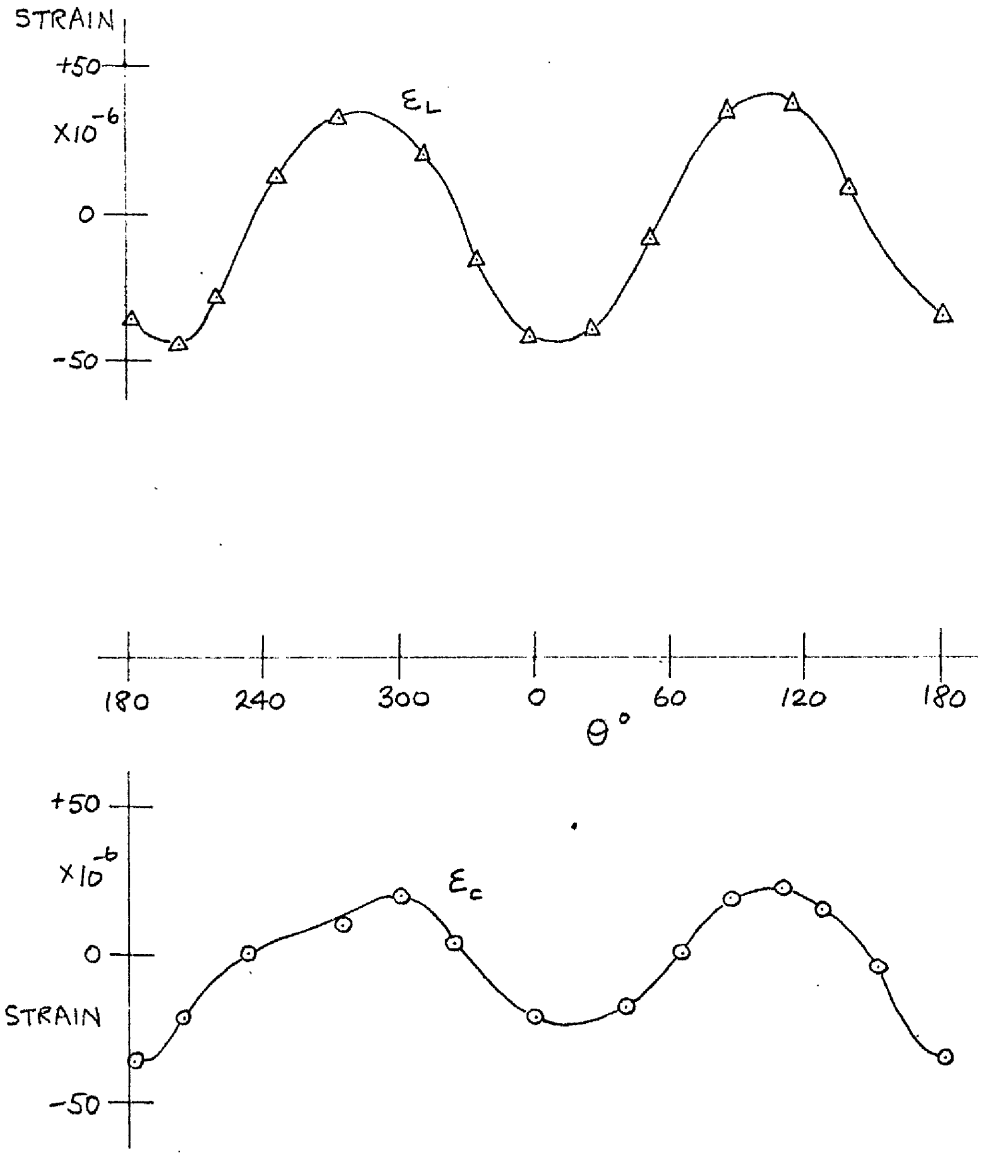

FIG. 70. FIRST CUT, TUBE 3A
ε_L, ε_c V θ

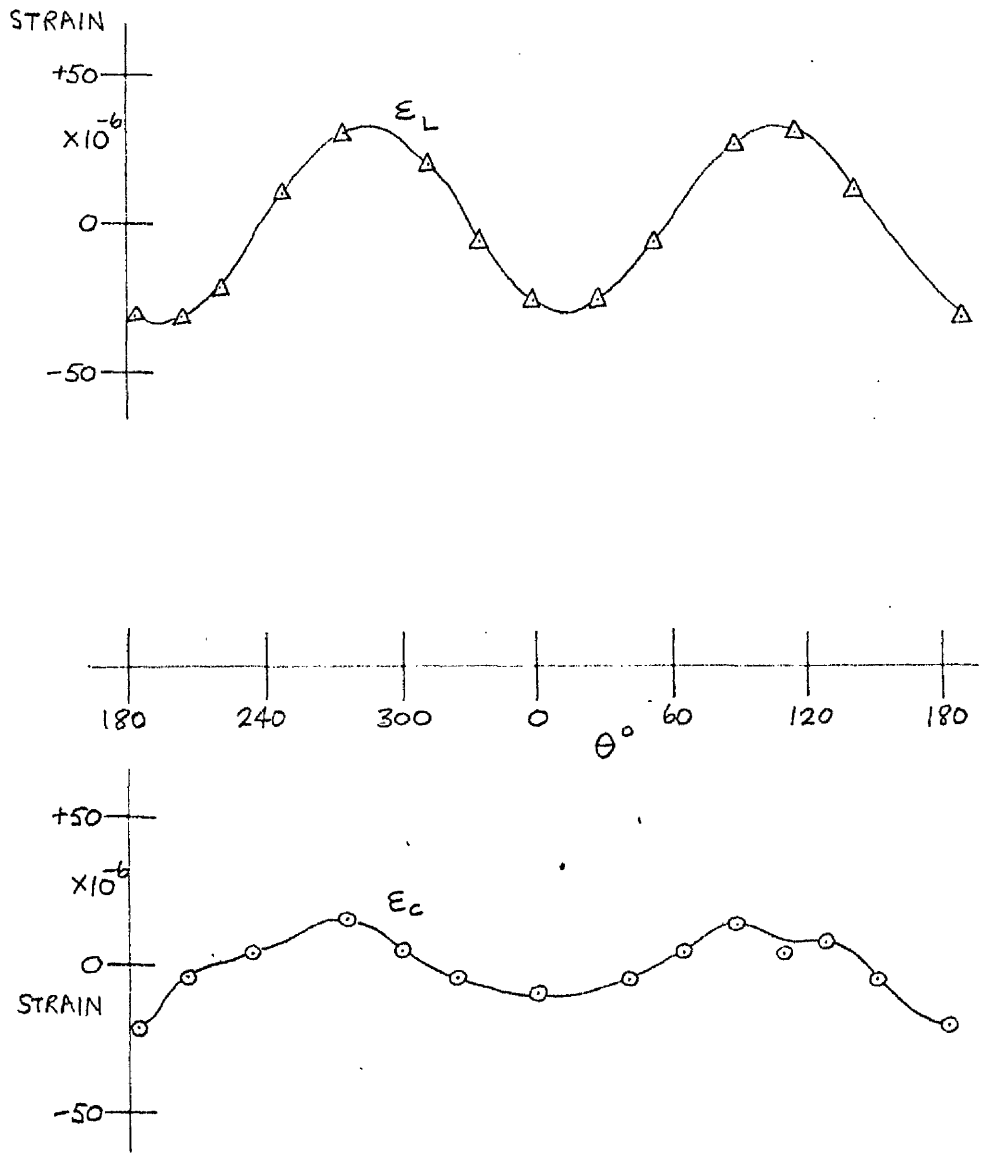

FIG. 71. SECOND CUT, TUBE 3A
ε_L, ε_c v θ

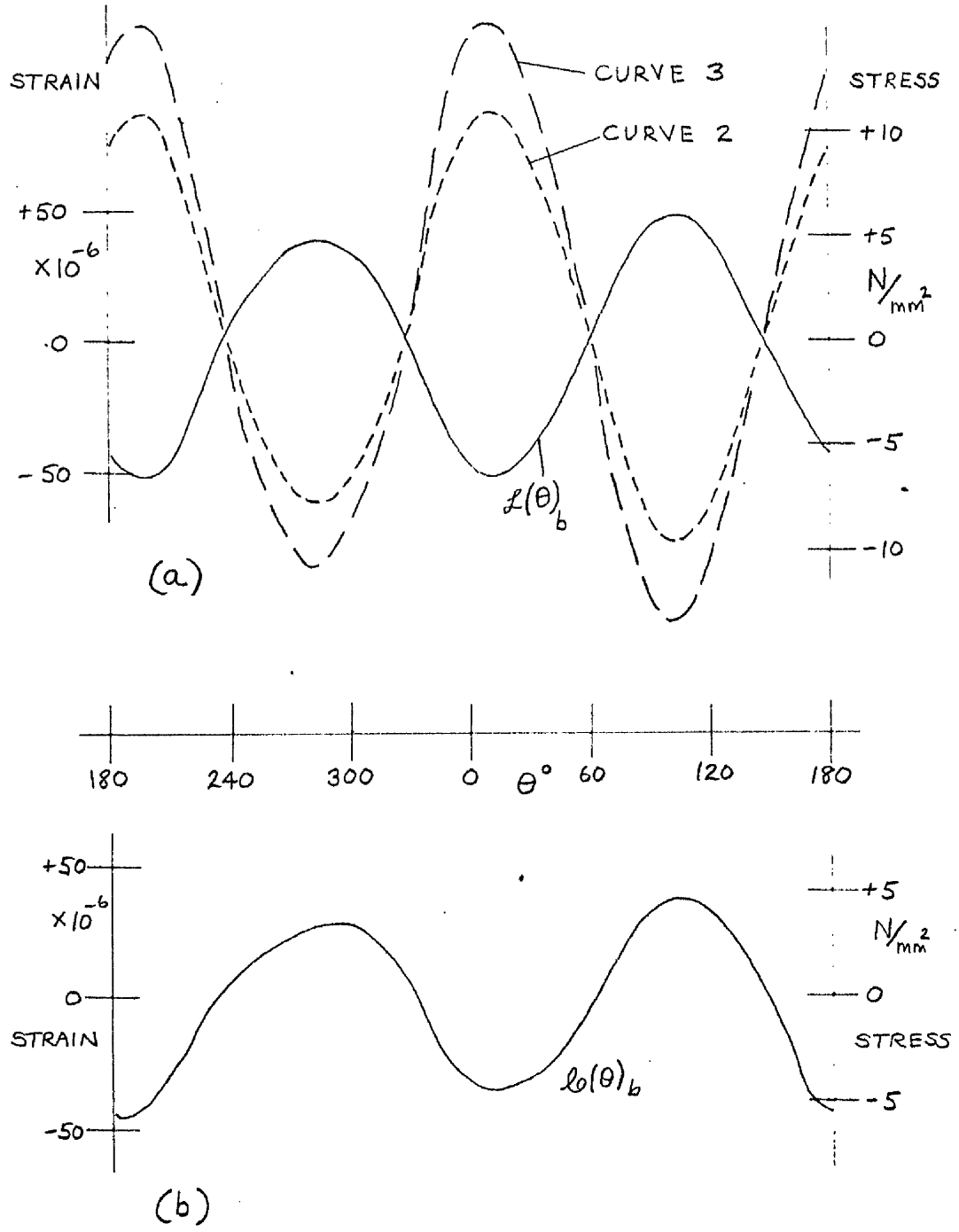

FIG. 72. FIRST CUT, TUBE 3A
$\mathcal{L}(\theta)_b$, $\ell o(\theta)_b$ v θ

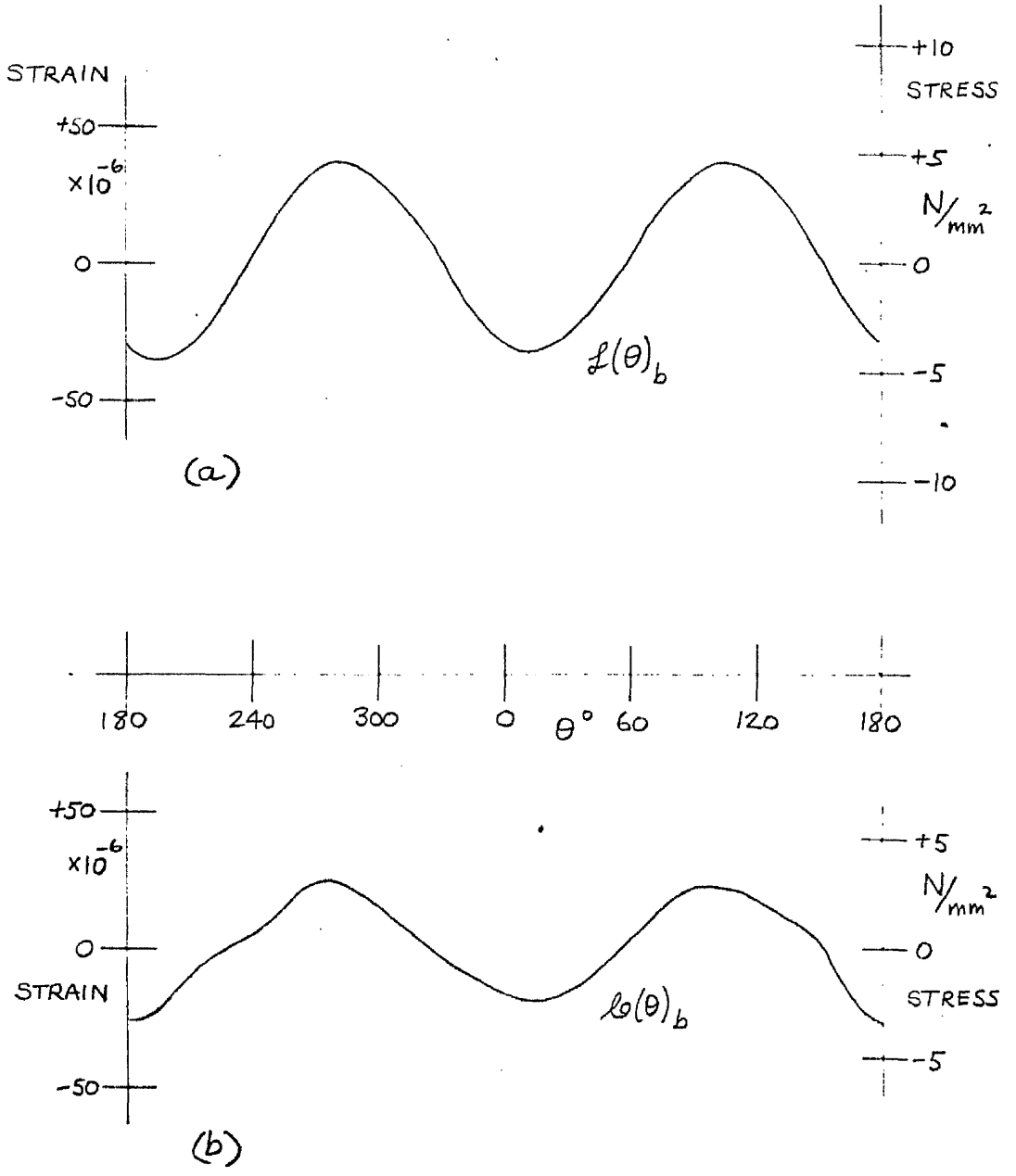

FIG. 73. SECOND CUT, TUBE 3A
$\mathcal{L}(\theta)_b$, $\mathcal{L}o(\theta)_b$ v θ

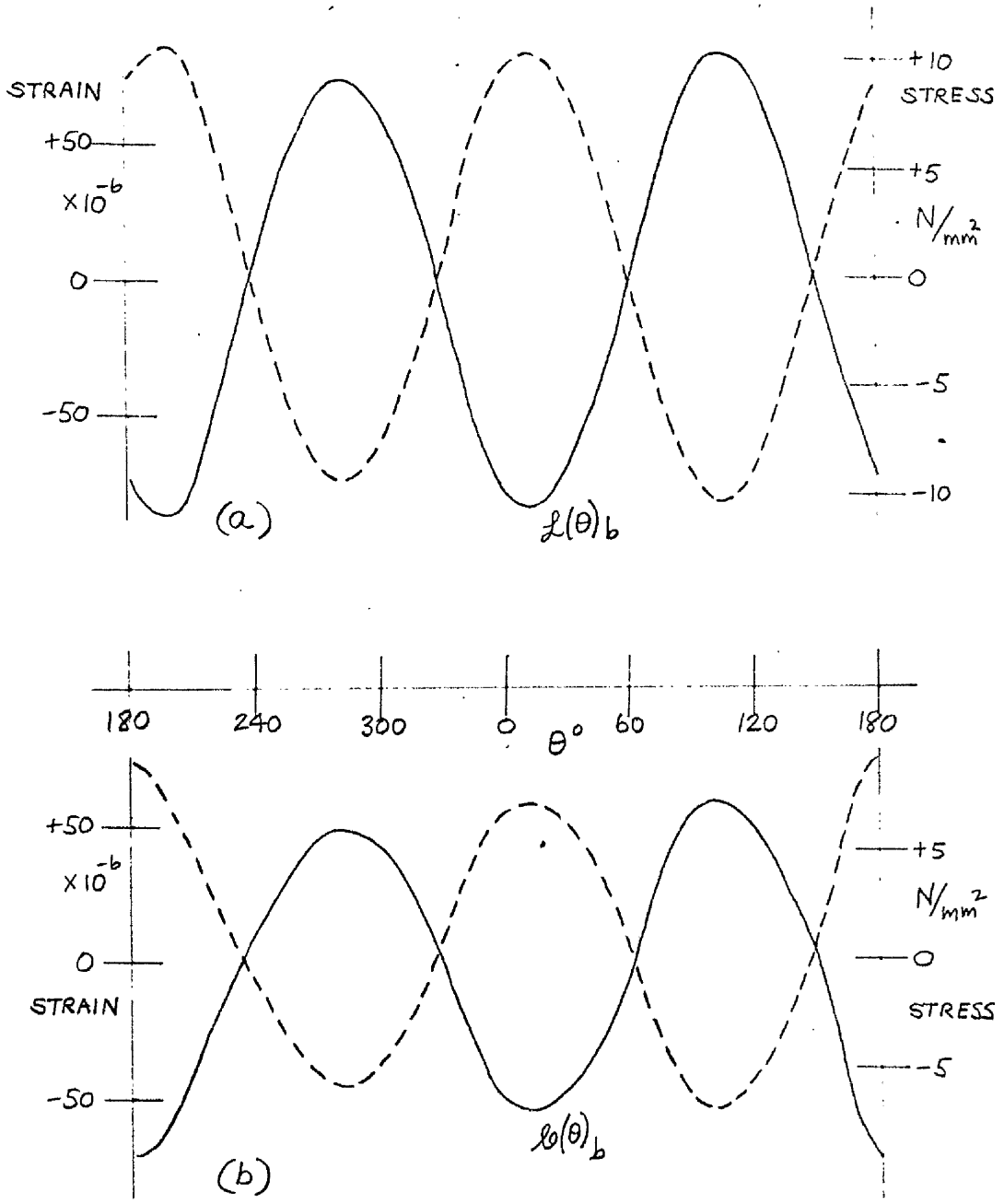

FIG. 74. FIRST & SECOND CUTS, TUBE 3A
$\mathcal{L}(\theta)_b$, $\mathcal{L}(\theta)_b$ TOTALS v θ

FIG. 75.

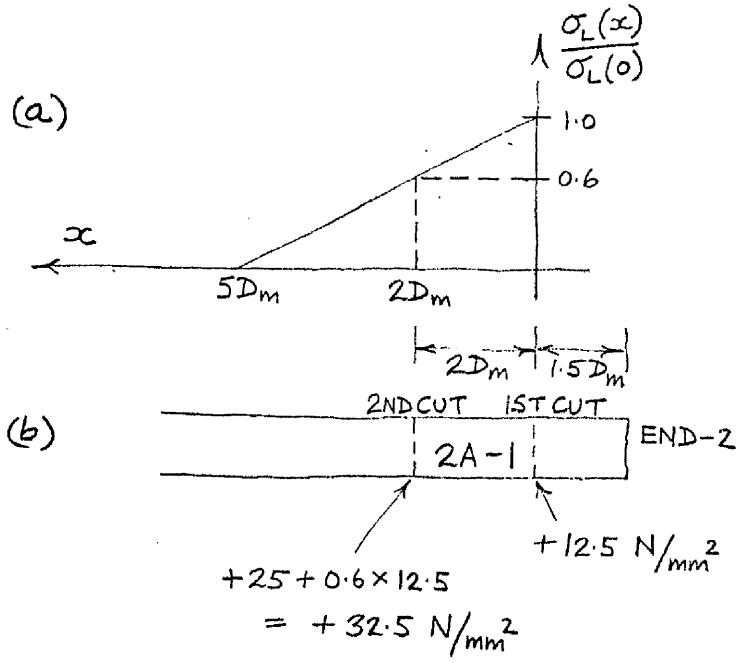
(a)
$\frac{\sigma_L(x)}{\sigma_L(0)}$
1·0
0·6
x
5Dm
2Dm
2Dm
1·5Dm
(b)
2ND CUT
1ST CUT
2A-1
END-2
+12·5 N/mm²
+25 + 0·6 × 12·5
= + 32·5 N/mm²

FIG. 76.

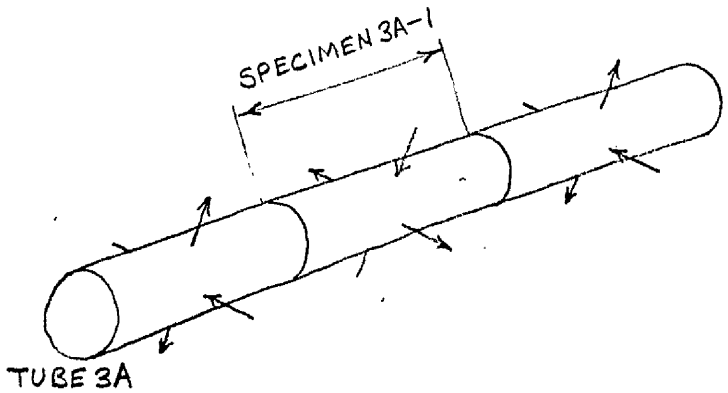
SPECIMEN 3A-1
TUBE 3A

FIG. 77.

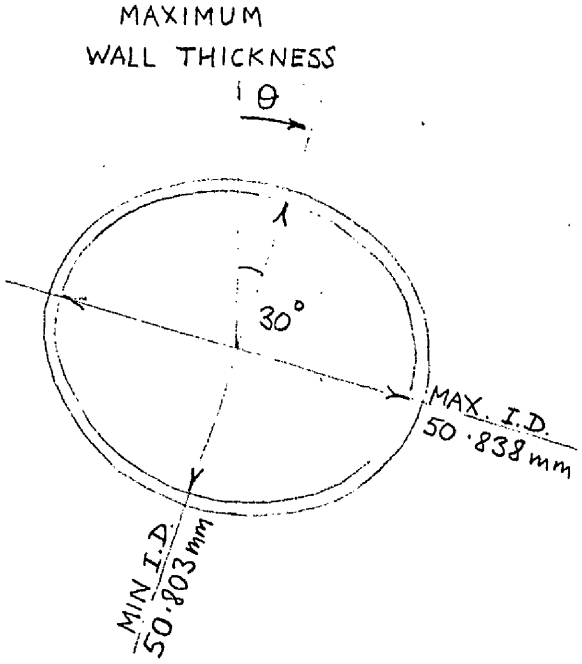

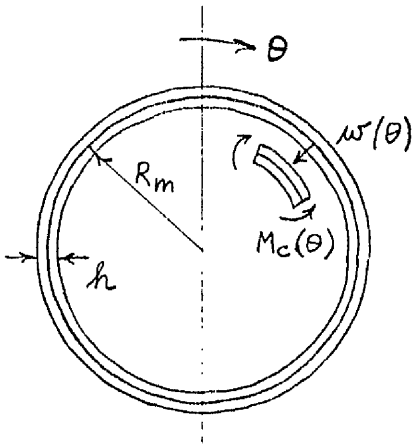

FIG. 78.

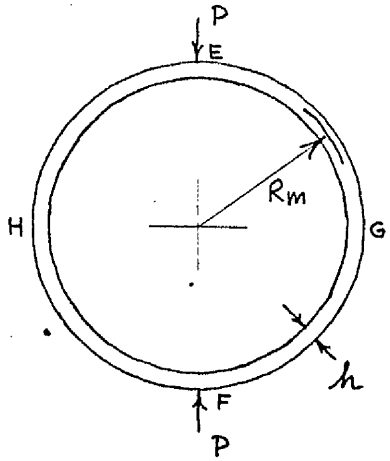

FIG. 79.

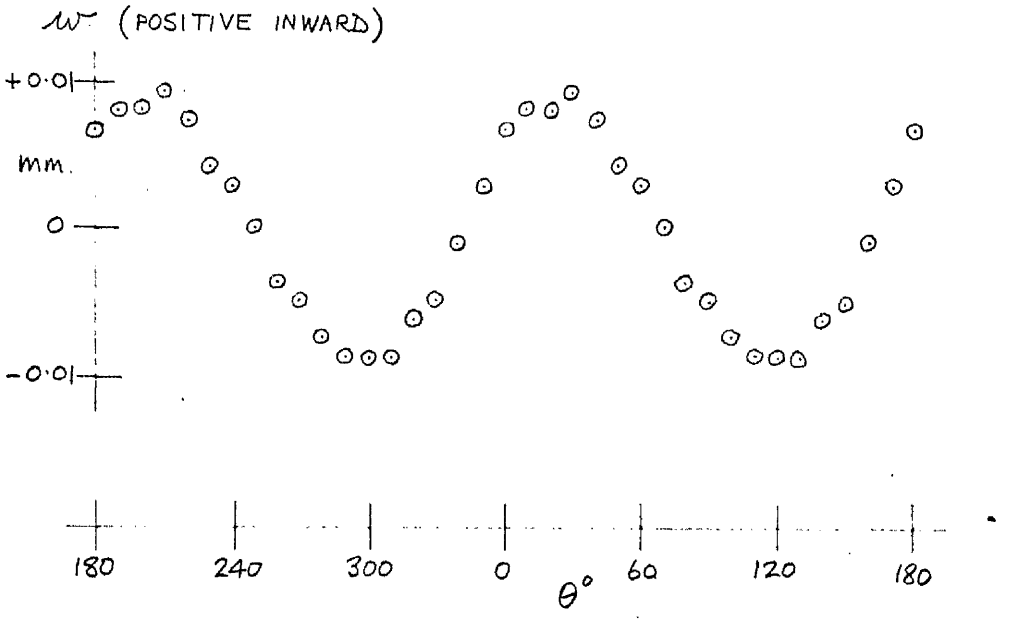

FIG. 80. INWARD RADIAL DISPLACEMENT w v θ, SPECIMEN 3A-1

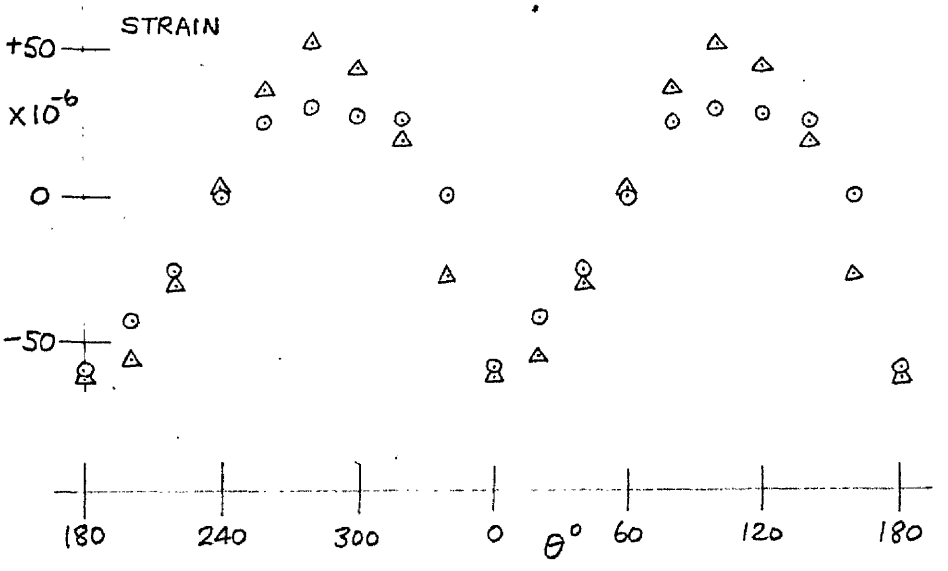

FIG. 81: $\ell_0(\theta)_b$ v θ, SPECIMEN 3A-1,
△ MEASURED BY STRAIN GAUGES,
⊙ CALCULATED FROM I.D. CHANGE.

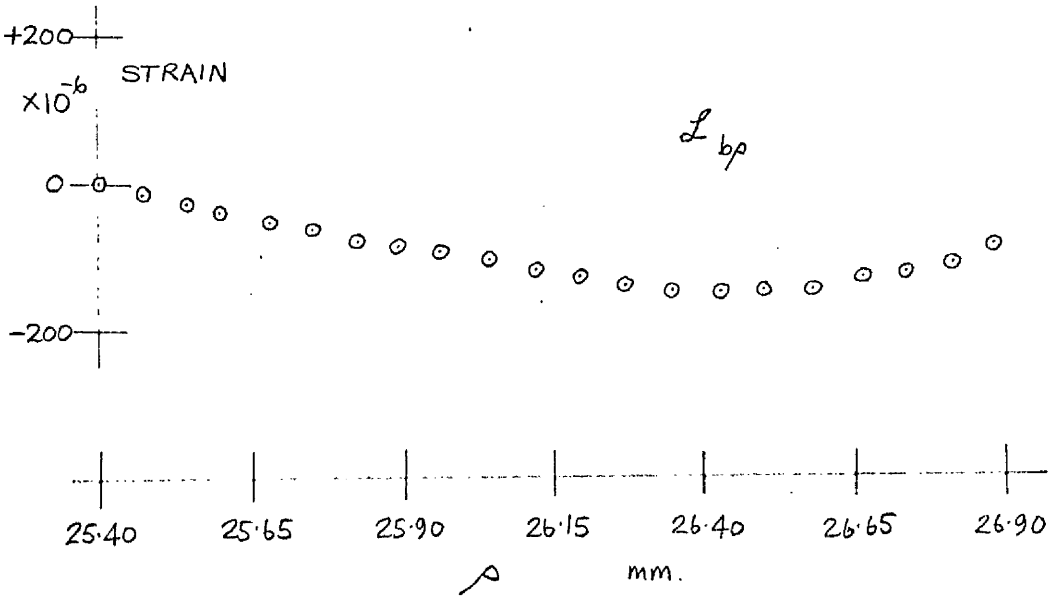

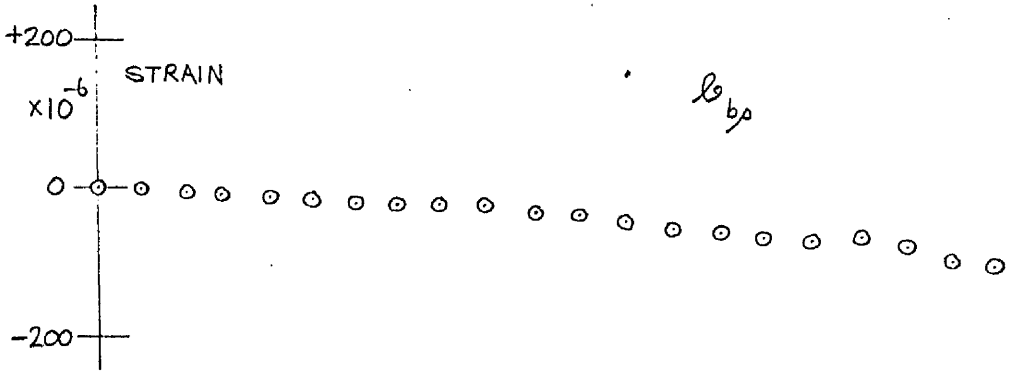

FIG. 82. SPECIMEN 2A-1 $\mathcal{L}_{bp}$, ℓ_{bp} V ρ AT MAXIMUM WALL THICKNESS

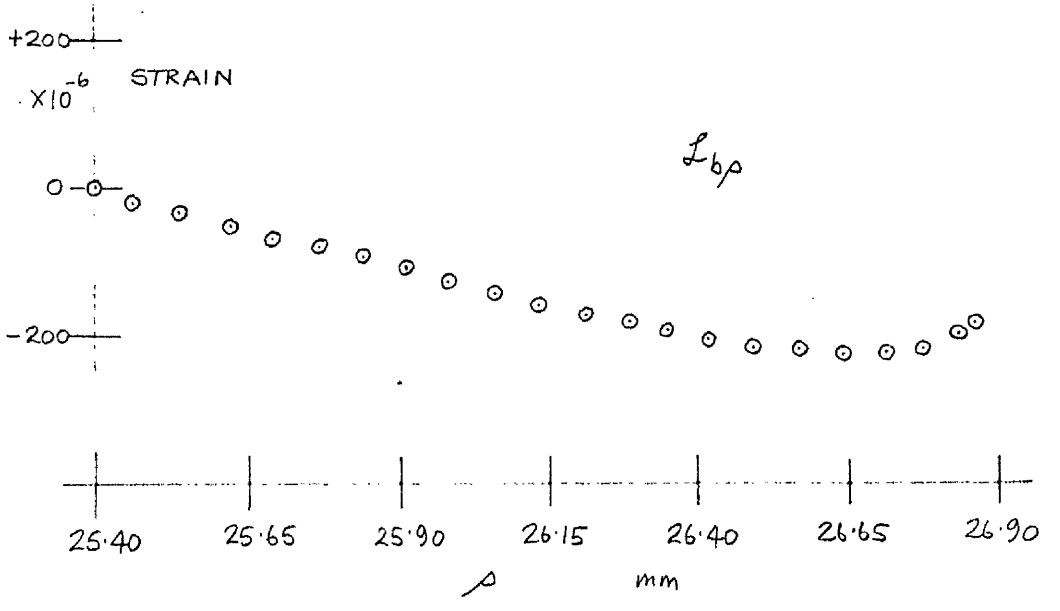

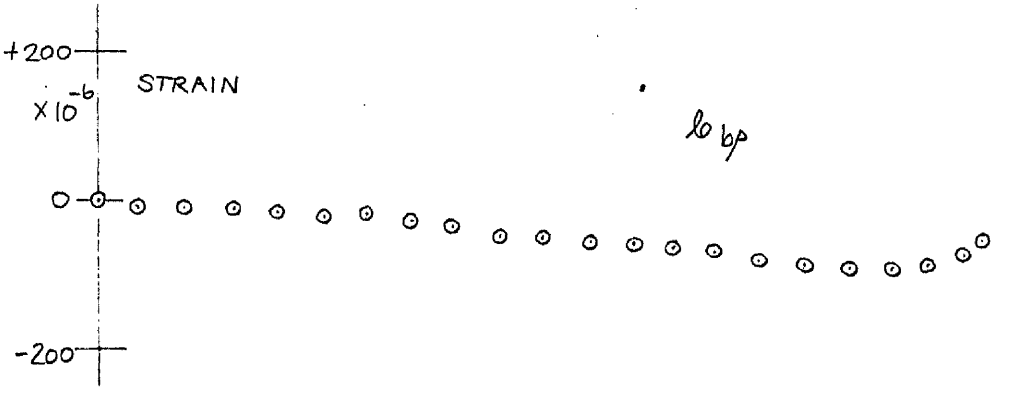

FIG. 83. SPECIMEN 1A-1 $\mathcal{L}_{bp}$, ℓ_{bp} V ρ AT MAXIMUM WALL THICKNESS

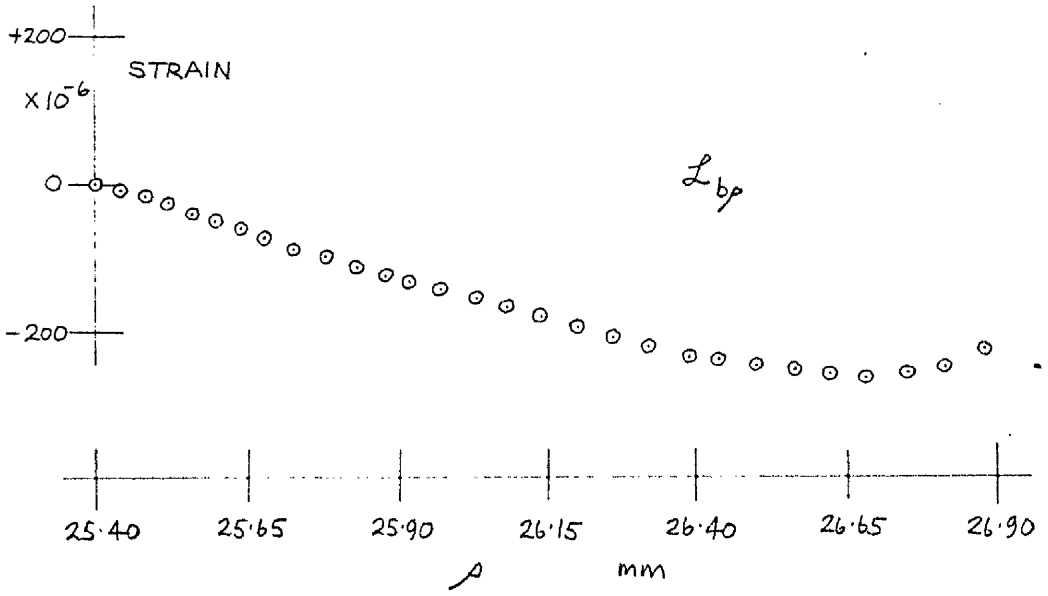

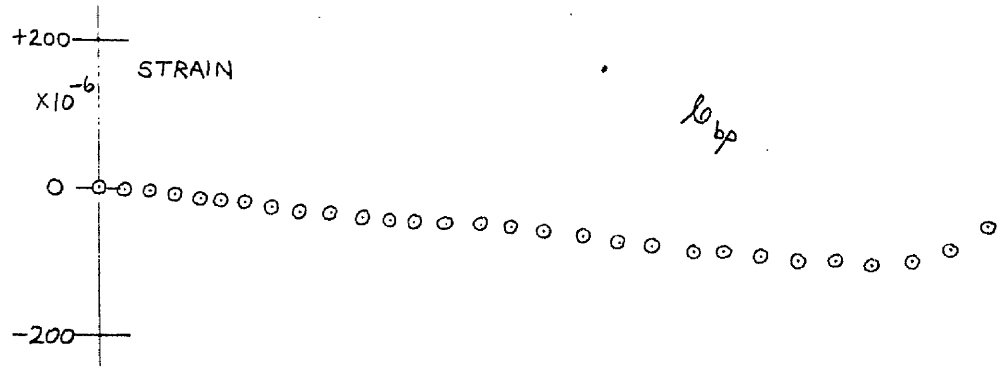

FIG. 84. SPECIMEN 1A-2 $\mathcal{L}_{bp}$, ℓ_{bp} V ρ AT MAXIMUM WALL THICKNESS

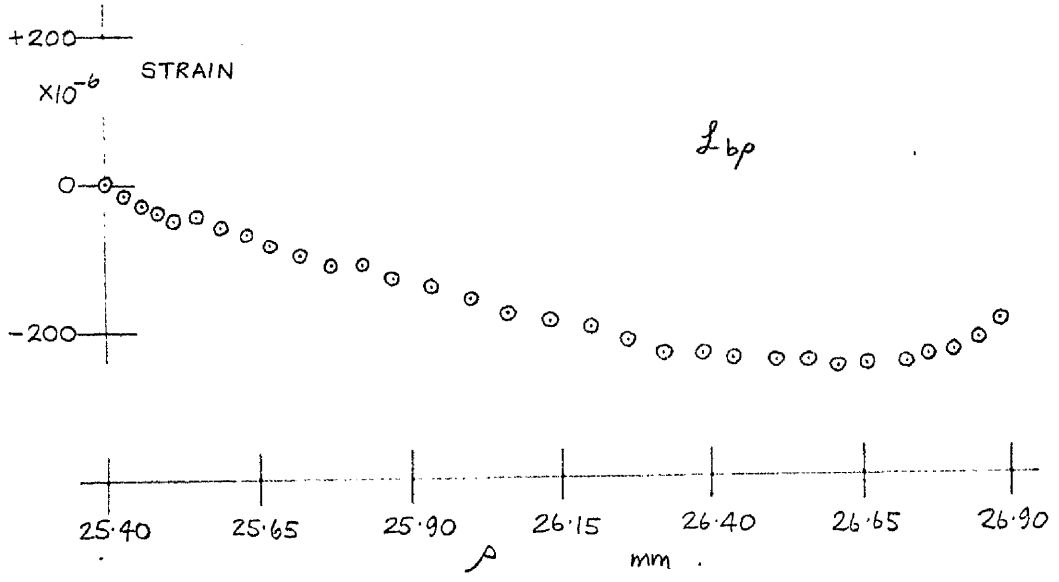

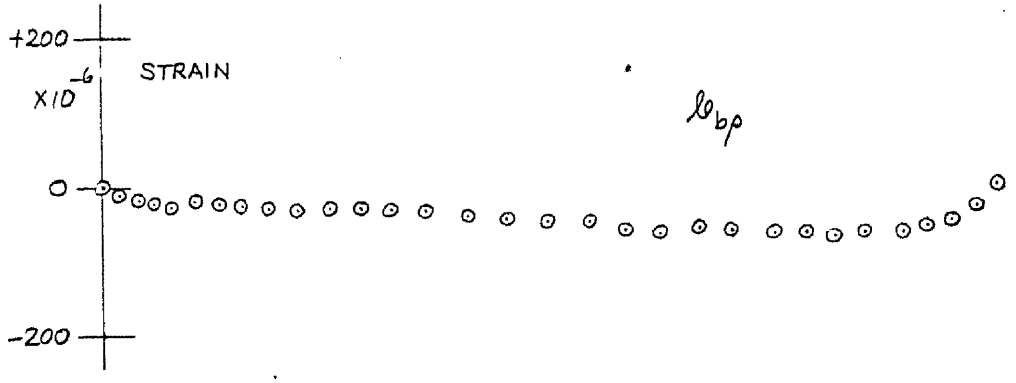

FIG. 85. SPECIMEN 3A-1 $\mathcal{L}_{bp}$, ℓ_{bp} v ρ AT MAXIMUM WALL THICKNESS

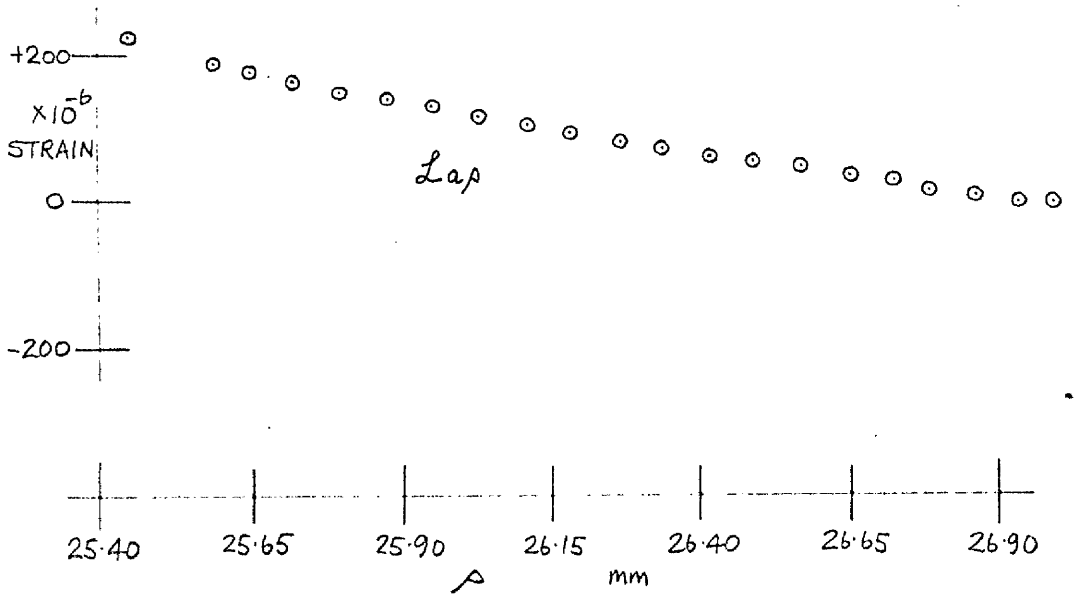

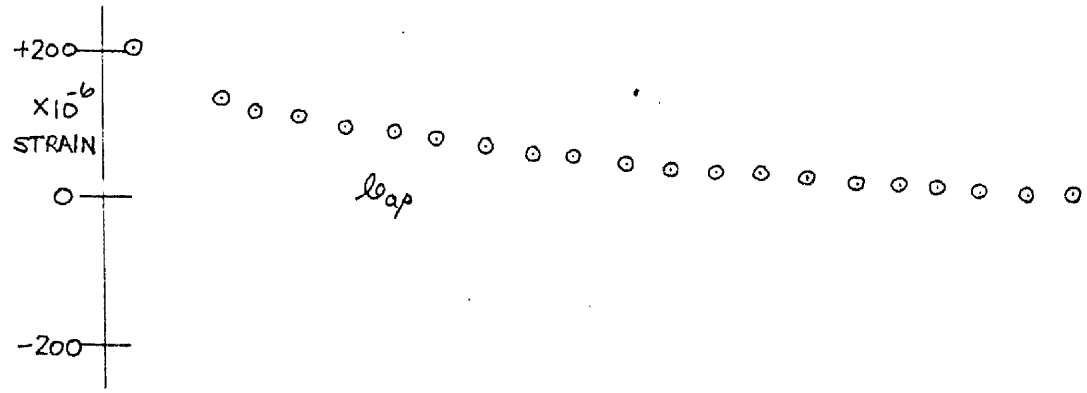

FIG. 86. SPECIMEN 2B-1 $\mathcal{L}_{ap}, \ell_{ap}$ V ρ AT MAXIMUM WALL THICKNESS

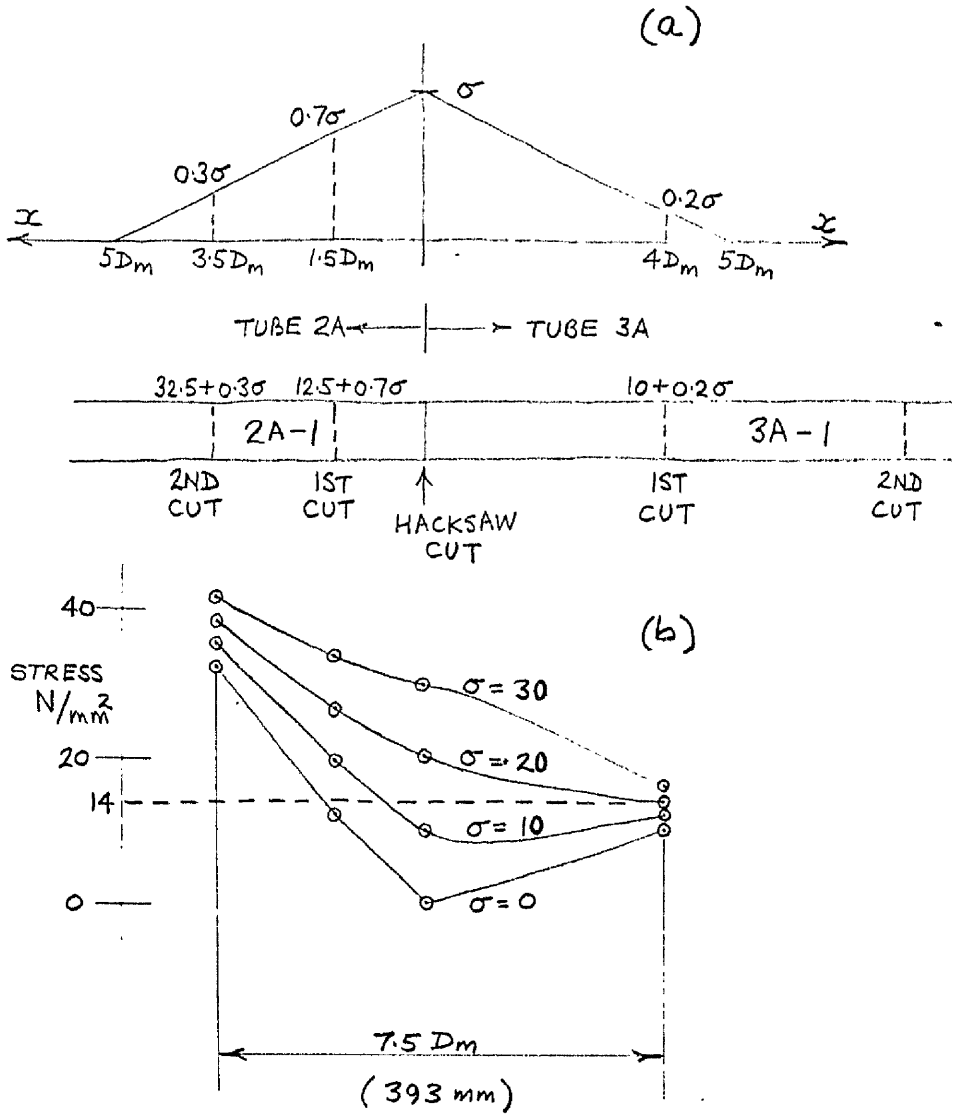
(a)
σ
0·7σ
0·3σ
0·2σ
x
y
5Dm
3·5Dm
1·5Dm
4Dm
5Dm
TUBE 2A
TUBE 3A
32·5+0·3σ
12·5+0·7σ
10+0·2σ
2A-1
3A-1
2ND CUT
1ST CUT
HACKSAW CUT
1ST CUT
2ND CUT
(b)
40
STRESS N/mm²
20
14
0
σ = 30
σ = 20
σ = 10
σ = 0
7·5 Dm
(393 mm)

FIG. 87.

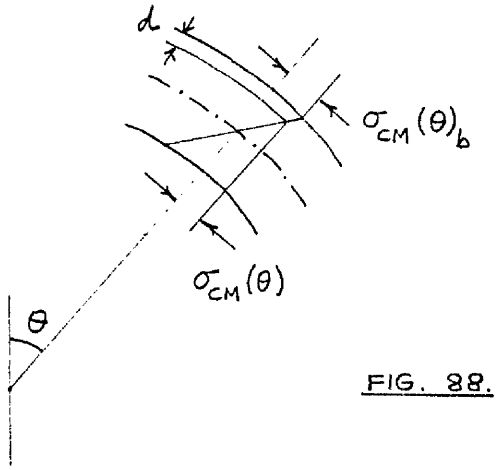
d
$\sigma_{CM}(\theta)_b$
$\sigma_{CM}(\theta)$
θ

FIG. 88.

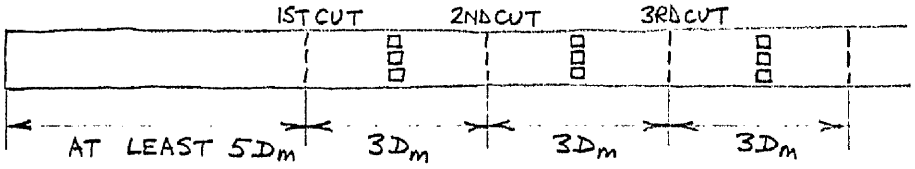
1ST CUT
2ND CUT
3RD CUT
AT LEAST $5D_m$
$3D_m$
$3D_m$
$3D_m$

FIG. 89.

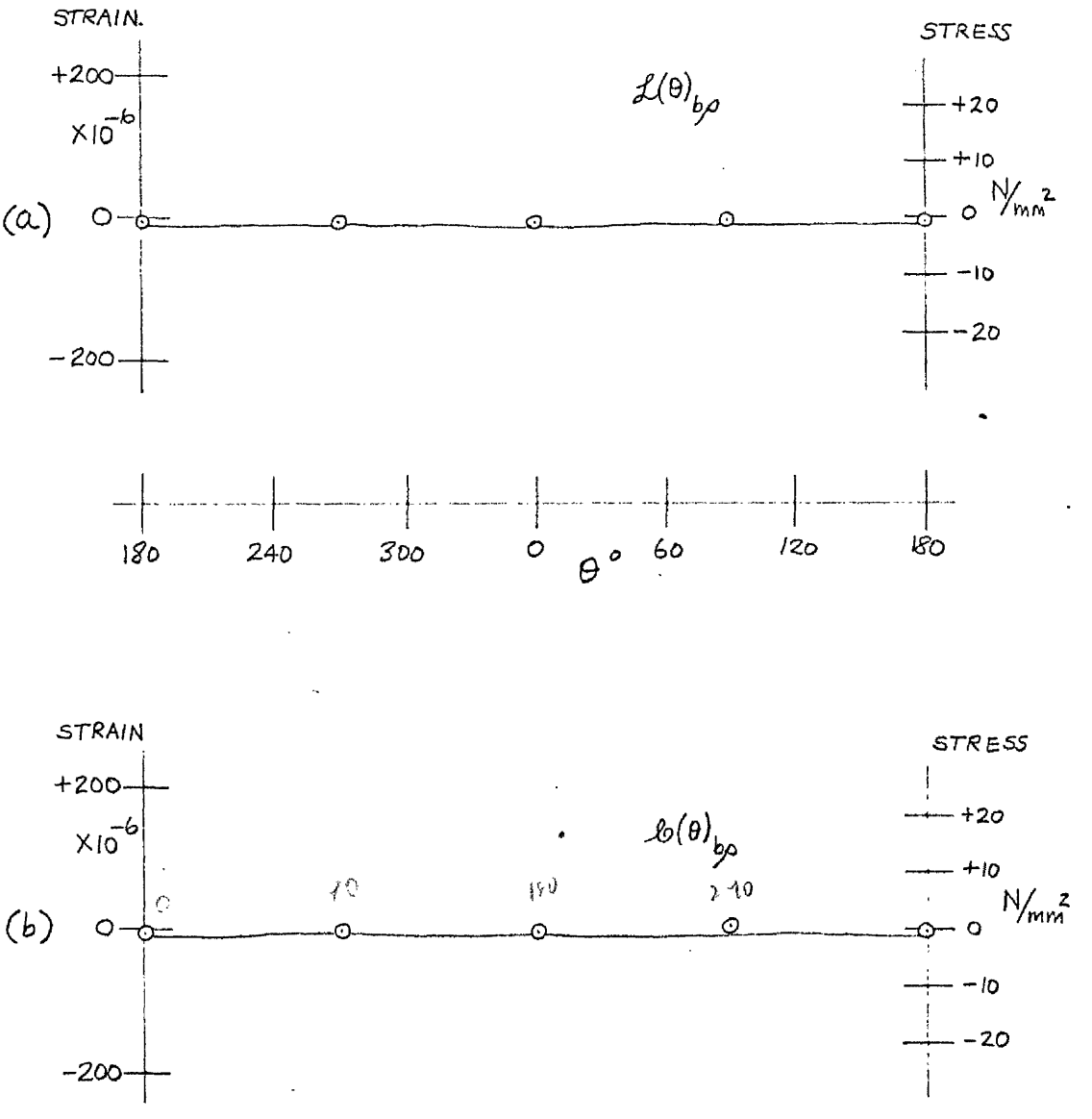

FIG.90. SPECIMEN 3A-1 $\mathcal{L}(\theta)_{bp}$, $\mathcal{b}(\theta)_{bp}$ v θ
AFTER FIRST ETCH.
$\rho/b = 0.942$, $e(\rho) = 0.061$

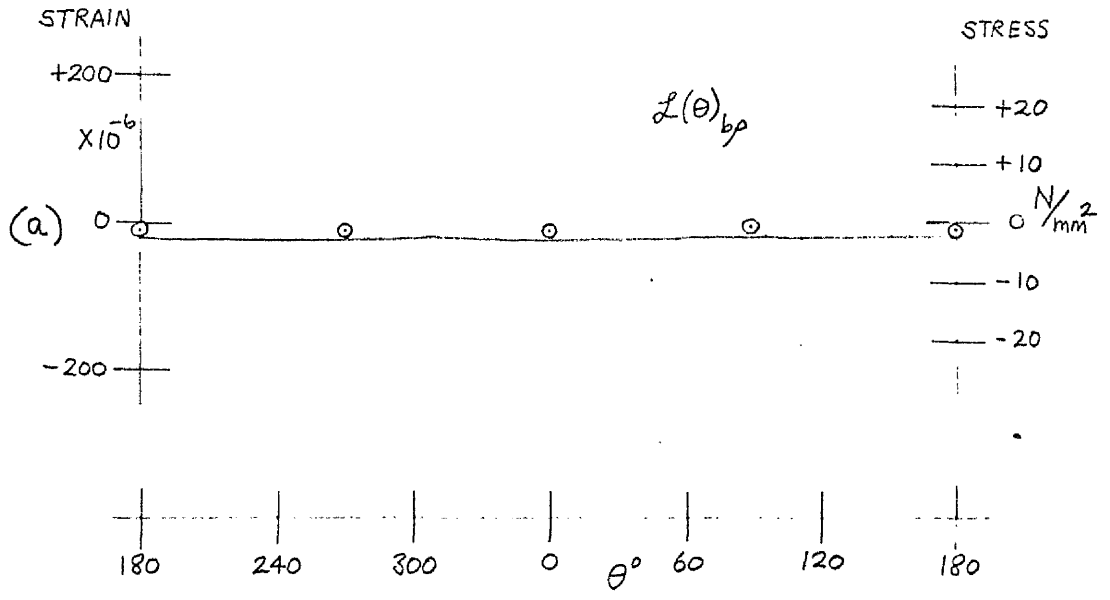

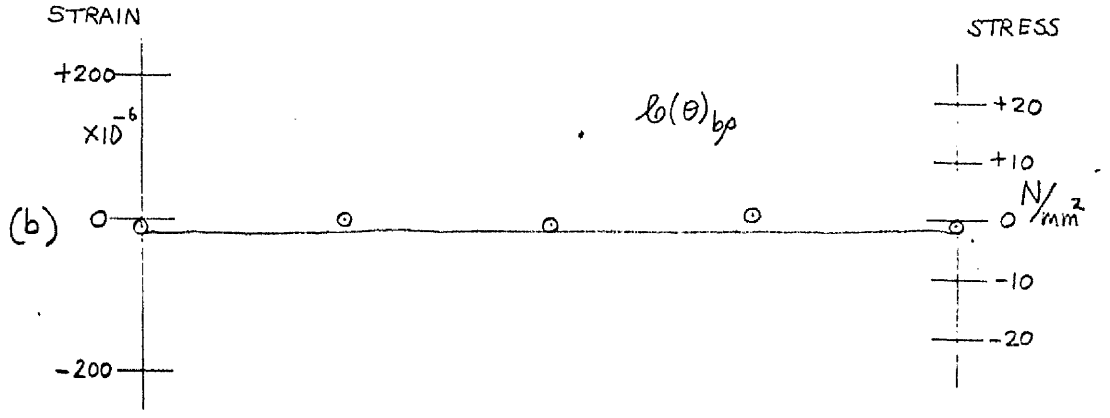

FIG. 91. SPECIMEN 3A-1 $\mathcal{L}(\theta)_{bp}$, $\ell_0(\theta)_{bp}$ v θ AFTER SECOND ETCH.
ρ/b = 0.943, $e(\rho)$ = 0.062

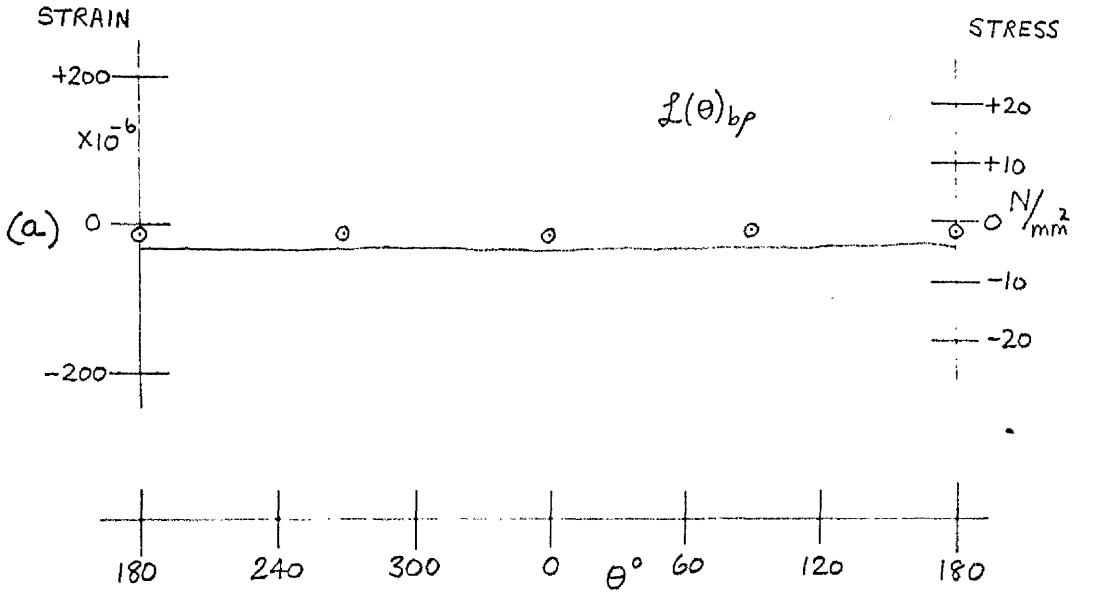

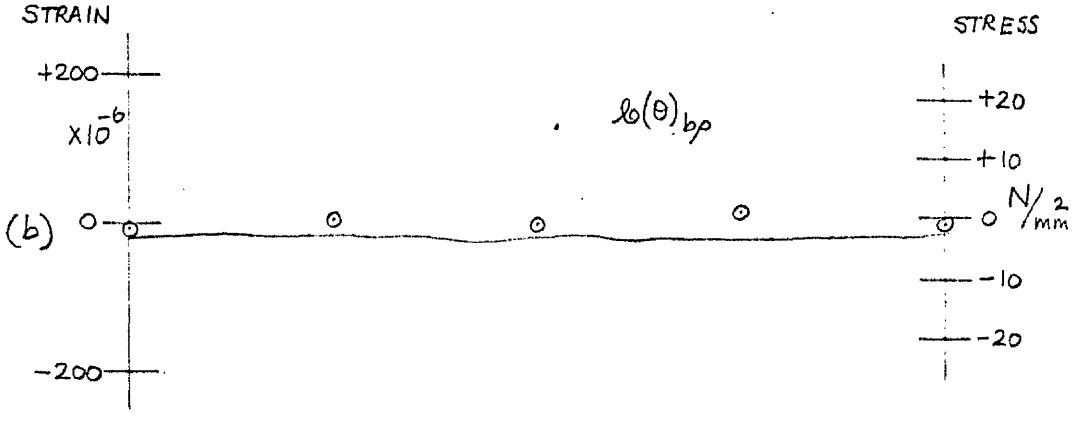

FIG. 92. SPECIMEN 3A-1 $\mathcal{L}(\theta)_{bp}$, $\ell_0(\theta)_{bp}$ V θ
AFTER THIRD ETCH.
$\rho/_b = 0.944$, $e(\rho) = 0.063$

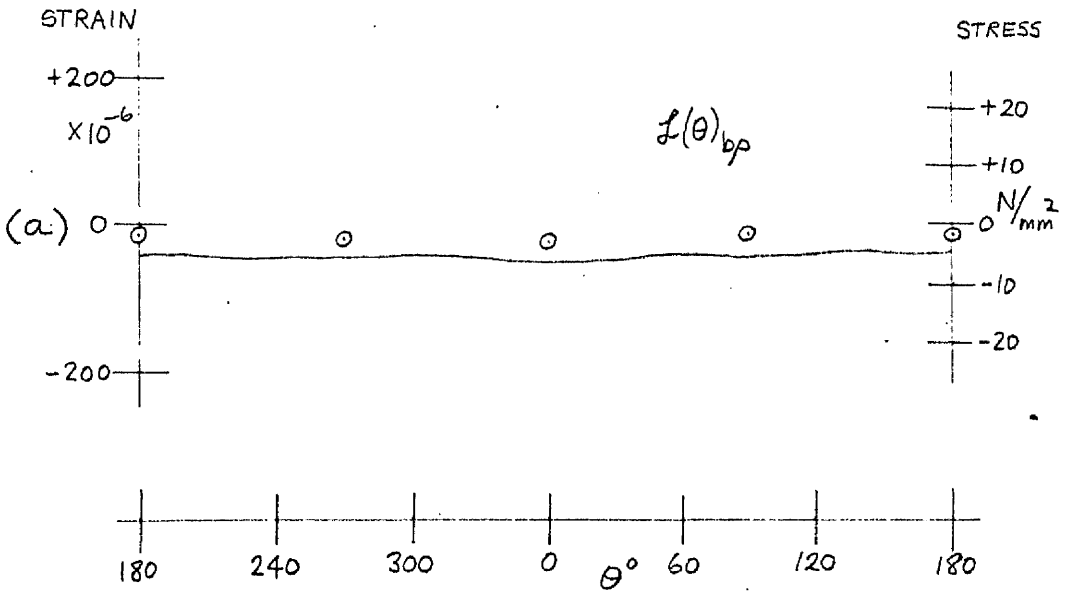

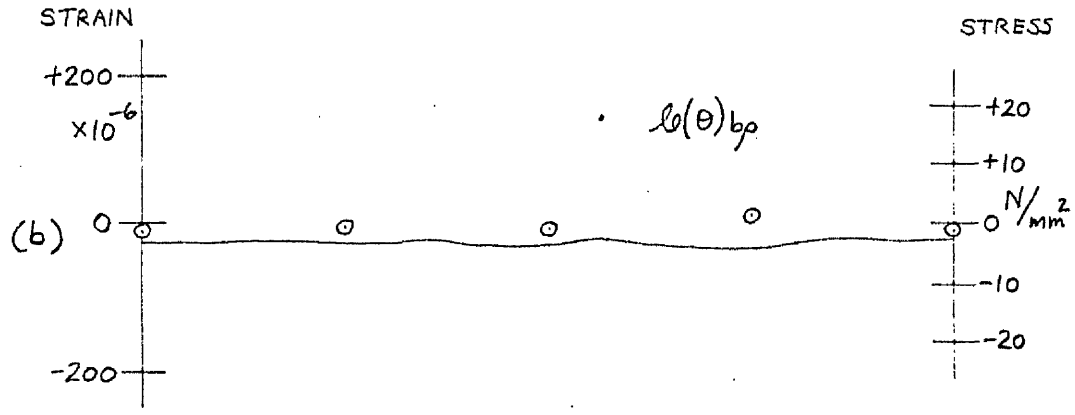

FIG. 93. SPECIMEN 3A-1 $\mathcal{L}(\theta)_{bp}$, $\mathcal{L}(\theta)_{bp}$ v θ
AFTER FOURTH ETCH.
$\rho/b = 0.945$, $e(\rho) = 0.065$

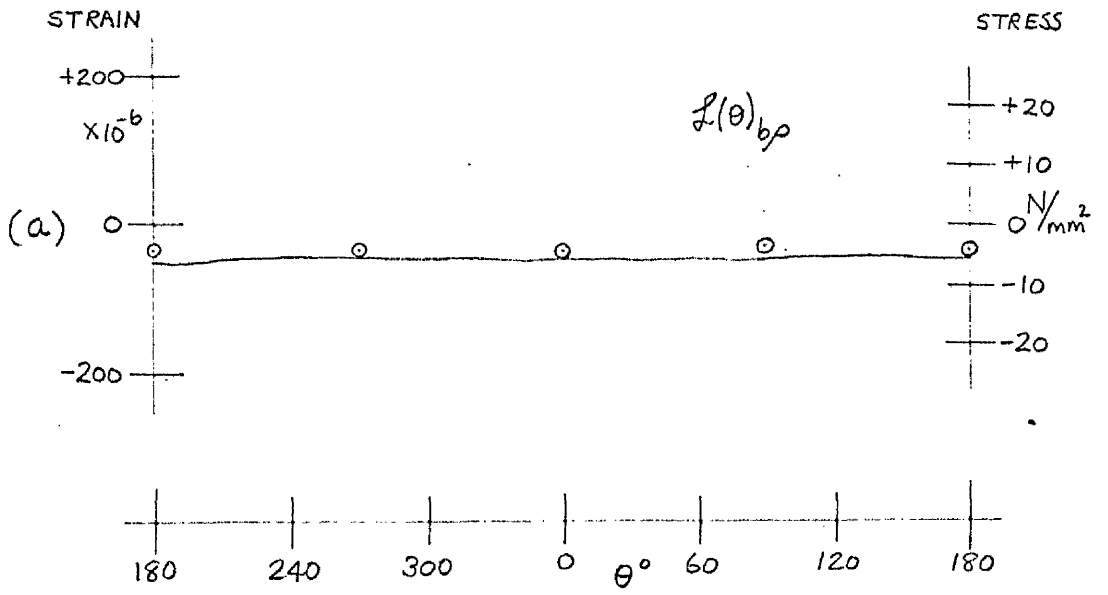

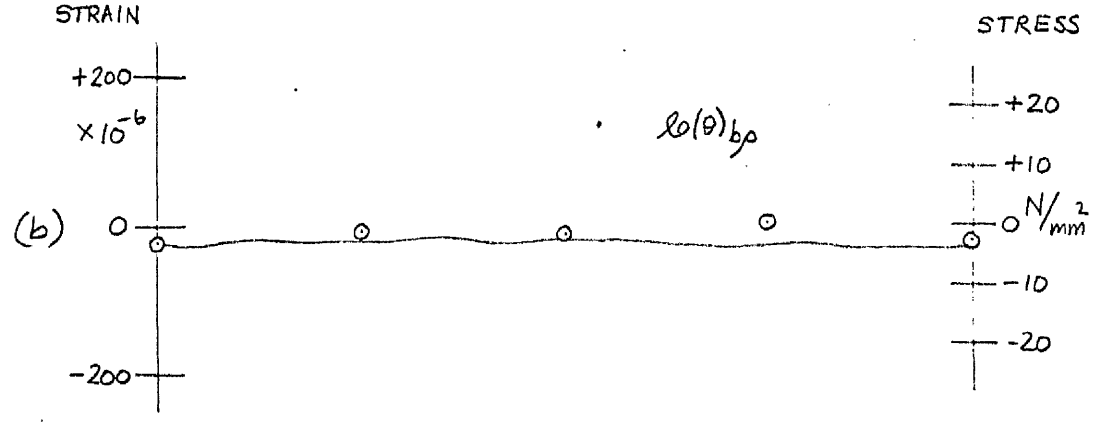

FIG. 94. SPECIMEN 3A-1 $\ell(\theta)_{b\rho}$, $\ell o(\theta)_{b\rho}$ v θ
AFTER FIFTH ETCH
$\rho/b = 0.946$, $e(\rho) = 0.066$

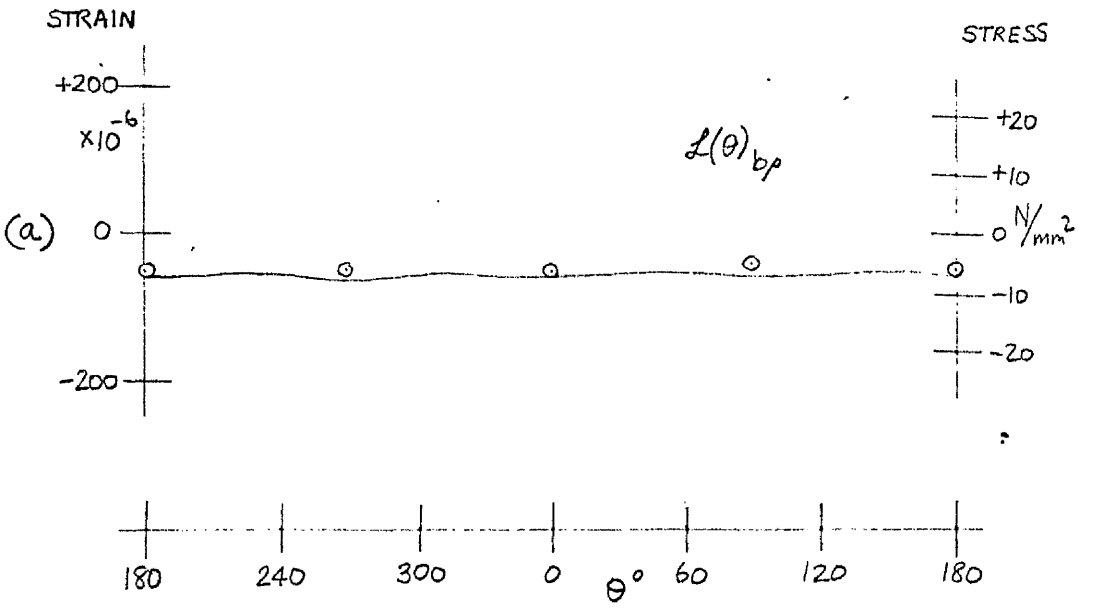

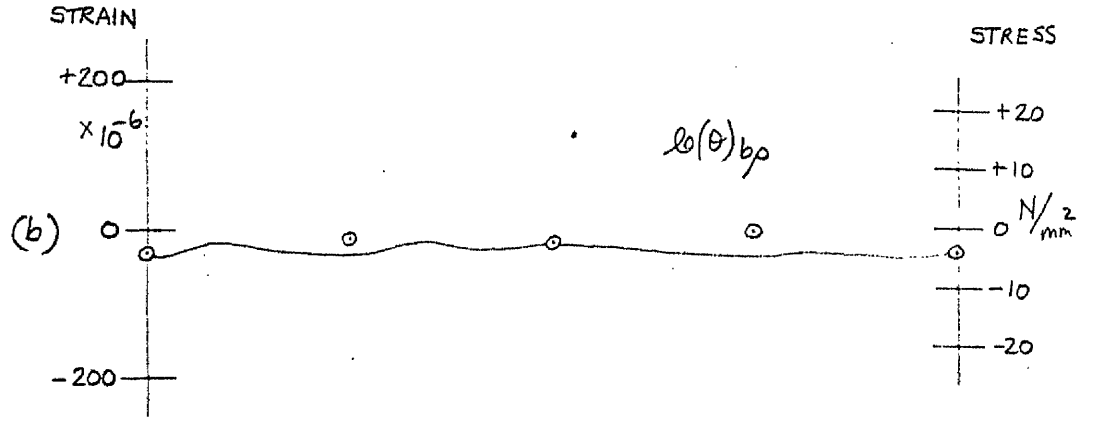

FIG. 95. SPECIMEN 3A-1 $\mathcal{L}(\theta)_{bp}$, $\ell_0(\theta)_{bp}$ V θ
AFTER SIXTH ETCH
ρ/b = 0·947, e/ρ = 0·067

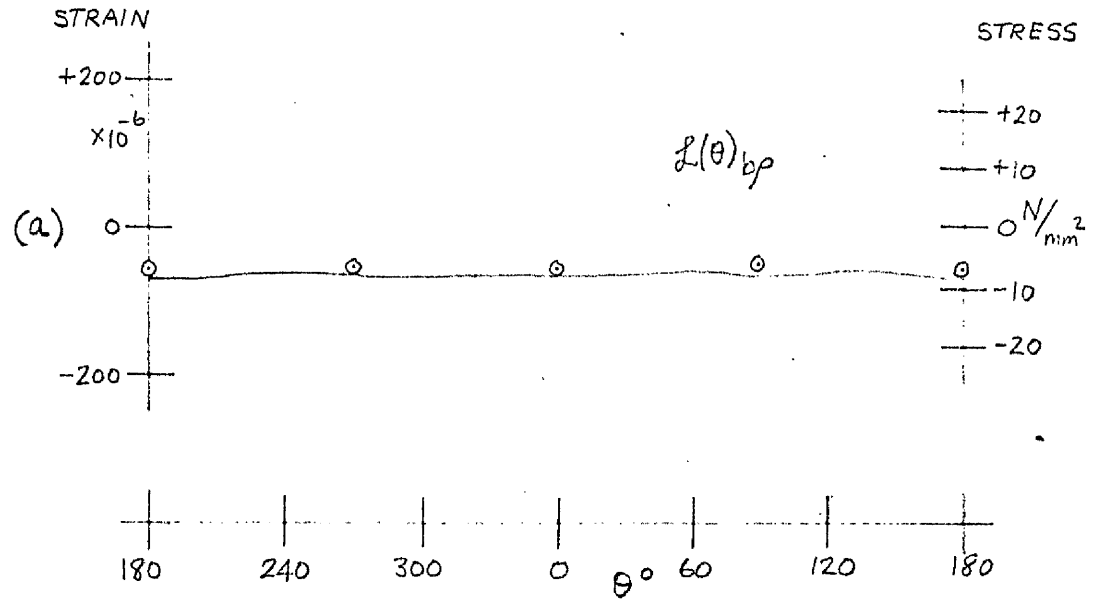

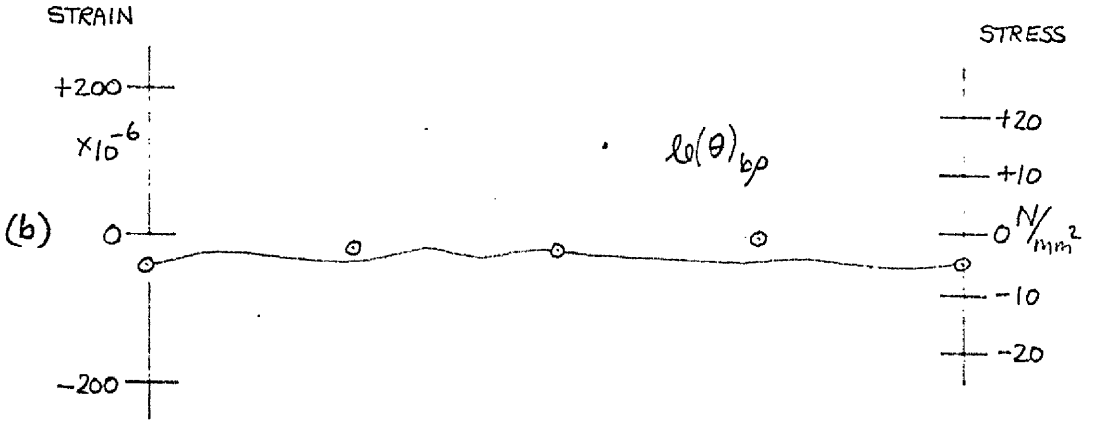

FIG. 96. SPECIMEN 3A-1 $\mathcal{L}(\theta)_{bp}$, $\ell\theta(\theta)_{bp}$ V θ
AFTER SEVENTH ETCH
$\rho/b = 0.949$, $e(\rho) = 0.070$

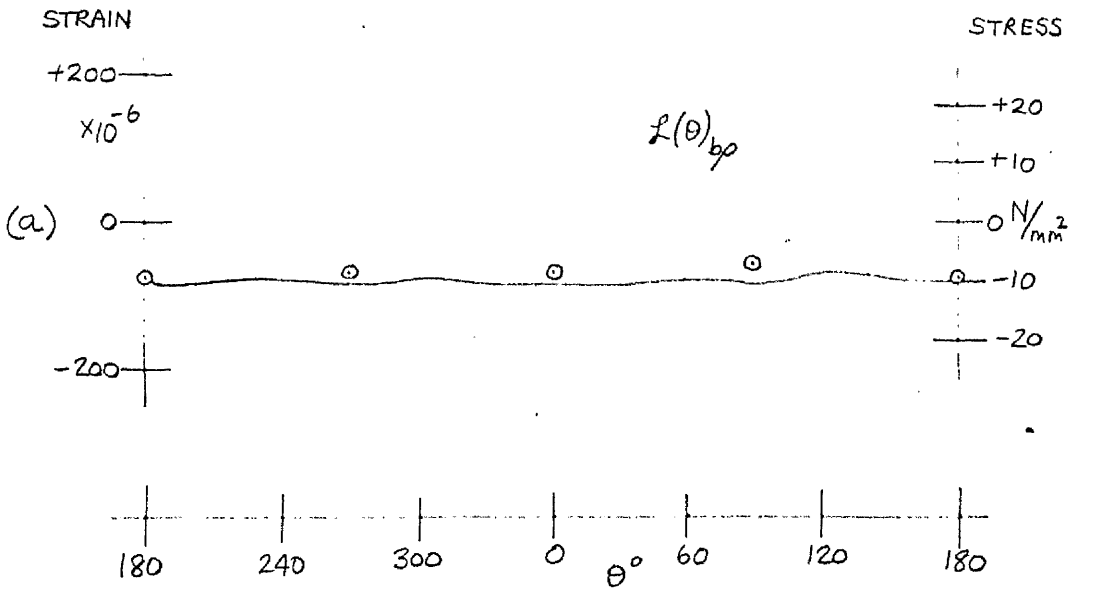

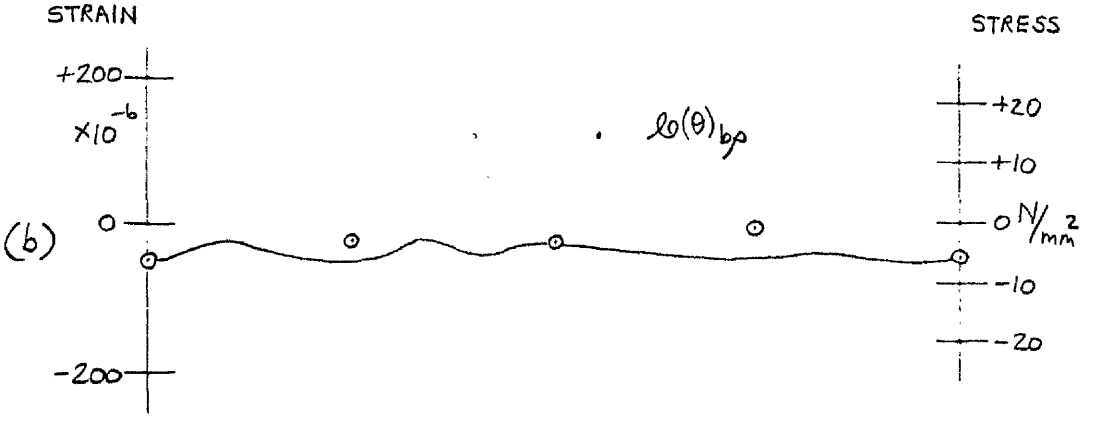

FIG. 97. SPECIMEN 3A-1 $\mathcal{L}(\theta)_{bp}$, $\mathcal{L}o(\theta)_{bp}$ v θ
AFTER EIGHTH ETCH
ρ_b = 0·951 , $e(\rho)$ = 0·072

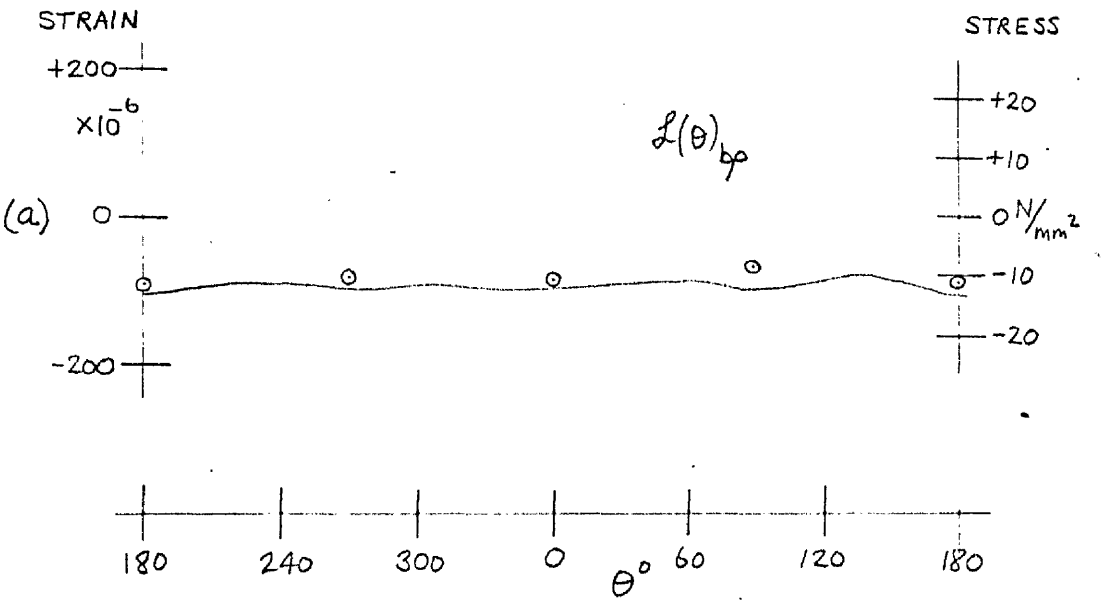

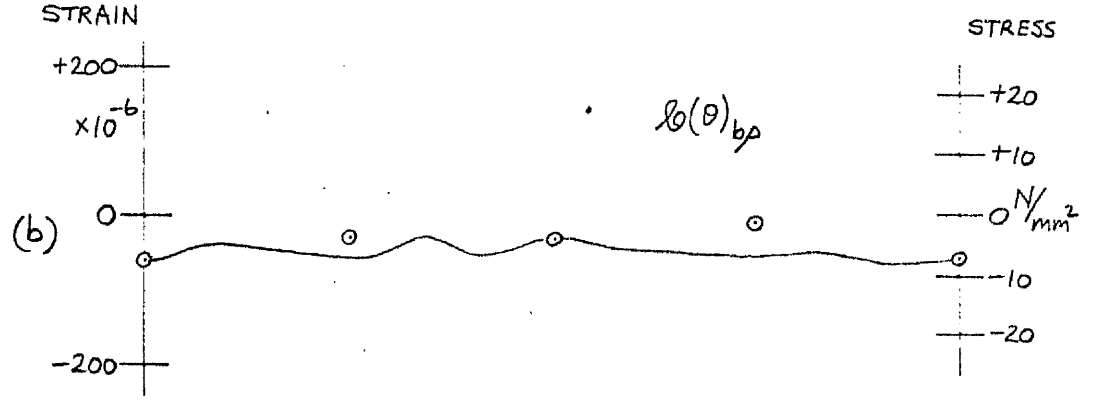

FIG. 98. SPECIMEN 3A-1 $\mathcal{L}(\theta)_{bp}$, $\mathcal{L}(\theta)_{bp}$ v θ AFTER NINTH ETCH.
$\rho/b = 0.953$, $e(\rho) = 0.077$

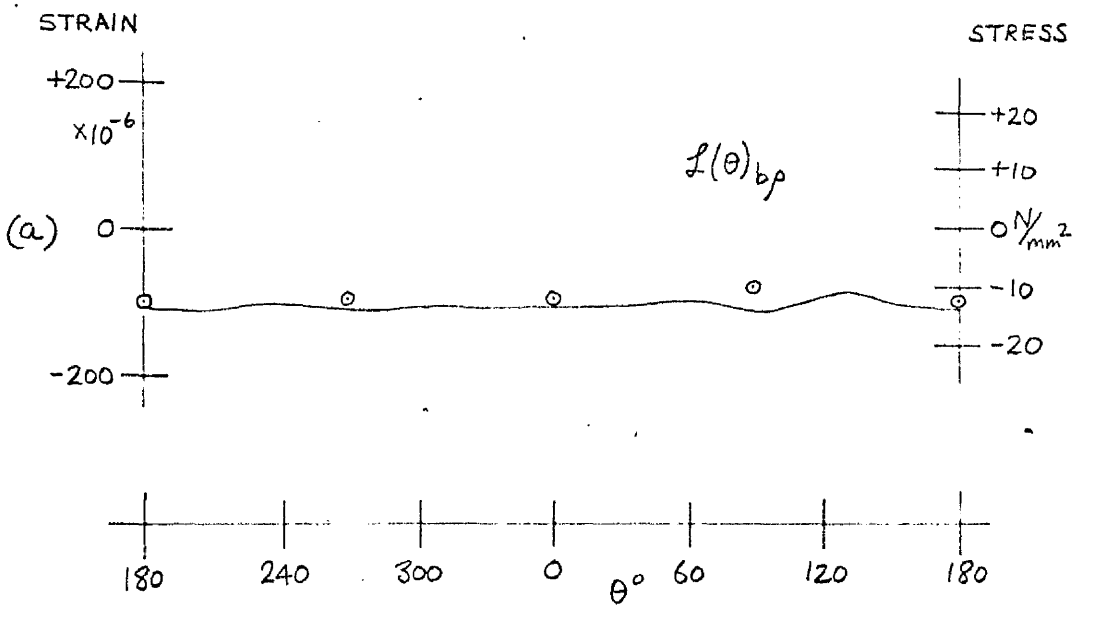

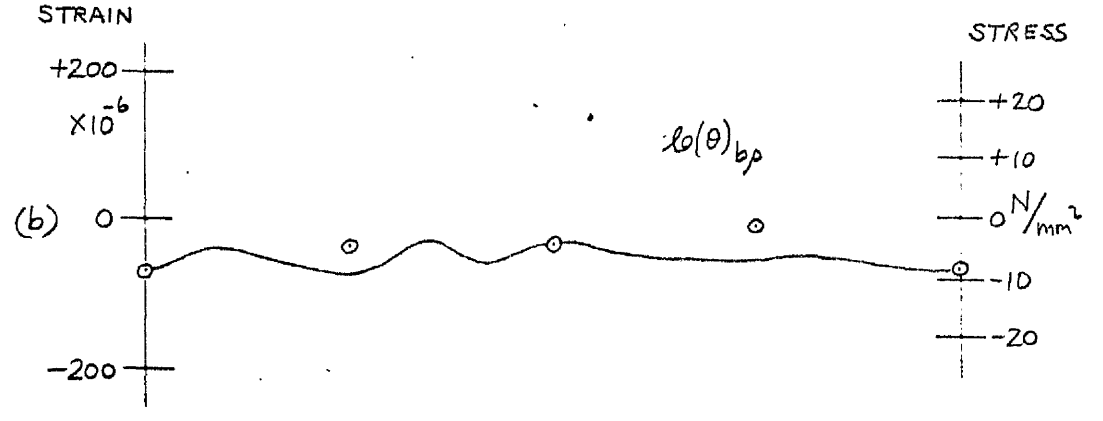

FIG. 99. SPECIMEN 3A-1 $\mathcal{L}(\theta)_{bp}$, $\mathcal{L}o(\theta)_{bp}$ V θ
AFTER TENTH ETCH
$\rho/b = 0.955$, $e(\rho) = 0.079$.

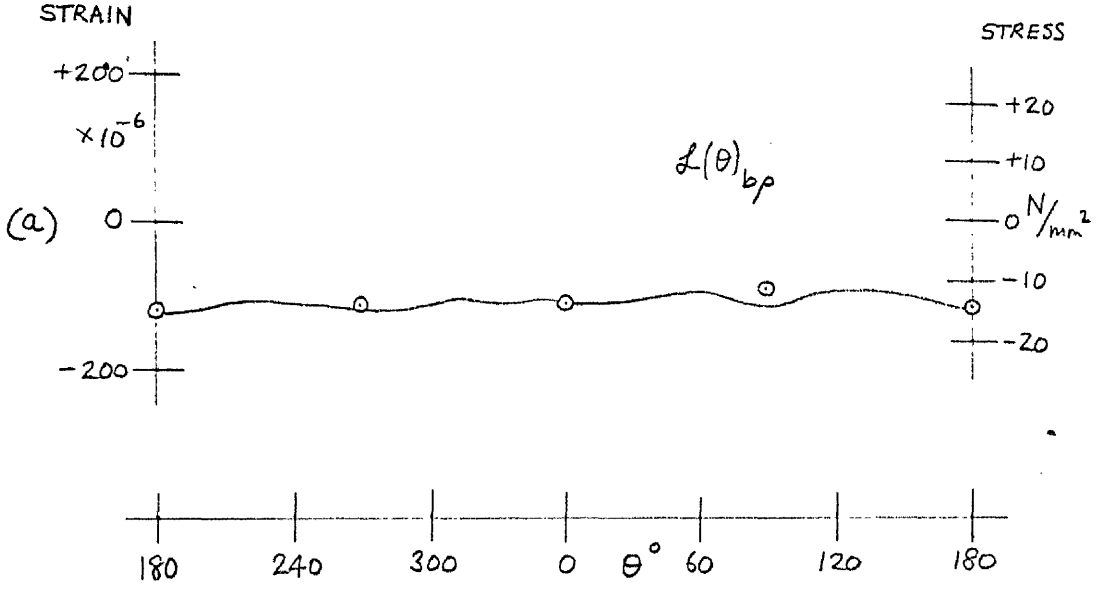

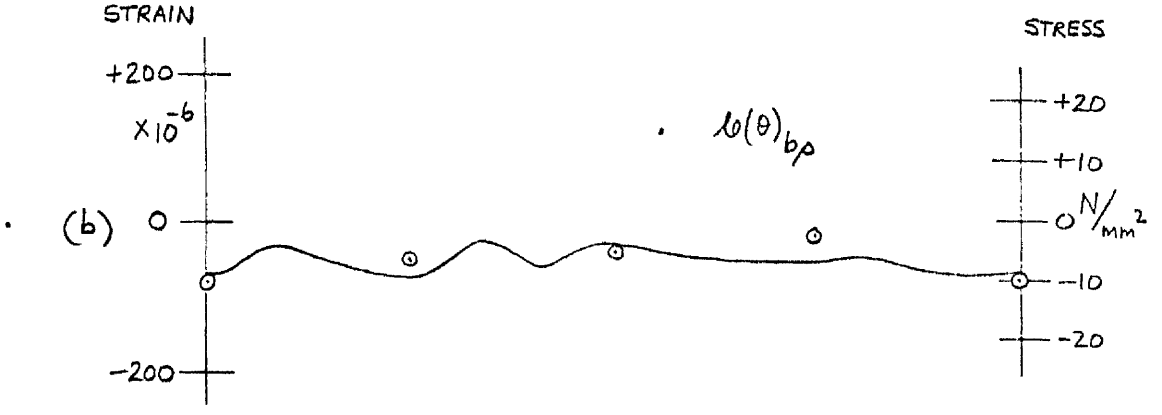

FIG. 100. SPECIMEN 3A-1 $\mathcal{L}(\theta)_{b\rho}$, $\ell(\theta)_{b\rho}$ v θ
AFTER ELEVENTH ETCH
$\rho/b = 0.957$, $e/\rho = 0.083$

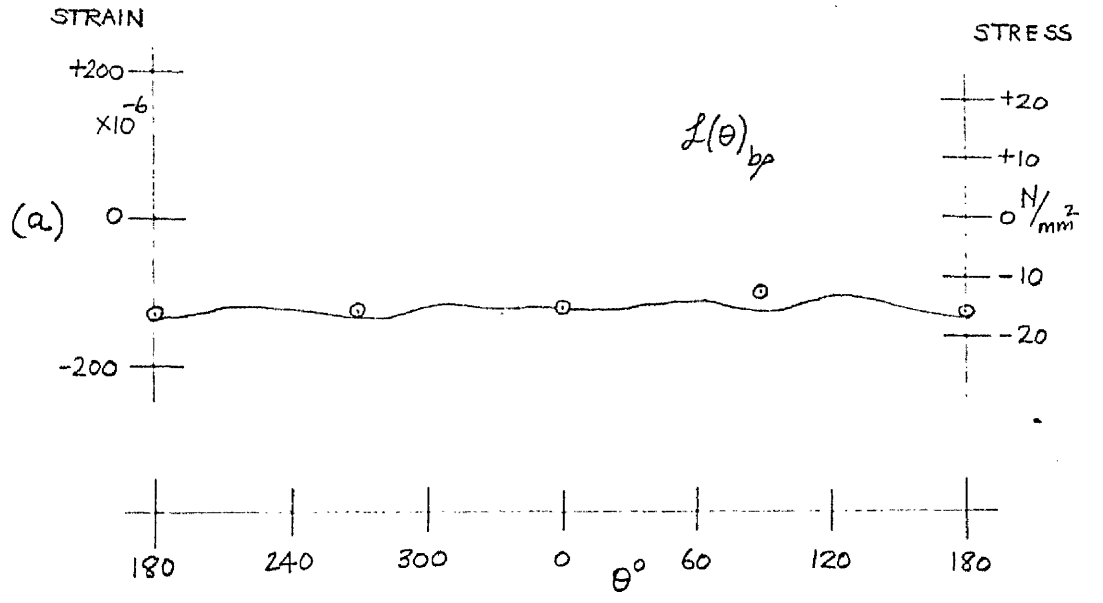

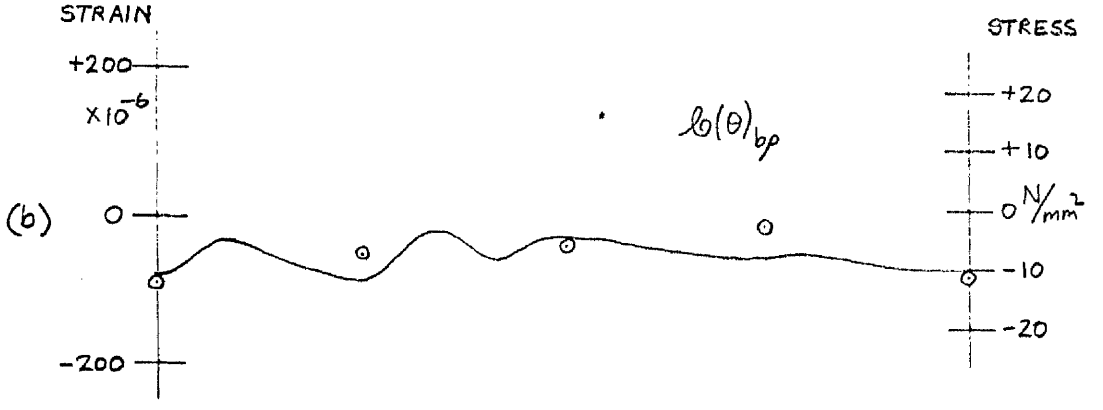

FIG. 101. SPECIMEN 3A-1 $\mathcal{L}(\theta)_{bp}$, $\ell(\theta)_{bp}$ v θ
AFTER TWELFTH ETCH
$\rho/b = 0.959$, $e(\rho) = 0.087$

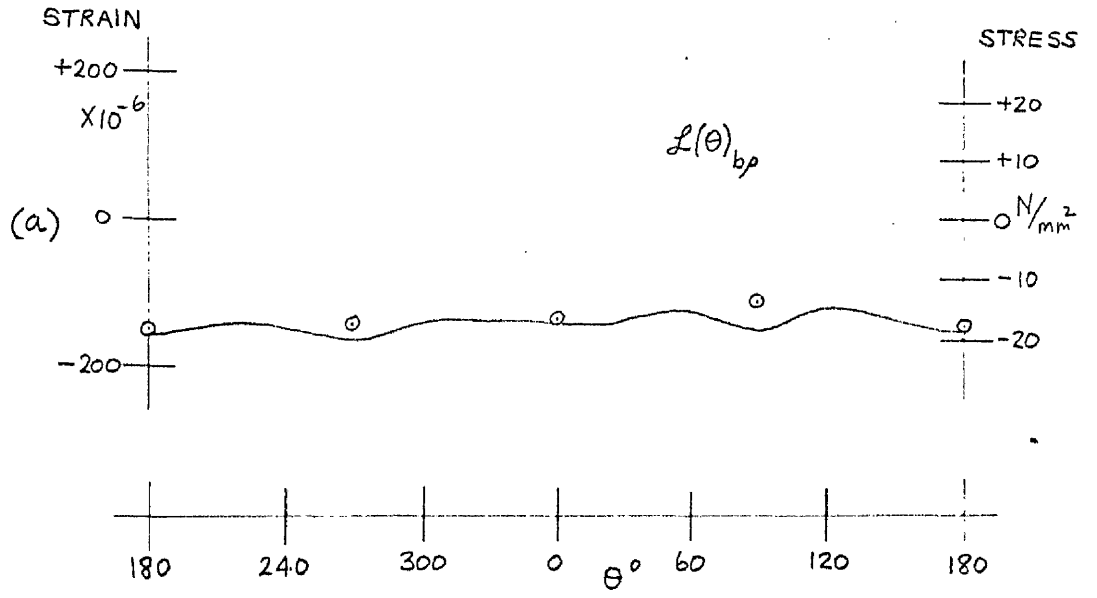

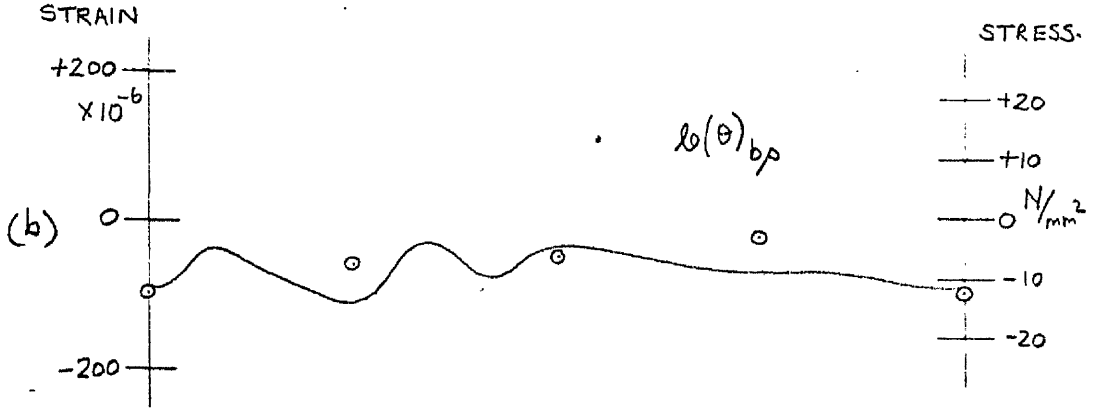

FIG. 102. SPECIMEN 3A-1 $\mathcal{L}(\theta)_{bp}$, $\mathcal{L}(\theta)_{bp}$ V θ
AFTER THIRTEENTH ETCH
$\rho/b = 0.961$, $e(\rho) = 0.091$

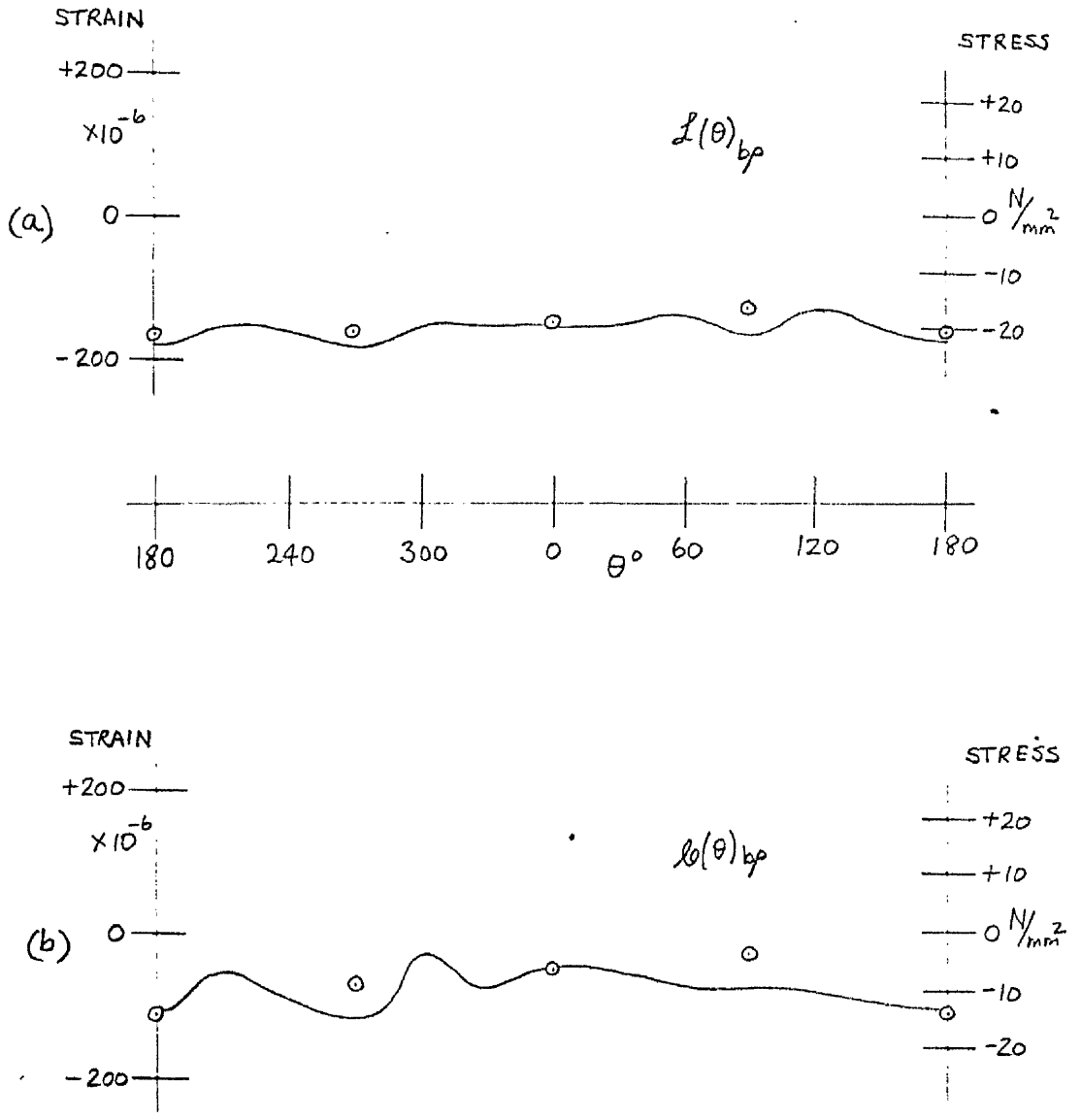

FIG. 103. SPECIMEN 3A-1 $\mathcal{L}(\theta)_{bp}$, $\mathcal{L}(\theta)_{bp}$ V θ
AFTER FOURTEENTH ETCH
$\rho/b = 0.963$, $e(\rho) = 0.096$

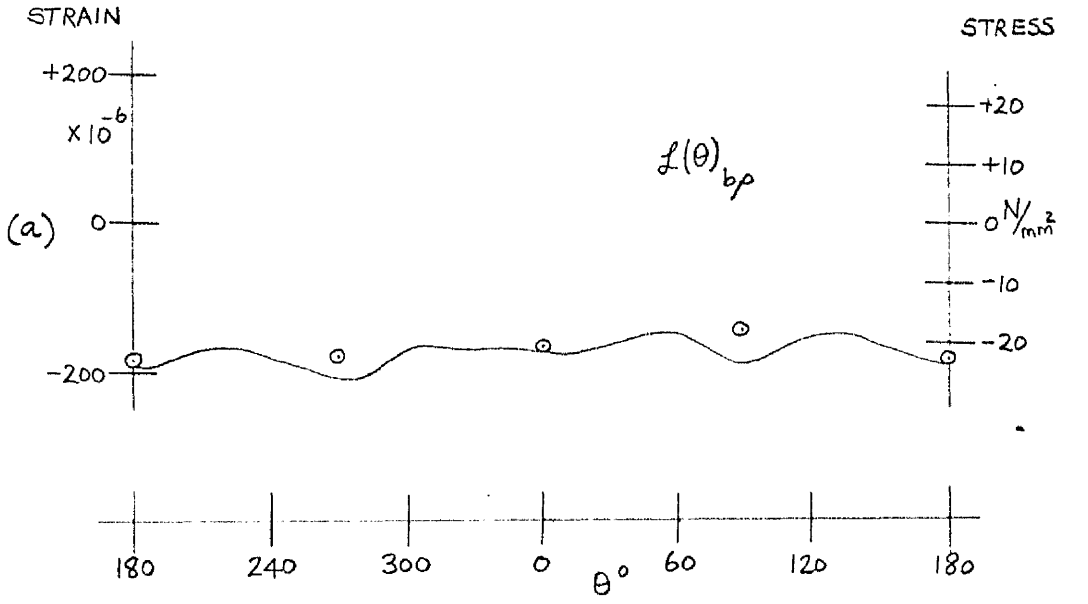

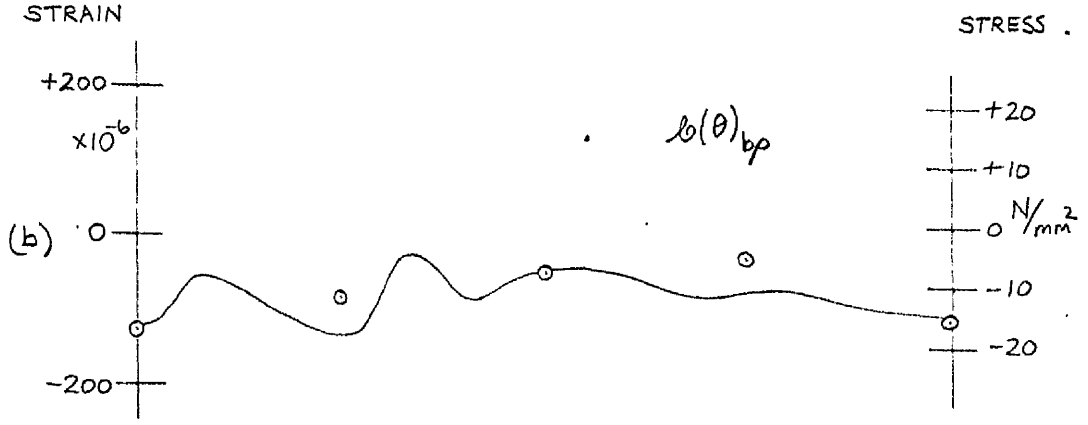

FIG. 104. SPECIMEN 3A-1 $\mathcal{L}(\theta)_{bp}$, $\mathcal{b}(\theta)_{bp}$ V θ
AFTER FIFTEENTH ETCH
$\rho/b = 0.966$, $e(\rho) = 0.104$

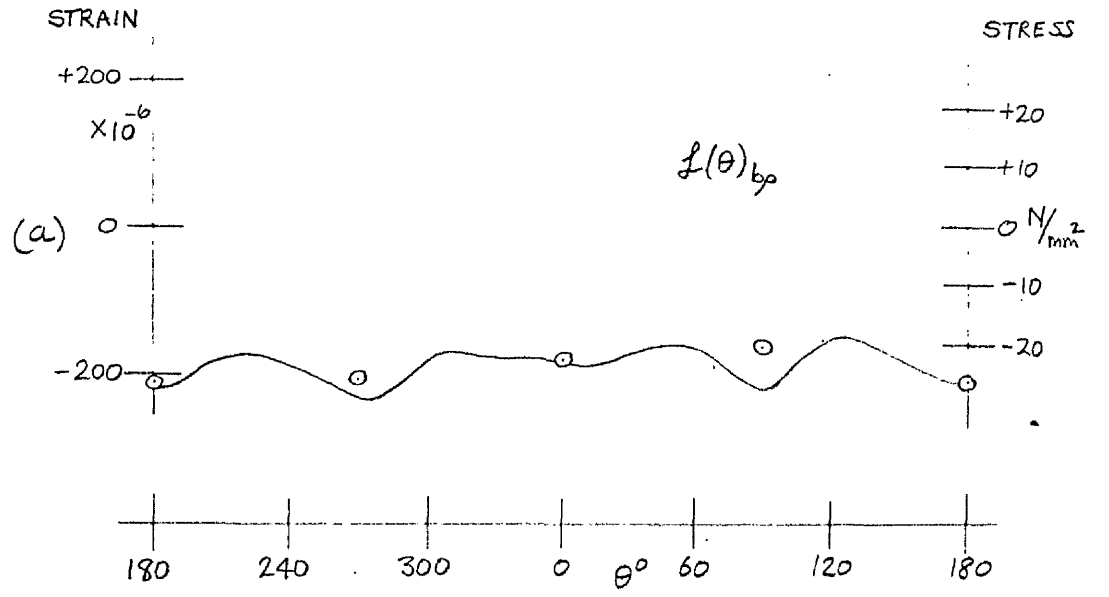

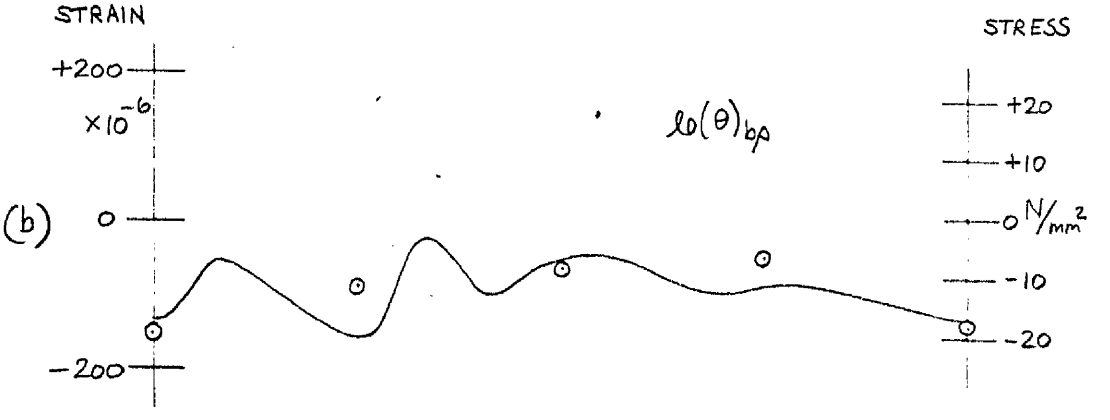

FIG. 105. SPECIMEN 3A-1 $\mathcal{L}(\theta)_{bp}$, $\ell o(\theta)_{bp}$ v θ
AFTER SIXTEENTH ETCH
$\rho/b = 0.969$, $e(\rho) = 0.115$

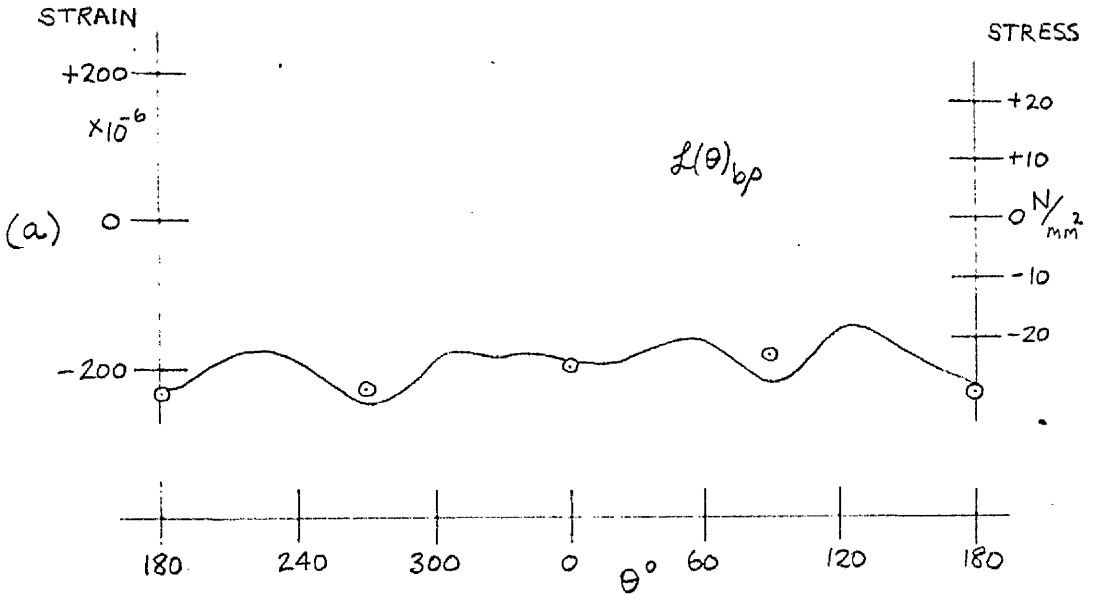

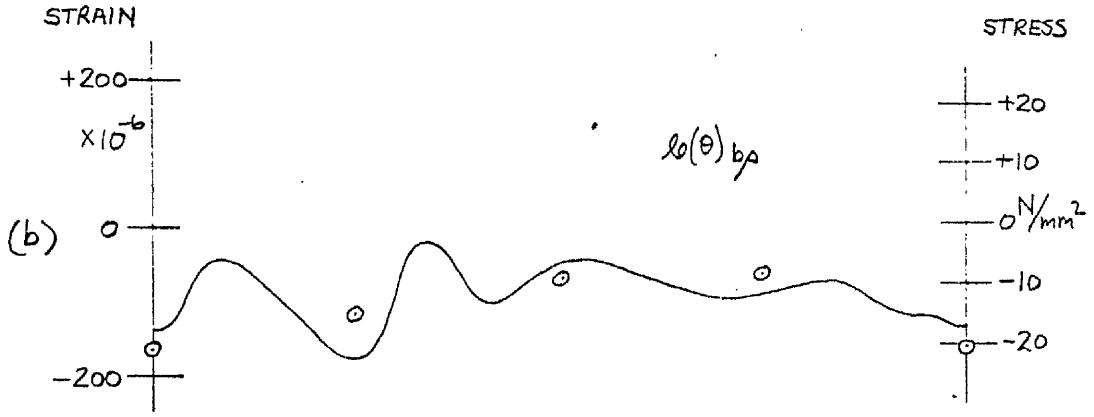

FIG. 106. SPECIMEN 3A-1 $\mathcal{L}(\theta)_{bp}$, $\ell_0(\theta)_{bp}$ v θ
AFTER SEVENTEENTH ETCH
$\rho/b = 0.971$, $e(\rho) = 0.122$

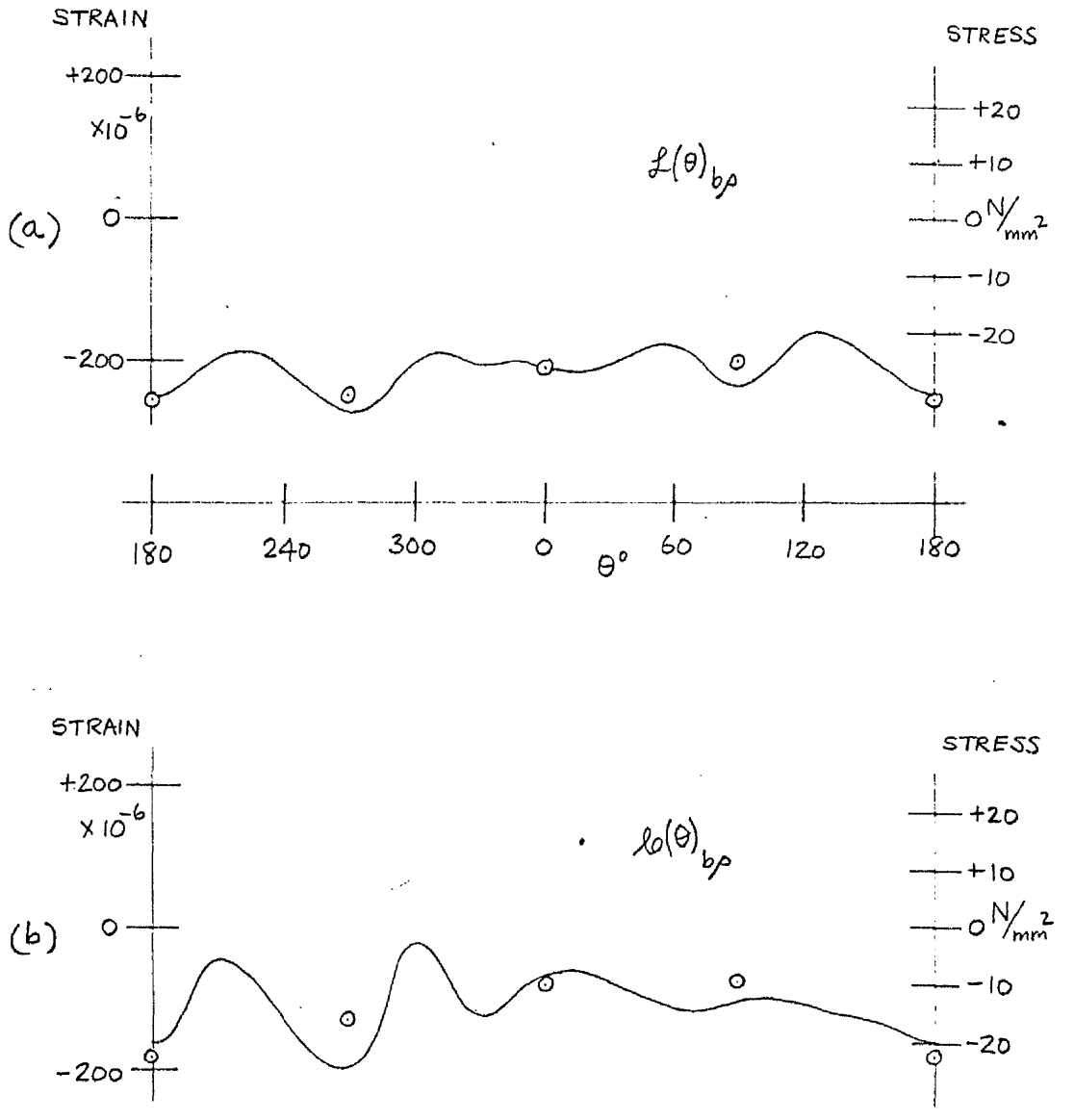

FIG. 107. SPECIMEN 3A-1 $\mathcal{L}(\theta)_{bp}$, $\mathcal{L}o(\theta)_{bp}$ v θ
AFTER EIGHTEENTH ETCH
$\rho/b = 0.973$, $e(\rho) = 0.131$

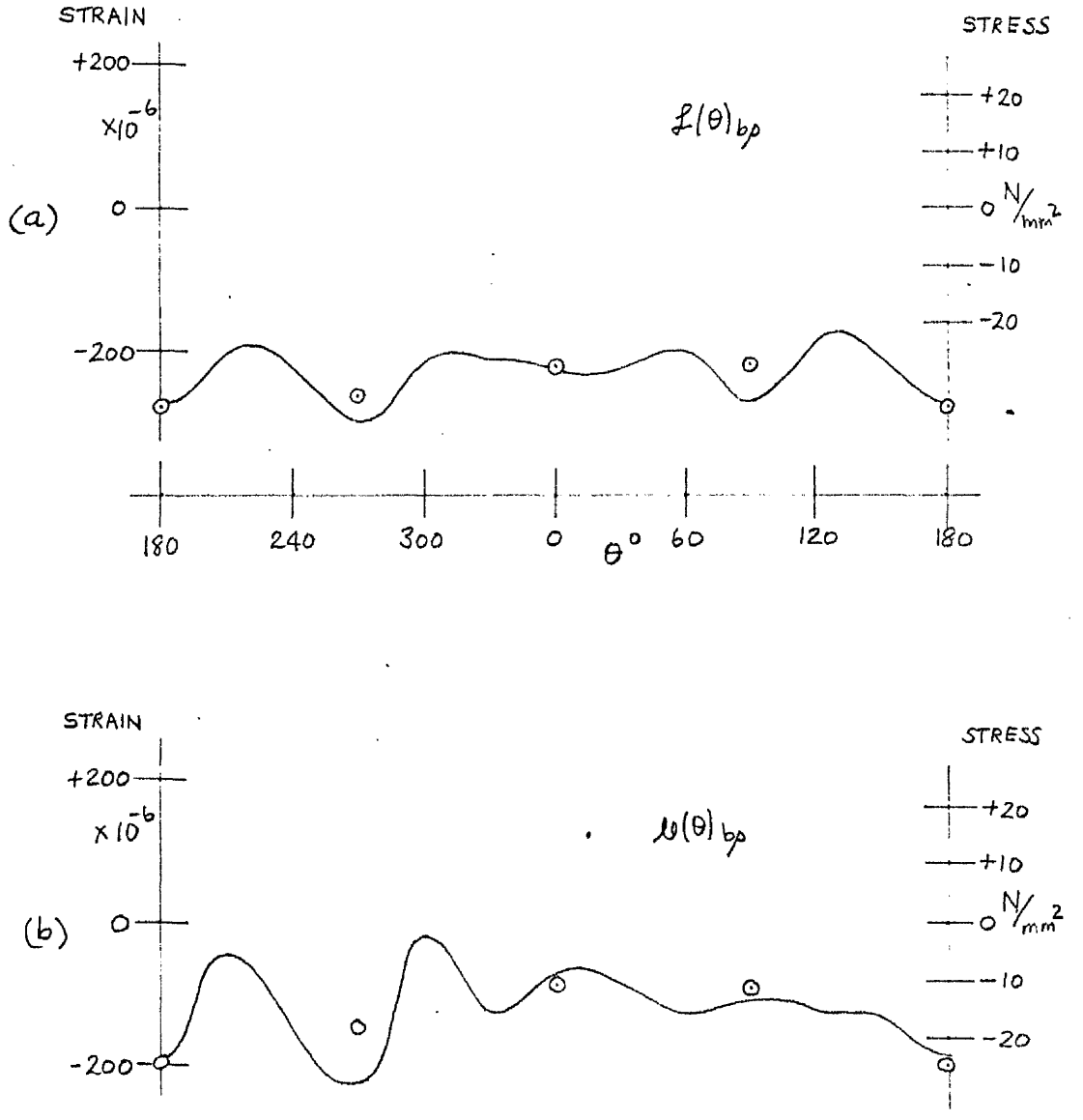

FIG. 108. SPECIMEN 3A-1 $\mathcal{L}(\theta)_{bp}$, $\mathcal{U}(\theta)_{bp}$ v θ
AFTER NINETEENTH ETCH
$\rho_b = 0.975$, $e(\rho) = 0.142$

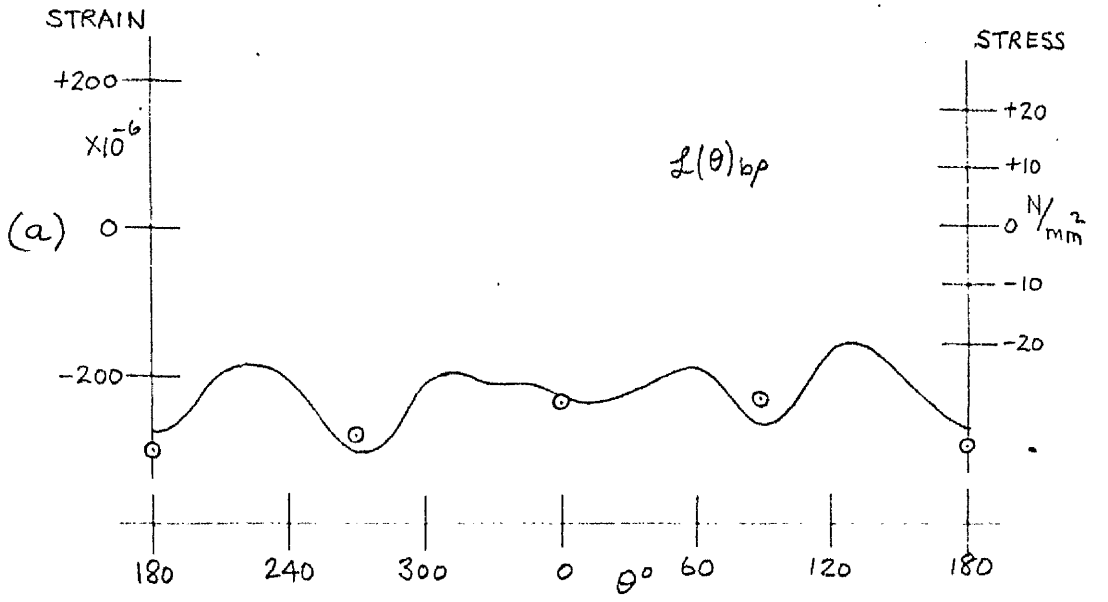

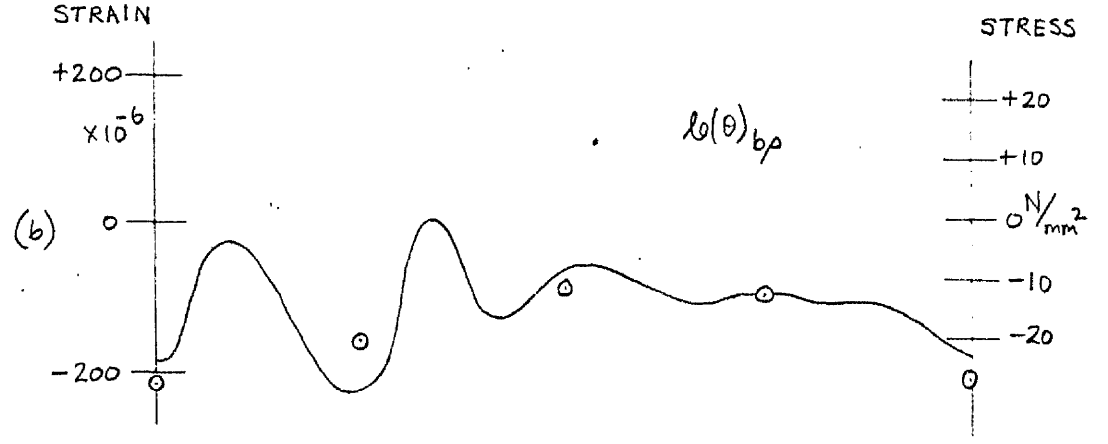

FIG. 109. SPECIMEN 3A-1 $\mathcal{L}(\theta)_{bp}$, $\ell(\theta)_{bp}$ v θ
AFTER TWENTIETH ETCH
$A/b = 0.978$, $e(\rho) = 0.161$

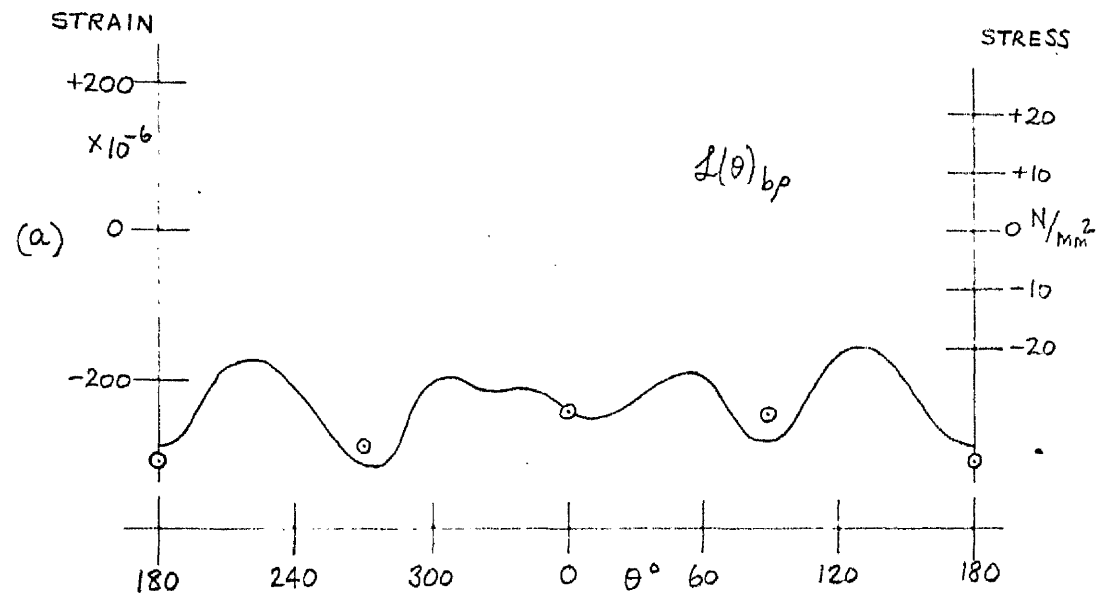

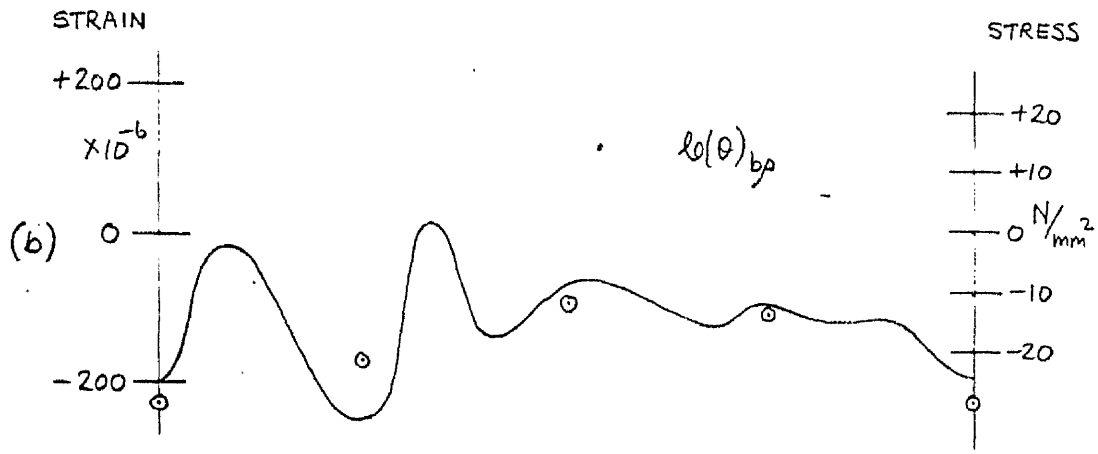

FIG. 110. SPECIMEN 3A-1 $\mathcal{L}(\theta)_{bp}$, $\ell o(\theta)_{bp}$ V θ
AFTER TWENTY-FIRST ETCH.
$\rho/b = 0.980$, $e(\rho) = 0.178$

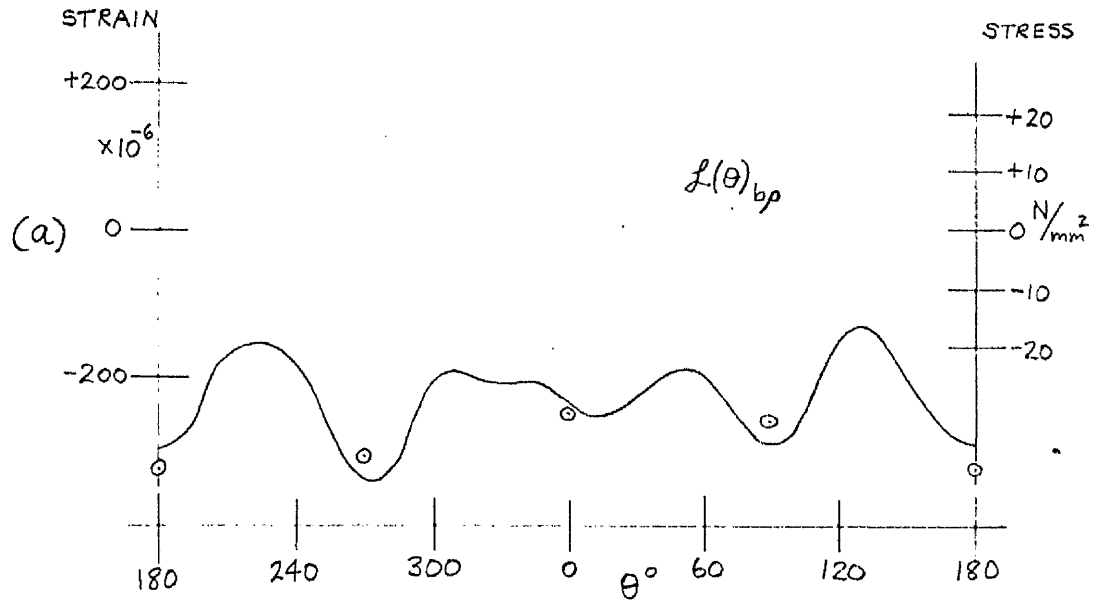

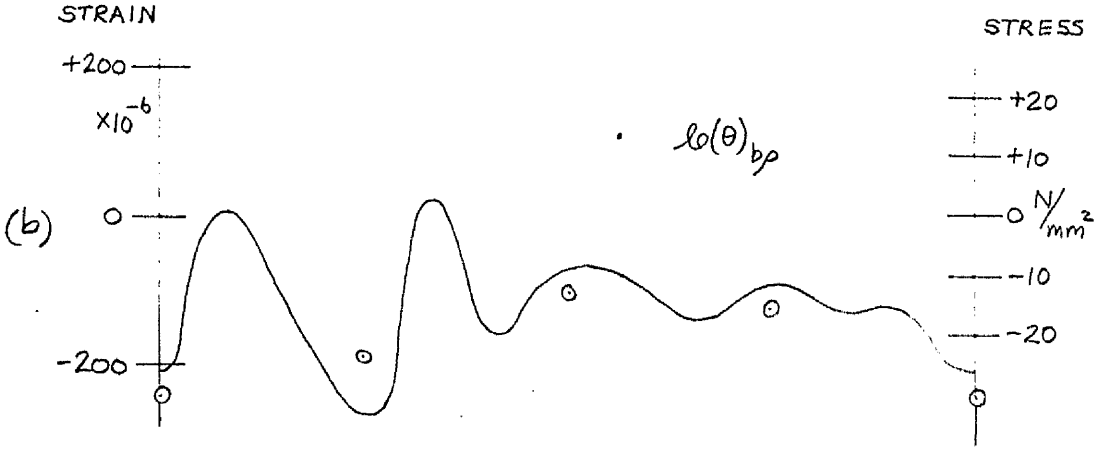

FIG. III. SPECIMEN 3A-1 $\mathcal{L}(\theta)_{bp}$, $\ell o(\theta)_{bp}$ v θ
AFTER TWENTY-SECOND ETCH
$\rho/b = 0.983$, $e(\rho) = 0.209$

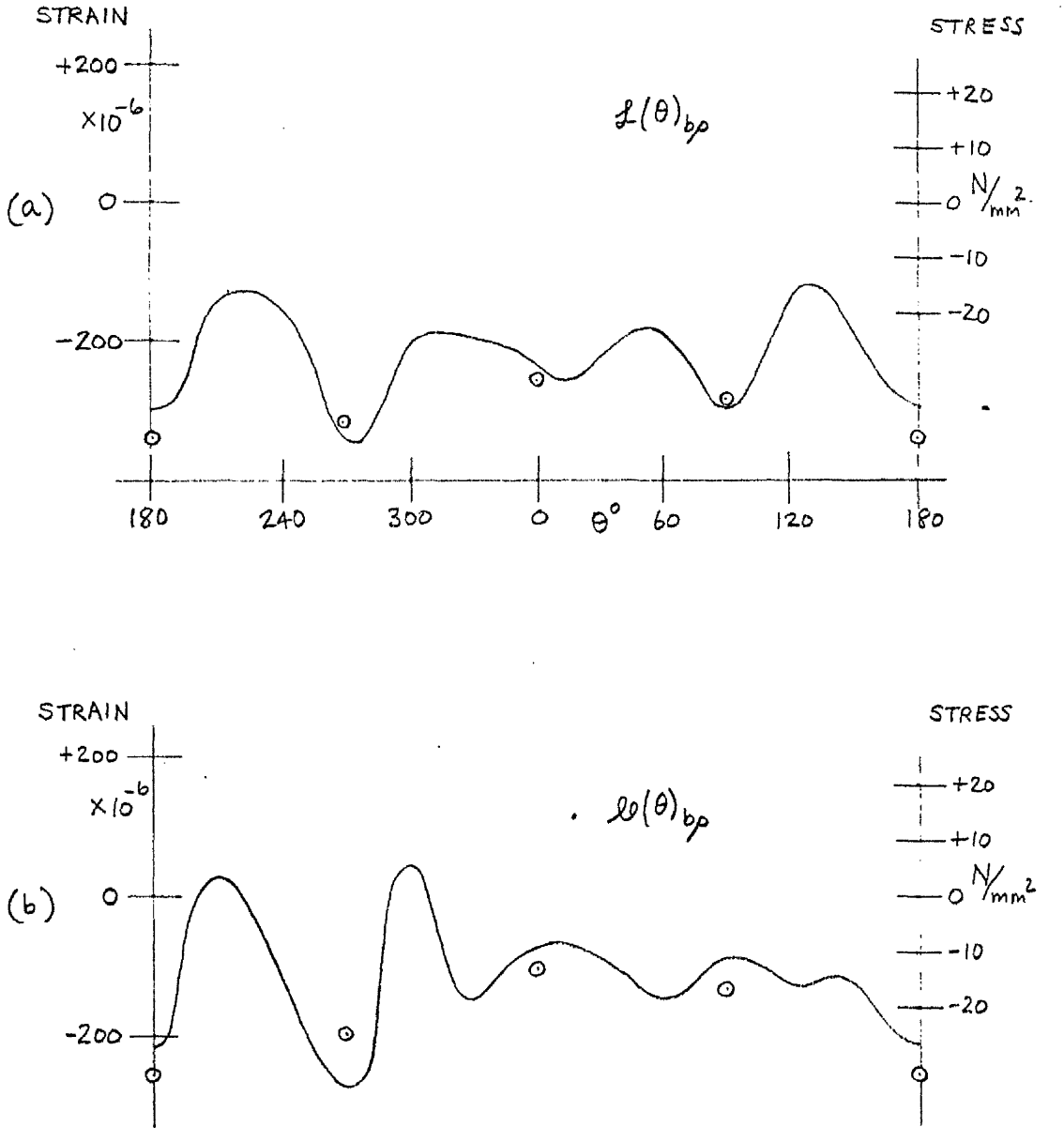

FIG. 112. SPECIMEN 3A-1 $\ell(\theta)_{bp}$, $\ell_0(\theta)_{bp}$ v θ
AFTER TWENTY-THIRD ETCH
$\rho/b = 0.985$, $e/\rho = 0.237$

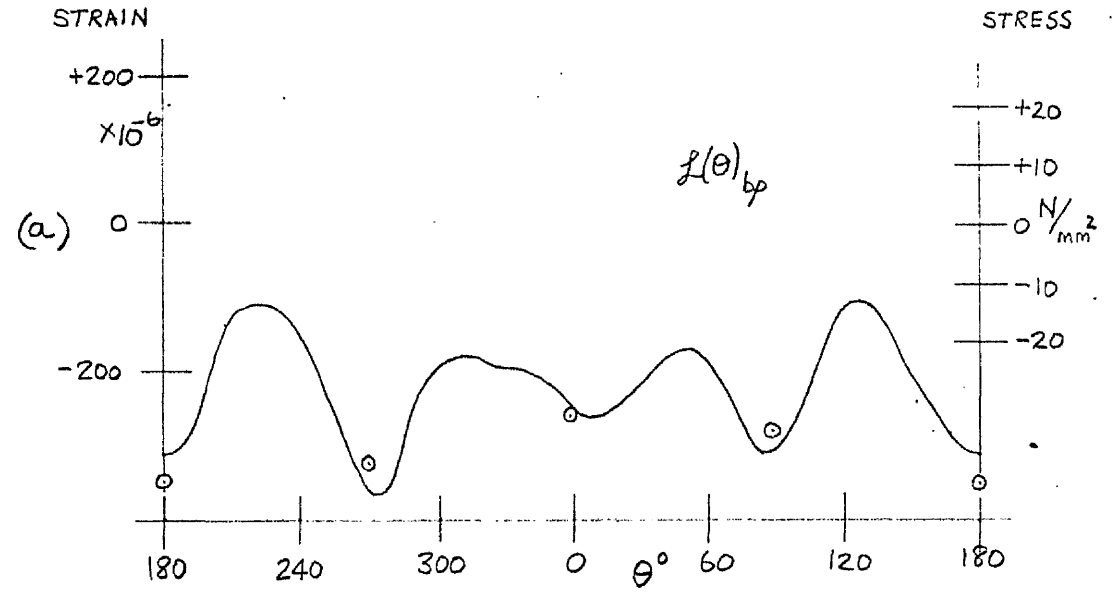

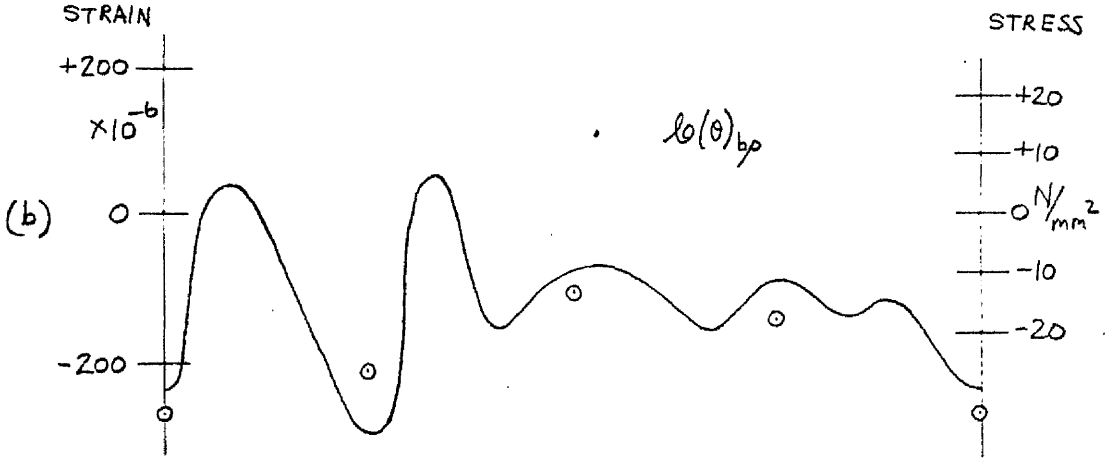

FIG. 113. SPECIMEN 3A-1 $\mathcal{L}(\theta)_{bp}$, $\mathcal{L}(\theta)_{bp}$ v θ
AFTER TWENTY-FOURTH ETCH
$\rho/b = 0.987$, $e(\rho) = 0.273$

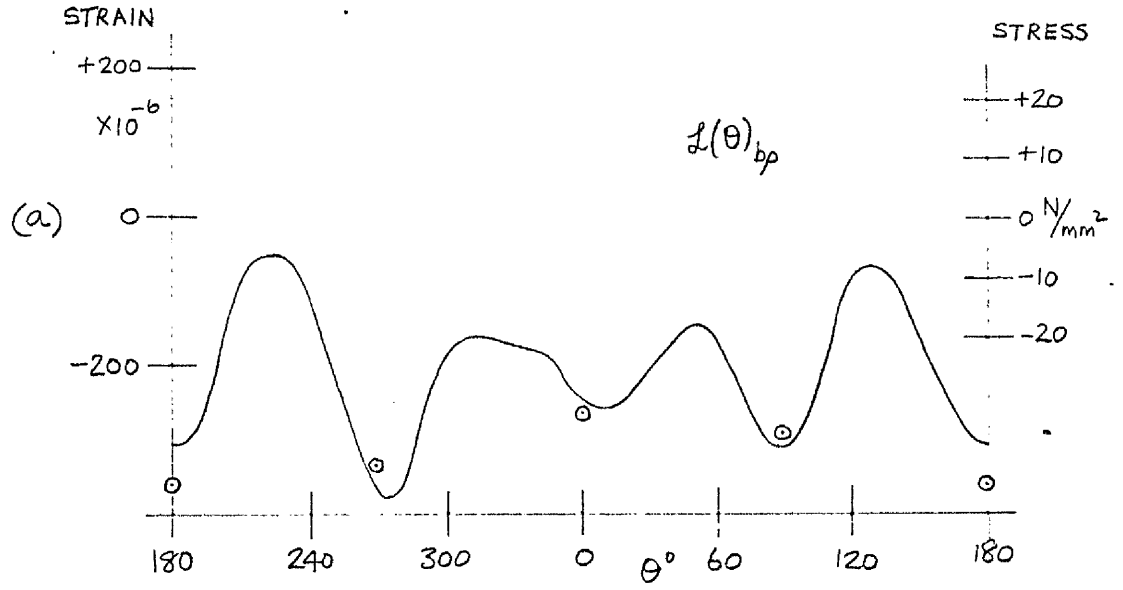

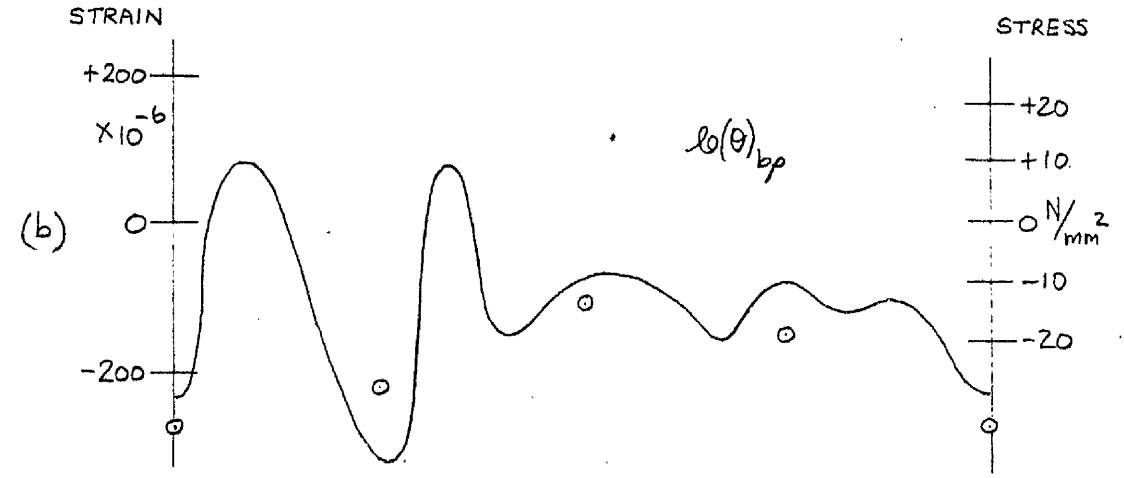

FIG. 114. SPECIMEN 3A-1 $\mathcal{L}(\theta)_{bp}$, $\mathcal{L}o(\theta)_{bp}$ v θ
AFTER TWENTY-FIFTH ETCH
$\rho/b = 0.988$, $e(\rho) = 0.296$

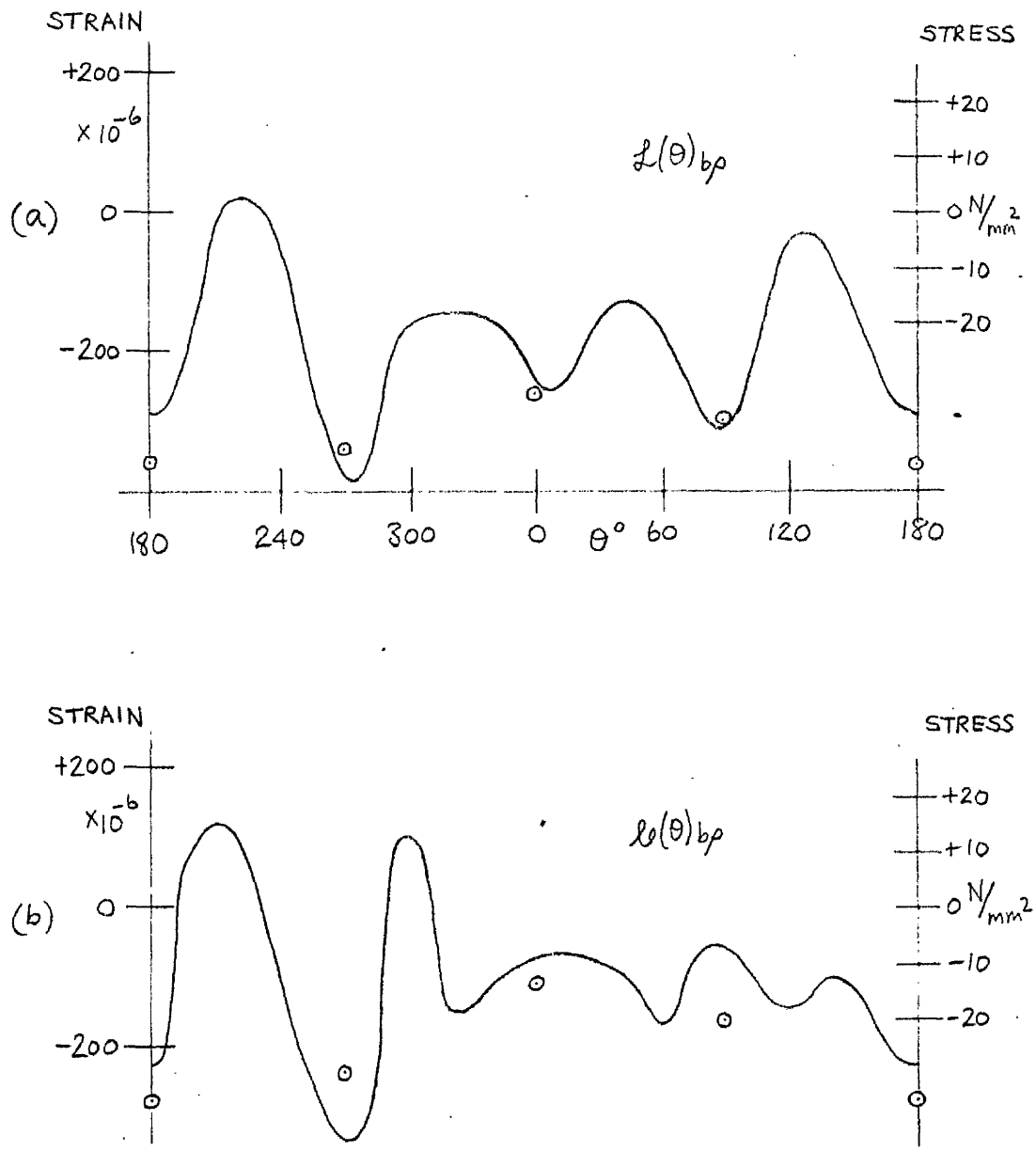

FIG. 115. SPECIMEN 3A-1 $\mathcal{L}(\theta)_{bp}$, $\ell_0(\theta)_{bp}$ V θ
AFTER TWENTY-SIXTH ETCH
$\rho/b = 0.990$, $e(\rho) = 0.355$

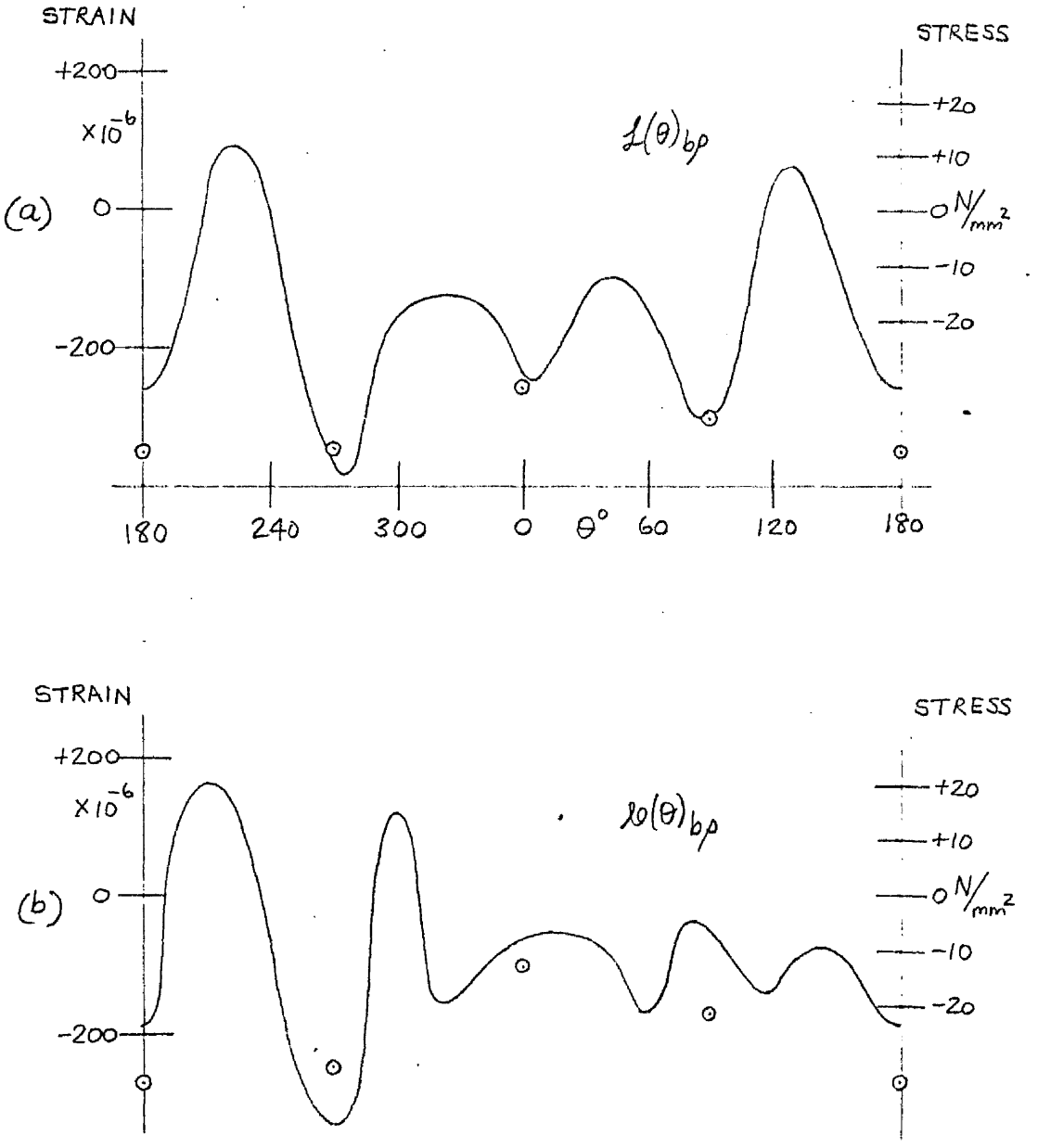

FIG. 116. SPECIMEN 3A-1 $\mathcal{L}(\theta)_{bp}$, $\ell o(\theta)_{bp}$ v θ
AFTER TWENTY-SEVENTH ETCH
$\rho/b = 0.992$, $e(\rho) = 0.444$

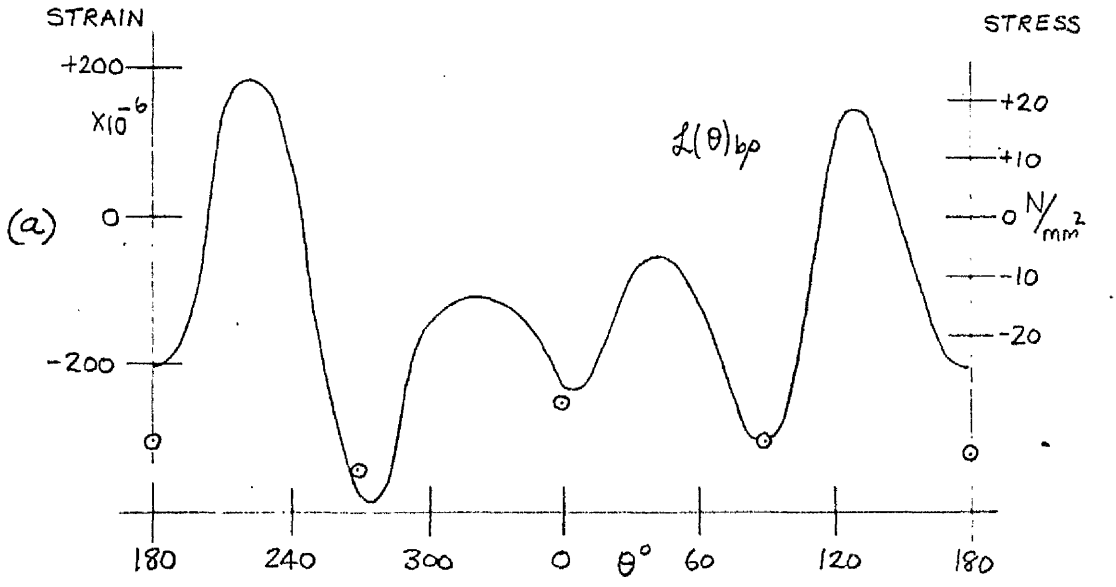

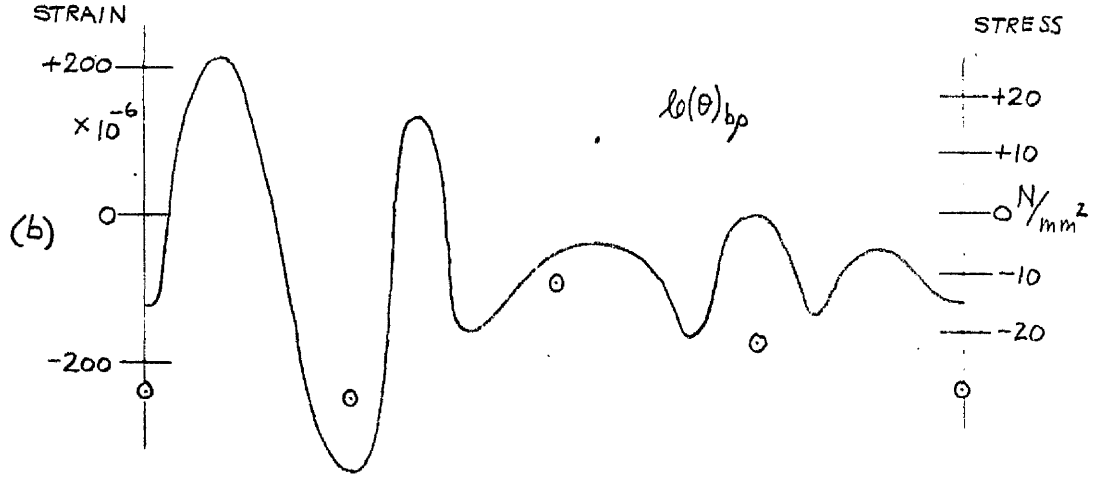

FIG. 117. SPECIMEN 3A-1 $\mathcal{L}(\theta)_{bp}$, $\mathcal{L}o(\theta)_{bp}$ v θ
AFTER TWENTY-EIGHTH ETCH
$\rho/b = 0.993$, $e(\rho) = 0.507$

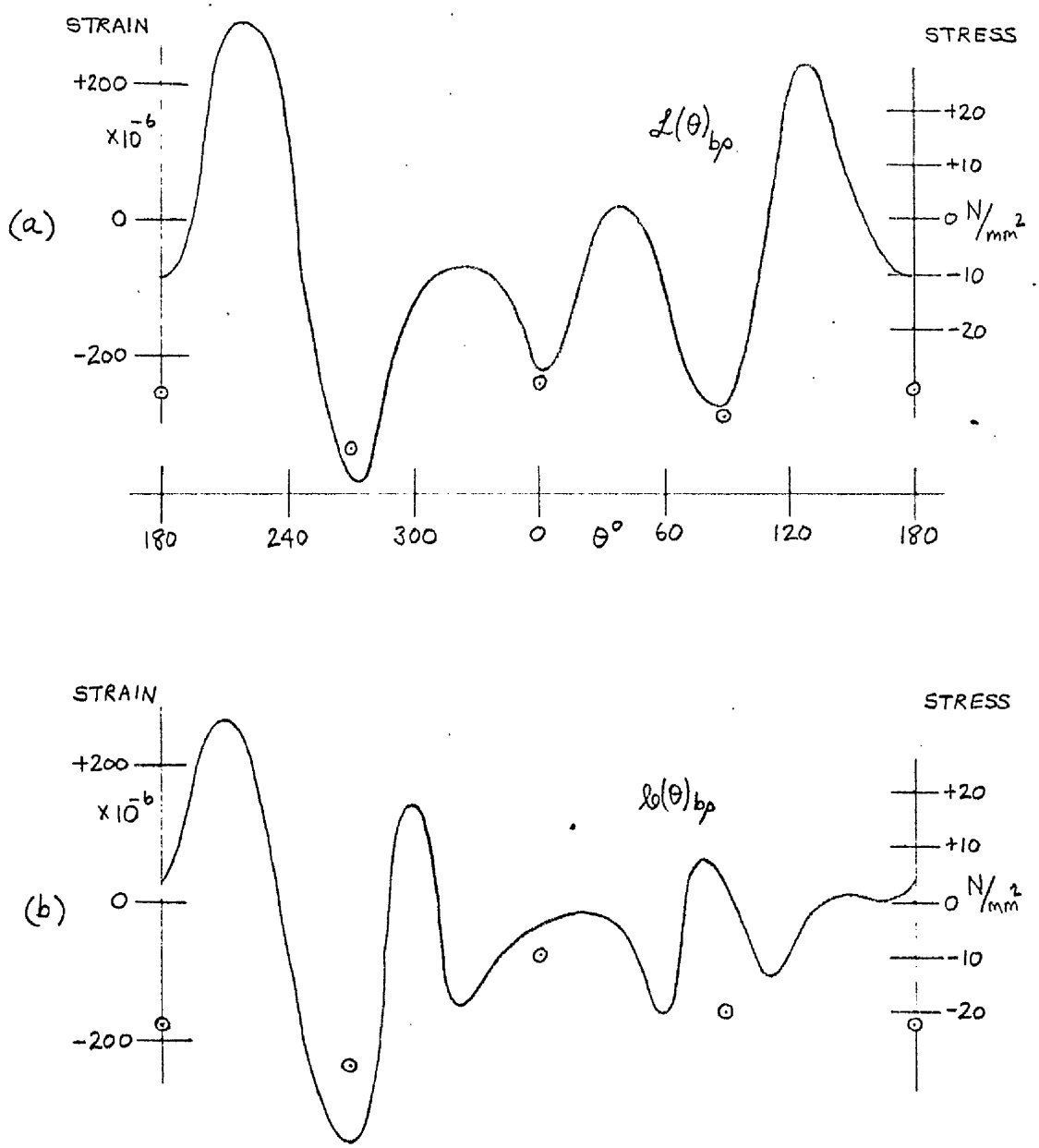

FIG. 118. SPECIMEN 3A-1 $\mathcal{L}(\theta)_{bp}$, $\ell_b(\theta)_{bp}$ V θ
AFTER TWENTY-NINTH ETCH
$\rho/b = 0.995$, $e(\rho) = 0.710$

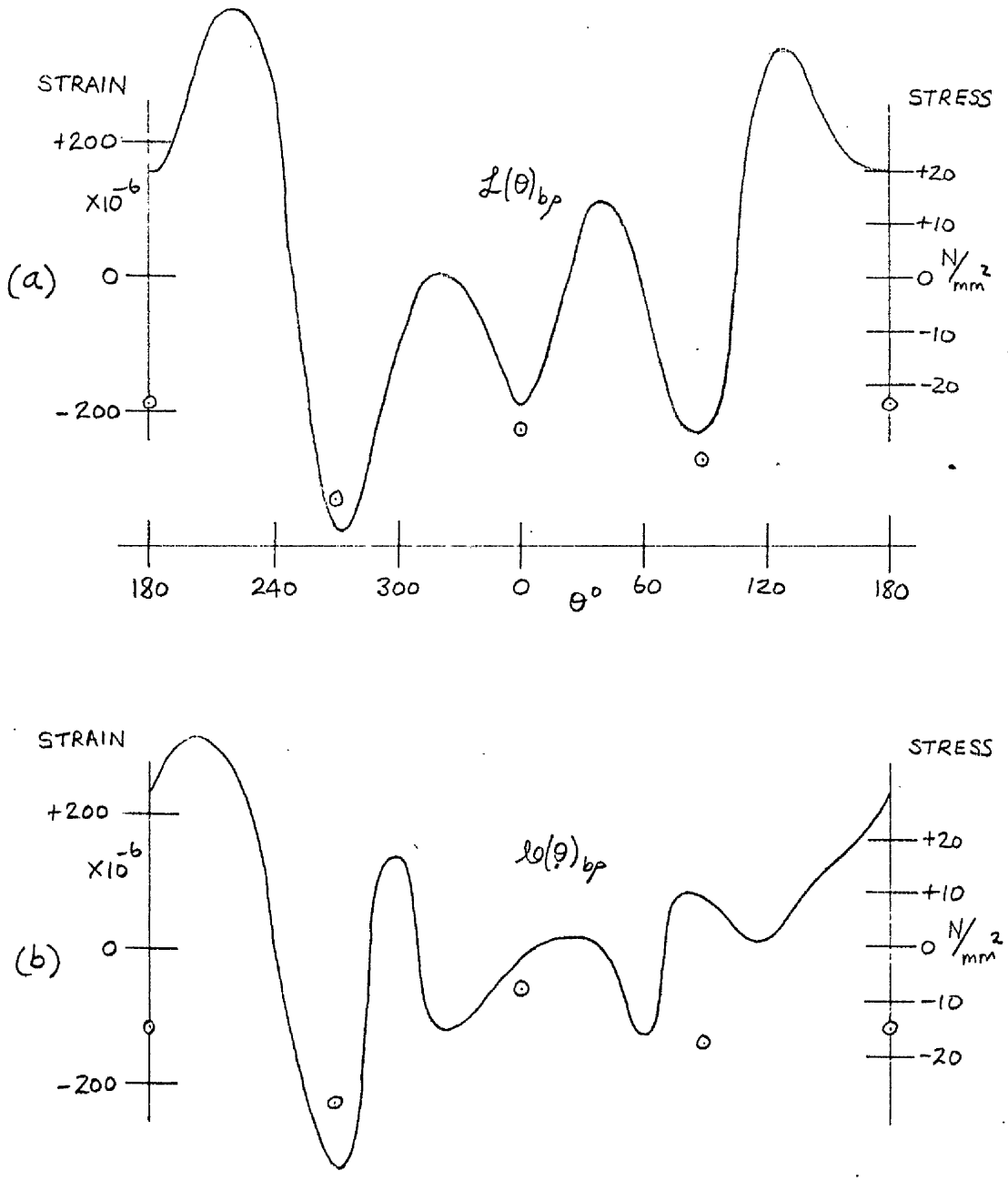

FIG. 119. SPECIMEN 3A-1 $\mathcal{L}(\theta)_{bp}$, $\ell\rho(\theta)_{bp}$ v θ
AFTER THIRTIETH ETCH
$A/b = 0.996$, $e(\rho) = 0.888$

FIG. 120. SPECIMEN 3A-1 $\mathcal{L}(\theta)_{bp}$ V θ AFTER EIGHTH, FIFTEENTH AND TWENTY-FOURTH ETCHES.

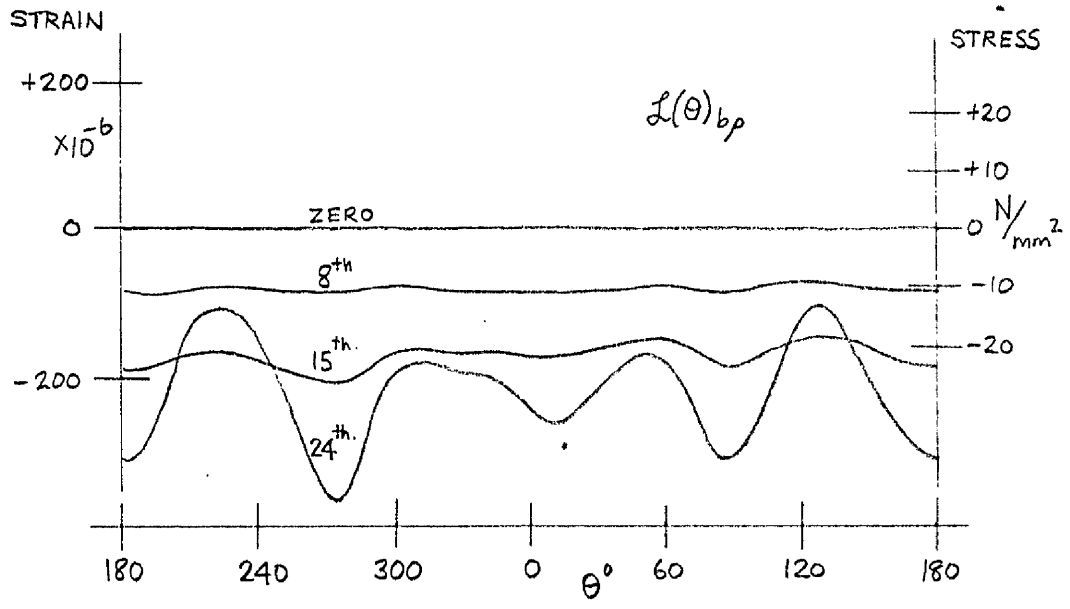

FIG. 121. SPECIMEN 3A-1 $\sigma(\theta)_{bp}$ V θ
AFTER EIGHTH, FIFTEENTH
AND TWENTY-FOURTH ETCHES

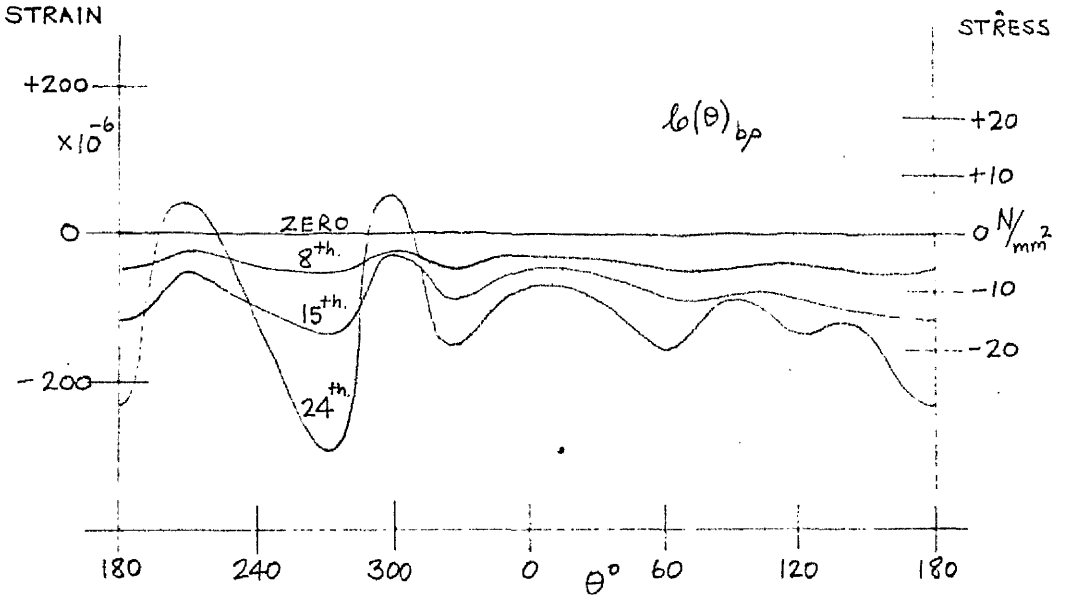

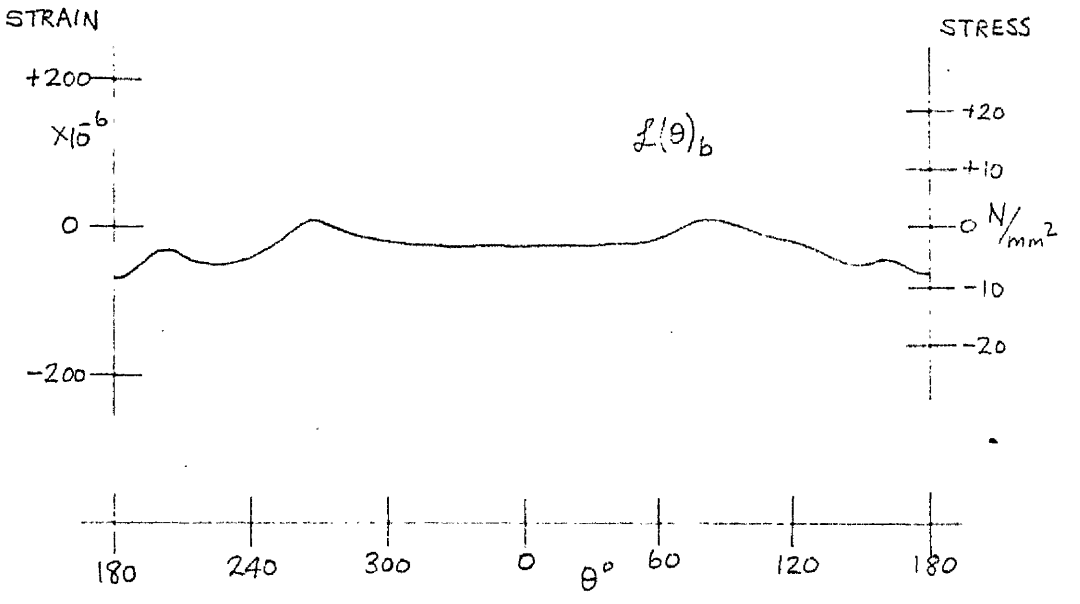

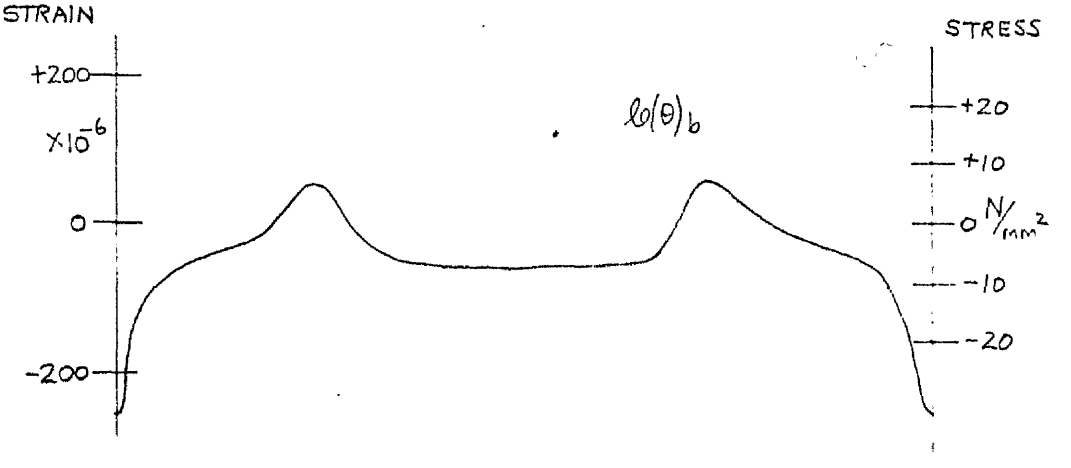

FIG. 122. SPECIMEN 3A-1, CHANGE IN $\mathcal{L}(\theta)_b$, $\mathcal{C}(\theta)_b$ ON FREEING SPECIMEN.

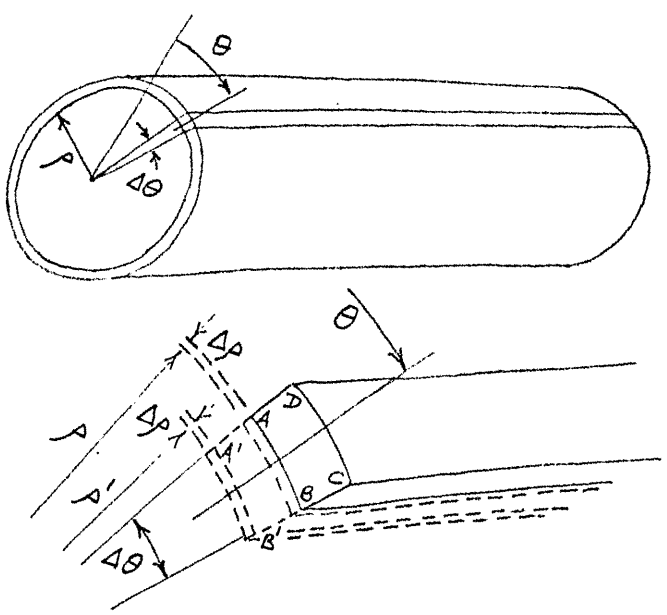

FIG. 123.

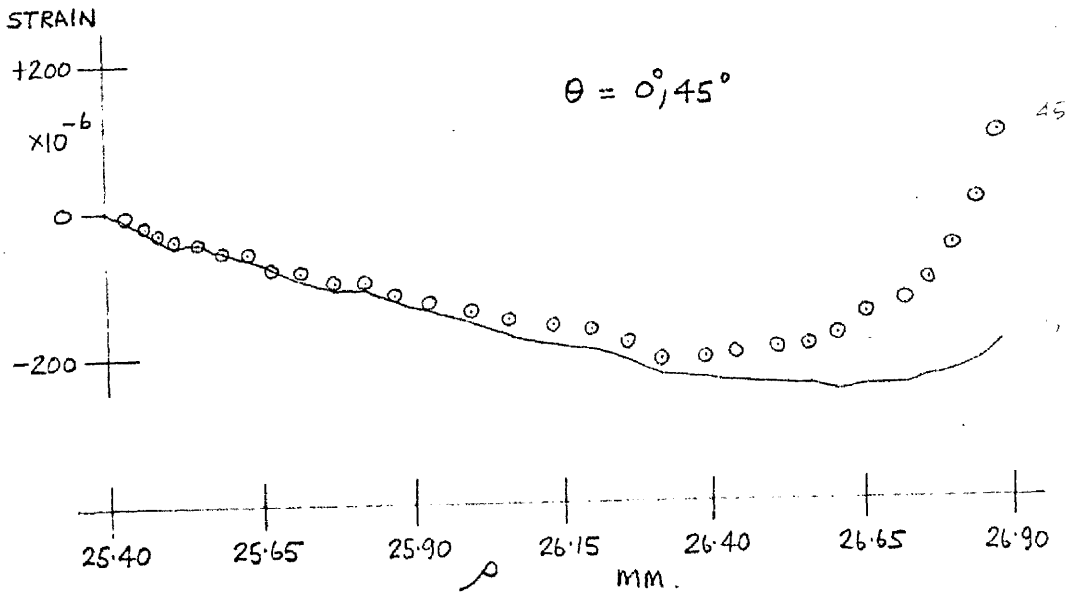

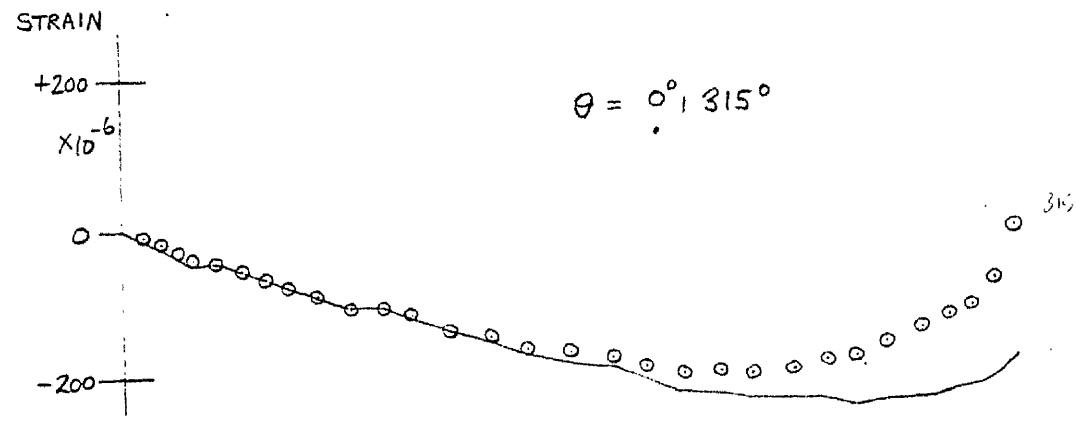

FIG. 124. SPECIMEN 3A-1 $\mathcal{L}(\theta)_{bp}$ V ρ AT $\theta = 0°, 45°, 315°$.

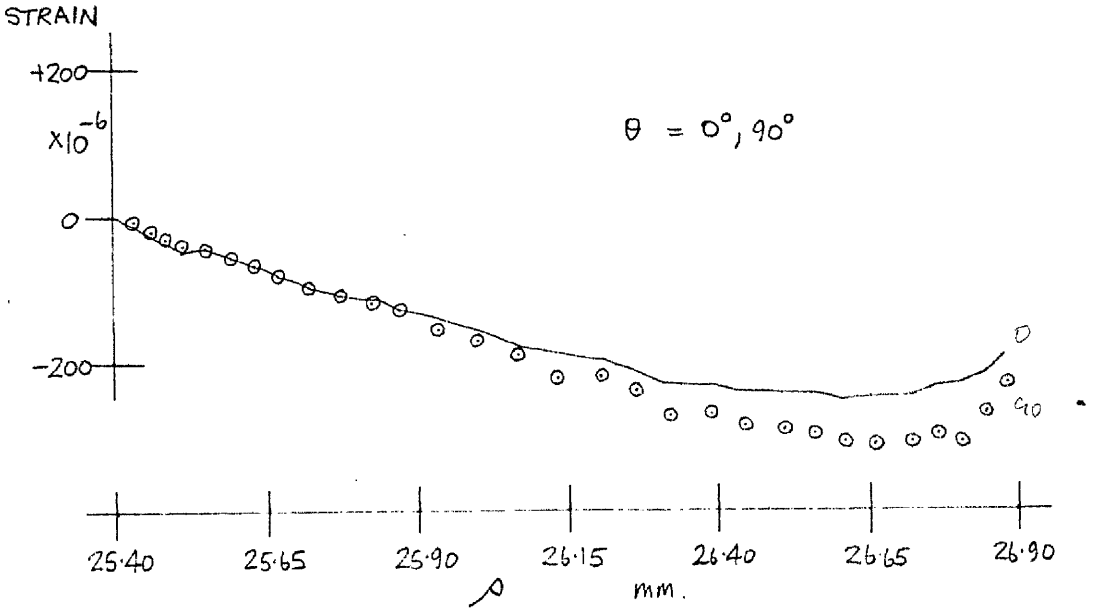

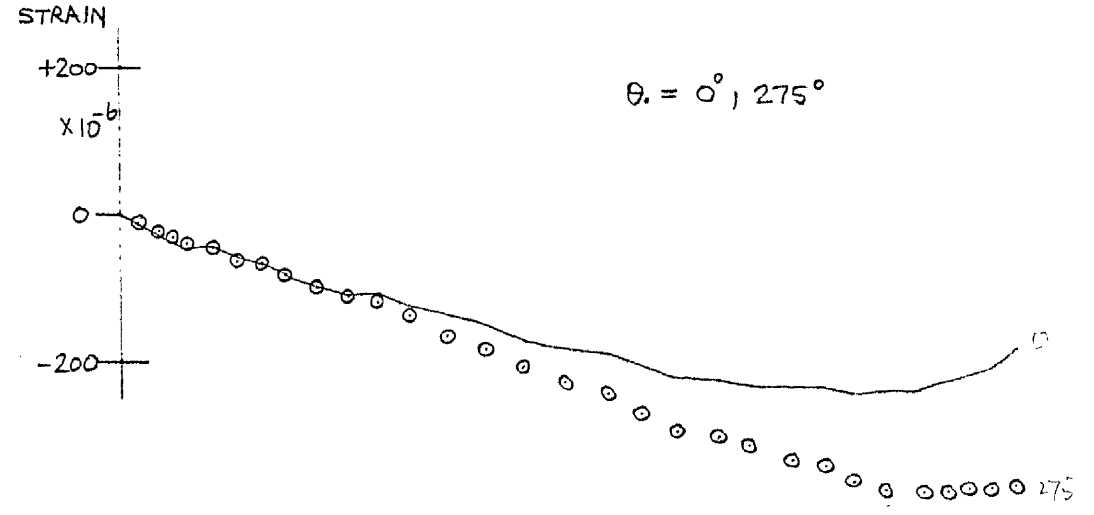

FIG. 125. SPECIMEN 3A-1 $\mathcal{L}(\theta)_{bp}$ V ρ AT $\theta = 0°, 90°, 275°$

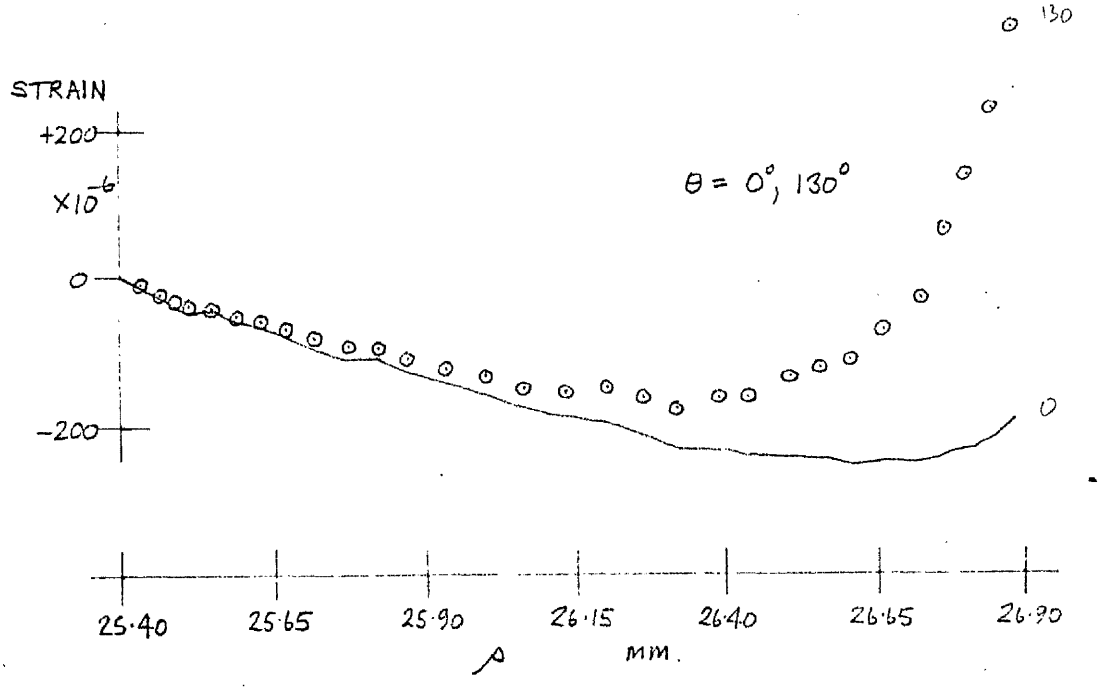

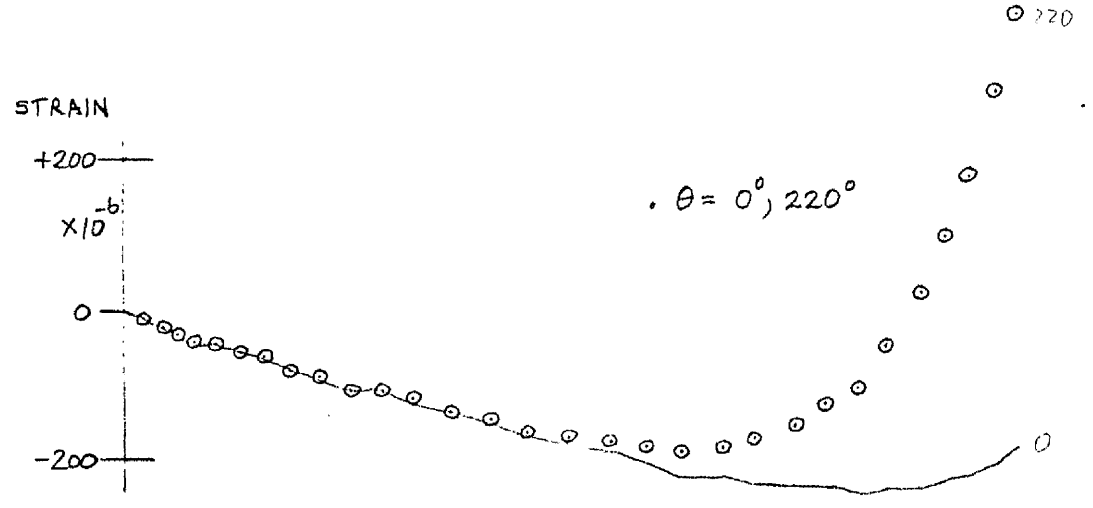

FIG. 126. SPECIMEN 3A-1 $\mathcal{L}(\theta)_{bp}$ V ρ AT θ = 0°, 130°, 220°

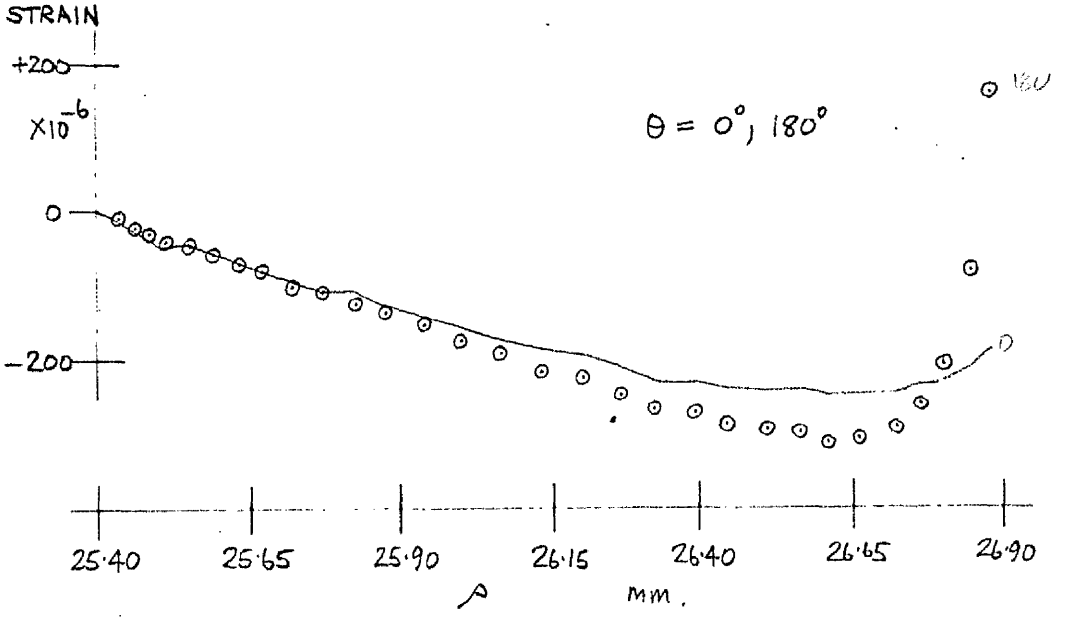

FIG. 127. SPECIMEN 3A-1 $\mathcal{L}(\theta)_{bp}$ V ρ AT $\theta = 0°, 180°$

FIG. 128. SPECIMEN 3A-1 $\frac{h\theta}{h_{MAX}}$ V ρ/b

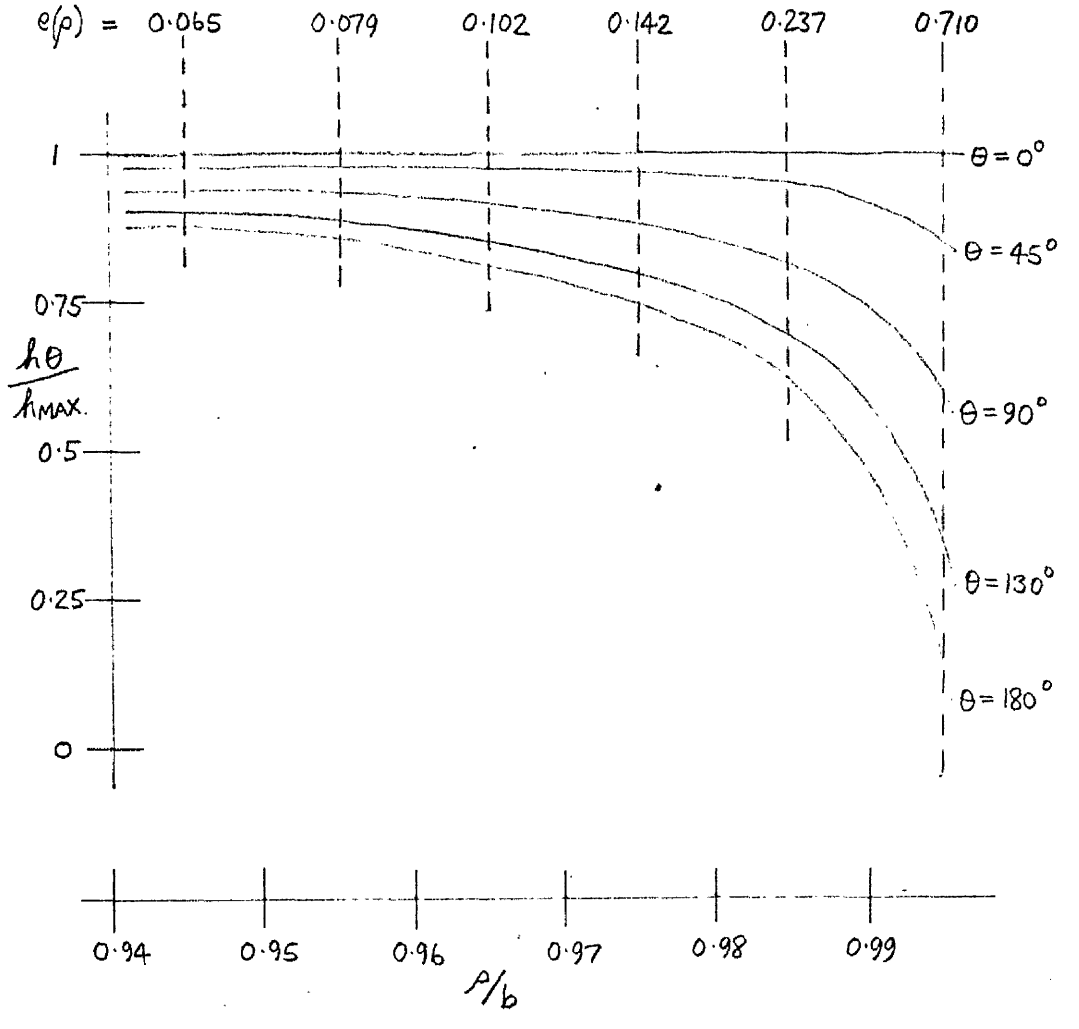

FIG. 129. SPECIMEN 3A-1 $\sigma_L(\theta)$ v ρ
AT $\theta = 0°, 45°$

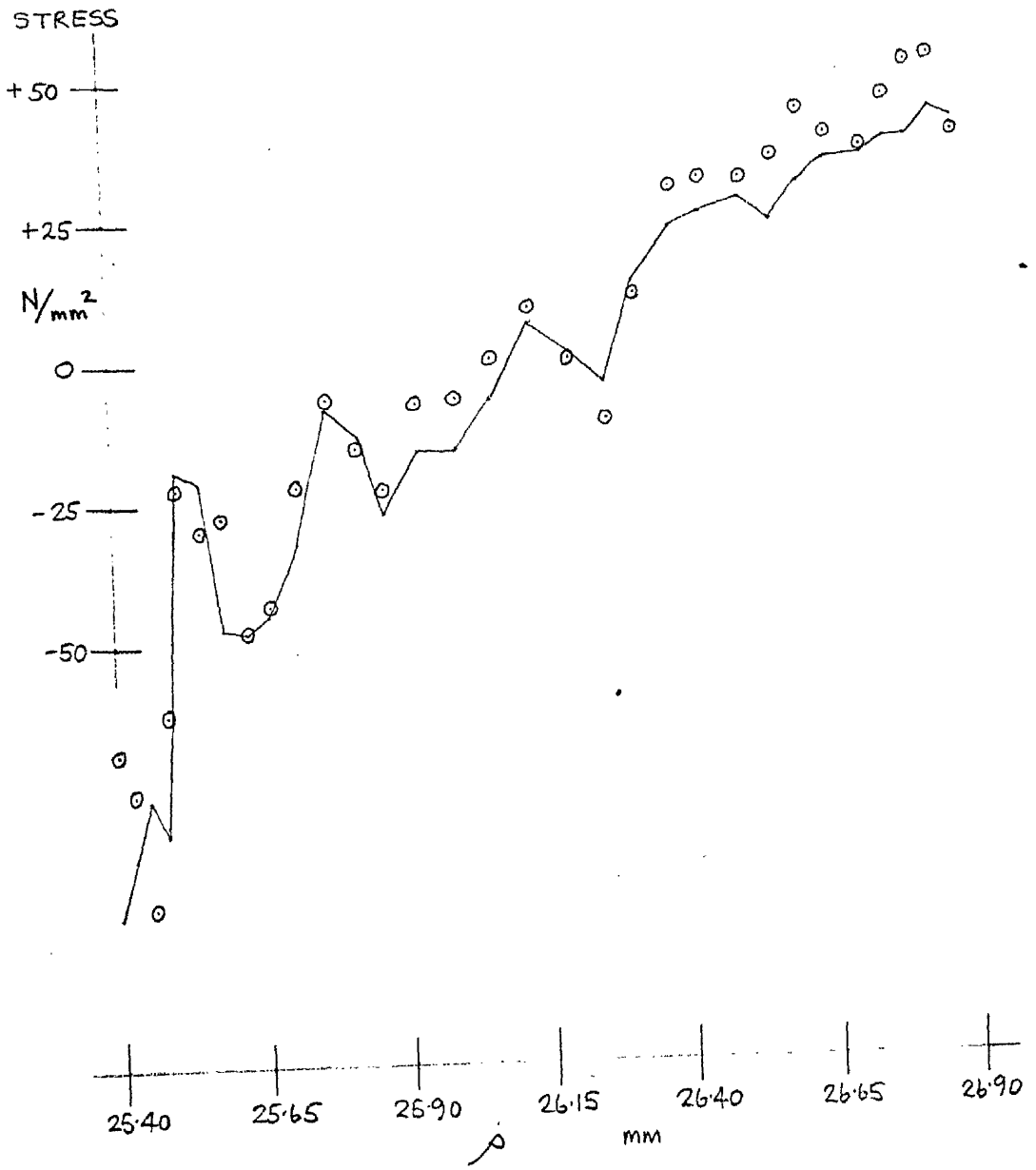

FIG. 130. SPECIMEN 3A-1 $\sigma_L(\theta)$ V ρ
AT $\theta = 0°, 90°$

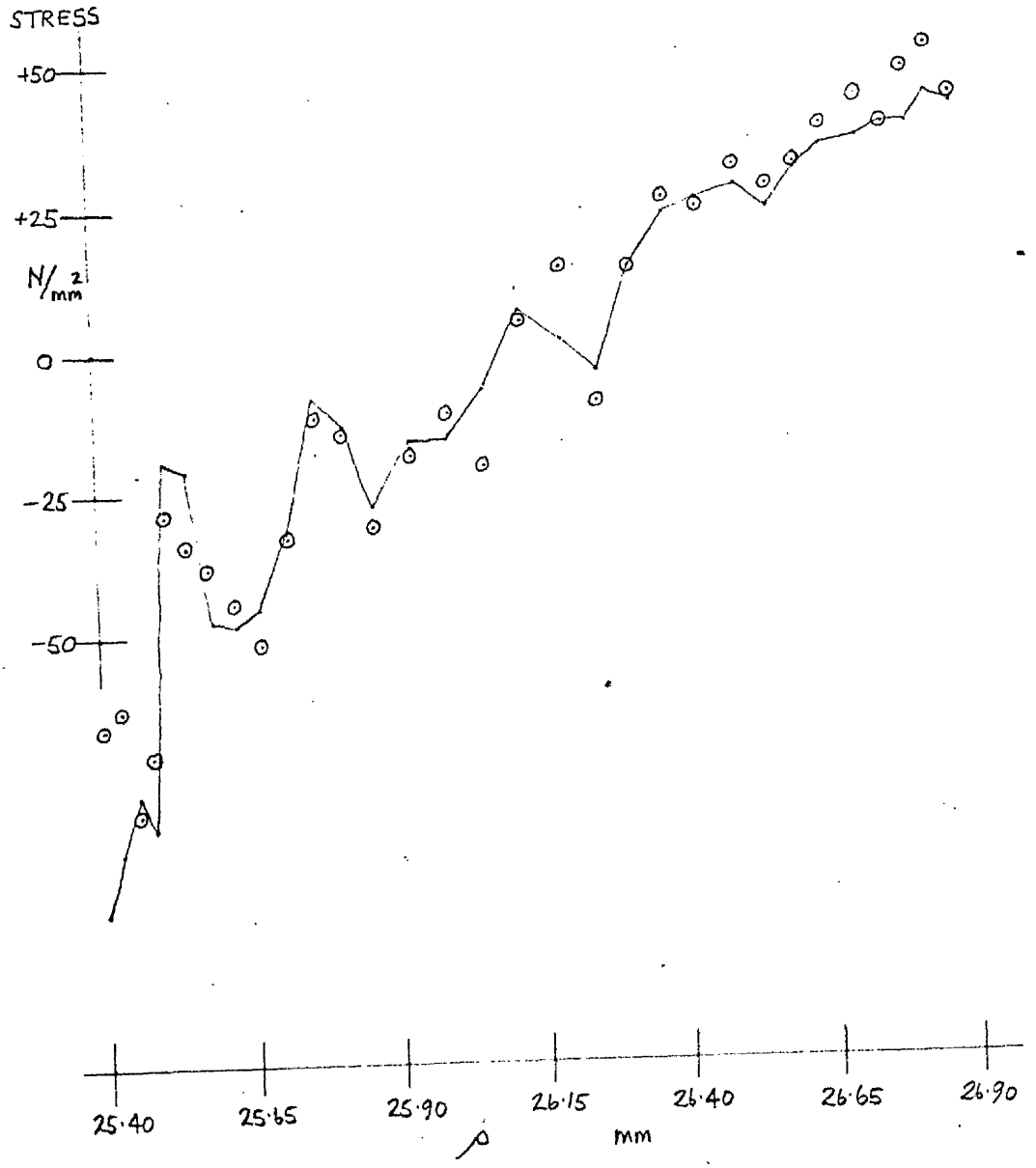

FIG. 131. SPECIMEN 3A-1 $\sigma_L(\theta)$ v ρ AT $\theta = 0°, 130°$

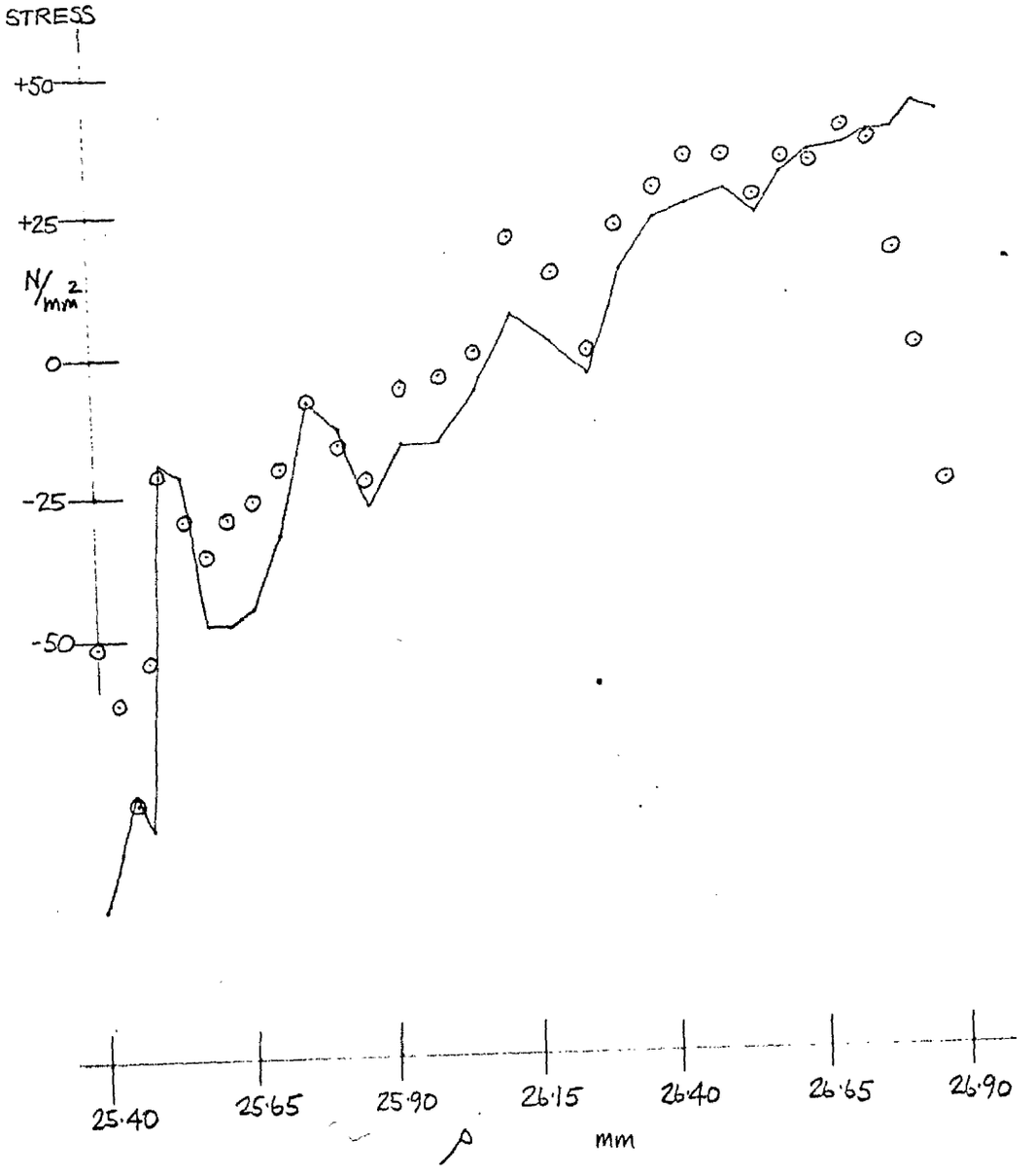

FIG. 132. SPECIMEN 3A-1 $\sigma_L(\theta)$ V ρ
AT θ = 0°, 180°

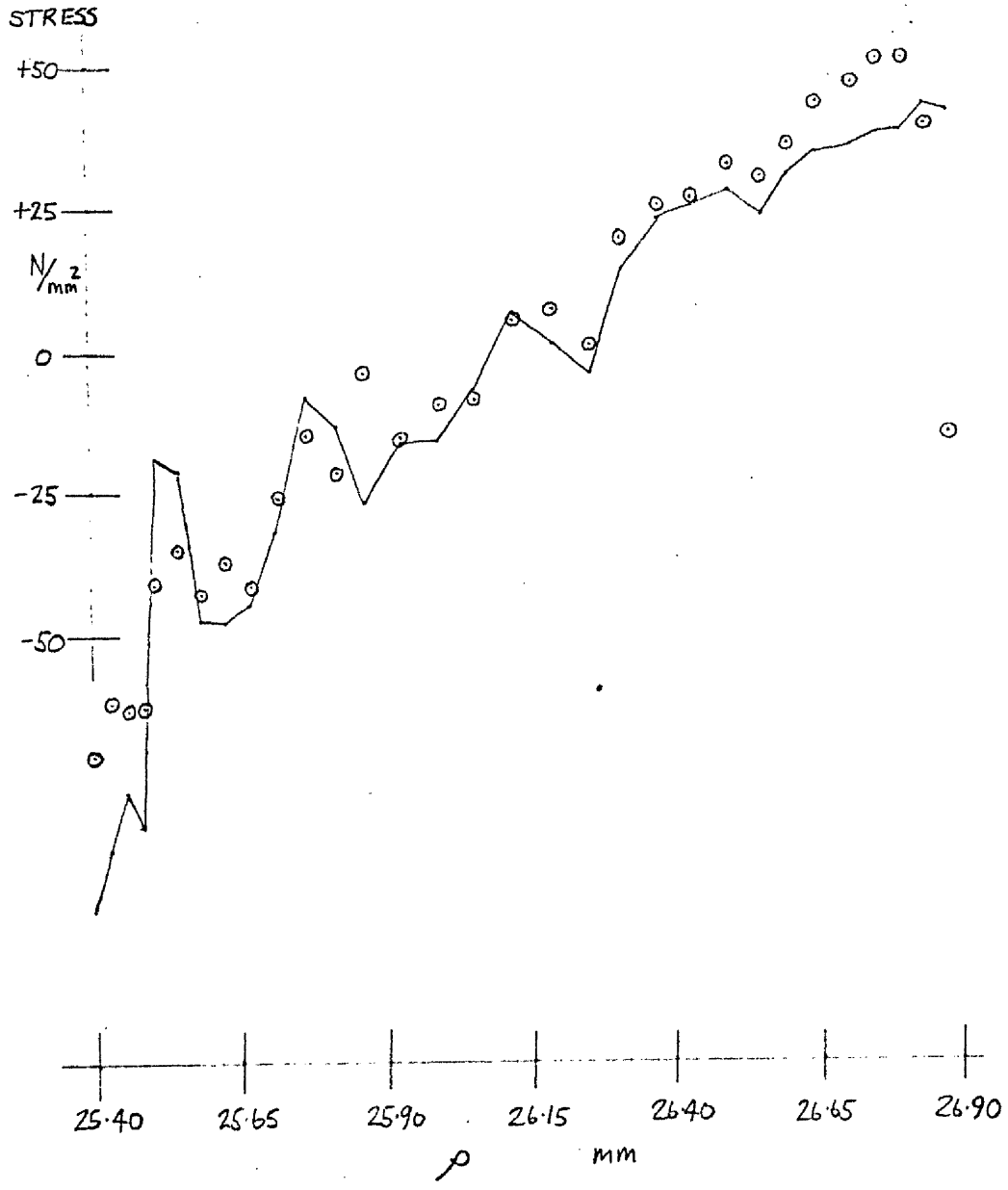

FIG. 133. SPECIMEN 3A-1

ℓ_{0_m} , $\ell_0(\pi/2)_{bp}$ V ρ

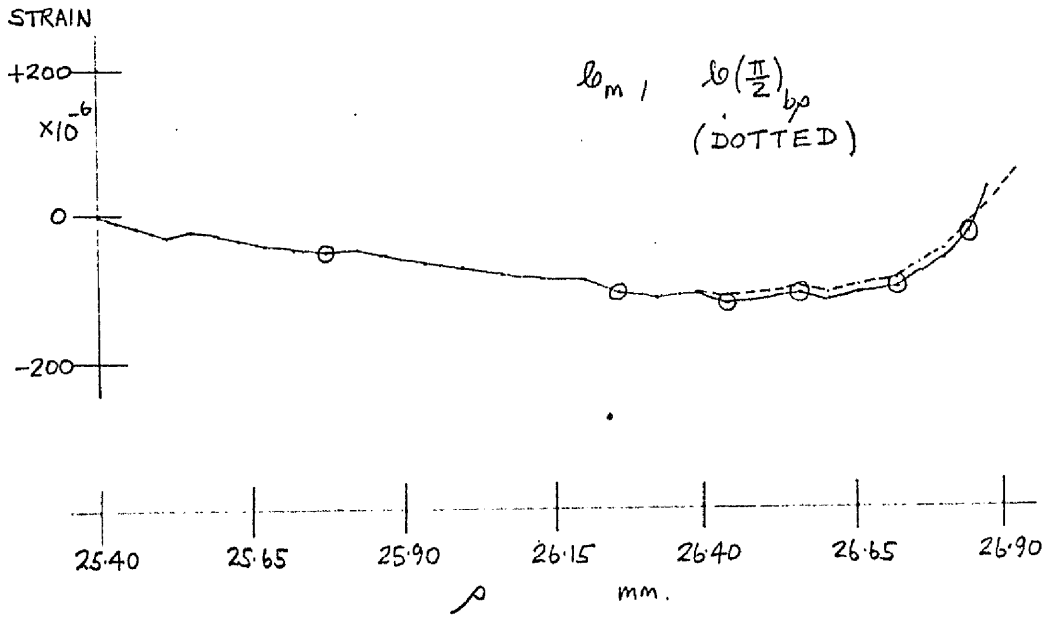

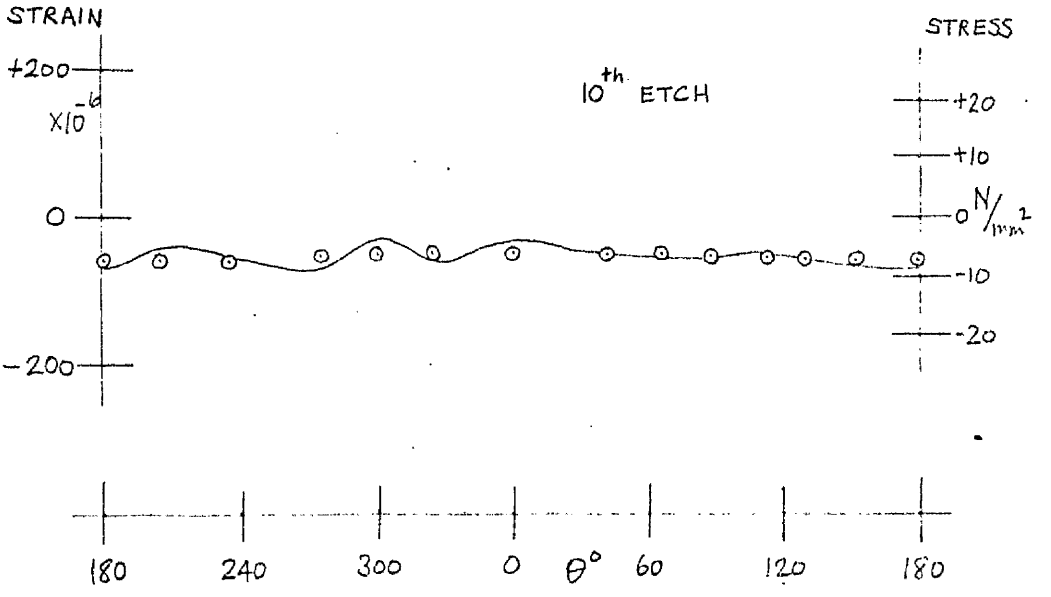

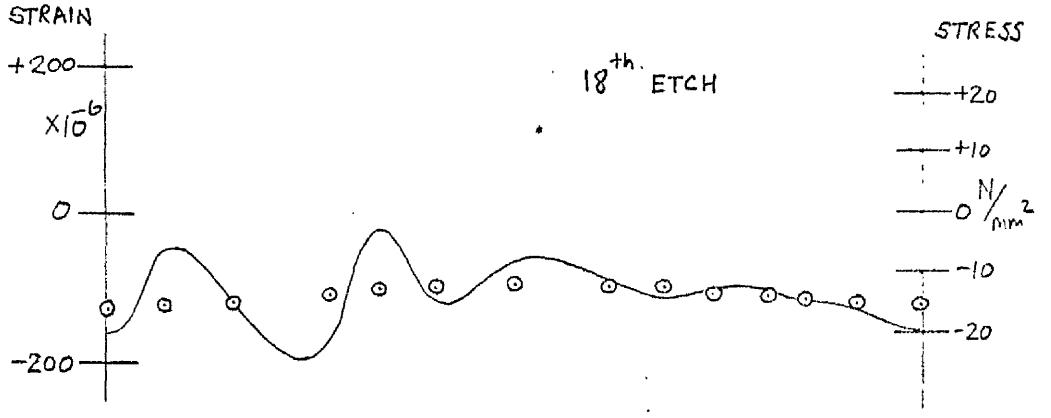

FIG. 134. SPECIMEN 3A-1

$\ell_b(\theta)_{bp}$, $\ell_m \cdot \frac{F_b(P_b, \theta)}{F_m}$ v θ

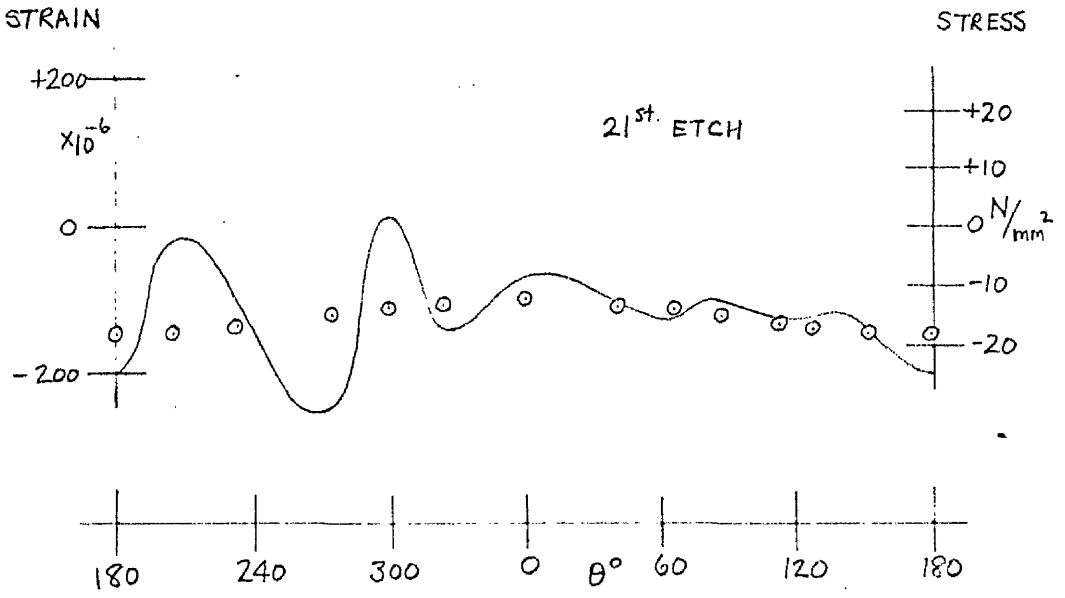

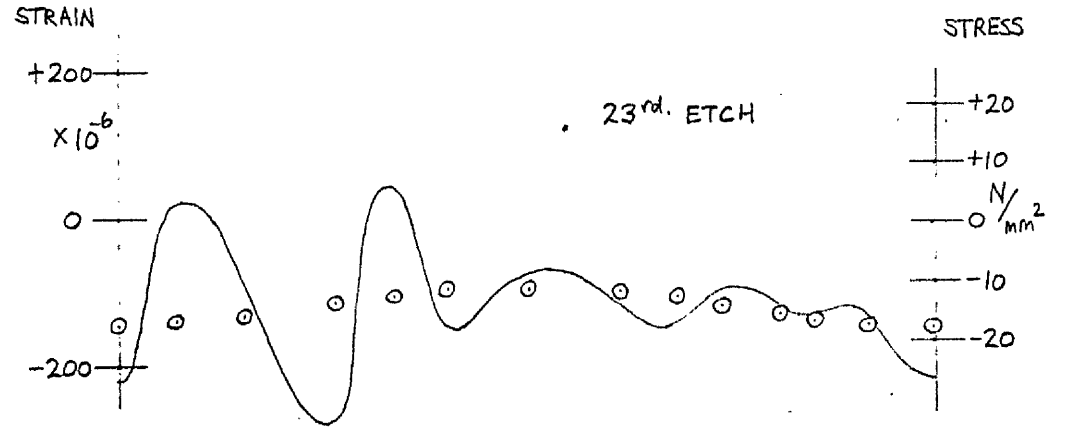

FIG. 135. SPECIMEN 3A-1

$\ell_b(\theta)_{b_0}$, $\ell_m \cdot \frac{F_b(\rho_b, \theta)}{F_m}$ $V\theta$

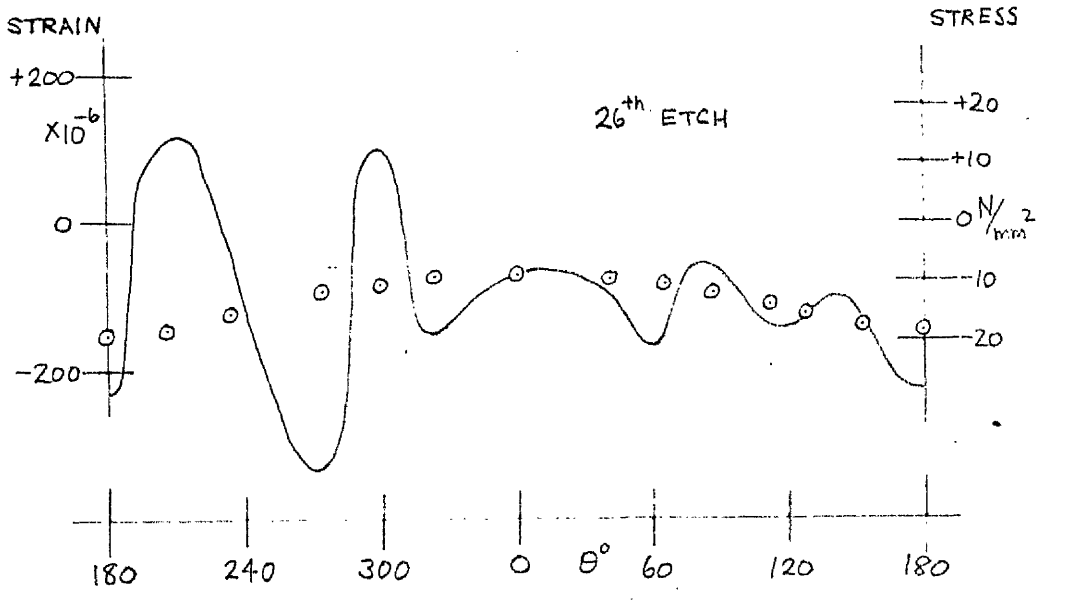

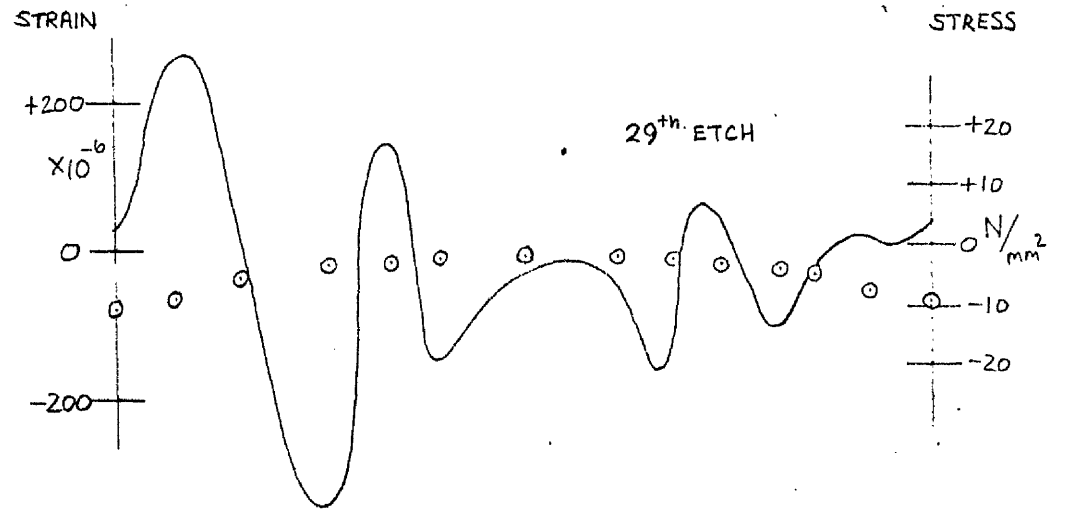

FIG. 136. SPECIMEN 3A-1

$l_o(\theta)_{bp}$, $l_{om} \cdot \frac{F_b(P/b, \theta)}{F_m}$ v θ

FIG. 137. SPECIMEN 3A-1 T V ρ/b, BASED ON MEAN WALL THICKNESS.

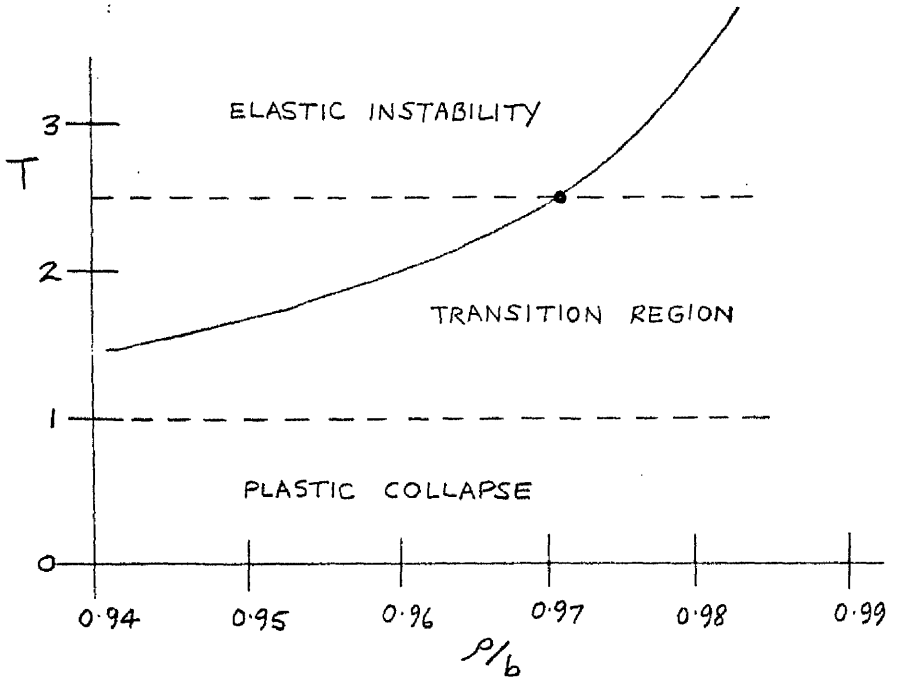

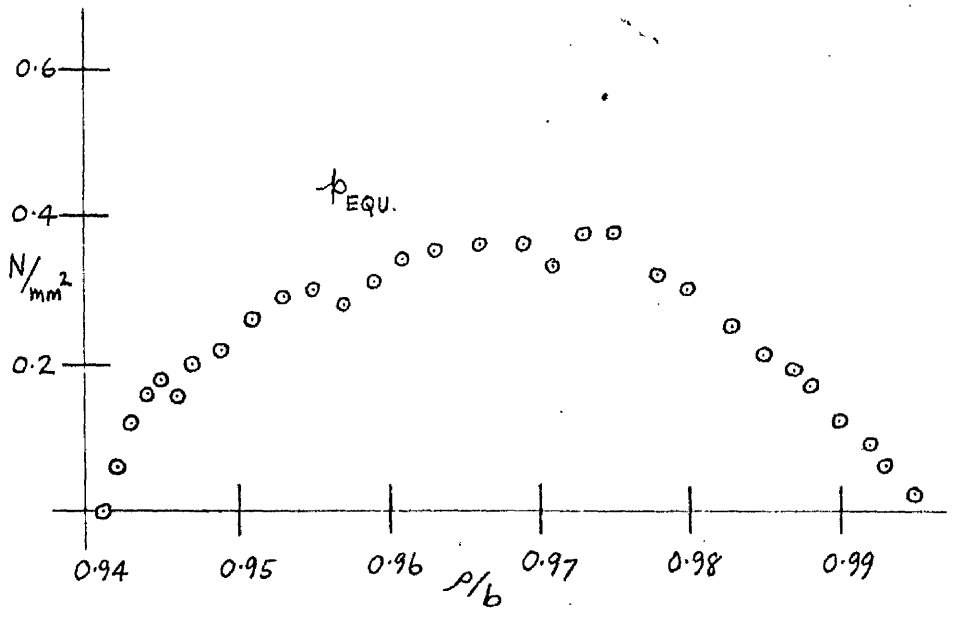

FIG. 138. SPECIMEN 3A-1 $p_{EQU.}$ V ρ/b

FIG. 139. COMPARISON OF $p_{CRIT.}$ FOR 3,4,5 LOBES (BASED ON MEAN WALL THICKNESS) AND $p_{EQU.}$ SPECIMEN 3A-1

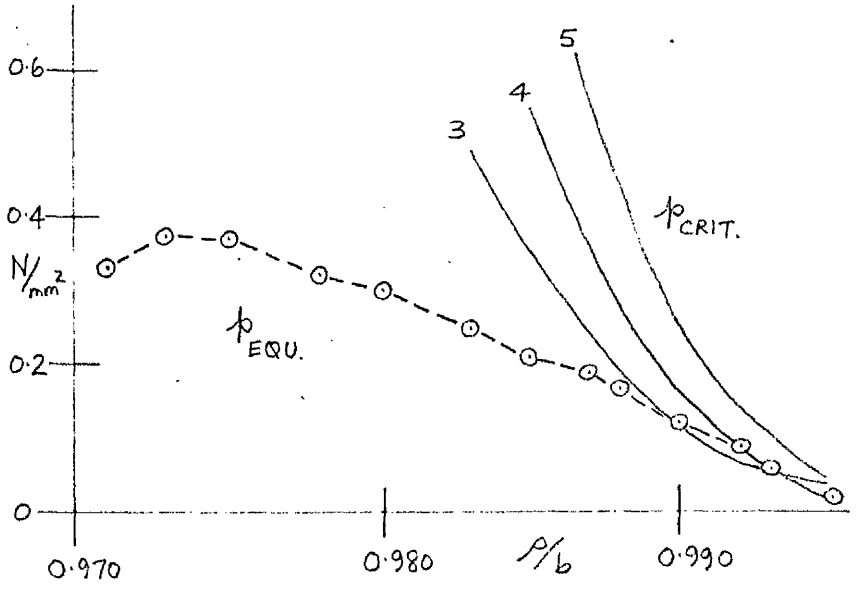

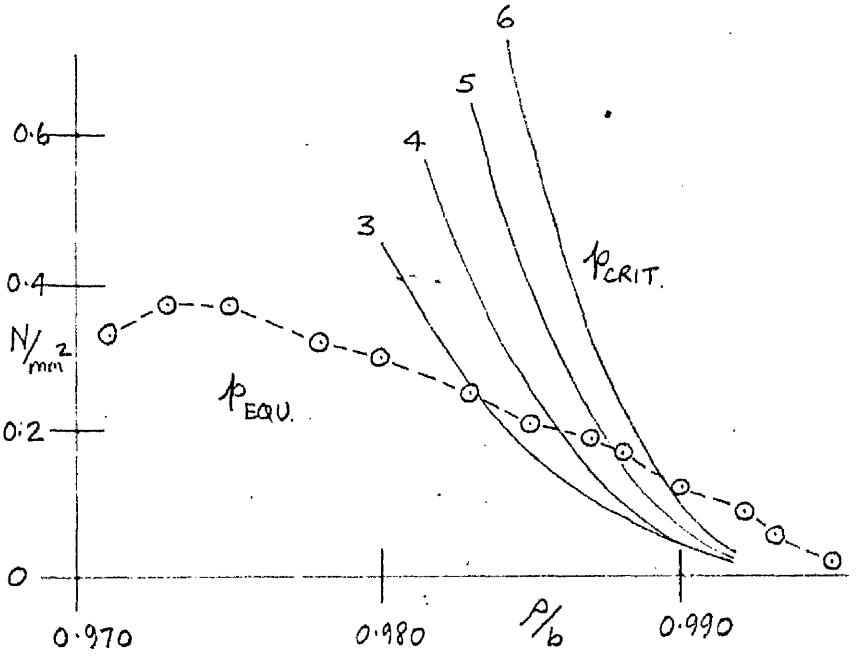

FIG. 140. COMPARISON OF $p_{CRIT.}$ FOR 3,4,5,6 LOBES (BASED ON MINIMUM WALL THICKNESS) AND $p_{EQU.}$ SPECIMEN 3A-1

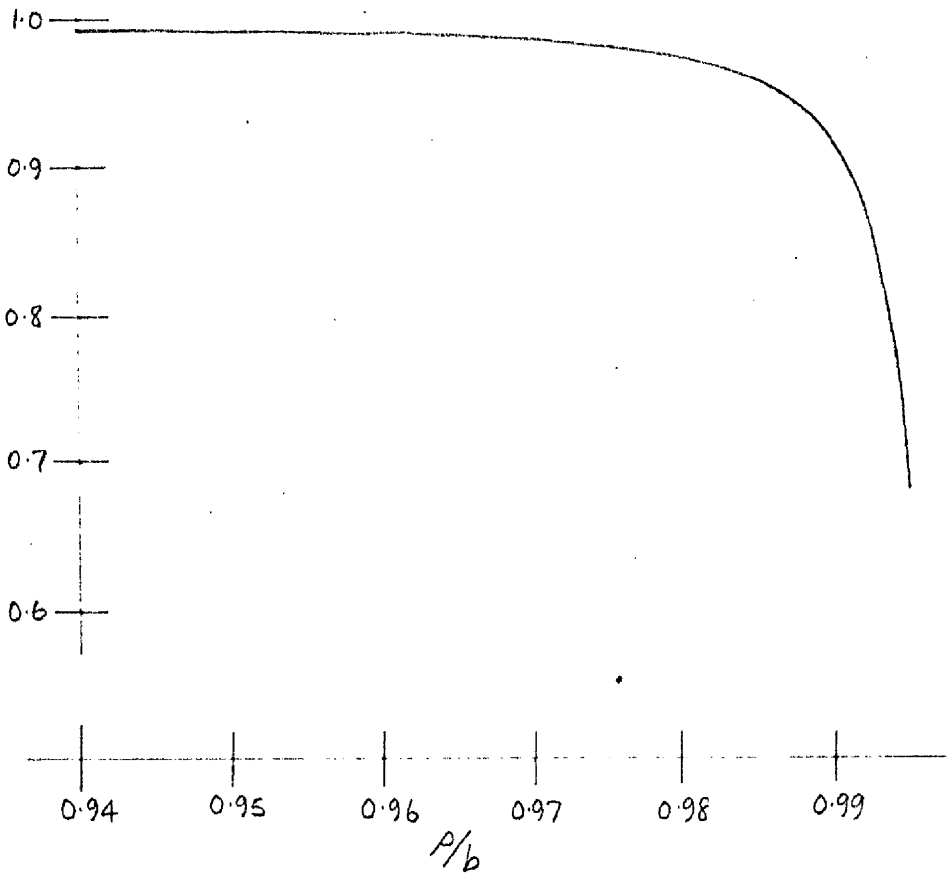

FIG. 141. $\frac{F_b(\rho/b, \pi/2)}{F_m}$ v ρ/b

SPECIMEN 3A-1

FIG. 142. SPECIMEN 3A-1 σ_c V/ρ

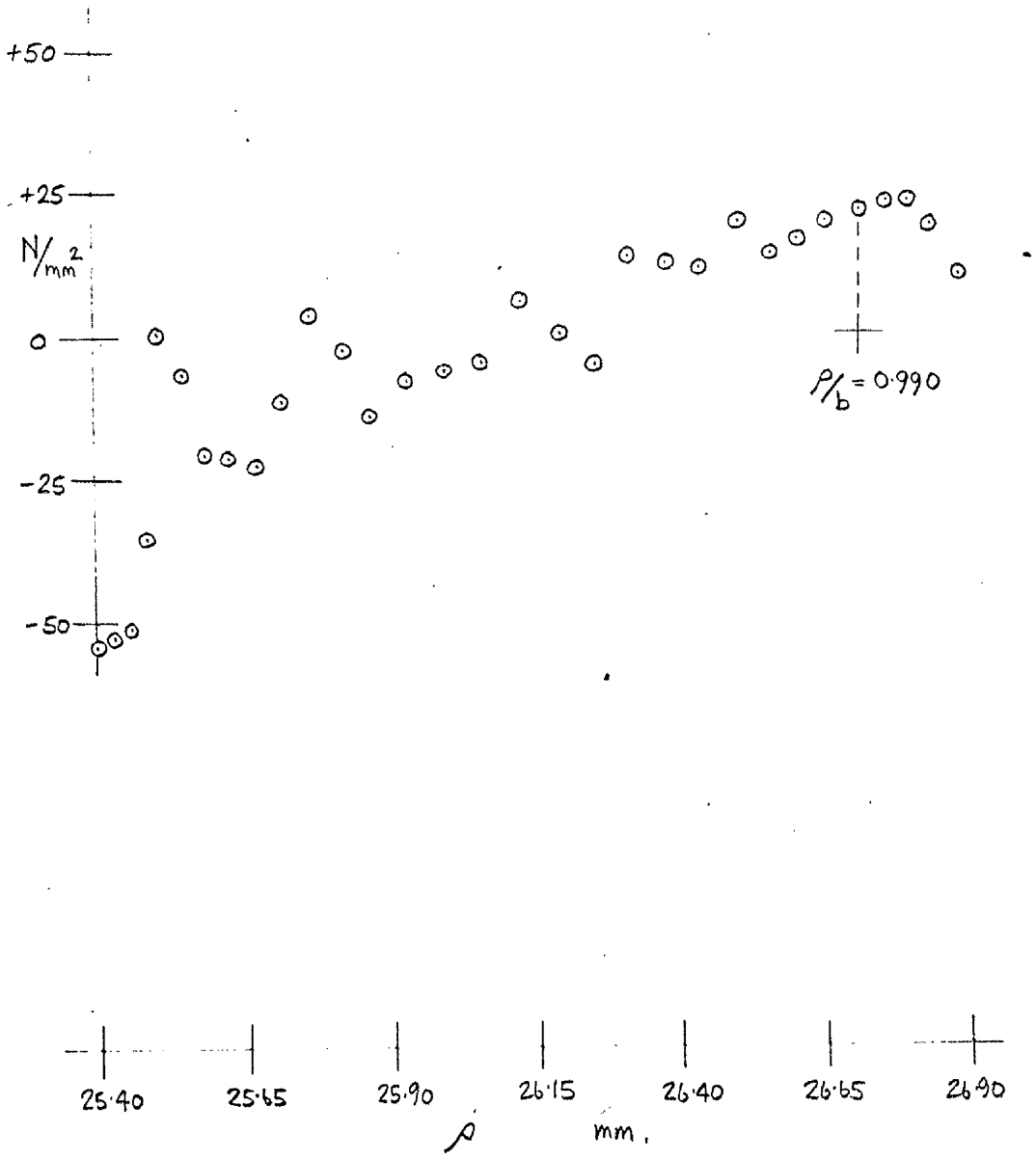

FIG. 143. SPECIMEN 3A-1 σ_R V ρ

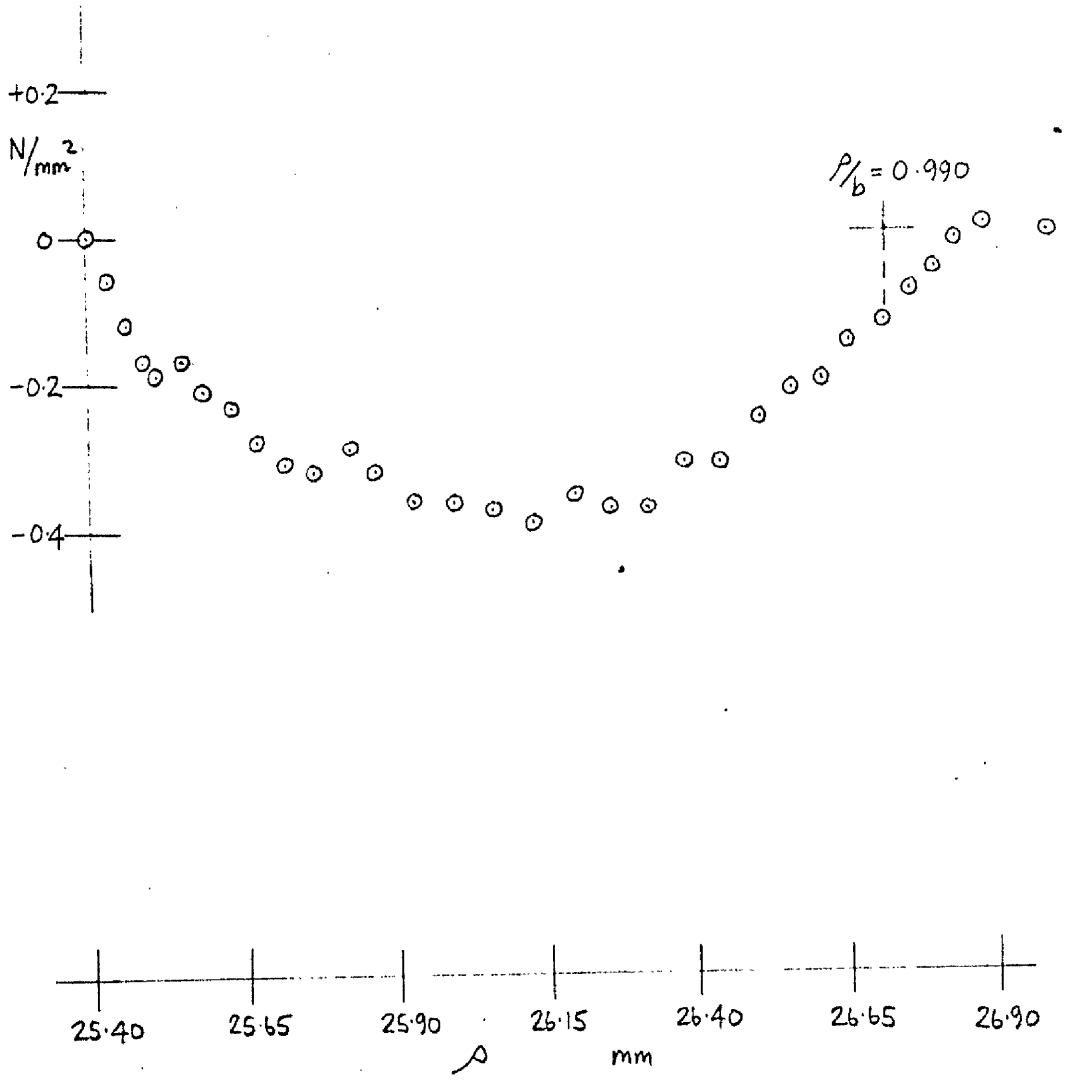

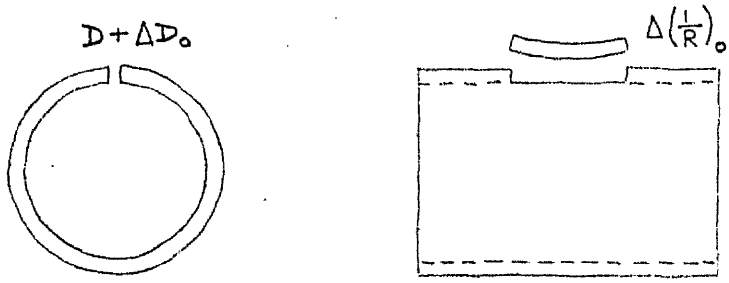

FIG. 144.

(a)

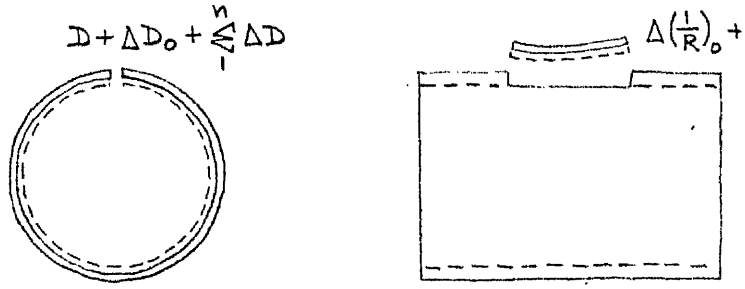

(b)

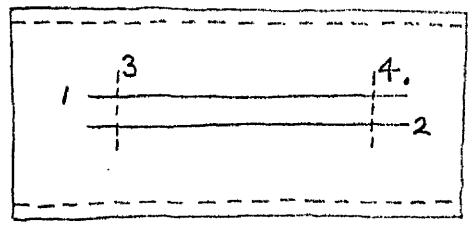

FIG. 145.

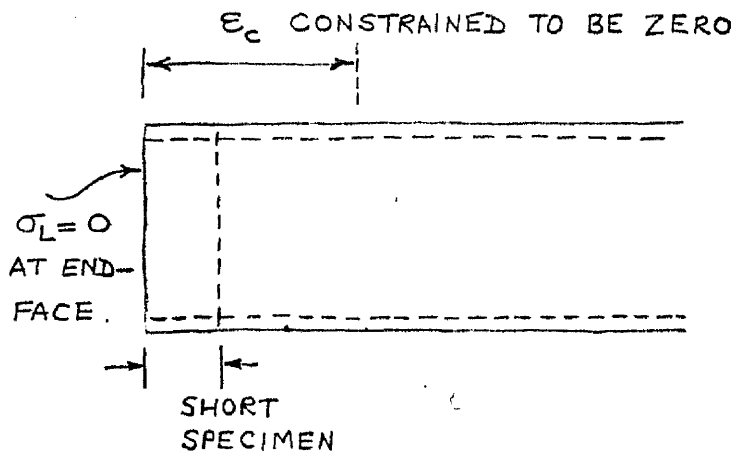

FIG. 146.

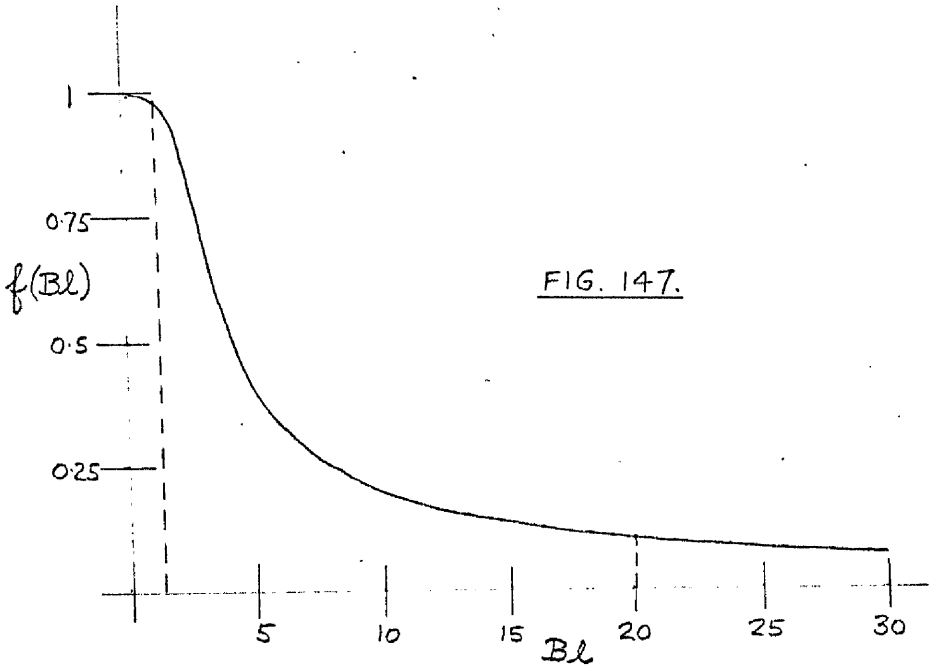

FIG. 147.

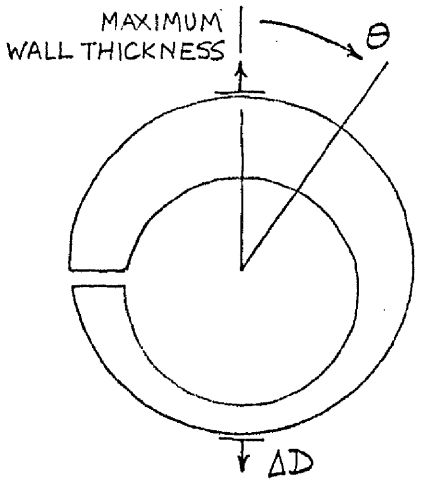

FIG. 148.

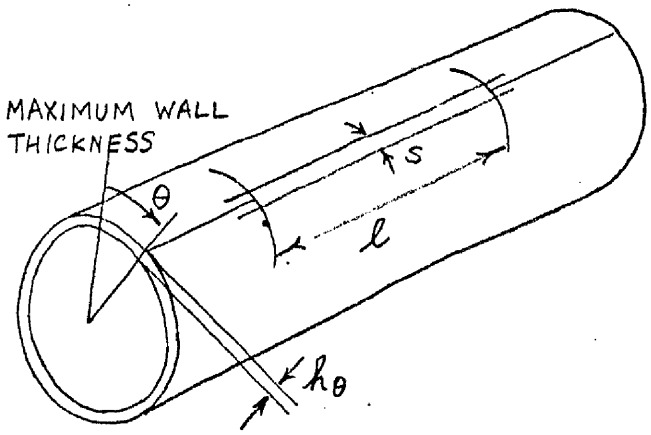

FIG. 149.

FIG. 150.

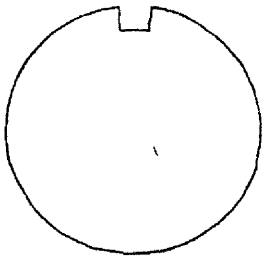

(a)

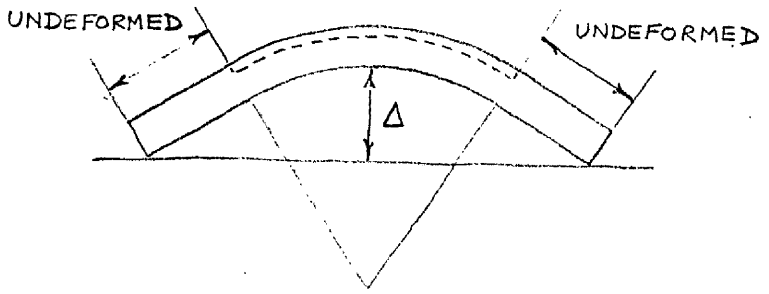
UNDEFORMED
UNDEFORMED
Δ

(b)

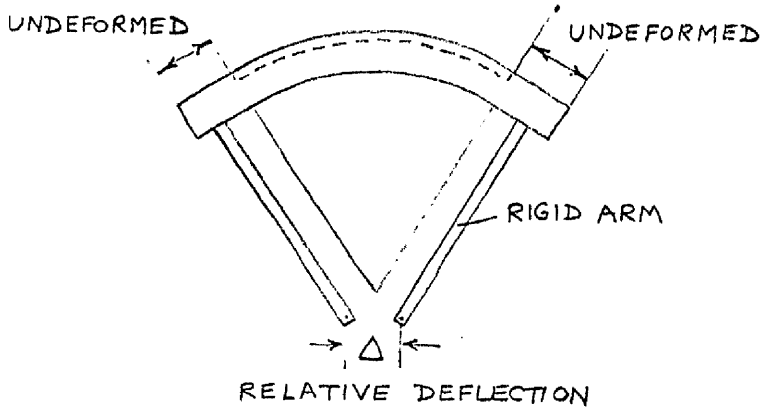
UNDEFORMED
UNDEFORMED
RIGID ARM
Δ
RELATIVE DEFLECTION

(c)

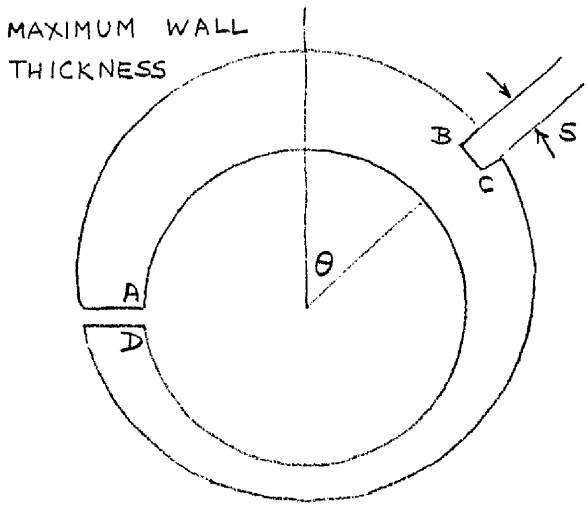

FIG. 151.

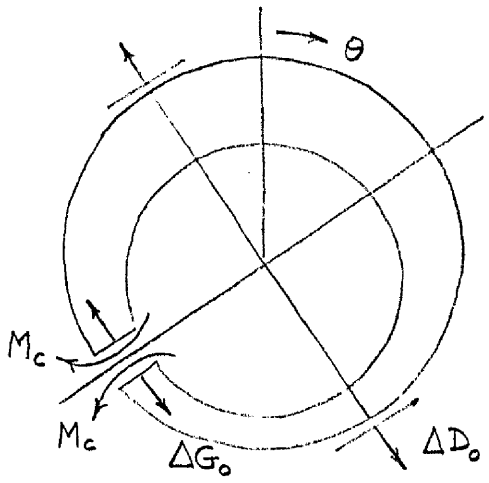

FIG. 152.

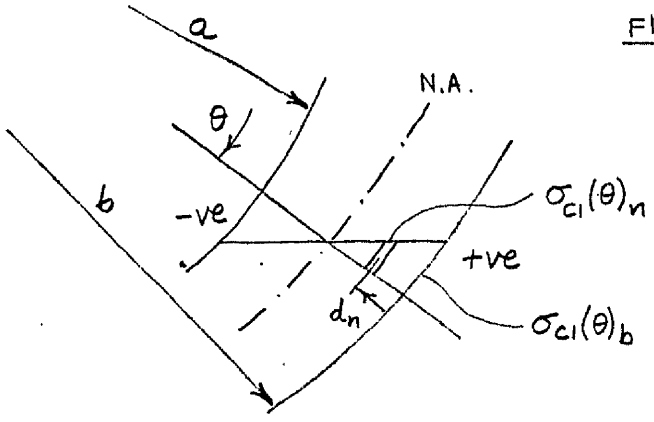

FIG. 153.

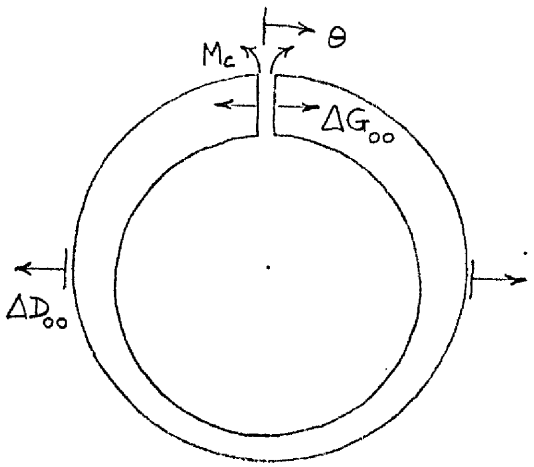
θ
M_c
ΔG_{oo}
ΔD_{oo}

FIG. 154.

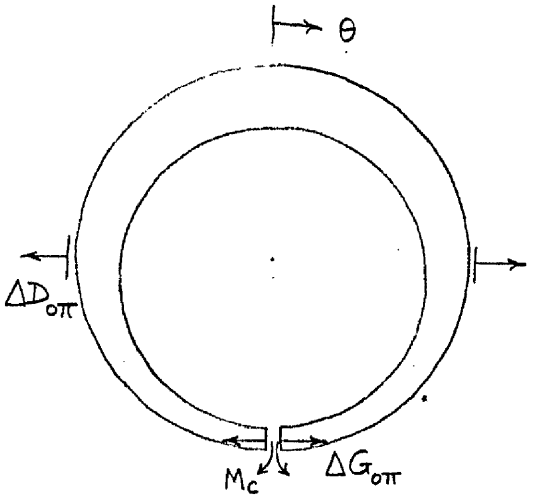
θ
$\Delta D_{o\pi}$
M_c
$\Delta G_{o\pi}$

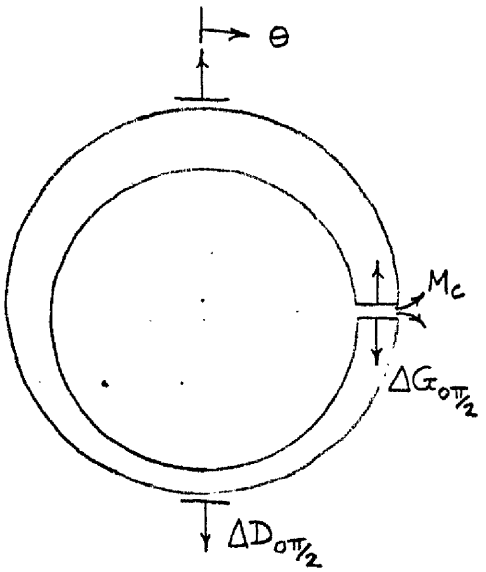
θ
M_c
$\Delta G_{o\pi/2}$
$\Delta D_{o\pi/2}$

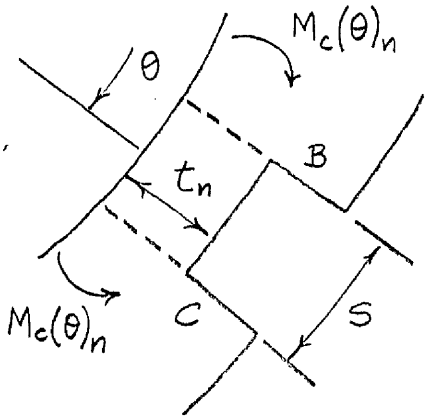

FIG. 155.

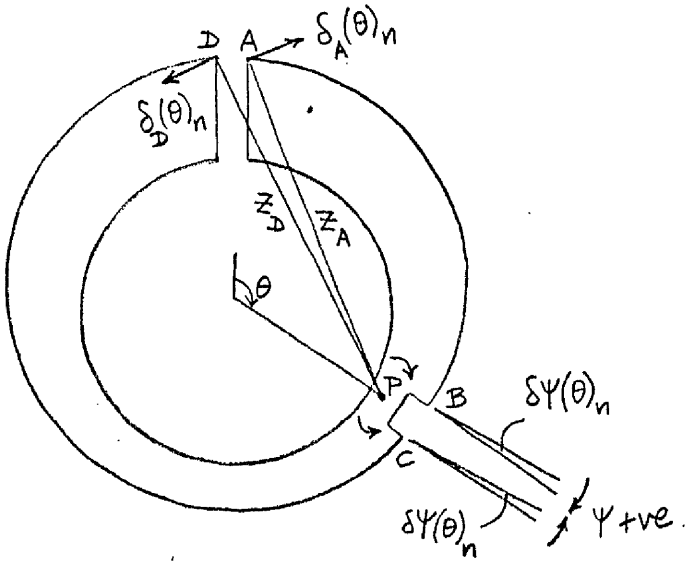

FIG. 156.

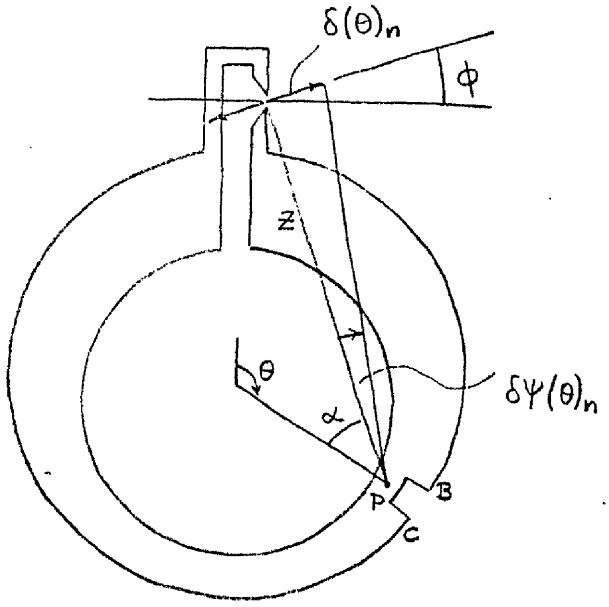

FIG. 157.

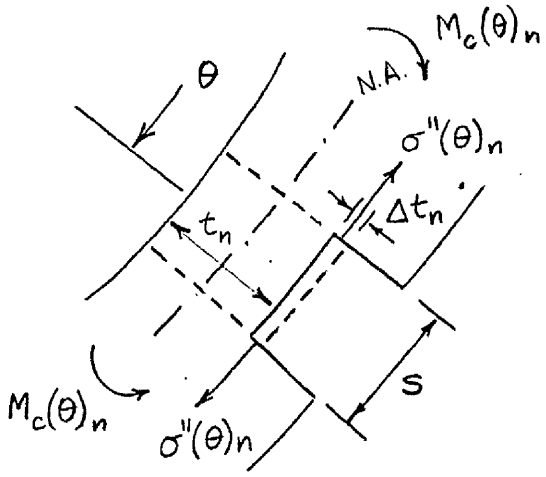

FIG. 158.

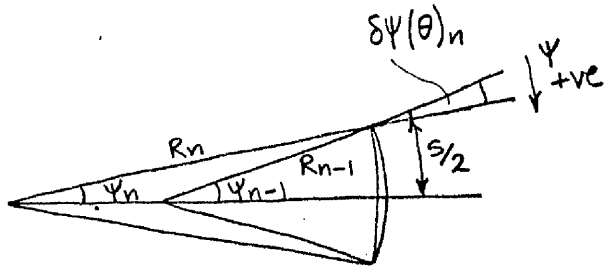

FIG. 159.

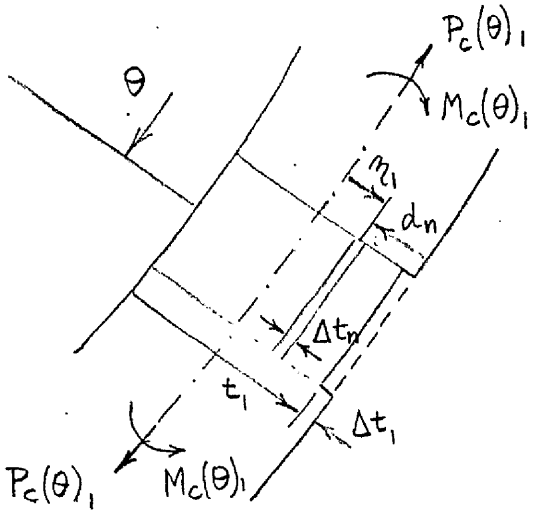

FIG. 160.

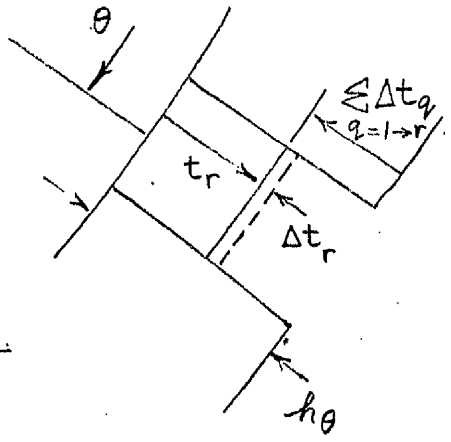

FIG. 161.

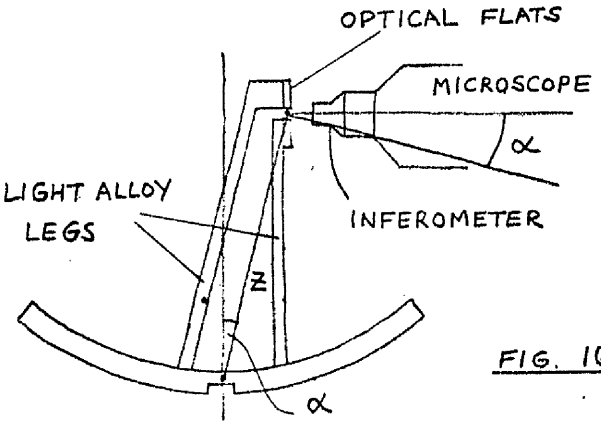

FIG. 162.

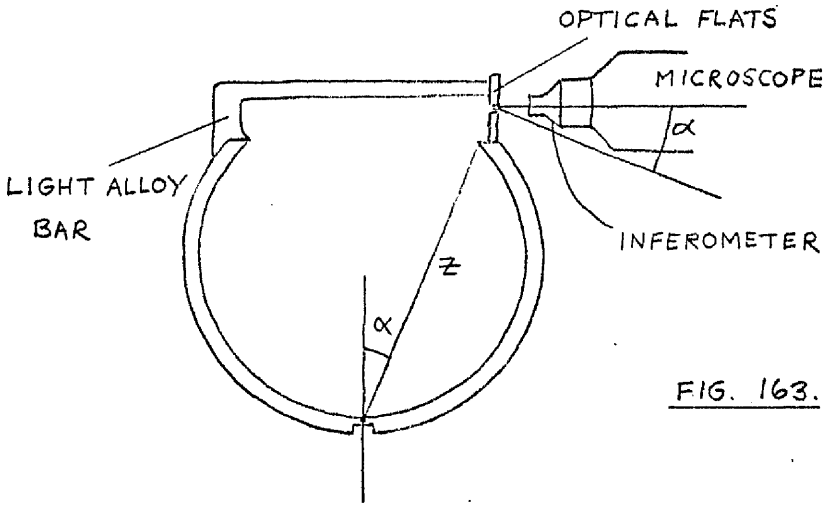

FIG. 163.

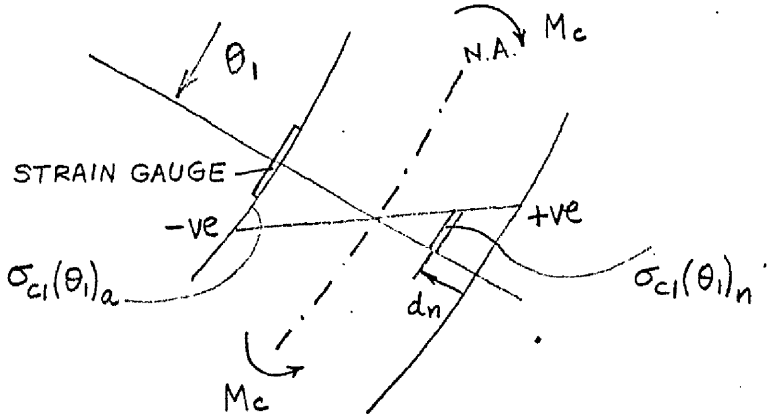

FIG. 164.

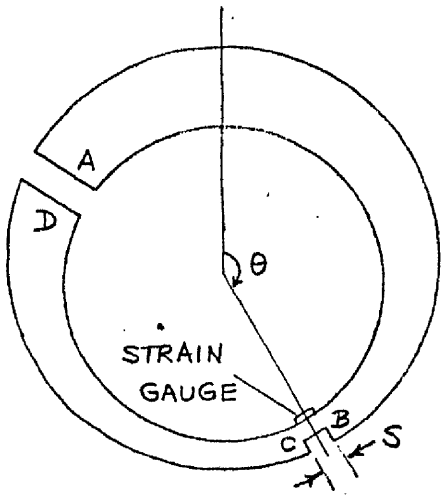

FIG. 165.

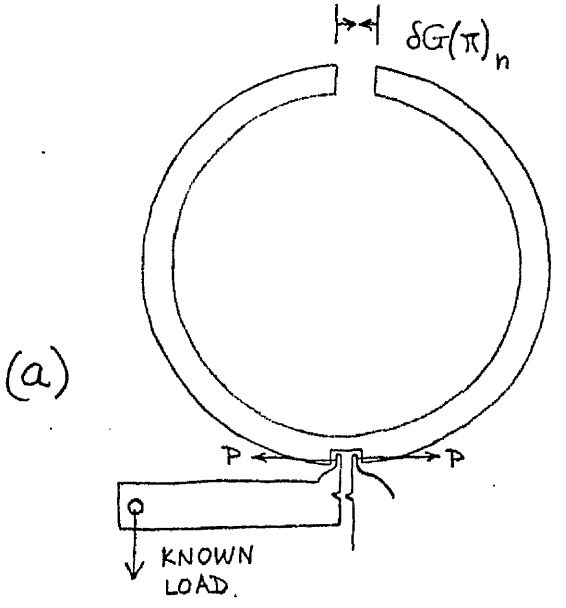

FIG. 166.

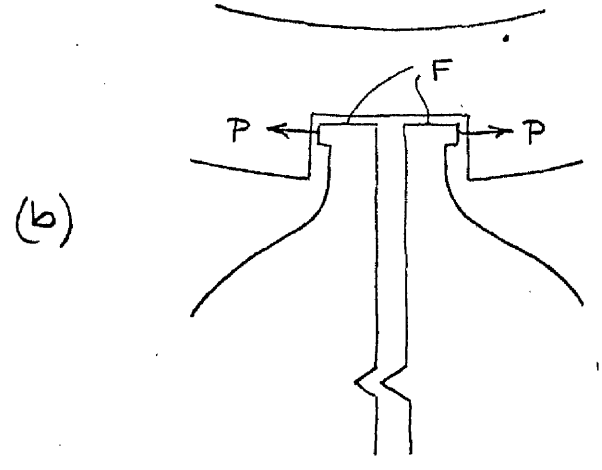

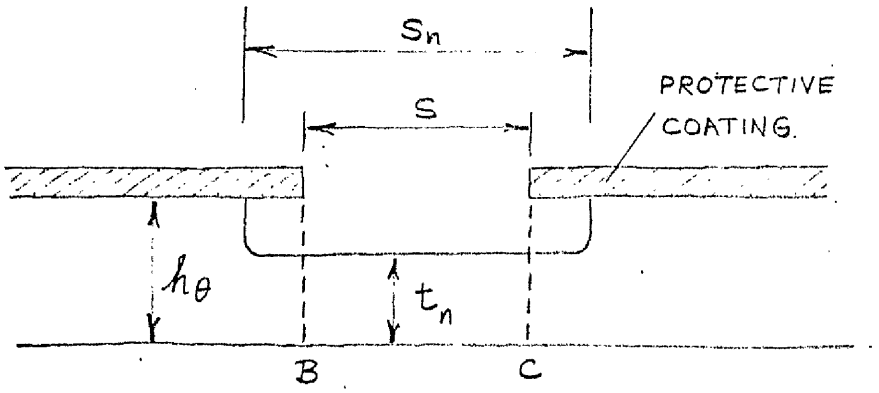

FIG. 167.

FIG. 168.

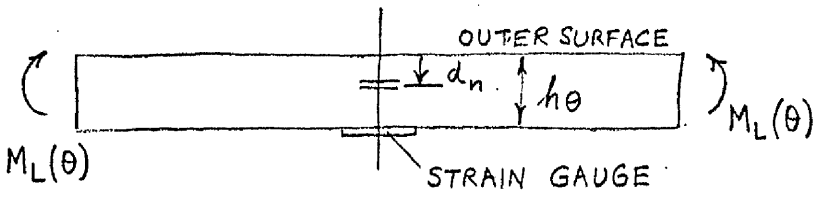

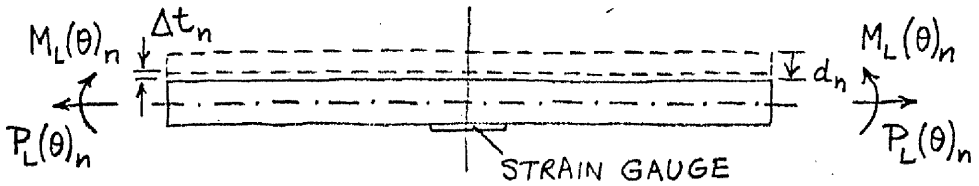

FIG. 169.

APPENDIX 2.

TABLES.

TABLE 1. : $F_b(\rho/b, \theta)$.

ρ/b =	0.940	0.945	0.950	0.955	0.960	0.965	0.970	0.974
θ°								
0	14.25	15.60	17.18	19.10	21.47	24.44	28.30	32.32
41.5	14.47	15.85	17.50	19.48	21.95	25.05	29.11	33.37
66	14.78	16.23	17.94	20.03	22.61	25.93	30.30	34.85
88.5	15.15	16.65	18.46	20.67	23.41	26.98	31.71	36.78
113	15.58	17.16	19.07	21.43	24.39	28.23	33.42	39.08
128.5	15.79	17.44	19.43	21.88	24.97	28.97	34.49	40.54
153	16.10	17.79	19.85	22.41	25.65	29.92	35.77	42.28
183	16.22	17.95	20.03	22.63	25.93	30.29	36.29	43.03
204	16.21	17.82	19.89	22.46	25.71	30.01	35.85	42.42
235	15.76	17.30	19.35	21.78	24.83	28.84	34.26	40.19
276	15.07	16.57	18.35	20.54	23.27	26.76	31.39	36.39
300	14.70	16.12	17.82	19.88	22.44	25.68	29.95	34.27
324	14.42	15.79	17.42	19.39	21.83	24.88	28.91	33.12
180	16.22	17.95	20.03	22.63	25.93	30.30	36.29	43.03
90, 270	15.19	16.69	18.53	20.72	23.50	27.08	31.84	36.93
F_m	15.27	16.79	18.64	20.90	23.73	27.38	32.29	37.60

TABLE 1. (continued)

ρ/b =	0.978	0.982	0.986	0.990	0.992	0.993	0.994	0.995
θ°								
0	37.61	44.87	55.43	72.18	84.25	93.00	102.8	114.5
41.5	39.03	46.86	58.42	77.34	92.08	101.7	113.3	128.1
66	41.11	49.85	63.14	85.67	104.0	116.4	132.5	152.3
88.5	43.71	53.69	69.33	97.27	121.6	138.8	161.6	193.2
113	46.93	58.65	77.73	114.4	149.1	175.9	214.0	272.6
128.5	48.96	61.72	83.20	126.1	170.3	202.2	260.5	353.8
153	51.62	65.91	90.59	144.8	204.9	259.1	350.5	549.6
183	52.67	67.67	94.12	153.4	223.0	287.8	405.9	685.7
204	51.83	66.24	91.43	146.5	208.4	264.6	361.3	565.8
235	48.53	61.06	81.96	123.6	165.5	198.6	249.5	333.0
276	43.15	52.85	67.95	94.64	117.4	133.6	154.6	183.1
300	40.52	49.00	61.90	83.20	100.5	111.9	126.3	145.0
324	38.68	46.37	57.69	76.03	90.28	97.54	110.7	124.6
180	52.69	67.69	94.14	153.5	223.1	288.2	406.4	687.7
90,270	43.90	54.08	69.95	98.60	123.8	140.8	164.7	192.0
F_m	44.95	55.75	73.29	107.3	141.0	168.4	211.0	291.7

TABLE 2. : $F_b(\rho_b, \theta)/F_m$.

(ETCH. NO.)	(10)	(18)	(2)	(23)	(26)	(29)
ρ/b =	0.940	0.955	0.973	0.980	0.985	0.990	0.995
θ°							
0	0.934	0.914	0.865	0.822	0.771	0.672	0.393
4.5	0.948	0.933	0.892	0.856	0.810	0.720	0.439
66	0.968	0.959	0.931	0.905	0.872	0 798	0.522
88.5	0.993	0.990	0.979	0.969	0.952	0.905	0.663
113	1.020	1.026	1.038	1.048	1.058	1.066	0.935
128.5	1.034	1.047	1.075	1.097	1.126	1.179	1.212
153	1.055	1.073	1.119	1.162	1.220	1.350	1.852
183	1.063	1.083	1.138	1.191	1.263	1.430	2.348
204	1.061	1.076	1.124	1.167	1.231	1.366	1.940
235	1.033	1.042	1.068	1.086	1.112	1.152	1.131
276	0.987	0.983	0.969	0.954	0.935	0.881	0.628
300	0.963	0.952	0.921	0.891	0.854	0.775	0.497
324	0.945	0.928	0.885	0.848	0.801	0.768	0.427
180	1.063	1.083	1.138	1.191	1.264	1.432	2.358
90, 270	0.995	0.992	0.984	0.974	0.960	0.918	0.679

TABLE 3. : Angular position of the strain gauges on specimen 3A-1 , (θ measured from maximum wall thickness in a clockwise direction, looking on end-1).

LONGIT. GAUGES	θ°	CIRCUMF. GAUGES	θ°
L_1	0	C_1	0
L_2	27	C_2	41·5
L_3	54	C_3	66
L_4	88·5	C_4	88·5
L_5	117	C_5	113
L_6	142	C_6	128·5
L_7	183	C_7	153
L_8	203	C_8	183
L_9	221	C_9	204
L_{10}	247·5	C_{10}	235
L_{11}	276	C_{11}	276
L_{12}	312	C_{12}	300
L_{13}	337	C_{13}	324

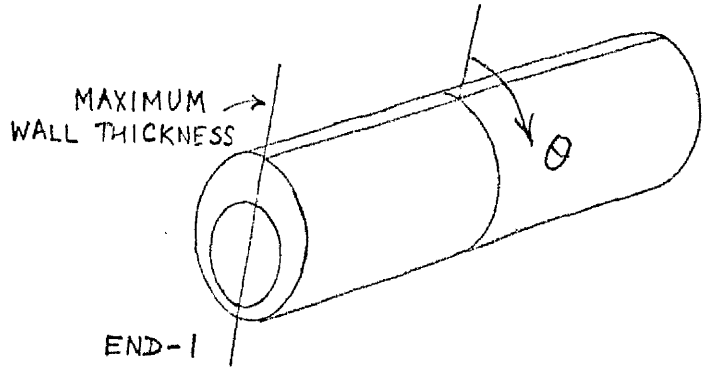

TABLE 4. : Surface strains and stresses on cutting-out specimens 1A-1 and 1A-2 , (gauges rezeroed between cuts).

(a) STRAINS $\times 10^{-6}$

GAUGE :	L_1	C_1	L_2	C_2	L_3	C_3	L_4	C_4	L_5	C_5
AFTER FIRST CUT	-7	0	0	0	-5	-6	+5	0	+1	+1
AFTER SECOND CUT	0	0	0	0	0	0	0	0	+12	+7
AFTER THIRD CUT	+5	+8	-6	-11	+6	+5	-1	-5	+5	+1
TOTALS	-2	+8	-6	-11	+1	-1	+4	-5	+18	+9

(b) TOTAL SURFACE STRESSES N/mm^2.

GAUGE NO.	1	2	3	4	5
LONGITUDINAL	0	-1·1	+0·1	+0·4	+2·5
CIRCUMFERENTIAL	+0·9	-1·6	-0·1	-0·5	+1·7

TABLE 5. : Surface stresses produced at maximum wall thickness, on cutting-out.

SPECIMEN	LENGTH	$E'\mathcal{L}_b$	$E'\mathcal{C}_b$ N/mm^2
2A-1	$2D_m$	-19.4	-3·7
1A-2	$4D_m$	0	+0·9
3A-1	$4D_m$	-9·6	-6·5
1A-1	$5D_m$	+2·5	+1·7

TABLE 6. : 'Type A' residual stress investigation, specimen 3A-1 ; internal radius ρ , at each stage of the etching process.

ETCH.	DURATION min.	TOTAL WEIGHT LOSS W (N)	ρ mm.	$\Delta\rho$ mm.
0	0	0	25.40	0
1	5	0.073	25.43	0.03
2	5	0.161	25.46	0.03
3	5	0.239	25.48	0.02
4	6	0.331	25.51	0.03
5	7	0.448	25.55	0.04
6	7	0.556	25.59	0.04
7	8	0.667	25.63	0.04
8	9	0.790	25.67	0.04
9	10	0.936	25.72	0.05
10	11	1.090	25.77	0.05
11	11	1.250	25.82	0.05
12	13	1.409	25.87	0.05
13	13	1.574	25.93	0.06
14	14	1.776	26.00	0.07
15	14	1.965	26.06	0.06
16	14	2.162	26.13	0.07
17	14	2.372	26.20	0.07
18	15	2.568	26.26	0.06
19	14	2.745	26.32	0.06
20	13	2.958	26.39	0.07
21	13	3.120	26.44	0.05
22	13	3.322	26.51	0.07
23	11	3.472	26.56	0.05
24	11	3.630	26.61	0.05
25	11	3.784	26.66	0.05
26	17	3.964	26.72	0.06
27	11	4.085	26.76	0.04
28	12	4.200	26.80	0.04
29	11	4.336	26.84	0.04
30	11	4.466	26.88	0.04

TABLE 7. : 'Type A' residual stress investigation, specimen 3A-1 ; measured strains after each etch.

(a) LONGITUDINAL STRAIN $\times 10^{-6}$

GAUGE: ETCH	L_1	L_2	L_3	L_4	L_5	L_6	L_7
0	0	0	0	0	0	0	0
1	-13	-11	-10	-10	-10	-7	-9
2	-24	-20	-19	-19	-19	-15	-19
3	-33	-29	-26	-29	-26	-23	-29
4	-45	-38	-36	-39	-35	-33	-38
5	-44	-39	-37	-41	-36	-34	-44
6	-58	-52	-42	-55	-48	-47	-57
7	-67	-60	-55	-63	-50	-51	-66
8	-83	-75	-67	-79	-63	-66	-78
9	-96	-85	-77	-93	-75	-77	-93
10	-110	-100	-87	-108	-84	-91	-102
11	-112	-102	-92	-112	-84	-91	-113
12	-128	-118	-105	-130	-96	-106	-128
13	-144	-134	-116	-146	-106	-117	-141
14	-159	-149	-128	-164	-119	-129	-160
15	-178	-165	-140	-185	-134	-140	-177
16	-188	-177	-146	-202	-139	-149	-197
17	-199	-186	-149	-210	-144	-152	-205
18	-215	-207	-162	-238	-153	-162	-224
19	-233	-224	-177	-263	-163	-171	-237
20	-238	-224	-174	-273	-149	-164	-241
21	-243	-231	-176	-284	-146	-160	-250
22	-244	-230	-170	-295	-129	-148	-258
23	-247	-225	-161	-304	-111	-133	-257
24	-253	-224	-156	-320	-96	-124	-265
25	-248	-204	-134	-323	-60	-91	-262
26	-247	-176	-110	-331	-10	-47	-252
27	-240	-141	-75	-331	+47	+8	-226
28	-235	-101	-40	-330	+105	+70	-193
29	-226	-29	+16	-319	+197	+153	-96
30	-207	+71	+94	-292	+303	+259	+102

TABLE 7. (continued)

GAUGE: ETCH	L_8	L_9	L_{10}	L_{11}	L_{12}	L_{13}
0	0	0	0	0	0	0
1	-10	-10	-11	-11	-13	-14
2	-18	-19	-20	-21	-21	-22
3	-28	-28	-28	-30	-30	-31
4	-40	-39	-39	-38	-41	-42
5	-40	-39	-39	-42	-40	-41
6	-55	-53	-56	-55	-54	-53
7	-64	-60	-61	-64	-63	-61
8	-78	-74	-75	-76	-77	-76
9	-91	-88	-87	-91	-91	-88
10	-105	-100	-101	-103	-104	-101
11	-109	-103	-104	-113	-105	-102
12	-125	-119	-120	-130	-120	-117
13	-141	-136	-139	-147	-136	-133
14	-155	-147	-153	-166	-149	-143
15	-171	-163	-169	-186	-166	-159
16	-184	-169	-180	-207	-173	-167
17	-194	-174	-188	-217	-181	-174
18	-209	-182	-201	-236	-197	-186
19	-224	-192	-212	-254	-208	-195
20	-223	-185	-206	-260	-204	-192
21	-225	-178	-204	-271	-203	-192
22	-222	-161	-190	-283	-177	-184
23	-219	-141	-174	-288	-187	-176
24	-220	-120	-164	-301	-184	-171
25	-203	-74	-135	-306	-165	-150
26	-183	-10	-96	-311	-149	-132
27	-146	+60	-49	-311	-129	-110
28	-91	+141	+8	-311	-107	-87
29	+25	+241	+99	-305	-74	-56
30	+256	+348	+223	-286	-16	-10

TABLE 7. (continued)

(b) CIRCUMFERENTIAL STRAIN $\times 10^{-6}$

GAUGE: ETCH	C_1	C_2	C_3	C_4	C_5	C_6	C_7
0	0	0	0	0	0	0	0
1	-4	-9	-8	-5	-3	-4	-6
2	-6	-13	-10	-10	-9	-10	-10
3	-8	-16	-15	-17	-16	-18	-19
4	-9	-17	-18	-15	-17	-16	-17
5	-2	-11	-15	-12	-13	-16	-16
6	-4	-16	-19	-15	-16	-22	-25
7	-5	-19	-21	-19	-18	-24	-27
8	-2	-18	-23	-19	-17	-28	-32
9	-4	-20	-25	-25	-22	-37	-37
10	0	-18	-28	-21	-23	-36	-39
11	+5	-15	-26	-17	-24	-39	-38
12	+4	-17	-29	-20	-30	-44	-41
13	+6	-17	-32	-20	-34	-44	-47
14	+5	-20	-38	-23	-43	-51	-57
15	+7	-25	-43	-23	-48	-56	-63
16	+4	-30	-53	-24	-54	-59	-67
17	+11	-30	-53	-22	-54	-60	-69
18	+3	-40	-66	-28	-63	-74	-79
19	+4	-46	-70	-25	-73	-75	-82
20	+10	-40	-65	-10	-65	-68	-76
21	+8	-46	-73	-4	-75	-74	-80
22	+5	-60	-89	+6	-88	-86	-85
23	+6	-65	-93	+25	-93	-88	-85
24	0	-70	-107	+40	-108	-99	-93
25	+4	-75	-115	+70	-123	-100	-88
26	+2	-72	-128	+101	-148	-113	-89
27	+11	-67	-135	+140	-160	-117	-78
28	+15	-75	-141	+171	-171	-120	-62
29	+31	-70	-140	+213	-160	-99	-10
30	+55	-48	-118	+260	-112	-43	+54

TABLE 7. (continued)

GAUGE: ETCH	C_8	C_9	C_{10}	C_{11}	C_{12}	C_{13}
0	0	0	0	0	0	0
1	-6	-4	-2	-6	-5	-7
2	-10	-8	-8	-10	-7	-10
3	-12	-9	-10	-13	-10	-16
4	-16	-10	-11	-17	-8	-19
5	-10	-6	-7	-10	-3	-13
6	-18	-7	-10	-18	-3	-16
7	-18	-7	-12	-19	-2	-14
8	-27	-7	-16	-28	0	-20
9	-31	-10	-22	-32	-1	-26
10	-37	-6	-21	-39	+2	-28
11	-33	0	-21	-39	+10	-22
12	-41	-2	-30	-47	+12	-25
13	-51	-2	-35	-62	+14	-31
14	-59	-6	-40	-69	+18	-35
15	-67	-7	-47	-83	+24	-44
16	-77	-9	-54	-94	+28	-48
17	-84	+2	-48	-102	+39	-49
18	-98	+3	-55	-117	+40	-64
19	-116	+8	-58	-139	+50	-76
20	-118	+30	-47	-145	+71	-70
21	-125	+42	-49	-159	+81	-80
22	-134	+55	-51	-173	+95	-91
23	-140	+78	-48	-186	+114	-94
24	-157	+95	-49	-207	+123	-111
25	-158	+131	-48	-223	+147	-122
26	-157	+165	-49	-246	+167	-133
27	-125	+200	-39	-260	+184	-141
28	-66	+222	-37	-266	+195	-153
29	+70	+229	-27	-254	+197	-152
30	+207	+237	-6	-226	+188	-146

TABLE 8. : Change in the surface strain parameters on rotating specimen 3A-1 by 180° about a longitudinal axis.

ETCH	ρ/b	$\theta = 0°$		$\theta = 88.5°$		$\theta = 183°$	
		$\mathcal{L}_b$	ℓ_{b}	$\mathcal{L}_b$	ℓ_{b}	$\mathcal{L}_b$	ℓ_{b}
		$\times 10^{-6}$		$\times 10^{-6}$		$\times 10^{-6}$	
0	0.941	+1	−1	0	0	0	0
5	0.946	0	0	0	0	0	0
15	0.966	0	−4	−1	0	−2	+1
23	0.985	0	0	−1	0	+1	+1
25	0.988	−1	−2	+1	−1	+2	+4
28	0.993	+6	+3	+3	−1	+7	+20
29	0.995	+1	−1	0	−1	+4	+20
30	0.996	0	−2	+3	+1	+6	+16

TABLE 9. : Number of circumferential lobes in elastically unstable collapse mode (61), for all-around pressure and $\ell/R = 8$.

R/h	n
50 → 125	3
143	3 OR 4
167 → 333	4
400	4 OR 5
500	5

TABLE 10. : Elastic critical pressure $p_{CRIT.}$,
specimen 3A-1 .

(a) BASED ON MEAN WALL THICKNESS N/mm^2

ρ/b	R/h	$n = 3$	$n = 4$	$n = 5$
0·980	50	0·76	1·29	2·04
0·983	58	0·49	0·80	1·26
0·985	66	0·35	0·55	0·86
0·987	76	0·24	0·36	0·56
0·988	83	0·20	0·28	0·44
0·990	100	0·12	0·16	0·25
0·992	125	0·07	0·09	0·13
0·993	137	0·06	0·06	0·10
0·995	200	0·03	0·02	0·03

(b) BASED ON MINIMUM WALL THICKNESS N/mm^2

ρ/b	R/h	$n = 3$	$n = 4$	$n = 5$	$n = 6$
0·980	60	0·45	0·73	1·15	
0·983	73	0·26	0·40	0·65	
0·985	86	0·18	0·25	0·39	
0·987	105	0·11	0·14	0·22	0·32
0·988	117	0·09	0·10	0·16	0·23
0·990	153	0·05	0·05	0·07	0·10
0·992	221	0·02	0·02	0·02	0·03
0·993	285	0·02	0·01	0·01	0·01
0·995	665	0·01			

TABLE 11. : The effect of eccentricity on the value of M_c/M_m.

(a) ΔD_{oo} MEASURED.

e	0	0·06	0·10	0·20
M_c/M_m	1	0·86	0·78	0·59

(b) ΔG_{oo} MEASURED.

e	0	0·06	0·10	0·20
M_c/M_m	1	0·91	0·84	0·68

APPENDIX 3.

DERIVATION OF THE SACHS EQUATIONS.

(a) Removal of uniform internal layers from a uniform cylinder containing axisymmetric residual stresses.

Defining the strain parameters:

$$\mathcal{L}_{b\rho} = \varepsilon_L + \mu . \varepsilon_C$$
$$\mathcal{C}_{b\rho} = \varepsilon_C + \mu . \varepsilon_L$$

where ε_L and ε_C are the measured surface strains on the outside surface of the cylinder, the object is to relate the stresses σ_L, σ_C and σ_R at some radius ρ to the changes in $\mathcal{L}_{b\rho}$ and $\mathcal{C}_{b\rho}$ which are produced when the material at radius ρ is removed.

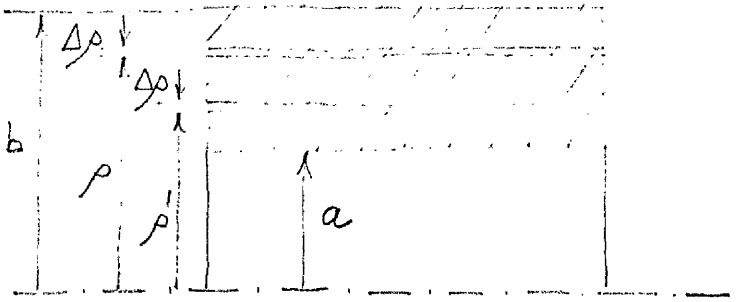

As layers of material at radius $\rho' < \rho$ are removed, the stresses at ρ undergo continuous alteration, so that:

$$\sigma_L'' = \sigma_L + \sigma_L'$$
$$\sigma_C'' = \sigma_C + \sigma_C'$$
$$\sigma_R'' = \sigma_R + \sigma_R'$$

where the components σ'' refer to that part of the original stress which is present in the layer $\Delta\rho$ at radius ρ when it is removed, and the components σ'

to the stress induced in the layer at radius ρ by removal of internal layers up to radius ρ .

The condition $\sigma'' < \sigma_y$ is assumed to apply at all times, so that only elastic strains are considered.

(i) Calculation of the stress components σ' .

If $(\Delta\sigma_c)_{\rho\rho'}$, $(\Delta\sigma_R)_{\rho\rho'}$ and $(\Delta\sigma_L)_{\rho\rho'}$ denote the stress changes produced at radius ρ by removal of a layer of thickness $\Delta\rho$ at radius $\rho' < \rho$ then:

$$(\Delta\sigma_c)_{\rho\rho'} = \frac{b^2+\rho^2}{2\rho^2}(\Delta\sigma_c)_{b\rho'}$$

$$(\Delta\sigma_R)_{\rho\rho'} = \frac{-(b^2-\rho^2)}{2\rho^2}(\Delta\sigma_c)_{b\rho'}$$

$$(\Delta\sigma_L)_{\rho\rho'} = (\Delta\sigma_L)_{b\rho'}$$

where $(\Delta\sigma_c)_{b\rho'}$ and $(\Delta\sigma_L)_{b\rho'}$ denote the stress changes produced at the outer surface. The first two equations are a consequence of Lame's equations (96) and the third follows from the fact that the distribution of the longitudinal induced stress over the cross-section of the cylinder is assumed to be uniform.

It follows from elementary stress analysis that:

$$(\Delta\sigma_c)_{\rho\rho'} = E' \cdot \frac{b^2+\rho^2}{2\rho^2}(\Delta\theta)_{b\rho'}$$

$$(\Delta\sigma_R)_{\rho\rho'} = -E' \cdot \frac{b^2-\rho^2}{2\rho^2}(\Delta\theta)_{b\rho'}$$

$$(\Delta\sigma_L)_{\rho\rho'} = E'.(\Delta\ell)_{b\rho'}$$

where $(\Delta\ell)_{b\rho'}$ and $(\Delta\theta)_{b\rho'}$ may be determined from the known strain changes at the outer surface, and since:

$$\sigma' = \sum_{\rho'=a\to\rho}(\Delta\sigma)_{\rho\rho'}$$

it follows that:

$$\sigma_c' = E'.\frac{b^2+\rho^2}{2\rho^2}.\sum_{\rho'=a\to\rho}(\Delta\theta)_{b\rho'} = E'.\frac{b^2+\rho^2}{2\rho^2}.\theta_{b\rho}$$

$$\sigma_R' = -E'.\frac{b^2-\rho^2}{2\rho^2}.\sum_{\rho'=a\to\rho}(\Delta\theta)_{b\rho'} = -E'.\frac{b^2-\rho^2}{2\rho^2}.\theta_{b\rho}$$

$$\sigma_L' = E'.\sum_{\rho'=a\to\rho}(\Delta\ell)_{b\rho'} = E'.\varepsilon_{b\rho}$$

(ii) Calculation of the stress components σ''.

If $(\Delta\sigma_c)_{b\rho}$ and $(\Delta\sigma_L)_{b\rho}$ denote the stress changes produced on the outer surface of the cylinder when the layer $\Delta\rho$ at radius ρ (containing the stresses σ_c'', σ_R'' and σ_L'') is removed, then:

$$(\Delta\sigma_c)_{b\rho} = \frac{2\rho^2}{b^2+\rho^2}(\Delta\sigma_c)_{\rho\rho}$$

$$(\Delta\sigma_L)_{b\rho} = (\Delta\sigma_L)_{\rho\rho}$$

where $(\Delta\sigma_c)_{\rho\rho}$ and $(\Delta\sigma_L)_{\rho\rho}$ denote the stress changes at radius ρ. The first equation again follows from Lame's theory, and the second from the fact that the longitudinal induced stress is uniformly distributed

over the cross-section.

It may easily be shown from considerations of longitudinal equilibrium that:

$$(\Delta\sigma_L)_{\rho\rho} = \frac{2\rho.\Delta\rho}{b^2-\rho^2}.\sigma_L''$$

so that:

$$(\Delta\sigma_L)_{b\rho} = \frac{2\rho.\Delta\rho}{b^2-\rho^2}.\sigma_L''$$

or:

$$\sigma_L'' = \frac{b^2-\rho^2}{2\rho}.\frac{(\Delta\sigma_L)_{b\rho}}{\Delta\rho}$$

It may also be shown using Lame's theory that:

$$(\Delta\sigma_c)_{\rho\rho} = \frac{b^2+\rho^2}{b^2-\rho^2}.\sigma_R''$$

and since σ_R'' is zero at the inner surface of the layer $\Delta\rho$, and has the average value $\frac{\Delta\rho}{\rho}.\sigma_c''$ (equilibrium of elemental cylinder, thickness $\Delta\rho$, radius ρ), it follows that:

$$(\Delta\sigma_c)_{\rho\rho} = \frac{b^2+\rho^2}{b^2-\rho^2}.\frac{\Delta\rho}{\rho}.\sigma_c''$$

so that:

$$\frac{b^2+\rho^2}{2\rho^2}.(\Delta\sigma_c)_{b\rho} = \frac{b^2+\rho^2}{b^2-\rho^2}.\frac{\Delta\rho}{\rho}.\sigma_c''$$

or:

$$\sigma_c'' = \frac{b^2-\rho^2}{2\rho}.\frac{(\Delta\sigma_c)_{b\rho}}{\Delta\rho}$$

and since:

$$\sigma_R'' = \frac{\Delta\rho}{\rho}.\sigma_c''$$

it follows that:

$$\sigma_R'' = \frac{b^2-\rho^2}{2\rho^2}.(\Delta\sigma_c)_{b\rho}$$

and using elementary stress analysis:

$$\sigma_L'' = E' \cdot \frac{b^2-\rho^2}{2\rho} \cdot \left(\frac{\Delta l}{\Delta \rho}\right)_{b\rho}$$

$$\sigma_C'' = E' \cdot \frac{b^2-\rho^2}{2\rho} \cdot \left(\frac{\Delta l\theta}{\Delta \rho}\right)_{b\rho}$$

$$\sigma_R'' = E' \cdot \frac{b^2-\rho^2}{2\rho^2} \cdot (\Delta l\theta)_{b\rho}$$

(iii) Determination of σ_L , σ_C and σ_R .

It follows from the general definition on p.146 , that:

$$\sigma_L = E'\left[\frac{b^2-\rho^2}{2\rho} \cdot \left(\frac{\Delta l}{\Delta \rho}\right)_{b\rho} - l_{b\rho}\right]$$

$$\sigma_C = E'\left[\frac{b^2-\rho^2}{2\rho} \cdot \left(\frac{\Delta l\theta}{\Delta \rho}\right)_{b\rho} - \left(\frac{b^2+\rho^2}{2\rho^2}\right) \cdot l\theta_{b\rho}\right]$$

$$\sigma_R = E' \cdot \frac{b^2-\rho^2}{2\rho^2} \cdot \left[(\Delta l\theta)_{b\rho} + l\theta_{b\rho}\right]$$

where $\left(\frac{\Delta l}{\Delta \rho}\right)_{b\rho} \rightarrow \left(\frac{dl}{d\rho}\right)_{b\rho}$, $\left(\frac{\Delta l\theta}{\Delta \rho}\right)_{b\rho} \rightarrow \left(\frac{dl\theta}{d\rho}\right)_{b\rho}$ and $(\Delta l\theta)_{b\rho} \rightarrow 0$ as $\Delta\rho$ tends to zero. With the substitution of $f = \pi\rho^2$ and $f_b = \pi b^2$, the equations 1.01 are obtained.

(b) Removal of uniform external layers from a uniform cylinder containing axisymmetric residual stresses.

In this case the derivation is almost identical (6,49), except that the surface strains ε_L and ε_C

are measured at the bore, and the change $\Delta\rho$ is taken as positive with decreasing radius. With this convention, the final equations are:

$$\sigma_L = E'\left[\frac{\rho^2-a^2}{2\rho}\cdot\left(\frac{\Delta\ell}{\Delta\rho}\right)_{a\rho} - \ell_{a\rho}\right]$$

$$\sigma_C = E'\left[\frac{\rho^2-a^2}{2\rho}\cdot\left(\frac{\Delta\theta}{\Delta\rho}\right)_{a\rho} - \left(\frac{\rho^2+a^2}{2\rho^2}\right)\cdot\theta_{a\rho}\right]$$

$$\sigma_R = E'\cdot\frac{\rho^2-a^2}{2\rho^2}\left[(\Delta\theta)_{a\rho} - \theta_{a\rho}\right]$$

and with the substitution of $f=\pi\rho^2$ and $f_a=\pi a^2$, the equations 1.02 are obtained as $\Delta\rho$ tends to zero.

APPENDIX 4.

DETERMINATION OF $\cos\beta_b(\rho,\theta)$ AND $\cos\beta_a(\rho,\theta)$ IN TERMS OF ρ, θ_b AND θ_a.

Expressions for $\cos\beta_b(\theta)$ and $\cos\beta_a(\theta)$ are derived for the general case shown below, and the particular solutions for internal and external layer removal are obtained by substitution of $a = \rho$ or $b = \rho$ respectively.

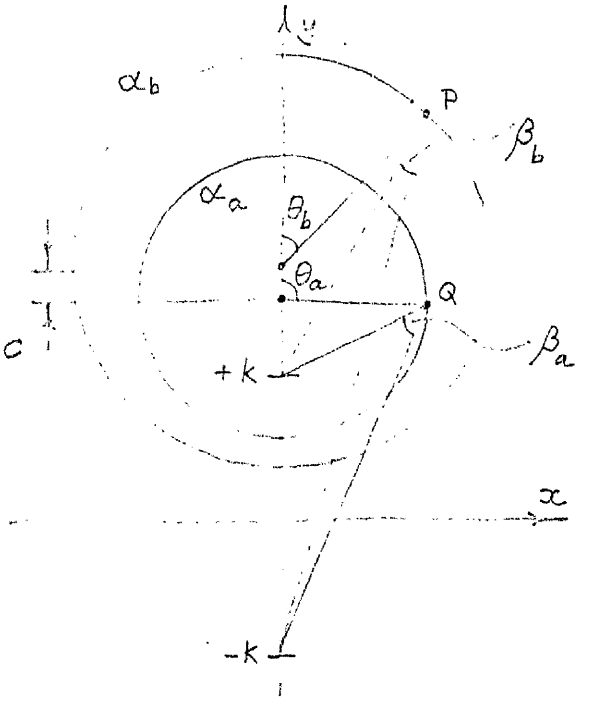

If c_a and c_b denote the distances of the centres of the circles α_a and α_b from the origin, a and b their radii and c the distance apart of their centres, so that $c = c_b - c_a$, it may be shown (44) that:

$$k^2 = \frac{1}{4c^2}\left[b^2-(a+c)^2\right]\left[b^2-(a-c)^2\right]$$

$$c_a = \frac{1}{2c}\left(b^2-a^2-c^2\right)$$

$$c_b = \frac{1}{2c}\left(b^2-a^2+c^2\right)$$

The first of these expressions may be written:

$$k^2 = \frac{1}{4c^2}\left[\left(b^2-a^2-c^2\right)^2 - 4a^2c^2\right]$$

from which it follows that:

$$k^2+a^2 = \frac{1}{4c^2}\left(b^2-a^2-c^2\right)^2 = c_a^2$$

$$k^2+b^2 = \frac{1}{4c^2}\left(b^2-a^2+c^2\right)^2 = c_b^2$$

(a) Determination of $\cos\beta_b(\theta)$.

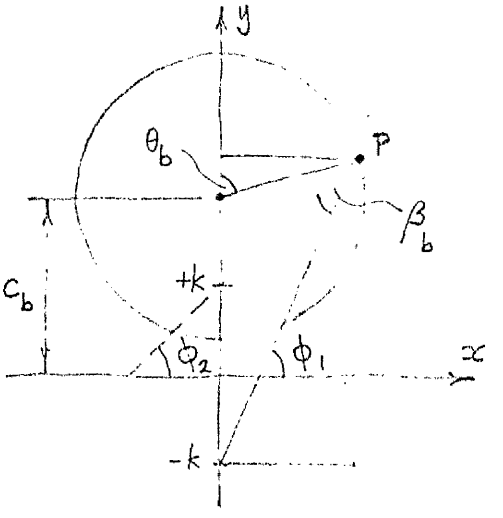

Recalling from equation 3.08 that:

$$\beta_b = \phi_1 - \phi_2$$

it may easily be shown that:

$$\tan\phi_2 = \frac{b\cos\theta_b + c_b - k}{b\sin\theta_b}$$

$$\tan\phi_1 = \frac{b\cos\theta_b + c_b + k}{b\sin\theta_b}$$

and, by using a standard trigonometrical formula, that:

$$\tan\beta_b(\theta) = \frac{2b.k.\sin\theta_b}{b^2+c_b^2-k^2+2b.c_b.\cos\theta_b}$$

and since $c_b^2 = k^2+b^2$, it follows that:

$$\tan\beta_b(\theta) = \frac{k\sin\theta_b}{b + c_b.\cos\theta_b}$$

so that:

$$\cos\beta_b(\theta) = \frac{b + c_b\cos\theta_b}{\sqrt{\left[(b+c_b\cos\theta_b)^2 + k^2\sin^2\theta_b\right]}}$$

and using the fact that $k^2 = c_b^2 - b^2$, it may be shown that:

$$\cos\beta_b(\theta) = \frac{b + c_b.\cos\theta_b}{b\cos\theta_b + c_b}$$

and replacing c_b by $\frac{1}{2c}(b^2 - a^2 + c^2)$ leads to:

$$\cos\beta_b(\theta) = \frac{2bc + \cos\theta_b(b^2 - a^2 + c^2)}{2bc\cos\theta_b + (b^2 - a^2 + c^2)} \qquad (A)$$

(b) Determination of $\cos\beta_a(\theta)$.

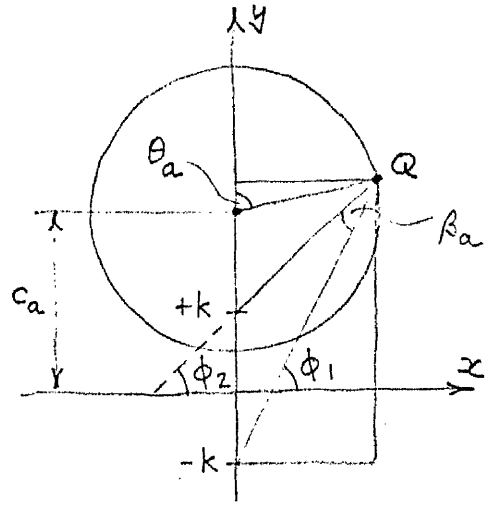

In this case $\beta_a = \phi_1 - \phi_2$ and it may similarly be shown that:

$$\tan\beta_a(\theta) = \frac{k\sin\theta_a}{a + c_a.\cos\theta_a}$$

so that:

$$\cos\beta_a(\theta) = \frac{a + c_a.\cos\theta_a}{\sqrt{\left[(a + c_a\cos\theta_a)^2 + k^2\sin^2\theta_a\right]}}$$

and by using the fact that $k^2 = c_a^2 - a^2$, it follows that:

$$\cos\beta_a(\theta) = \frac{a + c_a.\cos\theta_a}{a.\cos\theta_a + c_a}$$

and replacing c_a by $\frac{1}{2c}(b^2 - a^2 - c^2)$ gives:

$$\cos\beta_a(\theta) = \frac{2ac + \cos\theta_a(b^2 - a^2 - c^2)}{2ac\cos\theta_a + (b^2 - a^2 - c^2)} \qquad (B)$$

(c) Particular solutions.

In the case of internal layer removal $\cos\beta_b(\rho,\theta)$ is obtained by substituting ρ for a in expression (A) , and in the case of external layer removal $\cos\beta_a(\rho,\theta)$ is obtained by replacing b by ρ in expression (B) .

APPENDIX 5.

CALCULATION OF THE CHANGES IN DIAMETER AND GAP-WIDTH PRODUCED BY SLITTING AN ECCENTRIC TUBE ALONG A GENERATOR.

(a) Calculation of ΔD_{oo}.

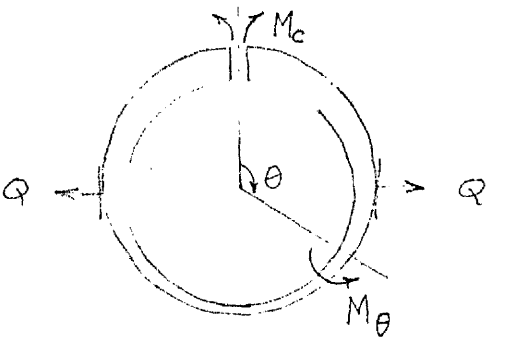

Taking as positive moments which tend to decrease curvature, it follows that:

$$M_\theta = M_c - Q.R_m.\cos\theta$$

where Q is a fictitious load applied for the purposes of calculating the diameter change ΔD_{oo}, and R_m is the mean radius of the tube, (it is assumed that the tube is sufficiently thin to regard R_m as constant).

Using Castigliano's theorem (96) :

$$\Delta D_{oo} = \left[\frac{\partial U}{\partial Q}\right]_{Q=0}$$

where:

$$U = \int_{\pi/2}^{3\pi/2} \frac{M_\theta^2.R_m.d\theta}{2E'.I_\theta} = \int_{\pi/2}^{3\pi/2} \frac{6(M_c - Q.R_m\cos\theta)^2.R_m.d\theta}{E'.l.h_m^3(1+e\cos\theta)^3}$$

and since:

$$\frac{\partial U}{\partial Q} = \frac{12R_m^2}{E'.l.h_m^3}\int_{\pi/2}^{3\pi/2} \frac{(-M_c + Q.R_m\cos\theta)\cos\theta.d\theta}{(1+e\cos\theta)^3}$$

it follows that:

$$\Delta D_{oo} = -\frac{12M_cR_m^2}{E'.l.h_m^3}\int_{\pi/2}^{3\pi/2} \frac{\cos\theta.d\theta}{(1+e\cos\theta)^3}$$

and from symmetry that:

$$\Delta D_{oo} = \frac{-24 M_c R_m^2}{E'.l.h_m^3} \int_{\pi/2}^{\pi} \frac{\cos\theta.d\theta}{(1+e\cos\theta)^3}$$

Using a table of integrals (102) it may be shown that:

$$-\int_{\pi/2}^{\pi} \frac{\cos\theta.d\theta}{(1+e\cos\theta)^3} = \frac{1}{(1-e^2)^2}\left\{1 + \frac{e^2}{2} + \frac{3e}{(1-e^2)^{1/2}}\left[\frac{\pi}{2} - \tan^{-1}\frac{(1-e^2)^{1/2}}{1+e}\right]\right\}$$

and so:

$$\Delta D_{oo} = \frac{24 M_c R_m^2}{E'.l.h_m^3 (1-e^2)^2}\left\{1 + \frac{e^2}{2} + \frac{3e}{(1-e^2)^{1/2}}\left[\frac{\pi}{2} - \tan^{-1}\frac{(1-e^2)^{1/2}}{1+e}\right]\right\}$$

(b) Calculation of $\Delta D_{o\pi}$.

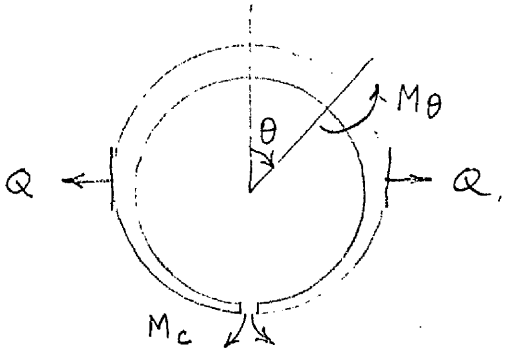

In this case:

$$M_\theta = M_c + Q.R_m.\cos\theta$$

and it may easily be shown that:

$$\Delta D_{o\pi} = \left[\frac{\partial U}{\partial Q}\right]_{Q=0} = \frac{12 M_c R_m^2}{E'.l.h_m^3} \int_{-\pi/2}^{\pi/2} \frac{\cos\theta.d\theta}{(1+e\cos\theta)^3}$$

and from symmetry:

$$\Delta D_{o\pi} = \frac{24 M_c R_m^2}{E'.l.h_m^3} \int_{0}^{\pi/2} \frac{\cos\theta.d\theta}{(1+e\cos\theta)^3}$$

It may be shown (102) that:

$$\int_0^{\pi/2} \frac{\cos\theta.d\theta}{(1+e\cos\theta)^3} = \frac{1}{(1-e^2)^2}\left\{1+\frac{e^2}{2}-\frac{3e}{(1-e^2)^{1/2}}\left[\tan^{-1}\frac{(1-e^2)^{1/2}}{1+e}\right]\right\}$$

and so:

$$\Delta D_{0\pi} = \frac{24 M_c R_m^2}{E'\ell.h_m^3(1-e^2)^2}\left\{1+\frac{e^2}{2}-\frac{3e}{(1-e^2)^{1/2}}\left[\tan^{-1}\frac{(1-e^2)^{1/2}}{1+e}\right]\right\}$$

(c) Calculation of $\Delta D_{0\pi/2}$.

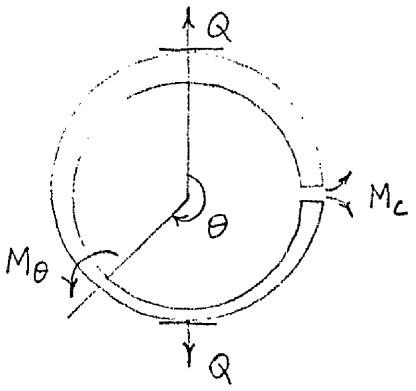

In this case:

$$M_\theta = M_c - Q.R_m.\sin\theta$$

and:

$$\Delta D_{0\pi/2} = \left[\frac{\partial U}{\partial Q}\right]_{Q=0} = \frac{12 M_c.R_m^2}{E'.\ell.h_m^3}\int_{\pi}^{2\pi}\frac{-\sin\theta.d\theta}{(1+e\cos\theta)^3}$$

$$= \frac{24 M_c R_m^2}{E'\ell.h_m^3(1-e^2)^2}$$

(d) Calculation of ΔG_{oo}.

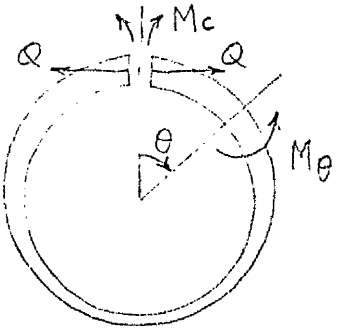

In this case the fictitious load Q is applied at the edges of the gap, and it follows that:

$$M_\theta = M_c + Q.R_m(1-\cos\theta)$$

so that:

$$\Delta G_{oo} = \left[\frac{\partial U}{\partial Q}\right]_{Q=0} = \frac{12 M_c R_m^2}{E'.l.h_m^3}\int_0^{2\pi}\frac{(1-\cos\theta).d\theta}{(1+e\cos\theta)^3}$$

and from symmetry:

$$\Delta G_{oo} = \frac{24 M_c R_m^2}{E'.l.h_m^3}\int_0^{\pi}\frac{(1-\cos\theta).d\theta}{(1+e\cos\theta)^3}$$

It may be shown (102) that:

$$\int_0^{\pi}\frac{(1-\cos\theta)\,d\theta}{(1+e\cos\theta)^3} = \frac{1}{(1-e^2)^2}\left[\frac{(1+e)(2+e)}{(1-e^2)^{1/2}}.\frac{\pi}{2}\right]$$

so that:

$$\Delta G_{oo} = \frac{24 M_c R_m^2}{E'.l.h_m^3(1-e^2)^2}\left[\frac{(1+e)(2+e)}{(1-e^2)^{1/2}}.\frac{\pi}{2}\right]$$

APPENDIX 6.

THE UPPER LIMIT FOR e.

Since the minimum value of $R_m/h\theta$ will occur at $\theta = 0$, the condition $R_m/h\theta \geq 11$ implies that:

$$\left(\frac{R_m}{h\theta}\right)_{\theta=0} \geq 11$$

from which it follows that:

$$\frac{\frac{1}{2}(b+a)}{(b-a)+c} \geq 11$$

or that:

$$(b-a)+c \leq \frac{1}{22}(b+a)$$

and since $e = \frac{c}{b-a}$, it follows that:

$$1 + e \leq \frac{1}{22}\cdot\left(\frac{b+a}{b-a}\right)$$

so that the upper limit for the initial eccentricity e is specified by:

$$e \leq \frac{1}{22}\left(\frac{1+a/b}{1-a/b}\right) - 1$$